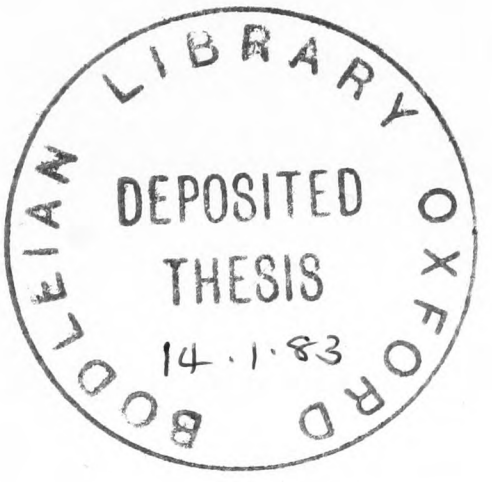
ION RAREFACTION WAVES AND ASSOCIATED PHENOMENA

ANDREW J. COATES

Keble College



This thesis is submitted in partial fulfilment of the requirements for the Degree of Doctor of Philosophy in the University of Oxford.

Hilary Term, 1982

TO MY PARENTS

ACKNOWLEDGEMENTS

Many thanks are due to my two supervisors, Drs. J. E. Allen and P. D. Edgley, who have offered me much advice and encouragement throughout my time in Oxford. Their guidance and the benefits of their experience have been much appreciated. Particular thanks are due to Dr. Edgley for his careful reading of the draft version of this thesis and to Dr. Allen for helpful comments on a later version.

I would also like to thank other members of the Oxford plasma physics group for many discussions. In particular I must thank Drs. N. St.J. Braithwaite and L. M. Wickens for taking such an interest in many of my problems. They both collaborated in the theoretical work described in this thesis. I am also grateful to Dr. A. H. von Engel for his interest in the operation of the multidipole device.

The financial support of the Science and Engineering Research Council in the form of a research studentship and an extension thereof is acknowledged.

Finally I should like to thank Katherine for her much-needed help and encouragement over the last three years, and in particular for typing the bulk of this thesis from a difficult manuscript.

ION RAREFACTION WAVES AND ASSOCIATED PHENOMENA

A. J. COATES, KEBLE COLLEGE.

A thesis submitted for the degree of Doctor of Philosophy
in the University of Oxford, Hilary Term 1982.

This thesis contains an experimental and theoretical study of the response of a plasma to the motion of the positive space-charge sheath which bounds it. It is known theoretically that, if a sheath edge is moved at a speed less than the speed of ion acoustic waves, a region of ion rarefaction propagates into the plasma at the ion acoustic speed. In the past, difficulty has been encountered with the theory of ion acoustic wave generation from moving sheath edges, where compressions are necessary in addition to rarefactions. The initial conditions of many previous calculations omit the formation of a steady-state presheath where ions are accelerated to form the sheath.

Some calculations are described which include the effects of an initial presheath by constructing a one-dimensional plasma solution where a production term balances the losses of ions to the walls. The plasma response to the motion of one boundary is found using the method of characteristics with appropriate boundary conditions. Ion rarefaction waves are associated with expanding sheaths while ion 'enhancement' waves (compressive features) are formed on sheath collapse. In each case the wavefront moves at the local ion acoustic speed which includes the effects of ion drift. The presence of the presheath is essential to the generation of enhancements.

The constructional details of a multidipole device are discussed, and the results of Langmuir probe and ion acoustic wave experiments are used to determine the parameters of a quiescent argon plasma. Some experiments on moving sheaths in such a plasma are then considered. Negative voltage ramps are applied to a plate and the plasma response is measured using sampled probe techniques. As the plate-plasma voltage increases, the ion-rich sheath expands at a speed which depends on the applied voltage waveform. For sheath edge speeds less than the ion acoustic speed, an ion rarefaction wave is formed. As the voltage decreases, the sheath collapses and an ion enhancement wave propagates into the plasma. Both wavefronts are observed to move at the local ion acoustic speed which increases with distance from the plate in agreement with theory.

CONTENTS

		Page
CHAPTER 1		
	PREVIOUS WORK ON MOVING PLASMA BOUNDARIES	
1.1	INTRODUCTION	1
1.2	BACKGROUND TO THE WORK	2
1.3	THE STRUCTURE OF THE STATIC SHEATH-PLASMA SYSTEM	8
1.4	THEORY OF MOVING SHEATHS	9
	1.4.1 Ion Rarefaction Waves With No Initial Presheath	10
	1.4.2 Movement of a Sheath Including Initial Presheath Effects	13
	1.4.3 The Dynamic Bohm Criterion	14
1.5	EXPERIMENTS ON MOVING SHEATHS	15
1.6	EXPANDING PLASMAS	18
1.7	TECHNIQUES FOR LAUNCHING ION ACOUSTIC WAVES	19
1.8	LAYOUT OF THE THESIS	20
CHAPTER 2		
	MOVING THE BOUNDARY OF A FINITE PLASMA	
2.1	INTRODUCTION	22
2.2	THE FLUID EQUATIONS IN CHARACTERISTIC FORM	23
2.3	PREVIOUS APPLICATIONS OF CHARACTERISTICS TO MOVING SHEATHS	27
2.4	THE STEADY-STATE SOLUTION	30
2.5	THE WAVEFRONT AND BOUNDARY CONDITIONS	32
2.6	PLASMA SOLUTION FOR AN ACCELERATING COLLAPSING SHEATH	35
	2.6.1 Method	35
	2.6.2 Results	36
2.7	PLASMA SOLUTION FOR AN ACCELERATING EXPANDING SHEATH	41
	2.7.1 Method	41
	2.7.2 Results	41

CONTENTS Page

CHAPTER 2
(continued)

2.8 NUMERICAL CHECKS 42

2.9 PLASMA SOLUTION FOR CONSTANT VELOCITY SHEATH COLLAPSE 44

2.9.1 Method 44
2.9.2 Results 46

2.10 PROOF THAT THE SHEATH EDGE IS NOT GENERALLY A CHARACTERISTIC 48

2.11 DISCUSSION OF THE BREAKDOWN OF QUASINEUTRALITY 50

2.12 SUMMARY OF THEORETICAL RESULTS 53

CHAPTER 3

THE MULTIDIPOLE DEVICE

3.1 INTRODUCTION 55

3.2 DOUBLE PLASMA MACHINES AND MULTIDIPOLE DEVICES 56

3.3 DESCRIPTION OF THE MULTIDIPOLE DEVICE 60

3.3.1 The Mechanical System 60
3.3.2 The Electrical System 63

3.4 SUMMARY AND RUNNING CONDITIONS 67

CHAPTER 4

BASIC PLASMA EXPERIMENTS

4.1 INTRODUCTION 68

4.2 LANGMUIR PROBE EXPERIMENTS 69

4.2.1 Current-Voltage Characteristics 69
4.2.2 Electron Velocity Distribution Measurements 75

4.3 CONTINUOUS ION ACOUSTIC WAVE PROPAGATION 78

4.4 ION ACOUSTIC PULSE PROPAGATION 83

CONTENTS Page

CHAPTER 4
(continued)

4.5 DISCUSSION AND COMPARISON OF RESULTS 90

4.6 SUMMARY OF PLASMA PARAMETERS 91

4.6.1 Summary 92
4.6.2 Effects of Different Anode Connections 93

CHAPTER 5

EXPERIMENTS ON MOVING SHEATHS

5.1 INTRODUCTION 95

5.2 EXPERIMENTAL TECHNIQUES 96

5.2.1 Details of Construction 96
5.2.2 Exciter and Receiver Electrical Circuits 100

5.3 ION RAREFACTION WAVE OBSERVATIONS 103

5.3.1 Slow ramp 105
5.3.2 Fast ramp 117

5.4 ION ENHANCEMENT WAVE OBSERVATIONS 121

5.4.1 Slow Ramp 121
5.4.2 Fast Ramp 124

5.5 OPTICAL MEASUREMENTS 129

5.5.1 Observations 129
5.5.2 Discussion of the Optical Results 131

5.6 SUMMARY OF EXPERIMENTAL RESULTS 134

5.7 ERRORS 135

CHAPTER 6

DISCUSSION AND SUMMARY

6.1 INTRODUCTION 137

6.2 RAREFACTION AND ENHANCEMENT WAVES 138

CONTENTS

CHAPTER 6
(continued)

6.3 OBSERVATIONS OF THE SHEATH EDGE

6.4 CURRENT TO THE PLATE

6.5 OTHER OBSERVATIONS

6.6 THE PRODUCTION OF ION ACOUSTIC WA

6.7 SUMMARY AND CONCLUSIONS

REFERENCES

CHAPTER 1

PREVIOUS WORK ON MOVING PLASMA BOUNDARIES

1.1 INTRODUCTION

This Chapter reviews previous work on moving plasma boundaries. The first Section briefly introduces the basic concepts of plasmas, sheaths, presheaths, moving sheaths and the production of ion waves. Next we consider the structure of the stationary ion-rich sheath formed at a negatively biassed electrode or a wall. Then we discuss the theory of sheath edges in motion, considering in particular the response of the previously undisturbed plasma. The conditions under which density rarefactions and compressions can be generated are outlined. Previous experiments on moving sheaths are then considered, followed by a review of the theory of plasma expansion into a vacuum, which is an extension of the moving sheath work. Experimental techniques previously used to launch ion acoustic waves are then discussed. The Chapter ends with a summary of the remainder of this thesis.

1.2 BACKGROUND TO THE WORK

The name 'plasma' is used to describe a particular state of matter which consists of approximately equal number densities of positive (n_+) and negative (n_-) charges. The plasma is said to be 'quasineutral' (i.e. $n_+ \approx n_-$) so that no large electric fields are allowed in the plasma itself. The use of $n_+ = n_- = n$ in plasma theory is known as the plasma approximation. In many situations, and for the purposes of this thesis, the positive charges are singly-charged ions and the negative charges are electrons. One of the features of a plasma is that it exhibits 'collective behaviour' associated with the long-range nature of the Coulomb force. This macroscopic electrical effect distinguishes plasma from an ordinary gas, the behaviour of which is dictated by microscopic collisions between the individual neutral particles. A plasma is often approximated by two electrically interacting fluids; an ion fluid and an electron fluid. Since the electrons are much lighter than the ions, the rate of energy transfer between the two fluids is slow, and the electron temperature T_e is, in many situations, much greater than the ion temperature T_i.

Because of an electrical screening effect similar to that found in electrolytes (DEBYE and HUCKEL, 1923), the sphere of influence of a particular charge is limited to a certain radius known as the Debye length ($\lambda_D = \sqrt{[\epsilon_o kT_e / ne^2]}$ where ϵ_o is the permittivity of free space, k is the Boltzmann constant and e is the electronic charge). It can be shown from Poisson's equation that this is the scale length over which we expect quasineutrality to break down. For distances of this order space-charge regions with $n_e \gg n_i$ or $n_i \gg n_e$ are allowed.

Let us consider the effect of placing an insulating surface (or an isolated metal surface) in the plasma. This is equivalent to considering the region near the wall of a plasma containment device if no magnetic fields are present. The electrons are lighter than the ions and their thermal velocities are much higher, particularly if $T_e \gg T_i$. The surface will thus charge up negatively, and the potential of the surface will be lower than that of the plasma if electron emission processes such as photoelectron emission are unimportant. This potential difference will tend to attract ions and repel electrons so that a region of positive ion space charge will form (Figure 1.1). In the steady state, the flux of electrons equals the flux of ions so that no net current is drawn; the surface is then at 'floating potential'. In general, the regions where $n_e \neq n_i$ have a scale length λ_d, so that we expect the scale length of the space-charge region (or 'sheath') will also be λ_d. The sheath almost shields out the potential difference between the plasma and the surface, but not completely, as we shall see.

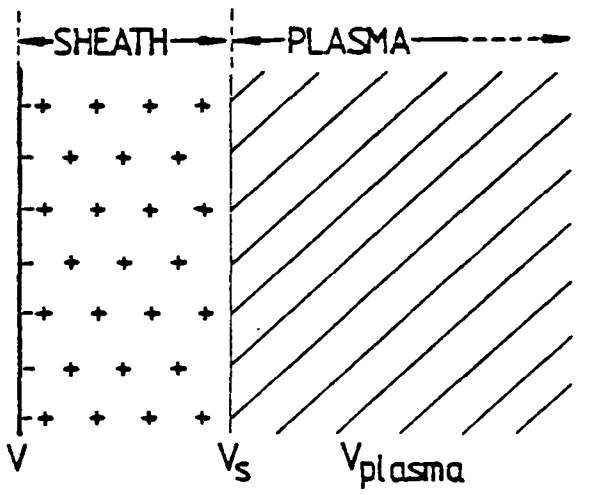


Figure 1.1
Plane geometry sheath: the wall potential $V < V_s < V_{plasma}$.

If there were no electric field in the plasma, then the ion flux across the sheath edge would be very low (the random flux associated with the low ion temperature). In practice, the slow ions are accelerated towards the sheath edge by a weak electric

field which penetrates the plasma. We shall consider this process from plasma and sheath viewpoints as follows:

(i) From the plasma viewpoint, TONKS and LANGMUIR (1929) considered a cylindrically symmetric positive column with a density and potential profile in the plasma (see Figure 1.2). The column was self-sustained, in that an ionization term balanced the loss of plasma to the walls. It was this balance of production and loss which gave the density profile. Using the plasma approximation ($n_e=n_i$), and assuming free-fall of the ions (no collisions), the variation of potential across the column was found. The plasma approximation clearly broke down when the electric field became infinite, and at this point the potential was shown to be near to $-kT_e/e$. This point was identified as the sheath edge, and the average ion velocity there was just above the ion acoustic speed c_s ($=\sqrt{(kT_e/M)}$, where M is the ion mass) directed towards the wall.

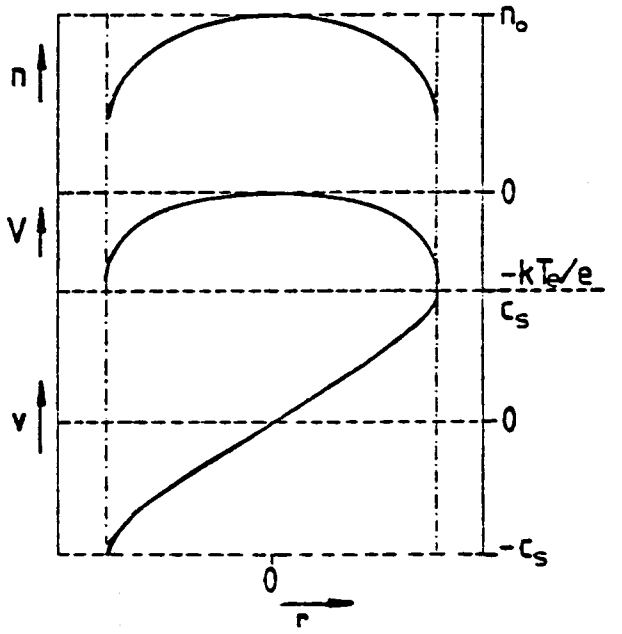


Figure 1.2

Plasma solution for a cylindrical positive column (schematic).

(ii) In the alternative approach, BOHM (1949) considered the situation in plane geometry and solved Poisson's equation in the sheath, again assuming free fall of ions. In order to find a non-oscillatory solution for the potential near the sheath edge the ions were required to move with a velocity of at least

c_s at the sheath edge directed into the sheath. This result is known as the 'Bohm criterion for sheath formation'. A modified version of this criterion will be used when we consider a moving sheath.

From both plasma and sheath points of view, then, and independently of geometry, it has been demonstrated that a region of influence extends beyond the Debye sheath in front of an isolated surface. In this 'presheath' (whose scale length is $\gg\lambda_d$) ions are accelerated towards the sheath edge but quasineutrality still holds.

If we now apply an external voltage to the previously isolated plate in the plasma, the sheath will tend to shield out this potential. If the voltage is more negative than floating potential a positive ion sheath (and also a presheath) is formed as previously described, and ion current is drawn to the plate. If the plate potential is sufficiently negative for all electrons to be reflected, the plate current may be written as:

$$i_+ = n_s e c_s A \qquad (1.1)$$

where n_s is the density of ions at the sheath edge, c_s is the ion acoustic speed (velocity of ions at the sheath edge), e is the electronic charge and A is the plate area. If Child's law (CHILD, 1911) for a space-charge limited diode can be applied to this situation, we have

$$i_+ = \frac{4}{9}\,\epsilon_o\,(\frac{2e}{M})^{1/2}\,\frac{V^{3/2}}{s^2} \qquad (1.2)$$

where V is the voltage across the sheath and s is the sheath width.

Expression (1.1) is independent of voltage if A is constant, so from (1.2) we have:

$$s^2 \alpha V^{3/2} \qquad (1.3)$$

Thus the sheath width depends on the applied voltage, increasing as the applied voltage goes more negative with respect to floating potential. If the voltage on the plate is made more positive than floating potential, the sheath width will decrease and more electron than ion current will be drawn. When the plate is at plasma potential, the sheath and presheath both disappear. Going more positive than plasma potential will push the ion fluid away from the plate and an electron-rich sheath will be formed, the current now consisting solely of electrons. A presheath is not necessary in this case because the electron thermal velocity is high compared to $(kT_i/m)^{1/2}$ (m is the electron mass) which is the appropriate speed for an electron 'Bohm' criterion; thus no pre-acceleration of the electrons is necessary.

We can see from this brief summary that changing the voltage on an electrode will change the nature of the sheath surrounding it. In this thesis we shall be concerned with the motion of a positive ion sheath when time-varying negative voltages are applied to a plane electrode. We shall see that a dynamic version of the Bohm criterion is applicable to the moving sheath.

At this point it is convenient to consider what happens in the plasma when an alternating voltage is applied to an electrode such that at all times the voltage stays below plasma potential. If the time scales involved are greater than the ion plasma period $(2\pi/\omega_{pi}=2\pi\sqrt{[\epsilon_0 M/ne^2]})$ the edge of the positive ion sheath will

alternately move towards and away from the electrode as the applied voltage varies. The application of an alternating voltage to the electrode results in the generation of waves in the plasma; if no magnetic field is present the low frequency mode is the ion acoustic wave. This is a longitudinal quasineutral plasma density disturbance which in the low frequency limit and for cold ions moves at a speed $c_s=(kT_e/M)^{1/2}$ relative to the plasma. It is an ion fluid wave (inertial term M) which relies on thermal electron neutralisation of space charge for its restoring force. The motion of the sheath edge is linked with the generation of plasma compressions and rarefactions, a combination of which gives the complete ion acoustic wave. It is the purpose of this thesis to clarify these processes experimentally and theoretically.

It will be seen that moving a sheath edge away from an electrode is associated with a density rarefaction and moving a sheath edge towards the electrode is associated with a density 'enhancement'. The latter is a compressive feature which will be explained fully in Chapter 2. The rarefaction and enhancement fronts both move at the local ion acoustic speed, that is the speed of ion acoustic waves in the drifting ion fluid. If the electrode is floating before any disturbances are created, the ion fluid streams towards the sheath edge to satisfy the steady-state Bohm criterion. The presence of such an ion velocity gradient in front of the sheath edge is essential to the launching of enhancements.

1.3 THE STRUCTURE OF THE STATIC SHEATH-PLASMA SYSTEM

Much work has been done on the sheath-presheath region, both theoretical and experimental. The main theoretical problem is that the plasma and sheath solutions must be matched (CARUSO and CAVALIERE, 1965). The matching procedure involves a number of mathematical 'transition regions' between the non-neutral sheath and the quasineutral plasma or 'presheath' (LAM, 1965, FRANKLIN and OCKENDON, 1970). Another approach is to solve Poisson's equation as formulated by Tonks and Langmuir numerically, making no artificial separation into plasma and sheath regions (SELF, 1965). Self's results clearly show both sheath and presheath regions for plane geometry, the division between the two being somewhat arbitrary. In common with others, the point at which the plasma solution breaks down is taken to be the sheath edge (e.g. ALLEN, BOYD and REYNOLDS, 1957, which was for spherical geometry).

Other theoretical work has been carried out by a number of authors. HARRISON and THOMPSON (1959) considered the case of a plane symmetric plasma and reformulated the BOHM (1949) criterion to account for a spread of ion velocities at the sheath edge. Their result was

$$M \langle v^{-2} \rangle^{-1} \geqslant kT_e$$

and is now known as the generalized Bohm criterion. For the case of warm ions, EMMERT et al (1980) have shown that electric fields are necessary in the plasma to accelerate ions even when T_i is as high as T_e .

Sheath thicknesses have been measured by a number of authors (e.g. LANGMUIR and MOTT-SMITH, 1924, WIDNER et al., 1972) and were found to be in agreement with the solutions of equations similar to (1.2). Experimental studies of the presheath region are complicated by the fact that any probing electrode will have its own sheath which will perturb the system. Some success has, however, been achieved by VAREY (1970) who measured the presheath with a plane Langmuir probe drawing electron saturation current. An approach which has given convincing results is the use of a perpendicular electron probing beam (GOLDAN, 1970). Deflections of the beam were used to measure the electric field perpendicular to a $5x5cm^2$ plate which was at floating potential in an argon discharge (electron temperature 4eV, pressure 0.8mtorr). The measurements agreed well with SELF's computations for plane geometry.

Theoretical and experimental results thus indicate that ion acceleration in the plasma is a necessity for ion-rich sheath formation.

1.4 THEORY OF MOVING SHEATHS

As we have seen, the application of an alternating voltage to an electrode in a plasma will lead to excursions of the sheath edge from its equilibrium position. We might also expect that movement of the sheath edge will disturb the equilibrium presheath. This process will depend on the timescale of the voltage change. If the timescale is very fast ($\ll \omega_{pi}^{-1}$), the ion fluid will not have time to respond, and will stay approximately stationary; this is known as the ion matrix model (VAREY and SANDER, 1969). If the timescale is very slow ($\gg \omega_{pi}^{-1}$), the ion fluid does have time to move and

dynamic presheath effects will be important. These presheath effects will be discussed in the following subsections. The motion of the sheath edge itself can be approximated by a dynamic version of Child's law (ANDREWS and VAREY, 1971).

1.4.1 Ion Rarefaction Waves With No Initial Presheath

The earliest work on slow timescale sheath motion concerned constant velocity sheath expansion in plane geometry (ALLEN and ANDREWS, 1970). The sheath edge moved away from a plate at a constant subsonic speed; the situation is illustrated in Figure 1.3. There was no ionization term in the equations, and so density and velocity gradients in the plasma were absent.

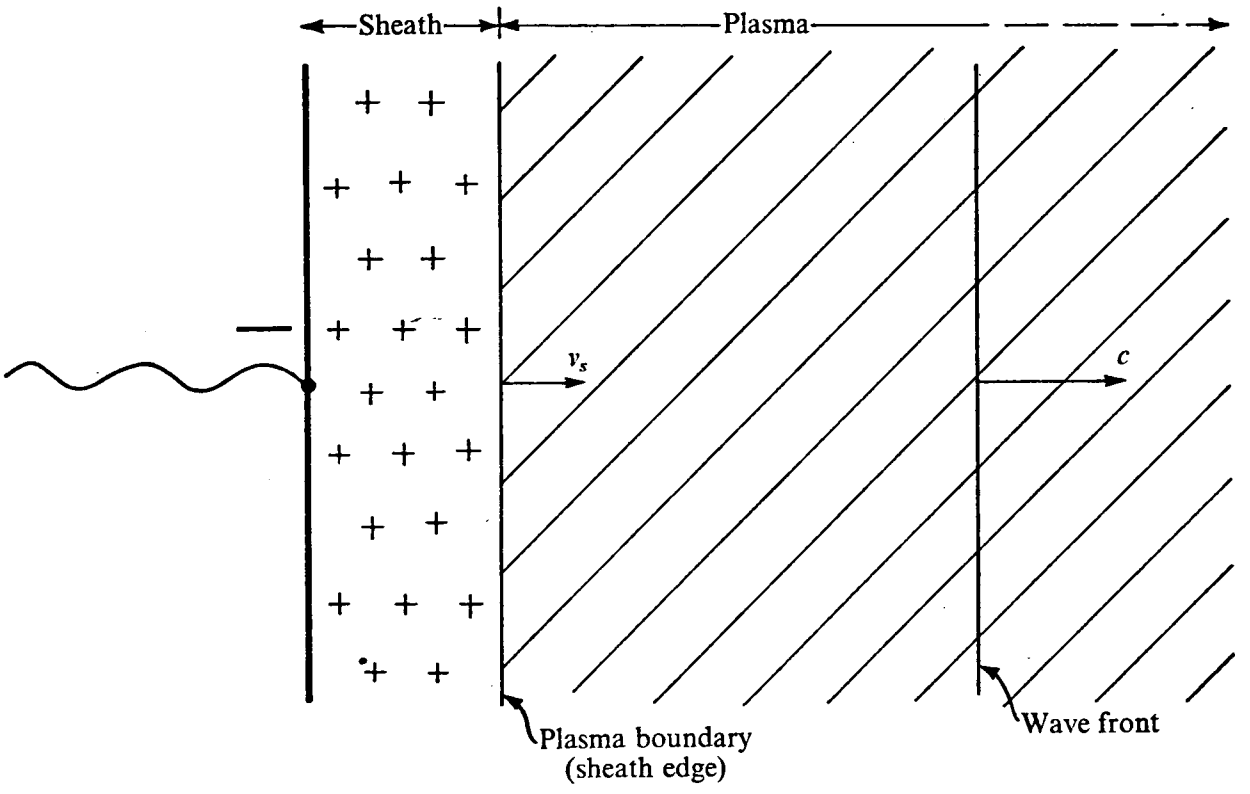


Figure 1.3

Schematic diagram showing the wavefront which moves ahead of a sheath boundary when $v_s < c_s$ (from ALLEN and ANDREWS, 1970).

The ion momentum and continuity equations were:

$$\frac{\partial v}{\partial t} + v\frac{\partial v}{\partial x} = \left(\frac{e}{M}\right)E \qquad (1.4)$$

$$\frac{\partial n}{\partial t} + \frac{\partial}{\partial x}(nv) = 0 \qquad (1.5)$$

The electrons were assumed to be in equilibrium with the applied potential so that

$$n_e = n = n_o \exp\left(\frac{eV}{kT}\right) \qquad (1.6)$$

where T denotes the electron temperature. Cold ions and quasineutrality were assumed. Combining (1.4) and (1.6) gave

$$\frac{\partial v}{\partial t} + v\frac{\partial v}{\partial x} = -\left(\frac{kT}{nM}\right)\frac{\partial n}{\partial x} \qquad (1.7)$$

which was noted to be very similar in form to an equation in fluid dynamics for an isothermal similarity rarefaction wave (LANDAU and LIFSHITZ, 1959). Since there are no characteristic lengths but there are characteristic velocities in (1.5) and (1.7) they were solved in terms of a similarity variable $\xi = \frac{x}{t}$. Solutions are shown in Figure 1.4. A large amplitude density rarefaction was predicted to propagate into the plasma at the ion acoustic speed. Behind the wavefront in the disturbed region the ions were accelerated (from zero velocity since there was no initial presheath) to reach the ion acoustic speed relative to the moving sheath edge. This is the dynamic form of the Bohm criterion, which will be discussed further in Section 1.3.3. The wavefront can be described as a carrier of information concerning the sheath edge motion into the undisturbed plasma. It will be noted that quasineutrality was not predicted to break down at the moving sheath edge (i.e. $\frac{\partial v}{\partial x}$ and $\frac{\partial n}{\partial x}$ did not approach infinity).

The results also applied to the case of sheath collapse at a constant velocity, in which case potential drops greater than $\frac{kT}{e}$ were predicted in the plasma to accelerate the ions to satisfy the dynamic Bohm criterion. A rarefaction wave was generated in this case also.

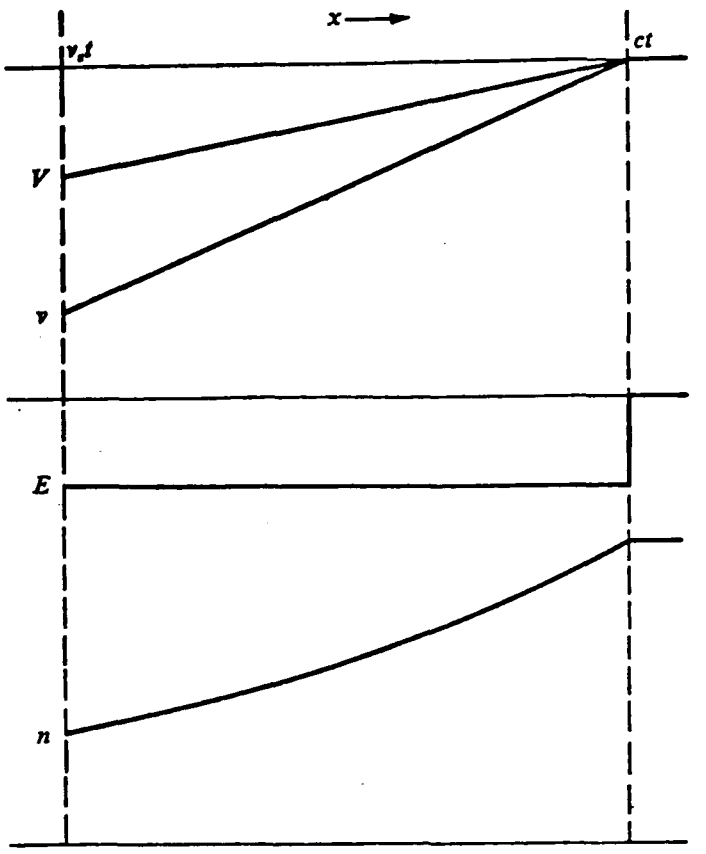


Figure 1.4

The spatial variation of potential, ion velocity, electric field and ion (or electron) density in the rarefaction wave (from ALLEN and ANDREWS, 1970).

Allen and Andrews' similarity variable solution has been extended to the case of cylindrical and spherical geometries (PREWETT and ALLEN, 1973). Again a constant sheath edge speed was assumed. In this case, the dynamic version of the Bohm criterion emerged naturally from the equations so that quasineutrality was predicted to fail at the moving sheath edge. Another difference to the plane geometry calculations was that the electric field in the disturbed region was not discontinuous (in the spherical case).

Another approach that has been adopted to study sheath growth is one involving a time-dependent numerical integration of Poisson's equation (WIDNER et al, 1970). Again there was no presheath before sheath expansion. A step change in the potential on a plane electrode was imposed at t=0, and the plasma response for t>0 was computed. The inclusion of space charge effects (using Poisson's equation) enabled two stages of sheath expansion to be identified:

(i) The rapid formation of a transient sheath (ALEXEFF et al, 1969a) due to electron motion with a stationary ion matrix

(ii) The formation of an ion rarefaction wave which moved into the plasma (similar to ALLEN and ANDREWS, 1970) at later times.

The authors also studied similar sheath expansion in cylindrical and spherical geometries, and in these cases the breakaway of a rarefaction pulse (rather than a monotonic rarefaction region) was predicted. Recently, CIPPOLA and SILEVICH (1981) have presented a similar simulation in which a planar isolated conductor was placed instantaneously into a plasma and the development of the floating sheath was followed. The computations revealed a similar ion rarefaction wave to the previous work. These calculations were then compared with results gained from the method of characteristics.

The method of characteristics is another approach which has been used to study this problem. The essence of the method is that information propagates along characteristic paths (see Chapter 2). This approach was suggested by ANDREWS (1970) who attempted to derive the dynamic Bohm criterion from this point of view. It was also used by PREWETT (1974) and WICKENS (1980) to study the effect of expanding a sheath edge with non-constant velocity. A rarefaction wave was still generated.

1.4.2 Movement Of A Sheath Including Initial Presheath Effects

In practice, the formation of a static sheath on an electrode necessitates an initial presheath. The effects of this will be seen to be vital in any theory of ion acoustic wave generation.

This topic will be covered more fully in Chapter 2. Basically, a bounded plasma model is constructed which includes a production term to balance the wall losses, and the method of characteristics is used to calculate the response of the plasma. Sheath expansion into such a plasma, and the associated rarefaction wave, have been studied by ANDREWS and SHRAPNEL (1972). Sheath collapse was studied

by ANDREWS (1971) and by WICKENS, BRAITHWAITE and COATES (1982); the former utilised an incorrect boundary condition, but both predicted waves of ion enhancement. A dynamic presheath was formed in the case of both expansion and collapse. The inclusion of the initial presheath is essential to the generation of enhancements as well as rarefactions.

1.4.3 The Dynamic Bohm Criterion

This concept, which we have seen emerging from the mathematics, may be understood physically by a transformation into the frame of reference of the moving sheath edge. In this frame, the Bohm criterion holds at the sheath edge, so that

$$v_{iS} \geq |-c_s|$$

where v_{iS} is the ion velocity at the sheath edge in the sheath edge frame of reference (see Figure 1.5). In the laboratory frame of reference

$$v_{iL} \geq |v_S - c_s| \qquad (1.8)$$

where v_{iL} is the ion velocity at the sheath edge in the laboratory frame of reference and v_S is the velocity of the sheath edge in the same frame (see Figure 1.5). The magnitude of v_{iL} is thus less than the laboratory frame ion acoustic speed. For negative values of v_S (i.e. a collapsing sheath), the ions move at a speed $>c_s$ in the laboratory frame at the sheath edge. Depending on initial conditions, dynamic presheath acceleration mechanisms may be necessary to satisfy relation (1.8); one example of this has been discussed in Section 1.4.1.

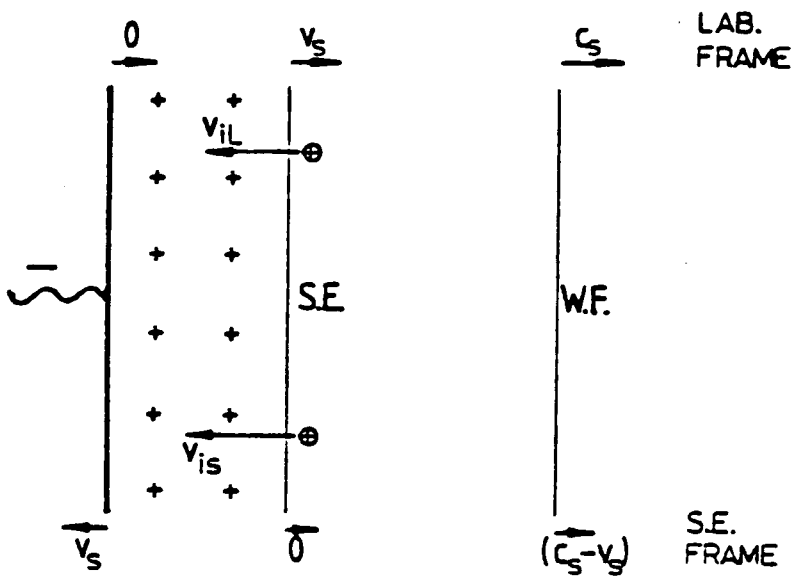


Figure 1.5
Frames of reference for the dynamic Bohm criterion.

1.5 EXPERIMENTS ON MOVING SHEATHS

In contrast to the large body of theory concerned with sheaths which move at speeds less than the ion acoustic speed, the experimental observations of sheath edge motion leading to rarefactive or compressive phenomena are not numerous. The first observation was made by CHESTER (1970), this work preceding the Allen and Andrews theory. The experiments utilised a mercury valve device similar to that used by VAREY and SANDER (1969) in their investigations of sheaths which moved faster than the ion acoustic speed. Chester used a Langmuir probe biassed to detect electron saturation current, and measured the plasma response to a negative-going voltage waveform applied to the planar anode of the valve. The sheath speed, initially supersonic because of the rapidly changing electrode voltage, eventually fell below the ion acoustic speed and an ion rarefaction wave was emitted. The oscillograms clearly showed the arrival of the wavefront and, later, the sheath edge (see Figure 1.6). The velocity of the sheath edge was by no means constant, but was well described by a quasi-static form of Child's law. The density rarefaction results agreed well with a theory which used the method of characteristics in the perturbed plasma region. The wavefront was seen to move at a

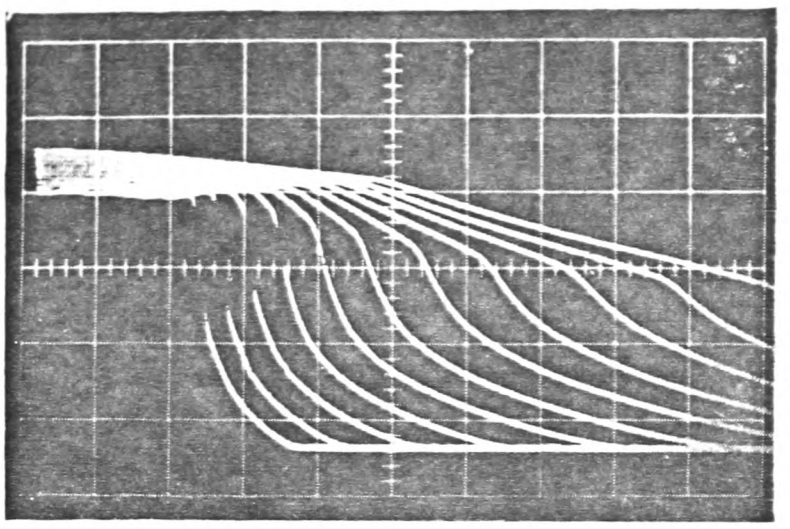


Figure 1.6
Saturation electron current to probe showing the arrival of wavefront and sheath boundary with probe at 0.5mm intervals from 6mm to 11mm from electrode (5μs/cm, from CHESTER, 1970).

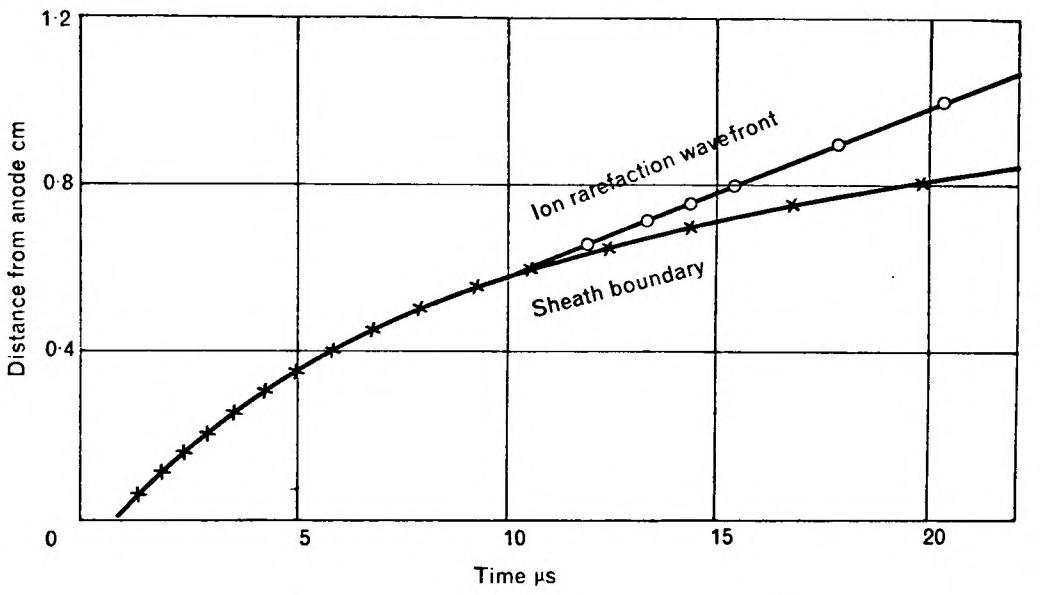


Figure 1.7
Plot of sheath growth against time, showing the breakaway of an ion rarefaction wave (from CHESTER, 1970).

constant speed away from the plate (see Figure 1.7).

The experimental results of WIDNER et al (1970), obtained in an electron-beam generated plasma, showed no evidence of the separation of the sheath edge and the rarefaction front. However the rarefaction front was observed to propagate into the plasma with a speed which was constant at large distances from the plate. The "initial slow-down" which was observed at small distances (Figure 1.8) is thought to be due to detection of the sheath edge prior to the emission of the rarefaction front (c.f. Figure 1.7). The same

paper also presented the results from expanding spherical sheath experiments, but the evidence for the "breakaway" phenomenon observed in their computer simulations was not convincing.

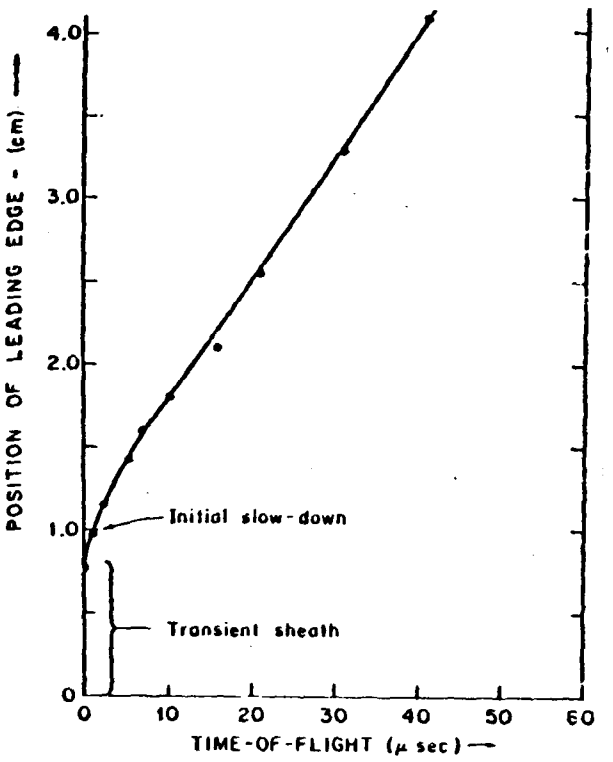


Figure 1.8

Distance-time diagram for leading edge of disturbance near a plane electrode to which a negative step voltage is applied (from WIDNER et al, 1970).

Some experiments have been performed by PREWETT (1974) and WICKENS (1980) in another electron-beam-produced plasma. An exponentially increasing negative voltage was applied to a plate and the fluctuations in saturation current to a nearby probe were studied. They observed a rarefaction front, though the sheath edge was not visible in their results. Similar results were obtained by COATES (1979) in the initial stages of the present work.

CHEN and SCHOTT (1977) have presented results of experiments in cylindrical geometry which support the supposition that the presheath is the origin of ion acoustic waves, though their results do not include measurement of the sheath edge.

Various experiments have been performed for faster-moving sheaths, mainly to check the validity of the ion-matrix model, the quasi-static Child's Law model or a transition between the two (VAREY and SANDER, 1969, HOLMES and YANABU, 1973). Similar experiments have been conducted in a high-pressure plasma (OLIVER et al, 1975); all these were studies of the sheath edge rather than

the plasma wave response.

1.6 EXPANDING PLASMAS

A major extension of the moving sheath theory is to the problem of plasma expansion into vacuum. This is a special case where no electrode is present, and so the plasma is free to expand with no current being drawn.

A quasineutral analysis of this situation necessarily involves non-physical initial conditions. If, for example, the initial condition is $n_e=n_i=n$ for $x<0$ and $n_e=n_i=0$ for $x>0$, all at $t=0$, then the electric field at $x=0$ is infinite, which means that ions will immediately be accelerated to unphysical speeds. A way around this is to include Poisson's equation (CROW, AUER and ALLEN, 1975) so that the mobile electrons "smear out" at $t=0$ to make the problem more physical. Their time-dependent numerical solution showed the formation of an ion front which moved at an increasing speed behind an electron cloud. The ions thus reached very high speeds, and the solution failed when the ion front velocity approached the electron thermal speed (in contrast to some earlier results by WIDNER et al (1971) where a similar ion front moved at a speed limited to $\sim 3c_s$). A rarefaction front moved back into the undisturbed plasma at the ion acoustic speed, similar to that predicted by ALLEN and ANDREWS (op. cit.) for a collapsing sheath. Comparable results were earlier obtained by GUREVICH et al (1966).

The problem with the quasineutral approach can also be avoided by the introduction of a finite scale length for the initial density variation as opposed to a step change in density (FELBER and DECOSTE, 1978). The essential features of the Allen and Andrews

self-similar solution were retained between the rarefaction wavefront and the ion front.

Self-similar calculations for an expanding two-electron temperature plasma have been performed (WICKENS and ALLEN, 1979, BEZZERIDES et al, 1978) and compared with experimental data from laser-produced plasmas (WICKENS, ALLEN and RUMSBY, 1978). The work has also been extended to the case of a multi-ion species plasma (WICKENS and ALLEN, 1981).

1.7 TECHNIQUES FOR LAUNCHING ION ACOUSTIC WAVES

A number of techniques have been used in the past to launch ion acoustic waves. The most well-defined method is to impress a small sinusoidal voltage variation onto the floating potential of a large plate in a plasma. The waves are then very nearly one-dimensional, and if $T_e \gg T_i$ the speed is $(kT_e/M)^{1/2}$. This was first confirmed by the experiments of JONES and ALEXEFF (1965).

A second approach is to use a grid instead of a plate. This procedure has been widely adopted (e.g. WONG et al, 1964) but there is the possibility of ballistic effects occuring (ALEXEFF et al, 1969b). The effect consists of ion bursts which can be confused with ion waves; the speed of the ion bursts depends on the applied potential (from $\frac{1}{2}mv^2=eV$). These "pseudowaves" are absent for the case of plate excitation. For a comparison of plate and grid (or wire) excitation see JOYCE et al (1969). A large grid has been used to generate ion acoustic solitons by WATANABE (1975).

More recently CHEN and SCHOTT (1976) have shown that waves may be excited more efficiently using an insulated probe. This was supposed to be a result of a more efficient coupling of the applied signal to the presheath since the sheath potential drop is less than in the case of a conducting probe at a high negative potential.

A technique which is often used to excite nonlinear ion wave phenomena is to change the potential of one plasma with respect to another in a "double plasma" device (see Chapter 3). IKEZI et al (1973) compared this method with plate excitation. A change of plasma potential with respect to a wall or electrode will also lead to the generation of ion acoustic waves; this was observed by CHRISTENSEN and HERSHKOWITZ (1977) and, independently, by us (see Chapter 4). The mechanism in these two methods involves a movement of sheaths due to a change in the potential of one plasma with respect to the other plasma or the wall.

The simplest technique for launching ion acoustic waves, and the one most amenable to theoretical analysis, is the use of a large plate to which an alternating voltage is applied. This is the method adopted for the purposes of this thesis.

1.8 LAYOUT OF THE THESIS

Chapter 2 introduces the method of characteristics which is then applied to the problem of the motion of one edge of a one-dimensional self-sustained bounded plasma. It is found that both enhancements and rarefactions of plasma density can be generated using such a model, whereas unbounded models without density gradients exclude the formation of enhancements.

Chapter 3 describes the multidipole device in which a quiescent argon plasma is produced for the experiments on sheath edge motion.

Chapter 4 contains results of basic plasma experiments (using Langmuir probes and ion acoustic waves as diagnostics) to determine the properties of the plasma generated in the multidipole device. Important knowledge is gained about the electron velocity distribution and the speed of ion acoustic waves.

In Chapter 5 the results of planar moving sheath experiments are presented. Sheath expansion and sheath collapse are separately investigated so that insight is gained into the generation process of ion rarefaction and enhancement waves.

Chapter 6 is a discussion of the experimental results and a comparison with the theoretical work described in Chapter 2. In the light of the experimental and theoretical results, the mechanism for ion acoustic wave generation from moving sheaths is considered. The Chapter ends with a summary of the work contained in this thesis.

CHAPTER 2

MOVING THE BOUNDARY OF A FINITE PLASMA

2.1 INTRODUCTION

Previous work on moving plasma boundaries was considered in Chapter 1. For a plasma with no initial presheath, slowly expanding and collapsing sheaths both caused ion rarefactions to travel into the plasma. Compressive features, which are necessary for ion acoustic wave generation, were not formed without initial plasma density and ion velocity gradients (i.e. presheaths). In this Chapter we include the effects of a presheath by considering a bounded self-sustained one-dimensional (x) plasma. The boundary of this plasma is moved and the subsequent plasma response ($t>0$) is calculated using the method of characteristics. Information concerning the motion of the plasma boundary propagates along the characteristic paths in (x,t) space into the disturbed region.

The method of characteristics is introduced by writing the fluid equations in characteristic form. A review of the previous applications of this method to the problem of moving sheath edges using similar equations is then given. The first step is to find the steady-state ($t\leq 0$) bounded plasma solution. Any disturbance of the plasma boundary at $t=0$ forms a wavefront which moves into the

undisturbed plasma, and its trajectory is calculated. The wavefront forms a boundary between the disturbed and the undisturbed regions. The plasma response for $t>0$ is computed for a plasma boundary which moves either away from or into undisturbed plasma; the former process is shown to result in plasma density enhancements and the latter in rarefactions. The use of the term "enhancement" will be discussed in Section 2.6.2. Care is taken over the boundary conditions applied at the sheath edge. Plasma boundaries which accelerate smoothly from rest are considered, and in addition the case of a constant velocity sheath collapse is discussed.

An interesting feature of the model used here is that the sheath edge itself cannot in general coincide with a characteristic path, and it is shown that this leads to a breakdown of quasineutrality at the moving sheath edge on application of the dynamic Bohm criterion. The final Section is a summary of the theoretical results.

2.2 THE FLUID EQUATIONS IN CHARACTERISTIC FORM

The one dimensional continuity and momentum equations for the ions may be written as follows:

$$\frac{\partial n}{\partial t} + \frac{\partial}{\partial x}(nv) = \lambda n \qquad (2.1)$$

$$\frac{\partial v}{\partial t} + v\frac{\partial v}{\partial x} = -(\frac{e}{M})\frac{\partial \rho}{\partial x} \qquad (2.2)$$

where n is the ion density, v is the ion velocity, ρ is the potential and λ is the ionization rate. The ions have been assumed cold and monoenergetic. The lack of a collision term in (2.2) will be discussed in the next section.

The electrons are assumed to be in equilibrium with the applied potential

$$n_e = n_o \exp(\frac{e\rho}{kT}) \qquad (2.3)$$

where T is the electron temperature. In addition, quasineutrality is assumed so that:

$$n_e = n \qquad (2.4)$$

The first step is to combine (2.1), (2.3) and (2.4) so that (2.1) becomes

$$(\frac{e}{kT})\frac{\partial \rho}{\partial t} + \frac{\partial v}{\partial x} + v(\frac{e}{kT})\frac{\partial \rho}{\partial x} = \lambda$$

This equation and (2.2) may now be normalized, giving

$$\frac{\partial \eta}{\partial \tau} + \frac{\partial u}{\partial X} + u\frac{\partial \eta}{\partial X} = \frac{L\lambda}{c} \qquad (2.5)$$

$$\frac{\partial u}{\partial \tau} + u\frac{\partial u}{\partial X} + \frac{\partial \eta}{\partial X} = 0 \qquad (2.6)$$

where $\eta=\frac{e\rho}{kT}$, $u=\frac{v}{c}$, $\tau=\frac{ct}{L}$, $X=\frac{x}{L}$, c is the ion acoustic speed $(\frac{kT}{M})^{1/2}$ and L is a scale length. The problem will be set up such that L is half the width of the bounded plasma at t=0 (see Figure 2.1).

Now equations (2.5) and (2.6) may be added and subtracted to give

$$\left[\frac{\partial}{\partial \tau} + (u + 1)\frac{\partial}{\partial X} \right] (u + \eta) = \frac{L\lambda}{c} \qquad (2.7)$$

$$\left[\frac{\partial}{\partial \tau} + (u - 1)\frac{\partial}{\partial X} \right] (u - \eta) = -\frac{L\lambda}{c} \qquad (2.8)$$

It should be noted that (u + 1) is the <u>local</u> speed of sound (u is a function of distance and time) for waves travelling in the

downstream direction (in the positive u direction), and (u - 1) is the local speed of sound for waves travelling in the upstream direction (in the negative u direction). The quantities in the square brackets in equations (2.7) and (2.8) are thus directional derivatives along wave (or information) propagation paths. These paths are called '<u>characteristic lines</u>' and differ from streamlines for which the velocity in the directional derivative would be u. Following the usual convention, we call the downstream path the f characteristic and the upstream path the g characteristic. These lines form a mesh of curves in the (X,τ) plane. Equations (2.7) and (2.8) are of the following form:

$$\left(\frac{d}{d\tau}\right)_f J_f = +A \qquad (2.9)$$

$$\left(\frac{d}{d\tau}\right)_g J_g = -A \qquad (2.10)$$

where $\frac{d}{d\tau}$ denotes a directional derivative, subscripts f and g refer to the f and g directions defined above, $J_f=(u+\eta)$, $J_g=(u-\eta)$, and A is $\frac{L\lambda}{c}$. The original fluid equations are now said to be in characteristic form.

The slopes of the characteristics may be written as the velocities appearing in the appropriate directional derivatives:

$$\left(\frac{dX}{d\tau}\right)_f = u + 1 \qquad (2.11)$$

$$\left(\frac{dX}{d\tau}\right)_g = u - 1 \qquad (2.12)$$

Integration of these equations would give the characteristic paths $X_{g,f}(\tau)$ if $u(X,\tau)$ were known. With no initial conditions only general equations may be written. When A is non-zero, as in this case, the characteristic paths found from these equations will be curved.

Equations (2.9) and (2.10) may be integrated along characteristic lines as follows:

$$u + \eta = \frac{L\lambda}{c}\tau + C_f \qquad (2.13)$$

$$u - \eta = -\frac{L\lambda}{c}\tau + C_g \qquad (2.14)$$

where C_f and C_g, the constants of integration, are the "Riemann invariants" along the f and g characteristics. This is a quantitative expression of the concept that information propagates along the characteristics. A particular f or g characteristic is uniquely defined by its Riemann invariant; thus by selecting a range of discrete values for C_f and C_g (subject to boundary conditions) an arbitrarily fine mesh of characteristics can be defined. At an intersection point in the mesh between an f and a g characteristic we may combine (2.13) and (2.14) to give

$$u = \frac{1}{2}(C_f + C_g) \qquad (2.15)$$

$$\eta = \frac{L\lambda}{c}\tau + \frac{1}{2}(C_f - C_g) \qquad (2.16)$$

Thus if C_f and C_g are known at a point in the disturbed region we may find u; if τ is known in addition we may find η. This gives n from equation (2.3) so that all variables are then known.

We have now set up the framework for this technique which allows us to solve the nonlinear fluid equations by simply writing them in a different form. Examples of the use of the method of characteristics will be considered in the following Sections.

2.3 PREVIOUS APPLICATIONS OF CHARACTERISTICS TO MOVING SHEATHS

In plasma experiments, sheath edge motion is effected by applying a varying voltage to an electrode. Depending on the applied waveform the sheath edge velocity may be directed either into or away from undisturbed plasma at a speed which is generally not constant. The method of characteristics allows us to solve the fluid equations for various initial conditions and sheath edge speeds in order to model experimental results. The limitation of the particular similarity technique discussed in Section 1.4.1 is that only constant sheath edge velocities may be considered because of the structure of the equations. A similar limitation is found in the piston problem of fluid mechanics (LANDAU and LIFSHITZ, 1959).

The method of characteristics has been adopted in previous studies of sheath edge motion, as was indicated in Chapter 1. Comparable equations to those in Section 2.2 were used, and we shall now discuss this work in more detail to highlight the differences in our calculations. We shall consider previous work which both excludes and includes an initial presheath. The latter approach is more physical since any electrode which in the steady state supports an ion-rich sheath will necessarily have an associated presheath.

For a semi-infinite plasma with no ionization (no static presheath), there has been interest in the expanding sheath case. PREWETT (1974) considered a sheath edge which moved into a plasma while decelerating from sonic speed at t=0. The f characteristic paths were all straight lines, corresponding to a "simple wave". This occured as a result of the term A in equations (2.9) and (2.10) being zero. Because of the initial conditions used, C_g was also zero, with the result that u and η were equal. The f

characteristics corresponded to lines of constant u. An ion rarefaction wavefront was predicted to move into the plasma at the ion acoustic speed which is constant in the absence of a presheath. A similar approach was used by WICKENS (1980), although the sheath edge speed was never sonic. A "centred" wave region (Section 2.9) was necessary in this case to accomodate a discontinuity in u at t=0, but in other respects the results resembled those of Prewett since an ion rarefaction wave was again formed. Both calculations imposed the dynamic Bohm criterion (Section 1.3.2). The application of this criterion was checked by CIPPOLA and SILEVICH (1981) who found a numerical solution (including the effects of space charge so that the dynamic Bohm criterion was unnecessary) for the evolution of a floating sheath on an isolated conductor immersed in a plasma. An ion rarefaction wave was again predicted moving into the plasma at constant speed. These results were compared with a solution of the same problem which used the method of characteristics and it was found that application of the dynamic Bohm criterion was accurate to about 12%. It was deduced that neglect of space charge, combined with the use of the dynamic Bohm criterion, was a reasonable approach to this problem.

A different initial condition is the inclusion of initial ion motion before the sheath edge is moved (ANDREWS, 1971). The initial plasma solution, including production and loss of ions to give profiles of density and ion velocity in the plasma, was found from the fluid equations presented in Section 2.2. The solution represented a one-dimensional bounded plasma as used in our work. The method of characteristics was used to study the plasma solution for a collapsing sheath. A wavefront, which was itself an f characteristic, was predicted to move into the plasma at a speed

which increased with distance across the plasma column. This speed was the "local" ion acoustic speed in the unperturbed, drifting plasma. All of the f characteristics were curved as a consequence of the ionization term (see Section 2.2). Unfortunately, ANDREWS' solution for the disturbed plasma region was incorrect because he assumed that the static sheath (Bohm) criterion held at the sheath edge, as opposed to a dynamic version (Section 1.3.2). The sheath edge velocity did not enter the calculations, and as a consequence of this the plasma approximation did not break down at the moving sheath edge.

An alternative steady-state plasma solution was studied by ANDREWS and SHRAPNEL (1972) who included a frictional term due to ionizing and other momentum transfer collisions in the momentum equation (2.2) of the form $-(\lambda + \nu)v$. This made the numerical procedure more difficult, since the term A in (2.9) and (2.10) depended on u. The response of this bounded plasma to an expanding sheath was computed using the dynamic Bohm criterion. A rarefaction wave was predicted to propagate into the plasma, and damping due to collisions was observed in the results. The equations were more physical than those in Section 2.2, although our simpler momentum equation has been shown to give fairly accurate results (BERTOTTI, CAVALIERE and GIUPPONI, 1966).

The case of an undisturbed plasma where there is a gradient of ion drift speed is an important one which is relevant to the experiments to be described in Chapter 5. In the rest of this Chapter we present some calculations which have been carried out using the method of characteristics to solve the equations in Section 2.2. Particular attention will be paid to the boundary

condition at the sheath edge. Sheath collapse and sheath expansion will both be considered. Some of the collapsing sheath results have been discussed by WICKENS, BRAITHWAITE and COATES (1982).

2.4 THE STEADY-STATE SOLUTION

In this Section we shall find the steady-state solution of equations (2.5) and (2.6) following ANDREWS (1971) and also define the initial conditions to be used here. We shall find a bounded plasma solution of half-width L using the equations of Section 2.2. The initial conditions are shown in Figure 2.1; the plasma is symmetrical about x/L=1. The ions reach the Bohm (sonic) speed at x/L=0 and 2, where the plasma approximation fails.

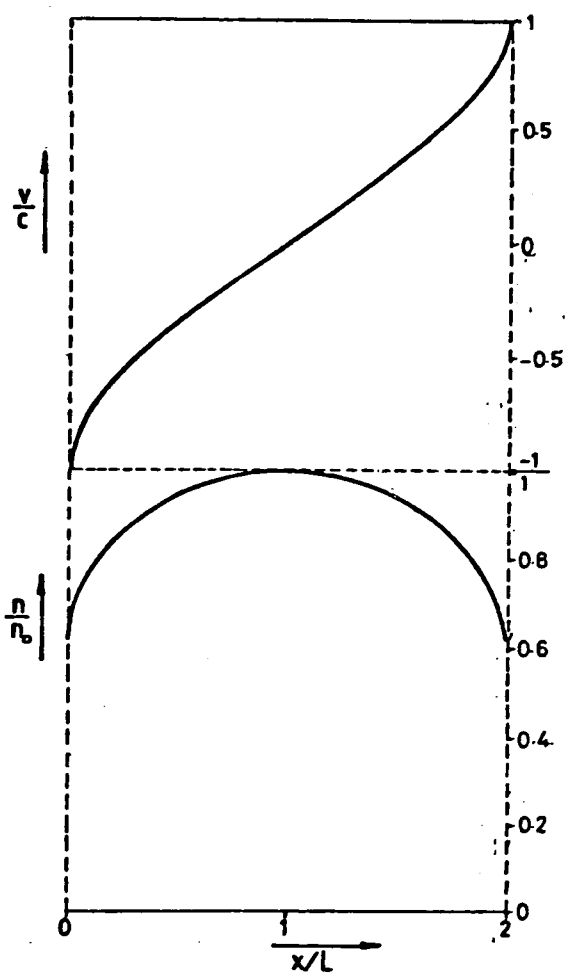


Figure 2.1

The steady state profiles of ion velocity and density from (2.20) and (2.22).

Setting $\frac{\partial}{\partial \tau}=0$ in equations (2.5) and (2.6) gives:

$$(1 - u^2)\frac{du}{dX} = \frac{L\lambda}{c} \qquad (2.17)$$

Integrating (2.17),

$$\frac{2}{3} + u - \frac{1}{3}u^3 = \frac{L\lambda}{c} X \qquad (2.18)$$

using the initial condition that u=-1 at X=0 (see Figure 2.1). Also, u=0 at X=1, which gives:

$$\lambda = \frac{2c}{3L} \qquad (2.19)$$

This value for λ is substituted into equations (2.5)-(2.18) so that A in (2.9) and (2.10) is $\frac{2}{3}$. The cubic equation (2.18) has the following solution for u (only one of the three real roots fits the boundary conditions):

$$u = 2\cos[(\cos^{-1}(1 - X) + 4\pi)/3] \qquad (2.20)$$

Setting η=0 at X=1 and integrating the time-independent version of (2.6) gives

$$\eta = -\frac{1}{2} u^2 \qquad (2.21)$$

from which the steady-state density profile is found:

$$n/n_o = \exp(\eta) = \exp(-\frac{1}{2} u^2) \qquad (2.22)$$

The results of (2.20) and (2.22) are plotted in Figure 2.1. The solution represents an analytic bounded positive column solution of half-width L. The Figure illustrates the initial density profile before sheath edge motion. A gradient of ion drift speed exists, the velocity being sonic at X=0 and X=2 to satisfy the steady-state Bohm criterion. Note also that at these positions the plasma approximation breaks down because $\frac{\partial n}{\partial X}$ (i.e. $\frac{\partial \eta}{\partial X}$) and also $\frac{\partial u}{\partial X}$ are infinite. The problem to be considered here is the plasma response to the motion of the plasma boundary at X=0, that at X=2 remaining fixed.

2.5 THE WAVEFRONT AND BOUNDARY CONDITIONS

If the plasma boundary at X=0 is moved, an unsteady flow will develop for $\tau>0$. The boundary between steady and unsteady flow has a particular distance-time relationship, and is called the wavefront. It travels at the local ion acoustic speed and is itself an f characteristic. The undisturbed plasma is given by the steady-state solution found in the previous Section.

For the wavefront we may obtain an analytic solution as follows. Using the value of λ from (2.19), equation (2.13) becomes

$$u + \eta = \frac{2}{3}\tau + C_f \qquad (2.23)$$

Let us consider an f characteristic originating from $(X,\tau)=(0,0)$. At $\tau=0$, we may write $u_o=-1$ (using the static Bohm criterion) and $\eta_o=\frac{1}{2}$ from equation (2.21). From (2.23), we may find the value of C_f for an f characteristic passing through $(X,\tau)=(0,0)$ as

$$C_{fo} = -\frac{3}{2} \qquad (2.24)$$

Substituting this into equation (2.23) gives:

$$u_w + \eta_w = \frac{2}{3}\tau - \frac{3}{2} \qquad (2.25)$$

where the subscript w refers to the wavefront. Now using equation (2.21) we may rearrange to give

$$u_w = 1 - 2(1 - \frac{\tau}{3})^{1/2} \qquad (2.26)$$

This is the time dependence of the ion velocity along the wavefront. When $\tau=3$, $u_w=1$ so the wavefront has reached the far side of the initial plasma column.

From (2.11) the velocity of the wavefront is:

$$\left(\frac{dX}{d\tau}\right)_w = 2\left[1 - \left(1 - \frac{\tau}{3}\right)^{1/2}\right] \qquad (2.27)$$

and we may integrate this equation to find the wavefront position as a function of time, giving

$$X_w = 4\left[\frac{1}{2}\tau + \left(1 - \frac{\tau}{3}\right)^{3/2} - 1\right] \qquad (2.28)$$

This equation is also the solution of

$$\left(\frac{dX}{d\tau}\right)_w = u(X) + 1$$

where u(X) is the initial velocity profile given by equation (2.20). The solution is plotted in Figure 2.2. Equation (2.28) describes the path of the wavefront produced by any disturbance at X and τ=0, and it represents propagation at the local ion acoustic speed in the undisturbed plasma. The wavefront is a weak discontinuity between the two regions.

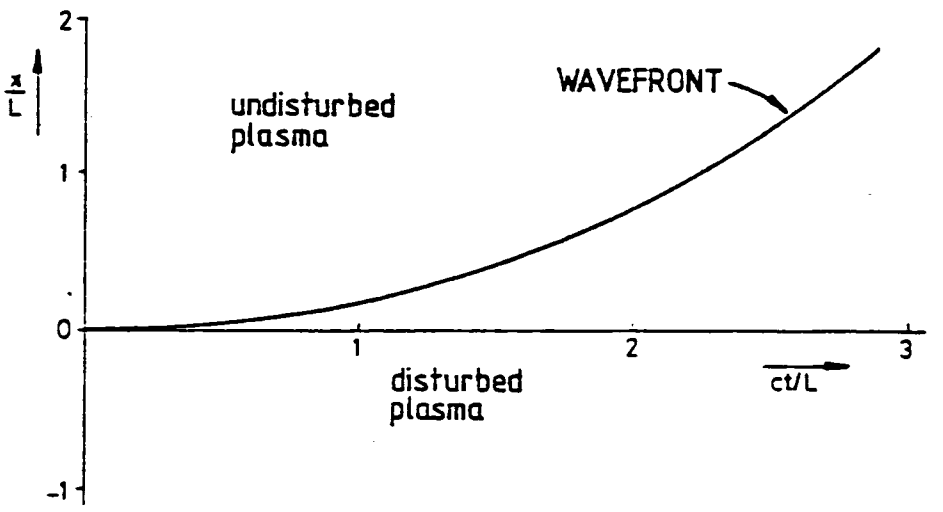


Figure 2.2
Distance-time diagram for the wavefront from (2.28).

We now consider the sheath edge. At this position, the ions have been accelerated from the steady-state speed at the wavefront (u_w) to cross the moving sheath edge.

To find the ion speed at this position we now impose the dynamic Bohm criterion (1.8), which may be written (using the equality sign) in the form

$$(\frac{dX}{d\tau})_s = u_s + 1 \qquad (2.29)$$

Comparing with (2.11), this equation shows that the f characteristics leave the sheath edge tangentially. This does not mean that the sheath edge itself is a characteristic, because any $X_s(\tau)$ relationship may be chosen as a boundary condition and C_f will not be conserved along an arbitrary line. The f characteristics, which affect the flow at later times, are launched from the sheath edge. It will be shown more rigorously in Section 2.10 that the sheath edge itself cannot in general coincide with a characteristic.

Equation (2.29) emphasizes the difference between this work and that of ANDREWS (1971) who used

$$0 = u_s + 1 \qquad (2.30)$$

which is the static form of the Bohm criterion. In our work the sheath edge velocity enters the calculations in (2.29) whereas no sheath edge velocity is present in Andrews' work except as a cut-off point for the solution.

To summarize this Section, the boundary conditions we shall apply are as follows:

(1) imposed sheath edge velocity $(\frac{dX}{d\tau})_s$; arbitrary function of time

(2) imposed dynamic Bohm criterion (equation 2.29)

In addition, the wavefront solution given by equations (2.24)-(2.28)

has been established.

2.6 PLASMA SOLUTION FOR AN ACCELERATING COLLAPSING SHEATH

We now present a particular application of the above theoretical framework to the case of a collapsing sheath.

2.6.1 Method

The sheath edge velocity boundary condition we shall use is

$$\left(\frac{dX}{d\tau}\right)_s = -0.2\tau \qquad (2.31)$$

As $\tau \to 0$, $\left(\frac{dX}{d\tau}\right)_s \to 0$ so that the sheath edge accelerates smoothly from rest. There is thus no discontinuity of u at $\tau=0$ (c.f. Section 2.9). The situation is illustrated in Figure 2.3 where the wavefront, the sheath edge and some f and g characteristics are shown schematically. The wavefront launches g characteristics while f characteristics are launched from the sheath edge. Every point in the disturbed region between the wavefront and the sheath edge is associated with an intersection between two particular f and g characteristics. There are some such intersection points on the sheath edge itself.

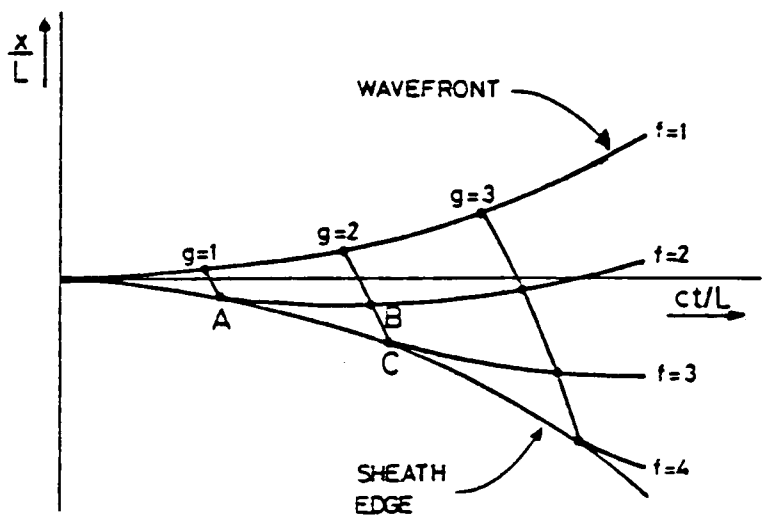


Figure 2.3
Schematic diagram of the mesh of f and g characteristics. The wavefront represents the first f characteristic; information propagates along the characteristics with increasing time.

The computational method may be described as follows. The values of all variables are known on the wavefront, so computations are started there. Equal time steps along the wavefront are taken. The value of C_g is calculated at the first time step from (2.14). The path of the first g characteristic is followed from the wavefront until it reaches the sheath edge at the point A (Figure 2.3). This path is calculated from equation (2.12). At the sheath edge, u is known from (2.29) and so C_f is found from equation (2.15). The values of all other variables may then be calculated. The next time step along the wavefront is then taken and the process is repeated. The second g characteristic intersects the previously found f characteristic at the point B, and using equations (2.11) and (2.12) the (X,τ) coordinates of B are found. All variables are then calculated, and the g characteristic is then followed to intersect the sheath edge at the point C. The next time step at the wavefront is then taken and the procedure is repeated. The computational method is summarized in the form of a flowchart (Figure 2.4).

A mesh of f and g characteristics is built up in the disturbed region between the wavefront and the sheath edge. The wavefront solution contains the initial conditions of the undisturbed plasma. The imposed boundary conditions, which are applied at the sheath edge, affect the whole solution.

2.6.2 RESULTS

At each intersection point, values of all disturbed parameters were stored. A time step of $\delta\tau=.025$ was used (see Section 2.8). The mesh was effectively tied to the disturbed flow rather than to

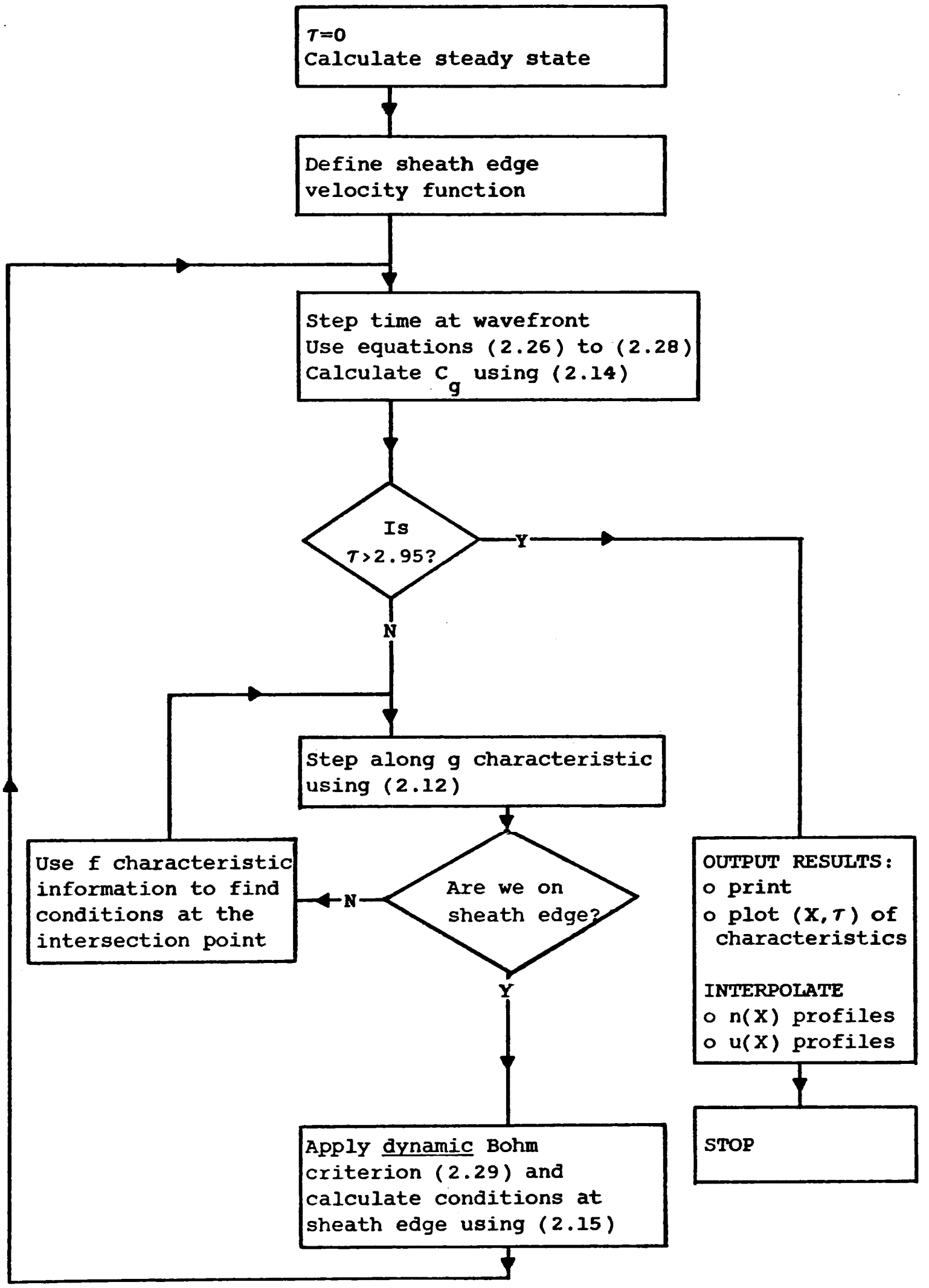


Figure 2.4
Flowchart for the computations.

constant X or τ values, so that different methods of examining results were available:

(i) Values of all the variables ($X, \tau, u, \eta, n/n_o$) were printed for each intersection point in the disturbed region.

(ii) The (X, τ) values of the intersection points were plotted and the characteristic lines were drawn.

(iii) Interpolation of the variables was performed for constant values of τ to obtain profiles of velocity and density with τ as a parameter. These were then drawn.

Results for the imposed sheath edge velocity in equation (2.31) are plotted in Figure 2.5 which is a computed distance-time diagram for the characteristics. The f characteristics leave the sheath edge tangentially, carrying information about the sheath edge motion into the plasma. The g characteristics carry information from the undisturbed plasma into the disturbed region with increasing time. The values of C_f start at -1.5 on the wavefront and become more negative with increasing f; the C_g values start at -0.5 when τ=0 (equation 2.14) and become more positive with increasing g.

Ion number density profiles with time as a parameter are shown in Figure 2.6. The steady-state density profile is shown at τ=0, and disturbed plasma profiles at time intervals of $\Delta\tau$=0.4 are plotted. The sheath edge moves with increasing speed into the plasma, and a point of particular interest is that behind the wavefront the perturbed plasma density becomes progressively larger than the unperturbed plasma density. The disturbance may thus be described as an ion enhancement wave. The word "enhancement" is used here in preference to "compression" since ionization

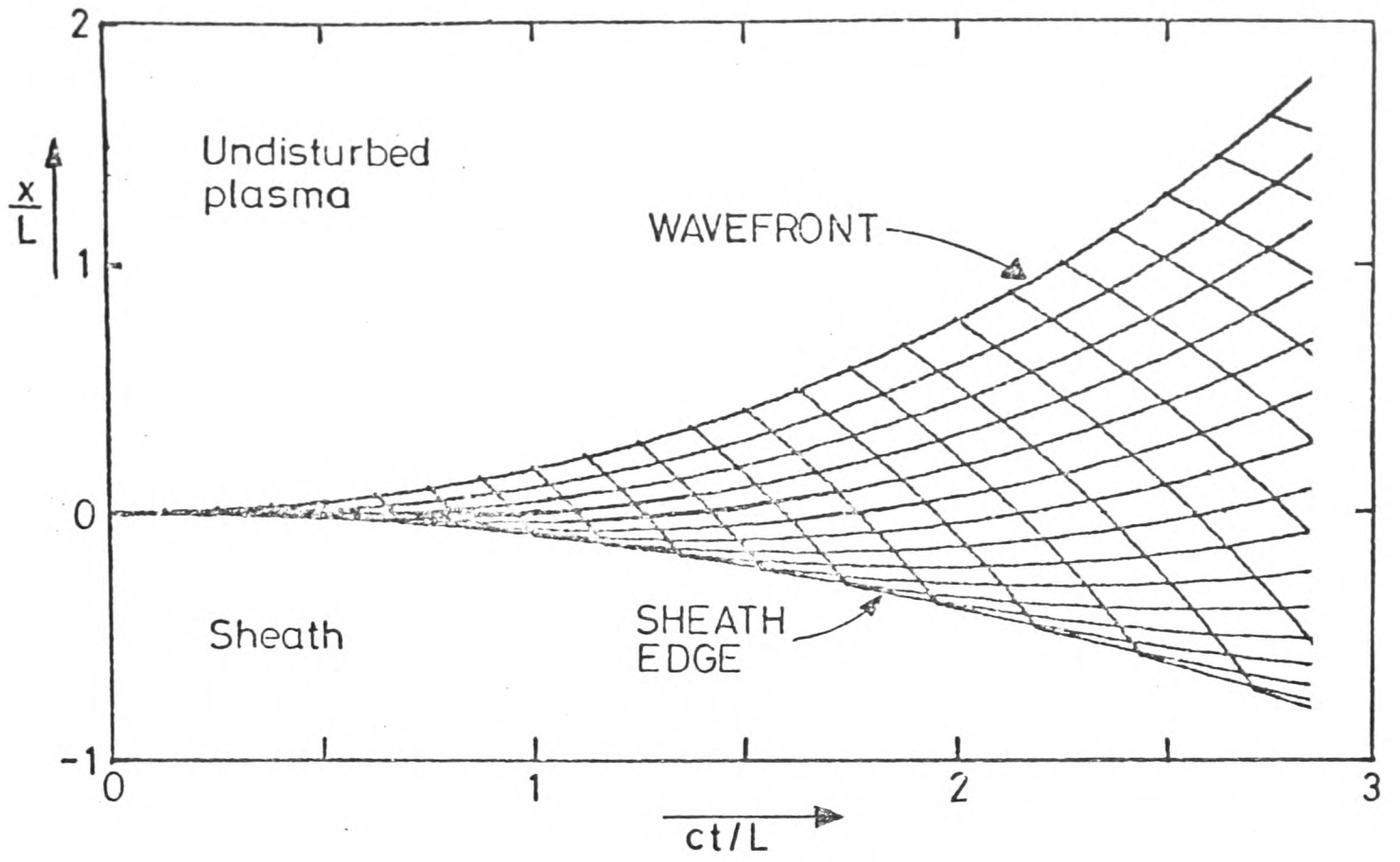


Figure 2.5
Some characteristic paths calculated for a collapsing sheath ($v_{sh}=-0.2c\tau$).

continually introduces new particles into the system to increase the perturbed density over its steady-state value. Another interesting feature in these results is that, at the moving sheath edge, the gradient of density $\frac{\partial n}{\partial X}$ (and hence of $\frac{\partial \eta}{\partial X}$) approaches infinity. This is similar to the unperturbed case ($\tau=0$) at the points where the plasma solution breaks down. Such behaviour will be discussed in Section 2.11.

The corresponding profiles of ion velocity with time as the parameter are shown in Figure 2.7. Ions are accelerated in the plasma to satisfy the imposed dynamic Bohm criterion at the moving sheath edge. The speeds of ions in the plasma are in places higher than the ion acoustic speed (i.e. $|u| > 1$). The gradient of ion velocity $\frac{\partial u}{\partial X}$ approaches infinity at the moving sheath edge.

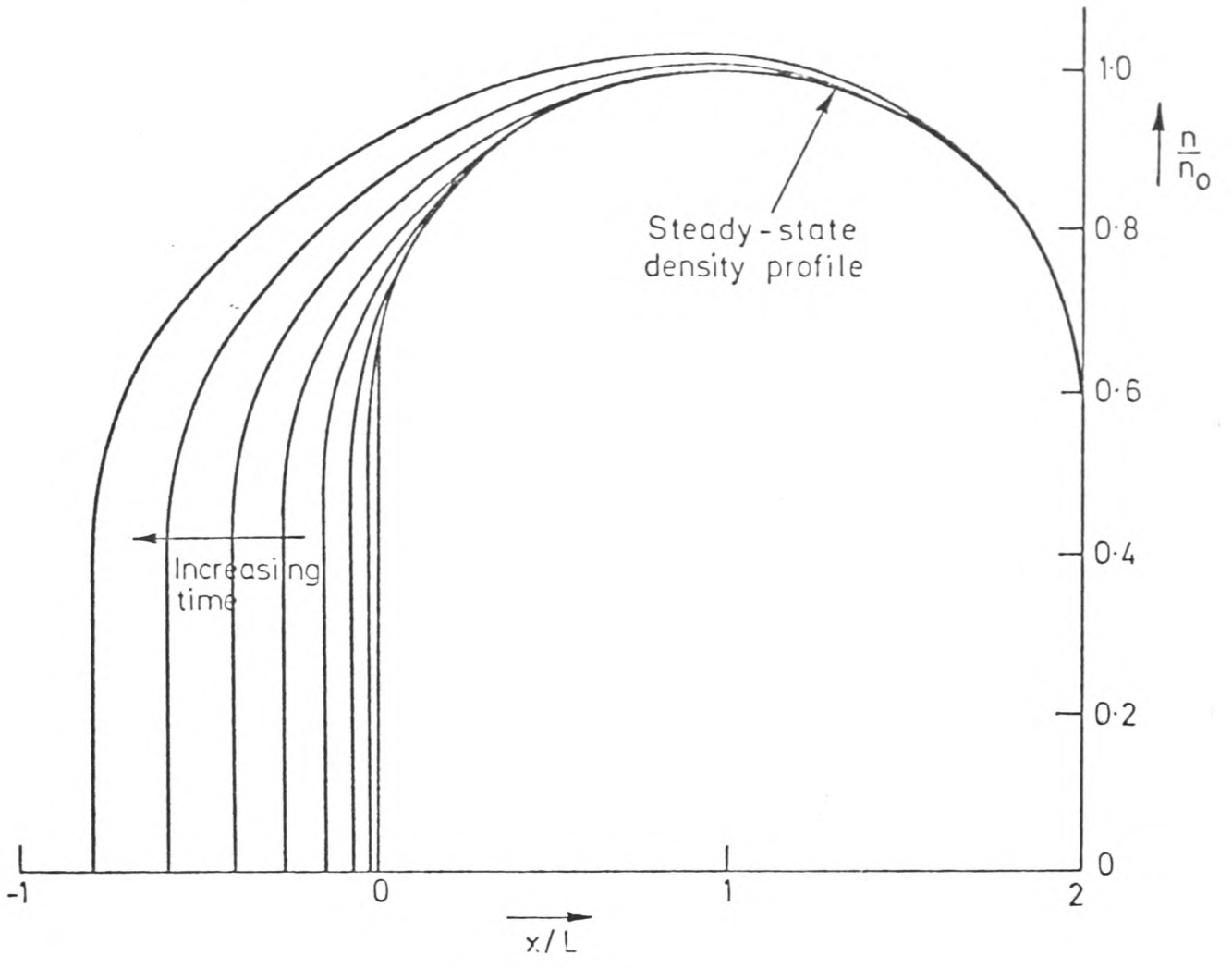


Figure 2.6

Ion number density profiles at successive times ($\Delta\tau$=0.4) for a collapsing sheath (v_{sh}=−0.2cτ).

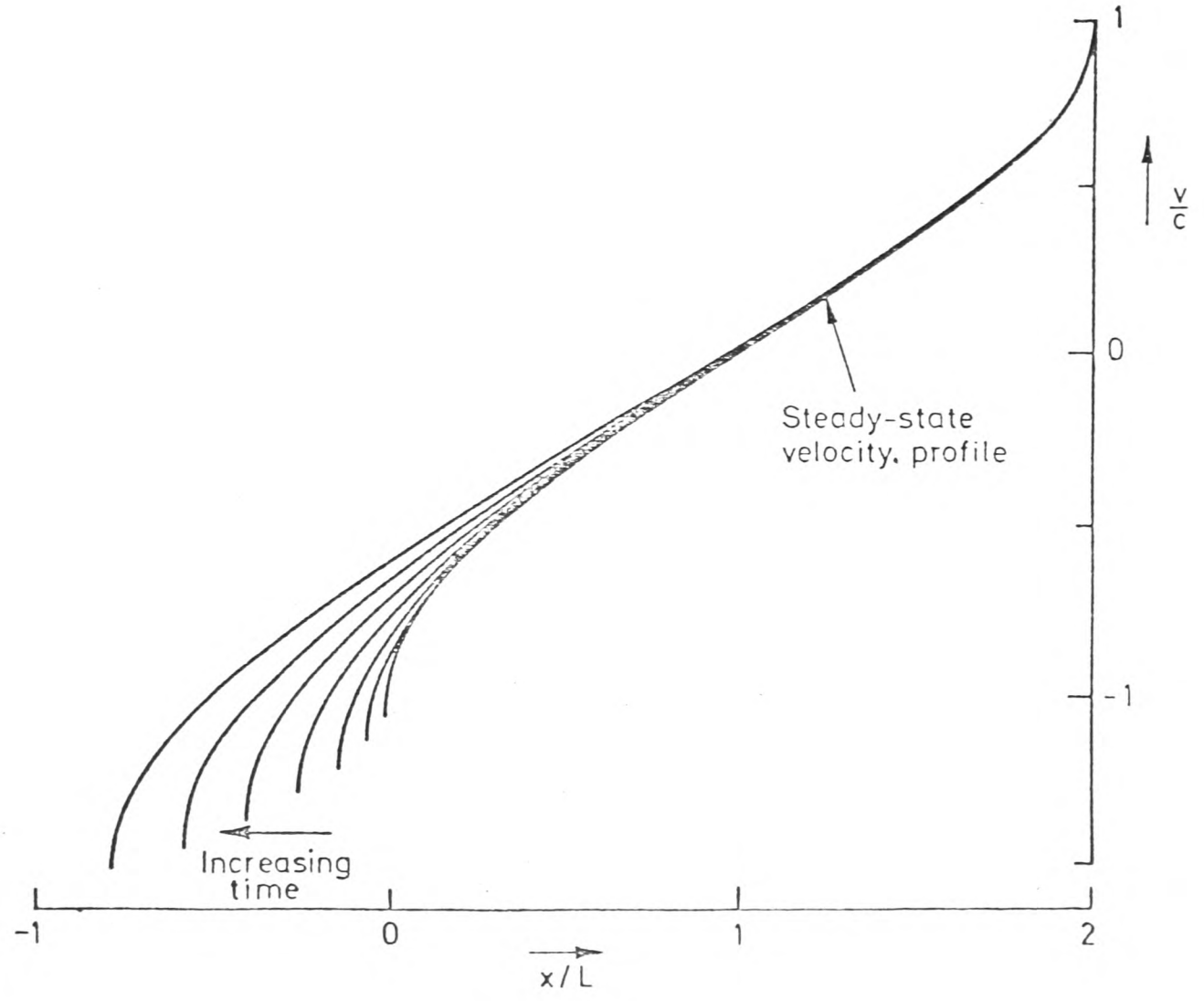


Figure 2.7

Ion velocity profiles at successive times ($\Delta\tau$=0.4) for collapsing sheath (v_{sh}=−0.2cτ).

2.7 PLASMA SOLUTION FOR AN ACCELERATING EXPANDING SHEATH

Another application of the theory is now given for a different sheath edge velocity boundary condition.

2.7.1 Method

The sheath edge velocity to be used here is:

$$\left(\frac{dX}{d\tau}\right)_s = +0.2\tau \qquad (2.32)$$

This represents a movement of the sheath edge into the plasma at a speed which increases smoothly from rest (i.e. an expanding sheath). A computational procedure similar to that for the collapsing sheath case (Section 2.6) was employed. The sheath edge now moves such that its position X is always greater than zero. The form of the imposed speed (2.32) means that the sheath edge does not cross the wavefront solution (see Figure 2.8) since its speed is less than the local ion acoustic speed. In addition, though the sheath edge accelerates, no f characteristics cross it.

2.7.2 Results

The computed distance-time diagram is shown in Figure 2.8. Again the f characteristics leave the sheath edge tangentially.

Figure 2.9 illustrates the density profiles with time as a parameter. A wavefront moves into the plasma, and the sheath edge moves in the same direction at a slower speed. Behind the wavefront, the density decreases compared with its initial value, corresponding to a rarefaction wave. Again, the density gradient approaches infinity at the moving sheath edge, corresponding to a

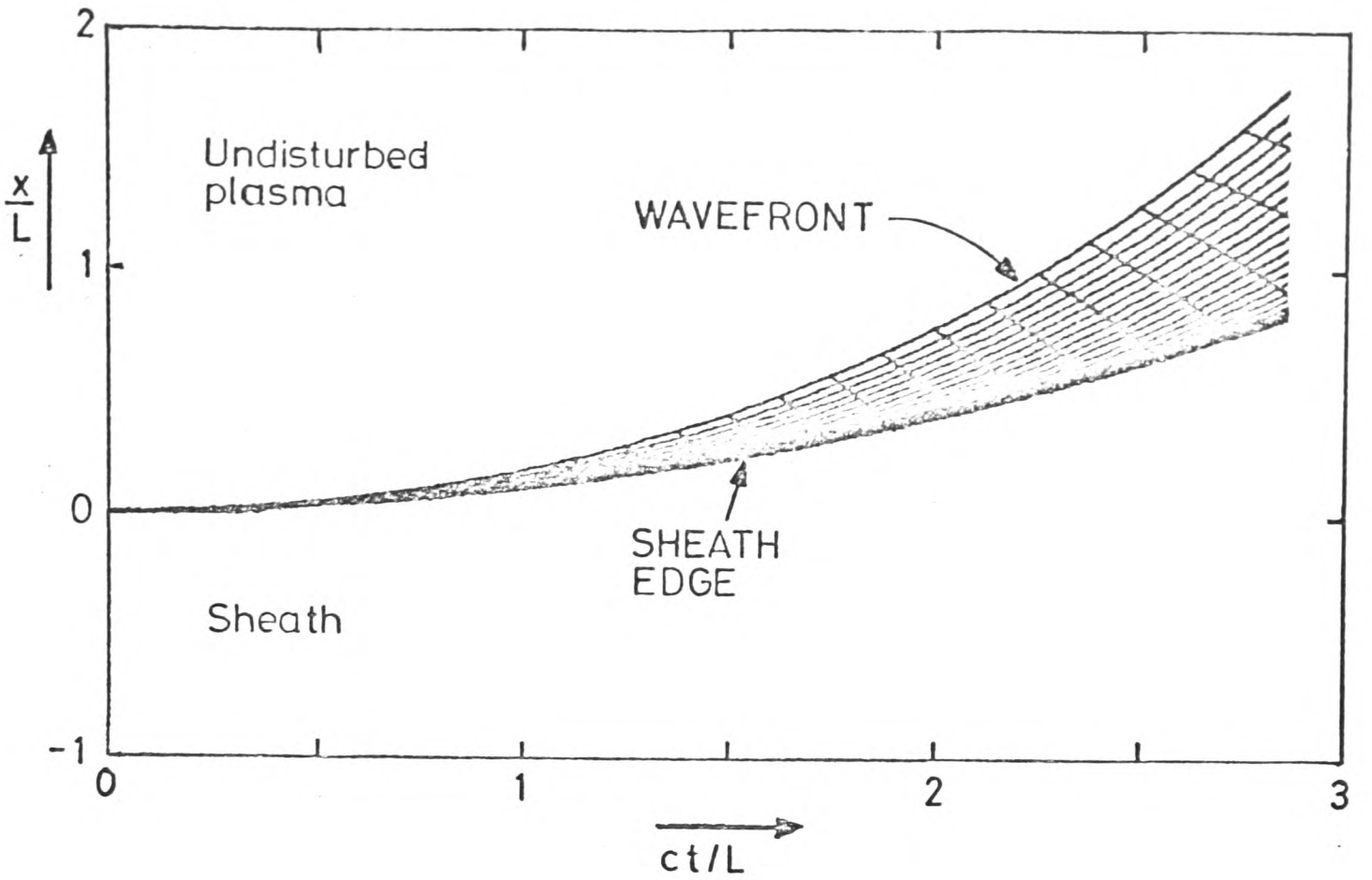


Figure 2.8

Some characteristic paths calculated for an expanding sheath (v_{sh}=+0.2cτ).

breakdown of the plasma solution (see Section 2.11).

For the same sheath edge speed, velocity profiles are plotted in Figure 2.10. The speeds of ions at the perturbed sheath edge are higher than their steady-state values at particular positions. The ions have been accelerated above their steady-state speeds at all points in the perturbed plasma to satisfy equation (2.29), the dynamic Bohm criterion.

2.8 NUMERICAL CHECKS

Two numerical checks were employed:

(i) The step length was increased by a factor 2; no significant differences appeared in the results, though they did begin to appear if the step length was increased by a factor 4.

(ii) The numerical method was checked by imposing the sheath edge boundary condition used by ANDREWS (1971) and making a comparison with his results, which were for a step length of

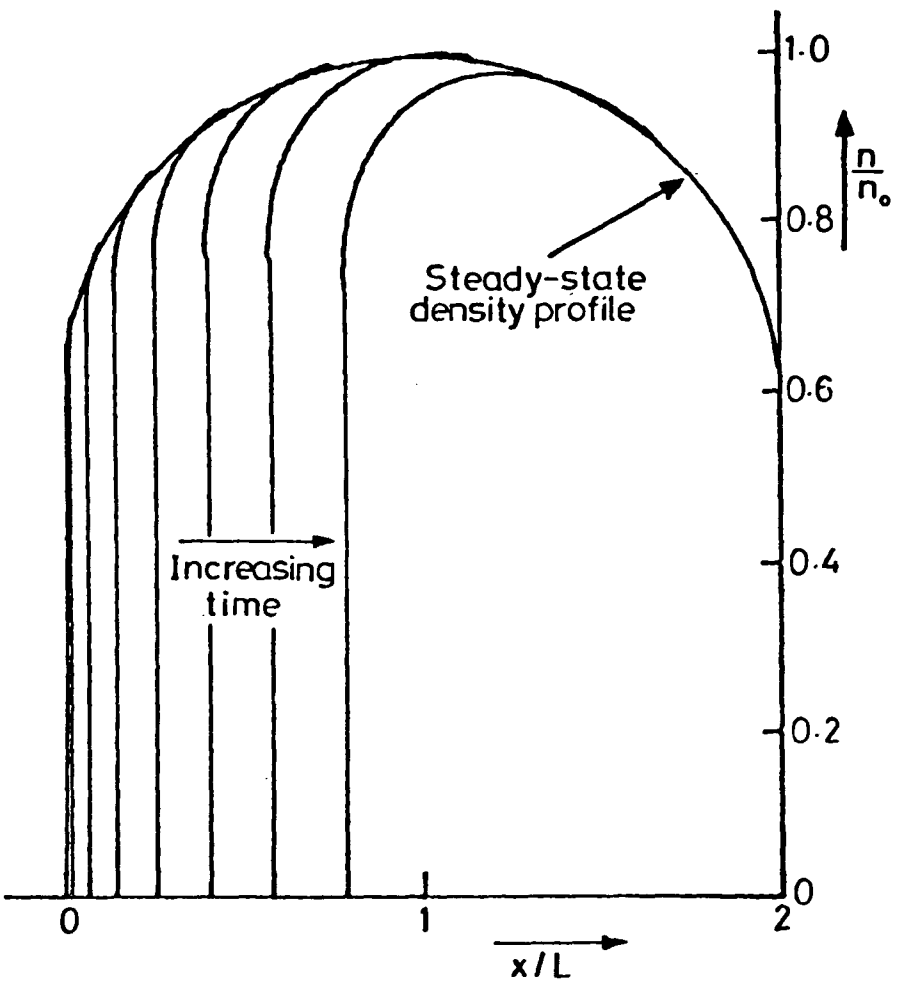


Figure 2.9

Ion number density profiles at successive times ($\Delta\tau$=0.4) for an expanding sheath (v_{sh}=+0.2cτ).

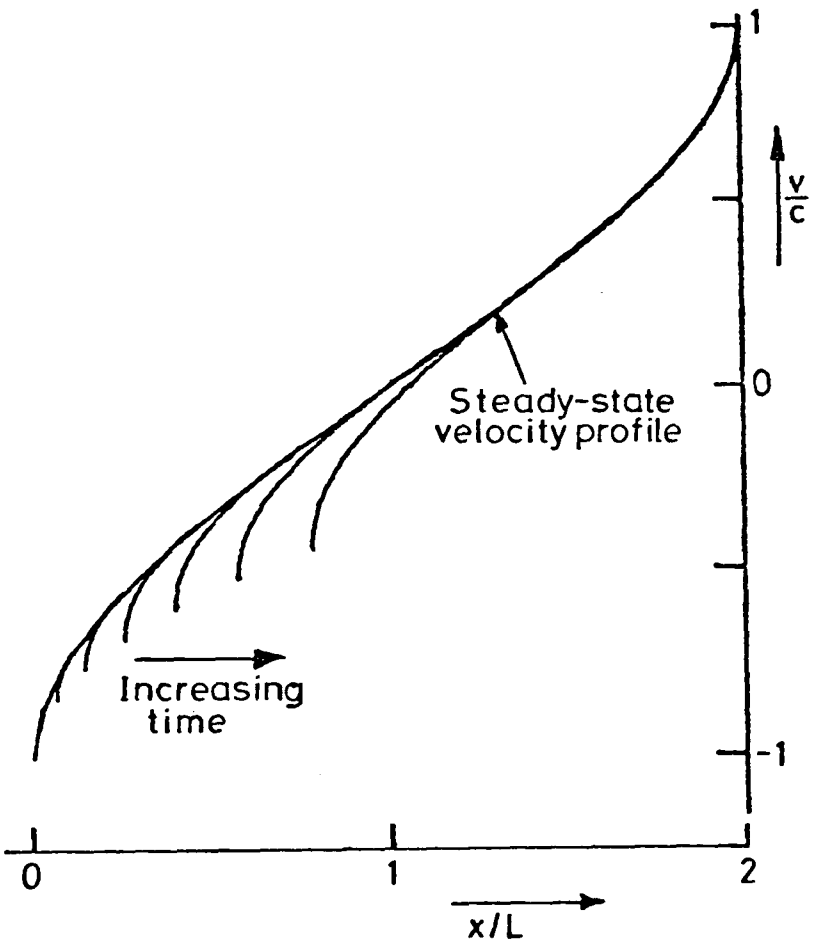


Figure 2.10

Ion velocity profiles at successive times ($\Delta\tau$=0.4) for an expanding sheath (v_{sh}=+0.2cτ).

$\delta\tau_w$=.01. Andrews' results were reproduced satisfactorily (see Figures 2.16 and 2.17).

2.9 PLASMA SOLUTION FOR CONSTANT VELOCITY SHEATH COLLAPSE

In the two examples studied above, the sheath edge accelerated smoothly from rest at the origin (curves A and B in Figure 2.11). The wavefront, which is an f characteristic, also accelerates smoothly from rest at (0,0) and is tangential to the curves A and B there. In this Section we consider sheath collapse at a constant velocity (line C in Figure 2.11). This imposed velocity function involves a discontinuity in $(\frac{dX}{d\tau})_s$, which is zero for $\tau \leq 0$ and finite for $\tau > 0$ (see Figure 2.11). From the dynamic Bohm criterion (equation 2.29), f characteristics must leave the sheath edge tangentially and thus a slightly different numerical technique is required for this case.

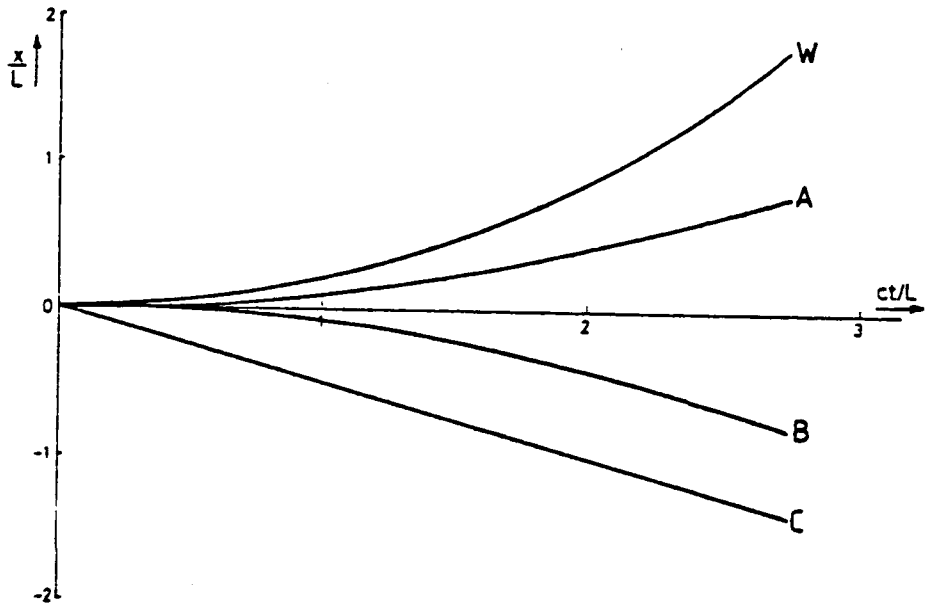


Figure 2.11
Distance-time diagram for the wavefront (W) and the sheath edge motions studied in this chapter (A, B and C). W is tangential to A and B, but not to C, at $\tau = 0$.

2.9.1 Method

The solution for the wavefront is still valid since it represents the fastest possible propagation velocity of ion acoustic waves in the undisturbed plasma. It is also an f characteristic since it separates the perturbed and unperturbed regions. Consider

that f characteristic which is a tangent to the sheath edge at the origin. This curve will differ from that which represents the wavefront. Between this "boundary" characteristic and the wavefront, both of which originate at (0,0), the intermediate f characteristics will also be "centred" at the origin. The boundary characteristic separates the centred region from the "normal" region where all characteristics are tangential to the sheath edge in a similar manner to the above calculations (see Figure 2.12).

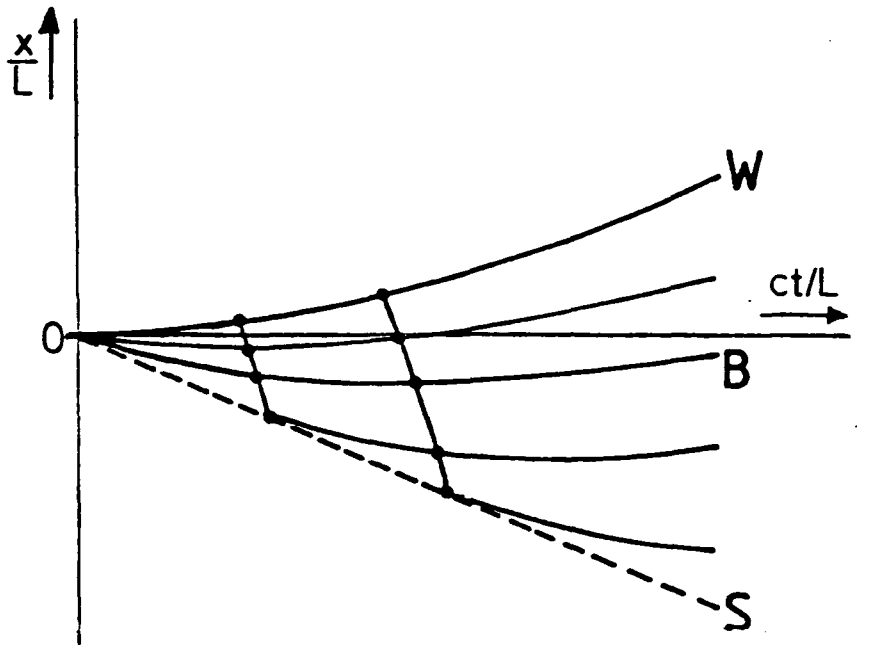


Figure 2.12
Schematic diagram showing the method of solution for constant velocity sheath collapse (S). The region between the wavefront (W) and the boundary characteristic (B) contains characteristics centred at the origin.

The computational method is as follows. An arbitrary number of centred f characteristics are fitted between the wavefront and the boundary characteristic. The latter is found from consideration of the discontinuity in u at the first time step which is a result of the step change in $(\frac{dX}{d\tau})_s$ at the origin. The centred region is now solved, using equations (2.11) and (2.12), and the values of all perturbed quantities are calculated. The boundary characteristic, where the values of all variables are now known, is used in the same manner as was the wavefront in the previous calculations for the remainder of the solution. In this normal region the f characteristics are launched from the sheath edge (see Figure 2.12).

2.9.2 Results

Results from these calculations are shown in Figure 2.13, which illustrates the characteristic mesh computed using a sheath edge velocity given by

$$\left(\frac{dX}{d\tau}\right)_s = -0.5 \qquad (2.33)$$

The centred characteristics originating from (0,0) are shown. In the non-centred region f lines are launched from the sheath edge as above.

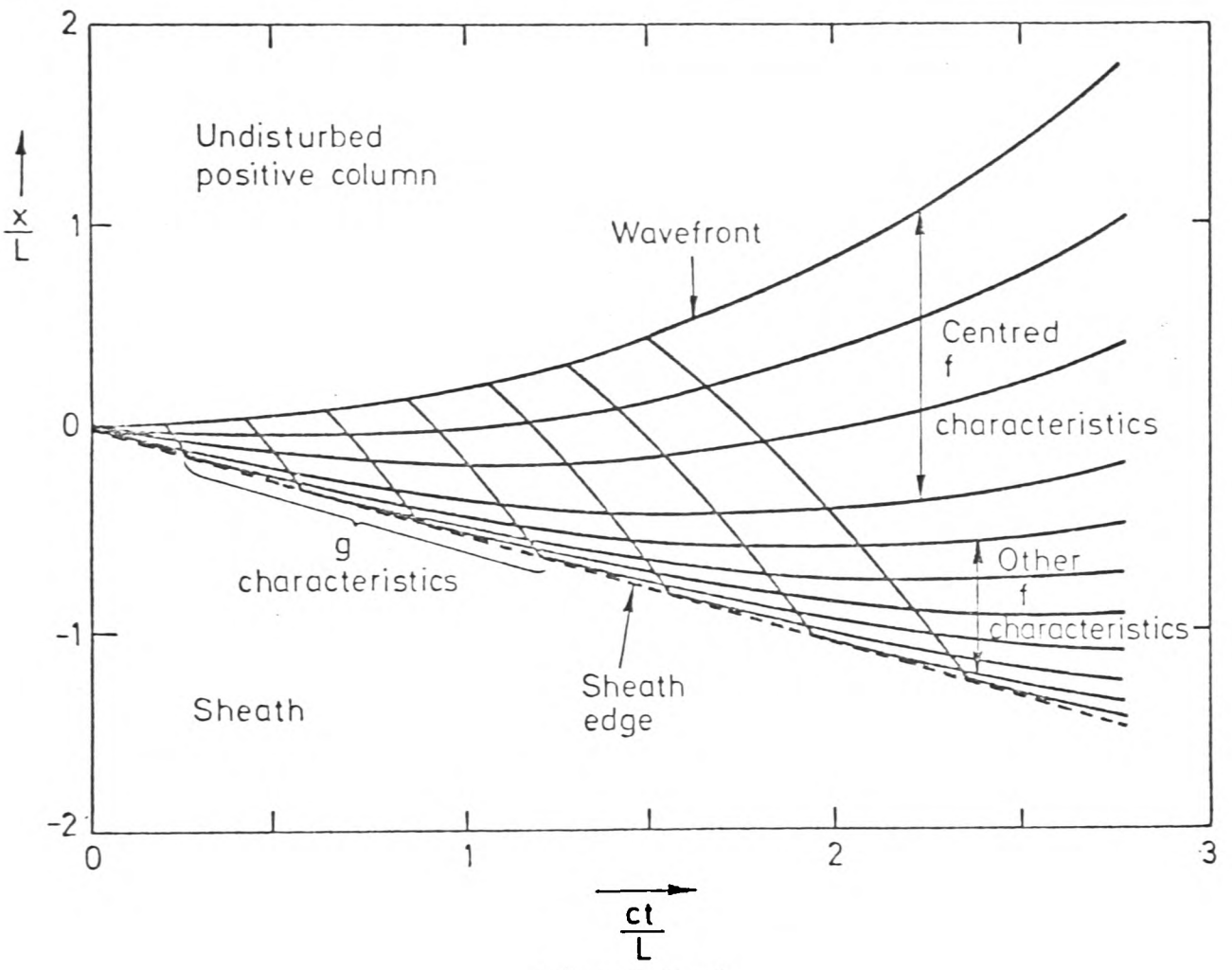


Figure 2.13

Some characteristic paths calculated for constant velocity sheath collapse (v_{sh}=-0.5c).

The density and velocity profiles are calculated in much the same way as before and are shown in Figures 2.14 and 2.15. The density profiles show a similar behaviour to the collapsing sheath results illustrated in Figure 2.6. An ion enhancement front again propagates into the plasma at the local ion acoustic speed. The velocity profiles show that the ions are accelerated to reach a constant speed at the sheath edge to satisfy equation (2.29).

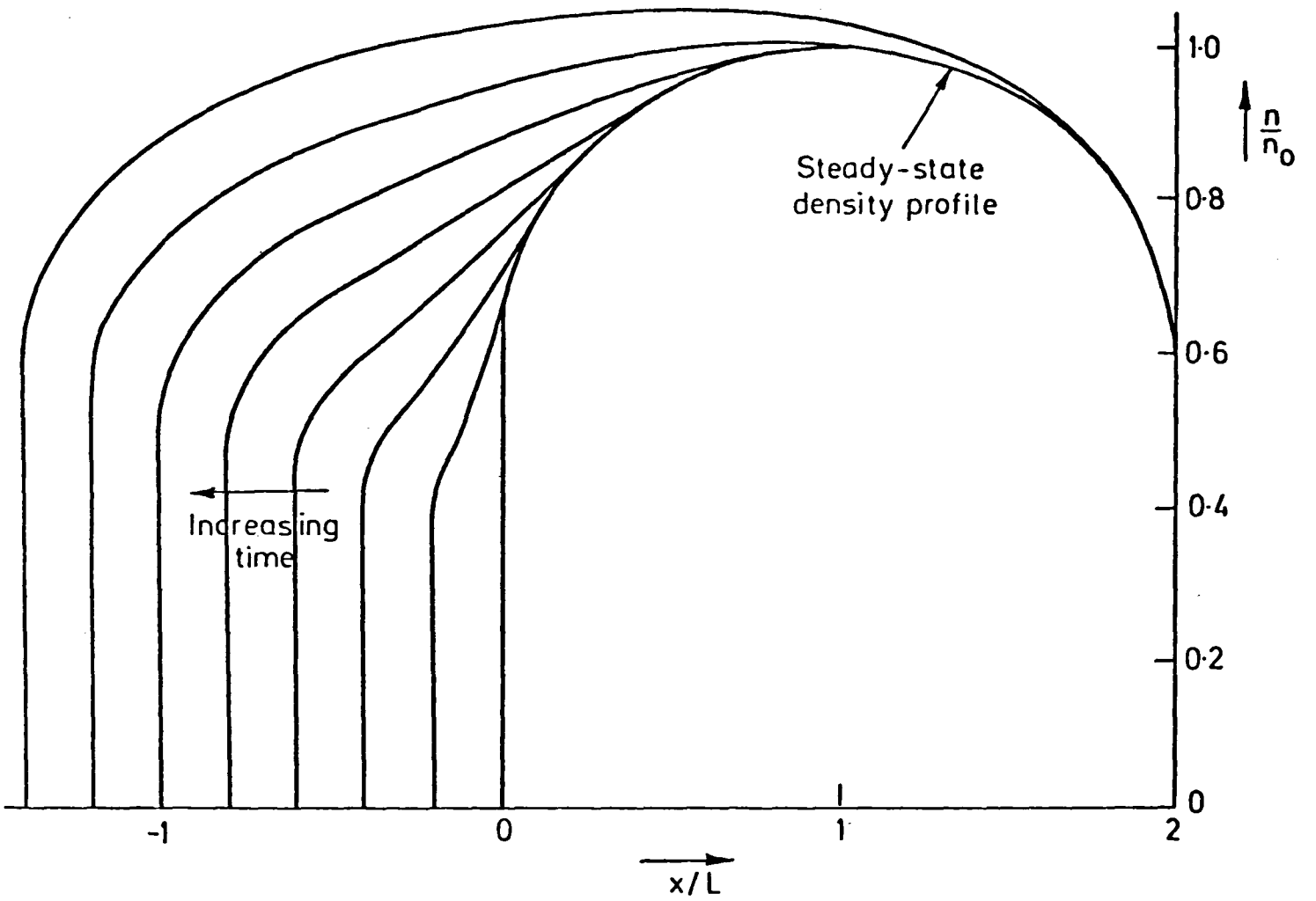


Figure 2.14

Ion number density profiles at successive times ($\Delta\tau$=0.4) for constant velocity sheath collapse (v_{sh}=-0.5c).

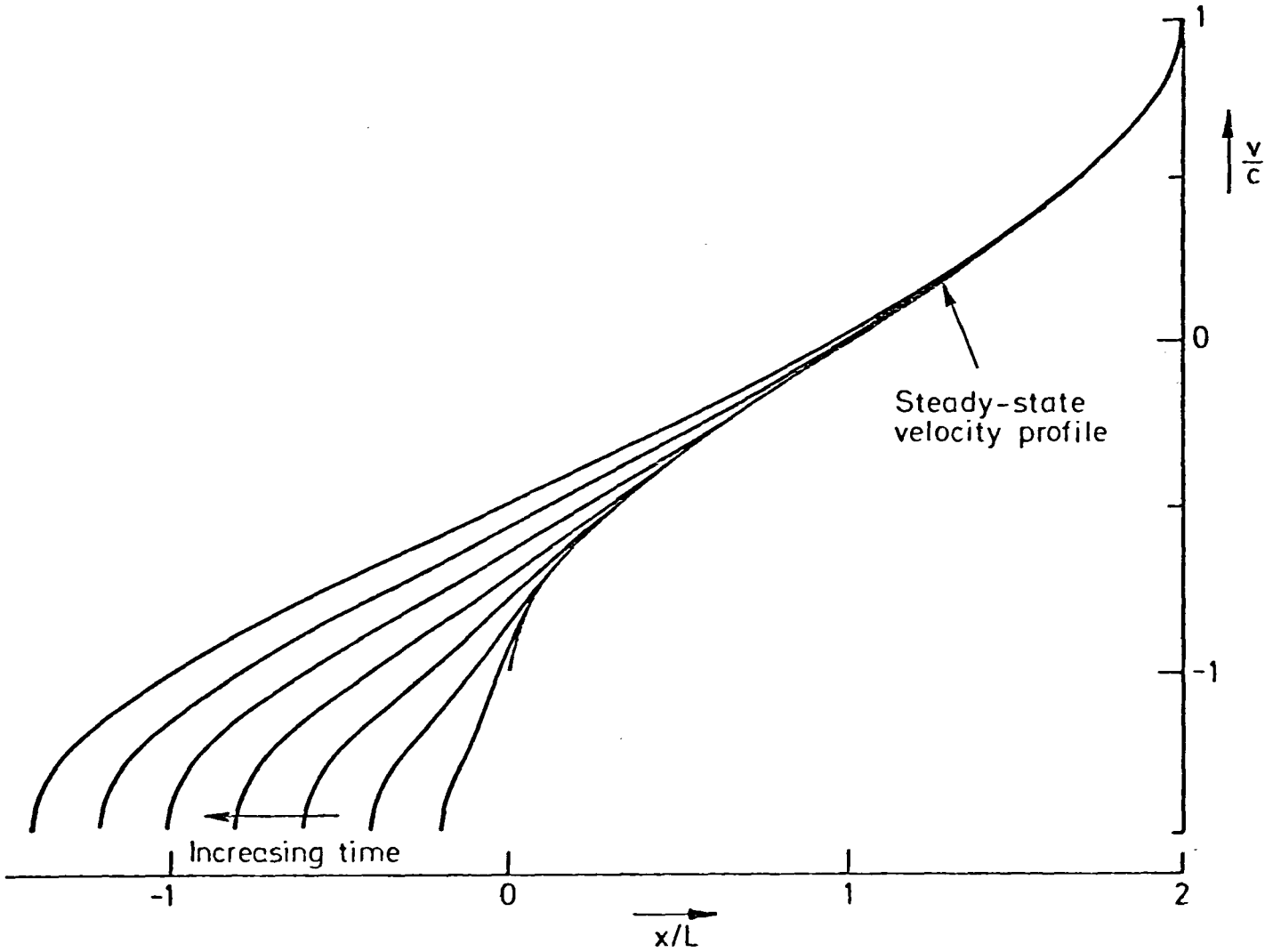


Figure 2.15

Ion velocity profiles at successive times ($\Delta\tau$=0.4) for constant velocity sheath collapse (v_{sh}=-0.5c).

For comparison, results obtained using the boundary conditions of ANDREWS (1971) are shown in Figures 2.16 and 2.17. These were calculated for the same sheath edge velocity function as our results. Though the steady-state and wavefront solutions are identical, the disturbed plasma solutions are not. This is a result of the different sheath edge boundary conditions applied. Our results are more physical because $\frac{\partial n}{\partial x}$ and $\frac{\partial u}{\partial x}$ are singular at the moving sheath edge. The results of ANDREWS and SHRAPNEL (1972) exhibited similar behaviour although this was not discussed.

2.10 PROOF THAT THE SHEATH EDGE IS NOT GENERALLY A CHARACTERISTIC

To show this, assume first that the sheath edge does coincide with a characteristic.

Consider the wavefront: this is an f characteristic, therefore C_f is a constant along it. Now u at the wavefront depends on τ from (2.26). Also we have relation (2.15):

$$u = \frac{1}{2}(C_f + C_g) \qquad (2.15)$$

Thus the g characteristics launched from the front will have values of C_g which depend on τ in a specified manner.

Now consider the sheath edge. If this is an f characteristic then C_f is conserved along it. From the dynamic Bohm criterion (2.29) we may write

$$u_s = \left(\frac{dX}{d\tau}\right)_s - 1 \qquad (2.34)$$

Thus, u at the sheath edge depends on the arbitrary sheath edge velocity function we apply in the initial conditions. Examining (2.15) at the sheath edge, C_f is a constant and u_s is arbitrary, so from this viewpoint C_g is an <u>arbitrary</u> function of τ.

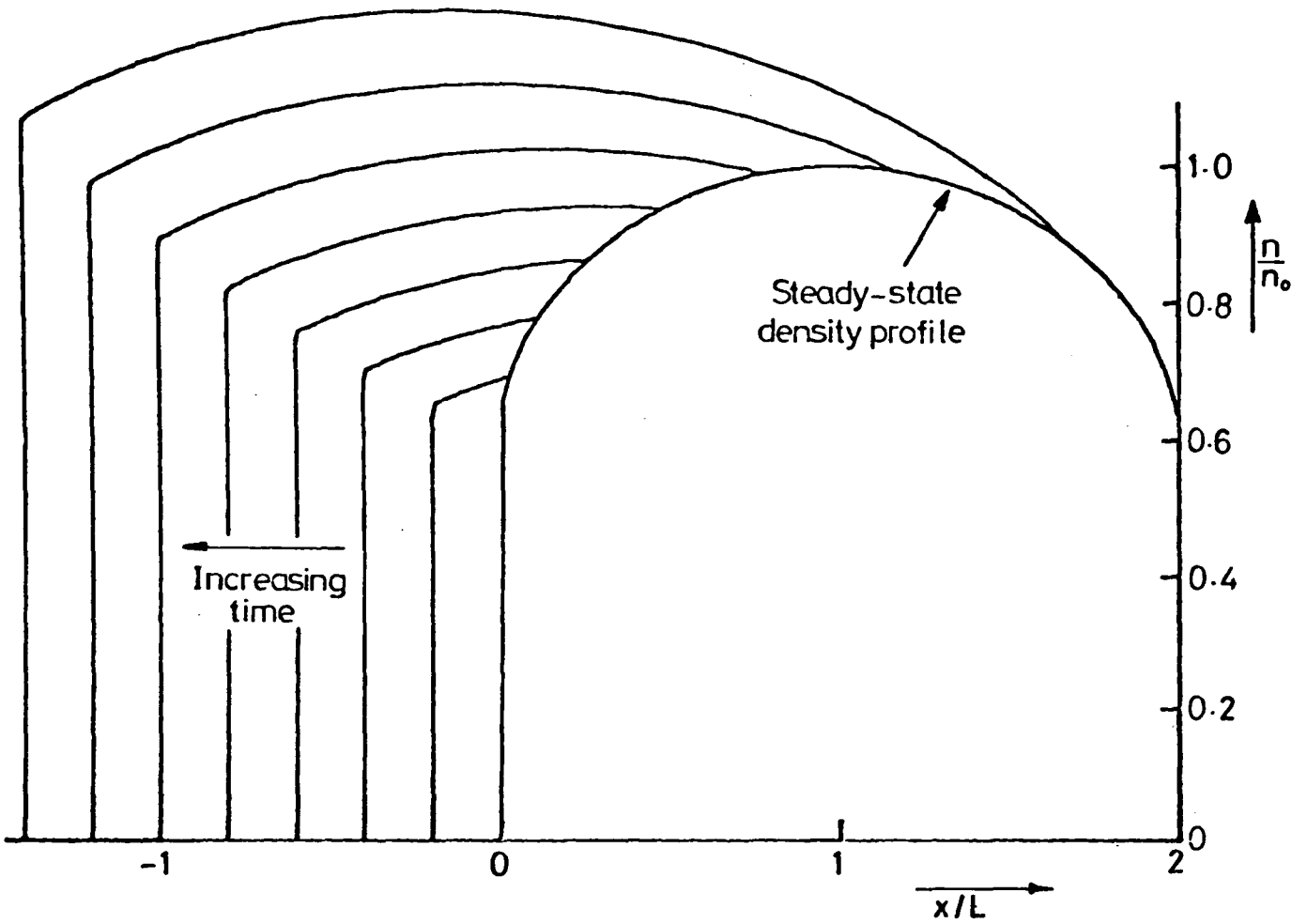


Figure 2.16

Ion number density profiles at successive times ($\Delta\tau$=0.4) using the boundary conditions of ANDREWS (1971) for constant velocity sheath collapse (v_{sh}=-0.5c).

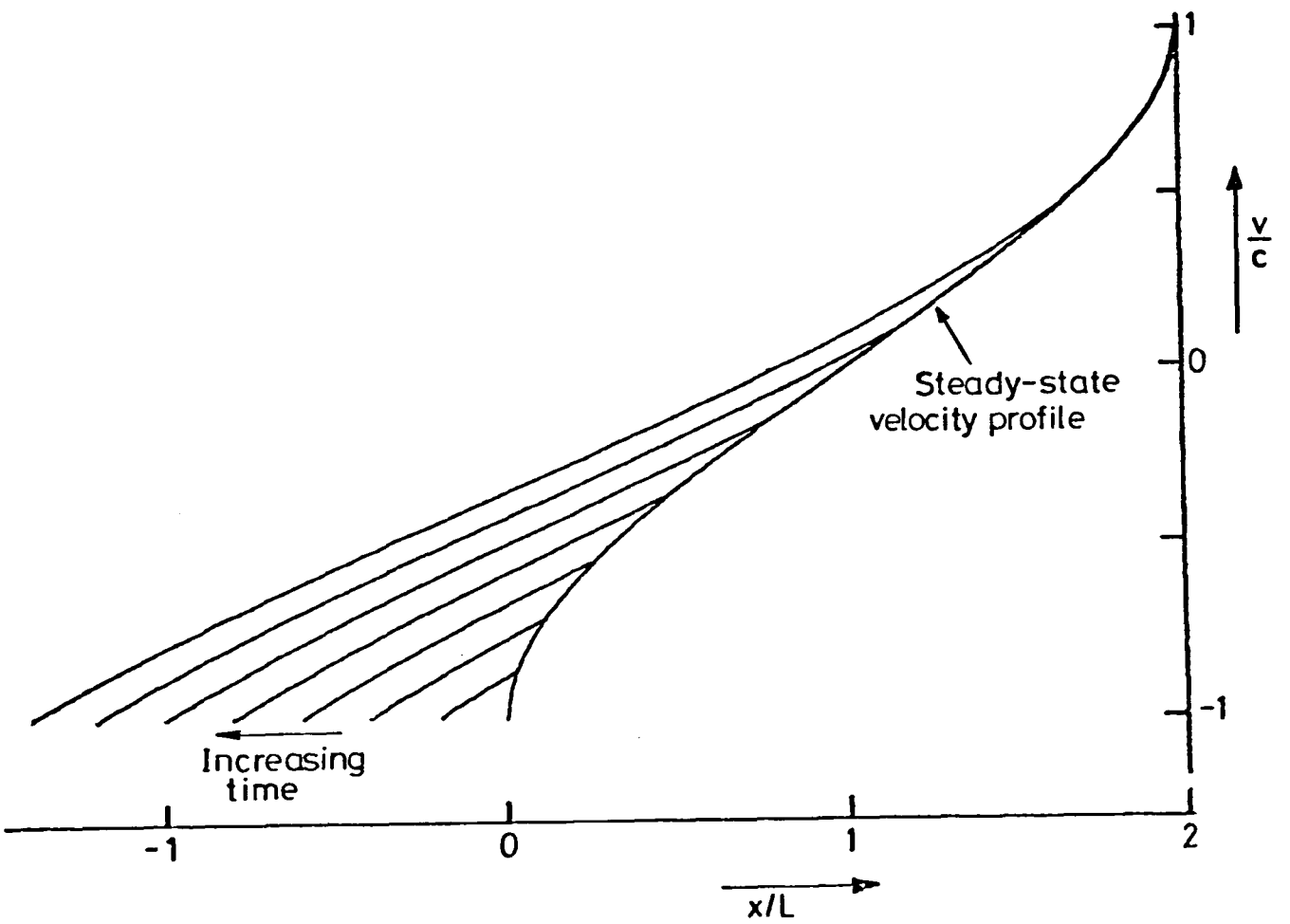


Figure 2.17

Ion velocity profiles at successive times ($\Delta\tau$=0.4) using the boundary conditions of ANDREWS (1971) for constant velocity sheath collapse (v_{sh}=-0.5c).

There is thus a contradiction since C_g is a specified function of τ as the g lines leave the wavefront. We may now state that the sheath edge cannot be a characteristic if the dynamic Bohm criterion is applicable, except where one very special choice of $(\frac{dX}{d\tau})_s$ is made.

2.11 DISCUSSION OF THE BREAKDOWN OF QUASINEUTRALITY

One of the most interesting aspects of the results presented in this Chapter is the breakdown of quasineutrality that has been observed at the moving sheath edge. This behaviour has not previously been noticed in plane geometry moving sheath calculations. In this Section it will be shown that, if the sheath edge is not a characteristic (Section 2.10), then use of the dynamic Bohm criterion and the breakdown of quasineutrality are related. This result adds credibility to the assumed dynamic Bohm crirerion.

Before proceeding it is interesting to note that a moving sheath edge has previously been associated with infinite potential gradients in the case of cylindrical and spherical sheath expansion (PREWETT and ALLEN, 1973). A self-similar technique was used to study a sheath expanding at constant speed, and the equations automatically gave a breakdown of the plasma solution at the moving sheath edge if the dynamic Bohm criterion was applied. The criterion thus emerged as an analytic result rather than being imposed. We shall now show that similar behaviour occurs for our case, as long as the sheath edge is not itself a characteristic.

Firstly, let us consider the directional derivative of $(u + \eta)$ along the sheath edge (c.f. equations 2.7 and 2.8). This may be written as follows:

$$\left(\frac{d}{d\tau}\right)_s (u + \eta) = \left[\frac{\partial}{\partial\tau} + v_s \frac{\partial}{\partial X}\right] (u + \eta) \qquad (2.35)$$

where v_s $(= \left(\frac{dX}{d\tau}\right)_s)$ is the velocity of the sheath edge. From (2.15) and (2.16) we have

$$\left(\frac{d}{d\tau}\right)_s (u + \eta) = \left[\frac{\partial}{\partial\tau} + v_s \frac{\partial}{\partial X}\right] (c_f) + \frac{2}{3} \qquad (2.36)$$

which is the directional derivative of c_f along the sheath edge plus a constant.

Along an f characteristic, (2.7) applies;

$$\left[\frac{\partial}{\partial\tau} + (u + 1)\frac{\partial}{\partial X}\right] (u + \eta) = \frac{2}{3} \qquad (2.7)$$

Equations (2.36) and (2.7) are valid simultaneously at particular points along the sheath edge, so that they may be subtracted:

$$(v_s - (u + 1)) \frac{\partial}{\partial X}(u + \eta) = \left[\frac{\partial}{\partial\tau} + v_s \frac{\partial}{\partial X}\right] c_f \qquad (2.37)$$

The particular form of this equation was suggested by BRAITHWAITE (1981, private communication). In discussion of this equation, we should remember the following points;

(i) $\frac{\partial u}{\partial X}$ and $\frac{\partial \eta}{\partial X}$ $(= \frac{1}{n}\frac{\partial n}{\partial X})$ have the same sign - see, for example, Figures 2.14 and 2.15 near the moving sheath edge.

(ii) On the sheath edge, the right hand side of equation (2.37) is finite and non-zero only if the sheath edge is <u>not</u> a characteristic; if the sheath edge <u>is</u> a characteristic this term is zero.

The value of the left hand side of equation (2.37) must therefore be finite and non-zero for our case. Consider the situation when $v_s = (u + 1)$, when (2.29) is applied at the moving sheath edge. Then we have

$$\frac{\partial}{\partial x}(u + \eta) \rightarrow \infty$$

An examination of the momentum equation (2.6) shows that the gradients of u and η separately become infinite since they have the same sign. This behaviour is observed in the numerical results. Thus application of the dynamic Bohm criterion is compatible with a breakdown of quasineutrality at the moving sheath edge if, as in our case, the sheath edge does not coincide with a characteristic.

A similar argument to the above may be applied in the zero ionization case, the only difference being the absence of the $\frac{2}{3}$ term in (2.36) and (2.7), which does not affect (2.37). A breakdown of the plasma solution is again expected. It is interesting to note that in the characteristics analysis by WICKENS (1980), infinite gradients appeared to be present at the moving sheath edge, but were not discussed. The sheath edge was not a characteristic, but was an imposed boundary condition as in our case. However, in the plane geometry self-similar calculations of ALLEN and ANDREWS (1970) the sheath edge formed the boundary of a centred simple characteristic fan, and infinite gradients did not occur despite the application of (2.29). This is because the sheath edge followed a characteristic path.

We now consider the curved geometry self-similar sheath expansion problem, which did give infinite gradients (PREWETT and ALLEN, 1973). Assuming cylindrical or spherical symmetry all

variations are radial, and equations (2.9)-(2.10) have the same form but with $A = -\frac{\alpha u}{R}$, where α is 1 or 2 for cylindrical or spherical geometry and R is the normalised radius coordinate (r/r_p). These terms come from the geometrical effects included in the continuity equation. The characteristics are thus curved in (R,τ) space and so the constant sheath edge velocity used by PREWETT and ALLEN (1973) did not follow a characteristic. Thus infinite gradients are expected from this argument, and were indeed observed.

2.12 SUMMARY OF THEORETICAL RESULTS

The method of characteristics has been used to examine the response of a self-sustained, bounded plasma to the motion of its boundary. The steady-state solution which was set up had gradients of density and velocity in the plasma, and so the region $0<x<L$ in our calculations (see Figure 2.1) may be likened to a presheath with scale length L. This presheath occured because of the introduction of ionization into the continuity equation which was balanced by loss to the walls.

On collapse of the sheath, an enhancement front was seen to propagate into the plasma at the local ion acoustic speed, while on sheath expansion a rarefaction front moved into the plasma at the same speed. In each case the characteristic paths were curved because of the ionization term in the initial fluid equations. The enhancement feature is of particular interest since such a phenomenon cannot be generated in the absence of a presheath.

The boundary conditions for the problem were the dynamic Bohm criterion for ion velocity at the moving sheath edge, and also the imposed sheath edge velocity function. Because of the arbitrary nature of the latter, infinite acceleration of the sheath edge was possible. This was accomodated for the case of constant velocity sheath collapse by the introduction of a centred wave component.

An interesting feature of the results presented here is the breakdown of the plasma approximation observed at the moving sheath edge. We have shown that this is to be expected theoretically on application of the dynamic Bohm criterion if the sheath edge is not itself a characteristic. This proof is also valid in the zero ionization case.

The generation of ion acoustic enhancements and rarefactions from the same model is an interesting development in the theory of ion acoustic wave generation. These results are thought to be due to the presence of an initial presheath in the calculations leading to the concept of curved characteristics. The problems encountered by WICKENS (1980) in explaining the wave generation process are now removed. It is possible that curved geometry may produce similar results, and this is an area for further study.

CHAPTER 3

THE MULTIDIPOLE DEVICE

3.1 INTRODUCTION

In this Chapter the experimental apparatus used in this work is described. Briefly, plasma is generated by the impact of accelerated electrons from hot filaments onto neutral argon gas atoms. Multidipole magnetic fields near the walls of the device confine the electrons.

Previous experiments on moving sheaths in this laboratory (PREWETT, 1974, WICKENS, 1980) were carried out in an electron beam-generated plasma which, due to the lack of magnetic confinement, required a background pressure not less than 2 mtorr. The multidipole device offered a simple method of producing a more quiescent, more uniform and less collisional plasma. The device itself is a modification of that used by MOORE (1979, 1981) in his experiments on thermal conduction in plasmas.

We commence with a review of multidipole devices in general, and subsequently give a detailed description of this device in particular.

3.2 DOUBLE PLASMA MACHINES AND MULTIDIPOLE DEVICES

Double plasma machines have been widely used in basic plasma physics experiments since their inception (TAYLOR et al, 1969). The original machines consisted of two similar metal chambers separated by a negatively biassed central grid which prevented the passage of electrons from one chamber into the other. Each chamber contained up to a hundred heated filaments which provided thermionic electrons. The filaments, equispaced near the walls for uniformity, were biassed at negative voltages with respect to the walls in order to accelerate the electrons. The electron population thus consisted of fast primary (or ionizing) electrons and secondary (or ultimate) electrons which were much slower. The two chambers were electrically isolated so that the electron accelerating voltages could be independently set, and thus two separately controllable plasmas were produced. The potential of the plasma in one chamber (the "driver") could be varied with respect to the other (the "target") and in this way electrostatic shocks (TAYLOR et al, 1970) and also beam-plasma interactions (e.g. TAYLOR et al, 1972) were studied.

A similar, spherical device was built (de HOOG and SCHOTT, 1970) without a separating grid but still using filaments near the walls. In these experiments a non-Maxwellian electron velocity distribution approximating to two temperatures (about 0.1 and 1 eV) was observed for the first time in this type of device. The higher temperature species was attributed to "thermalized primary electrons". Another version of the original device used electrostatic confinement of electrons by the use of a cylindrical grid as the anode as opposed to the relatively large vacuum chamber

(SPIELMAN et al, 1976). There was thus less area for the electrons to be collected at and in this sense they were confined. This technique increased the plasma density by a factor of 3 to 4, and also led to a non-Maxwellian electron velocity distribution.

The use of permanent magnetic confinement (the multidipole technique) was first demonstrated by LIMPAECHER and MacKENZIE (1973). They used a short-range cusped magnetic field produced by a large number of permanent magnets inside the vacuum chamber. The pole faces acted as the anodes, the bulk of the volume was magnetic field-free and the filaments were not in the cusp regions. The plasma confinement time was improved, and the plasma density increased by at least an order of magnitude compared to a device using no magnets. The improvement was most marked at low (<0.1mtorr) pressures, where relatively high plasma densities could be reached. The noise level was reported to be $\delta n/n \simeq .02\%$ which is of the same order as noise levels in devices without magnets. No deviation from a Maxwellian distribution for electrons was reported. Plasma potentials which were negative with respect to the anode were observed at low ($<5 \times 10^{-5}$ torr) neutral pressures.

Following this work, optimization of the confinement was considered important and results of experiments showed that a line-cusp arrangement was the most efficient (LEUNG, SAMEC and LAMM, 1975). A thin-walled non-magnetic metal vacuum chamber with externally mounted magnets was used. A schematic diagram of this arrangement is shown in Figure 3.1. A large number of individual permanent magnets produced lines of North and South poles running along the length of the device. It was suggested that the primary electrons in such a device should show a "shell-like" velocity

distribution (i.e. they were monoenergetic and isotropically distributed in velocity space). These electrons were well-confined, making many bounces before being collected. The ions, due to their larger Larmor radius, were not confined as efficiently. For low pressure (less than 0.1mtorr) a linear portion in the Langmuir probe characteristic was observed (TAYLOR and LEUNG, 1976), and this was explained in terms of a monoenergetic distribution of primary electrons. The ultimate electron population was considered to have a Maxwellian distribution.

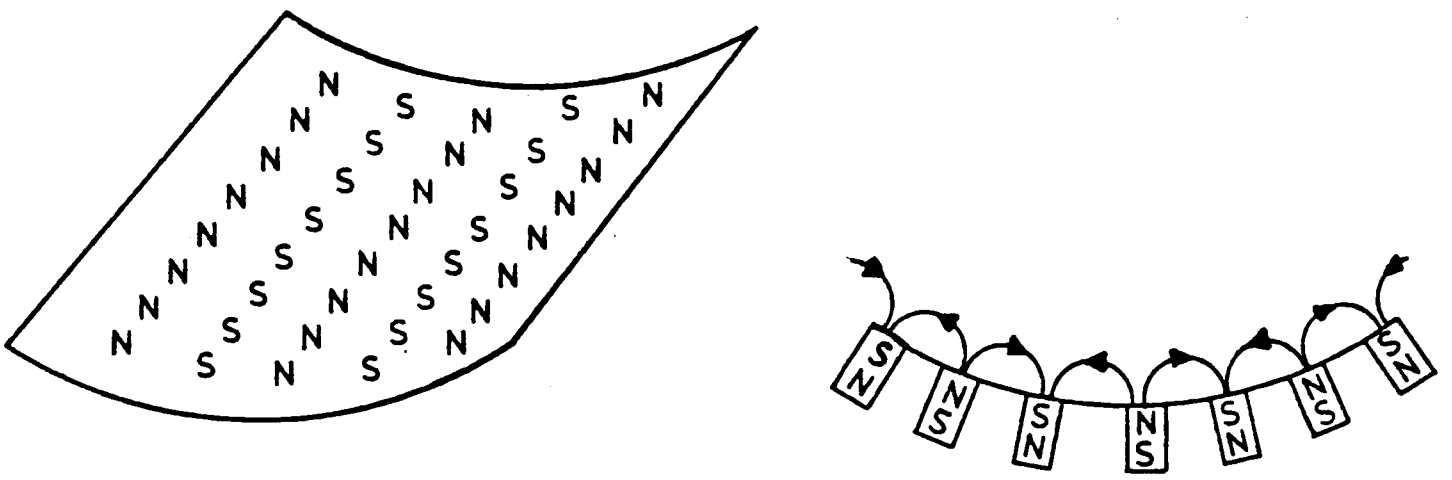


Figure 3.1
Schematic diagram of the full line cusp configuration of permanent magnets. The localized cusp regions extend the length of the device.

The device described by SCHOTT (1978) used magnetic strips as opposed to bar magnets, and his results showed that the electron velocity distribution function approximated to a two-temperature distribution, the effect being more marked than in the case without magnets.

A number of DP and multidipole devices are currently in use around the world because of their ease of construction and the quiescent nature of the plasma. Multidipole devices are used both with and without central grids. One application of these machines outside pure plasma research is the use of the multidipole technique in ion sources for neutral injection in Tokamaks, where the efficiency of the devices makes them a good choice for this

application. An interesting measurement in such a device was that of the primary electron velocity distribution (GOEDE et al, 1980), which was found to be appreciably spread out in energy. These results disagree with the conjecture of a monoenergetic distribution. When measured electron velocity distributions approximate to the sum of two Maxwellian distributions, the higher temperature distribution (usually 3-10eV) is sometimes explained in terms of thermalized primary electrons. The results of GOEDE et al would also appear to rule out this possibility since the measured number density is similar at all energies up to the electron accelerating voltage. It seems likely that the 3-10eV electrons are an ultimate population (i.e. the slow electrons formed in ionizing e-A collisions) rather than a primary one.

Primary electrons may be eliminated from the main plasma volume by placing the filaments within the cusped magnetic field regions (HERSHKOWITZ et al, 1980). This technique may be important in certain experimental situations where volume ionization must be excluded. Such a procedure has been used for double layer experiments in a triple plasma device (COAKLEY et al, 1978).

The presence of secondary electrons from ion or electron bombardment of the walls of multidipole devices has been investigated (COAKLEY and HERSHKOWITZ, 1980). At low pressures, secondary electrons were detected in the main plasma volume. Also negative plasma potentials have been produced in such plasmas by supplemental (cold) electron emission from subsidiary filaments (HERSHKOWITZ et al, 1979).

3.3 DESCRIPTION OF THE MULTIDIPOLE DEVICE

In this section our multidipole containment device will be described. This device has been modified and rebuilt since its original use (MOORE, 1979, 1981), a major difference being that no central grid was used in our experiments. The mechanical system and the electrical arrangements will be described in the following subsections.

3.3.1 The Mechanical System

The vacuum system of the original apparatus used by MOORE (op. cit.) was completely refurbished. The improved version consisted of a 4" Genevac oil diffusion pump backed by a Genevac mechanical rotary pump together with two Pirani gauges, an ionization gauge (I.T.L. gauge head controlled by a Mullard unit) and the main chamber (see Figure 3.2). The backing pressure was less than 50 mtorr while the base pressure of the chamber was better than $3x10^{-6}$torr with the cold trap full of liquid nitrogen. In normal operation a steady flow of argon at about $3.5x10^{-4}$torr was maintained and thus 99% purity was achieved in the main chamber. Note that this pressure was corrected from an actual gauge reading of $5x10^{-4}$torr using the gauge calibration factor for argon quoted by EDWARDS (1974) as (1/1.4).

The vacuum system control unit (see Figure 3.3) was arranged in such a way that the diffusion pump could be switched on only if various safety conditions were fulfilled (COATES, 1979). The vacuum system was safe to leave pumping overnight to achieve the lowest base pressure and impurity level possible.

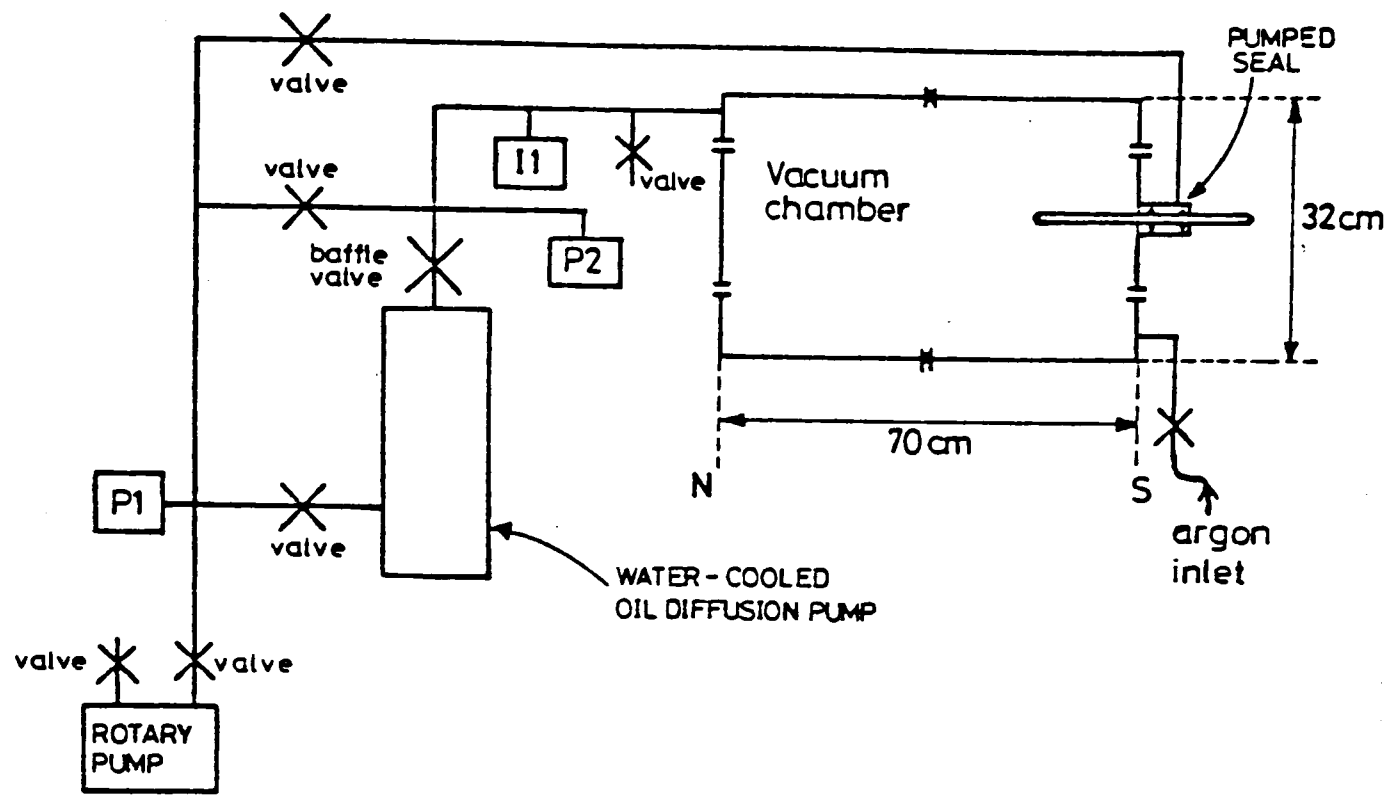


Figure 3.2
The vacuum system.

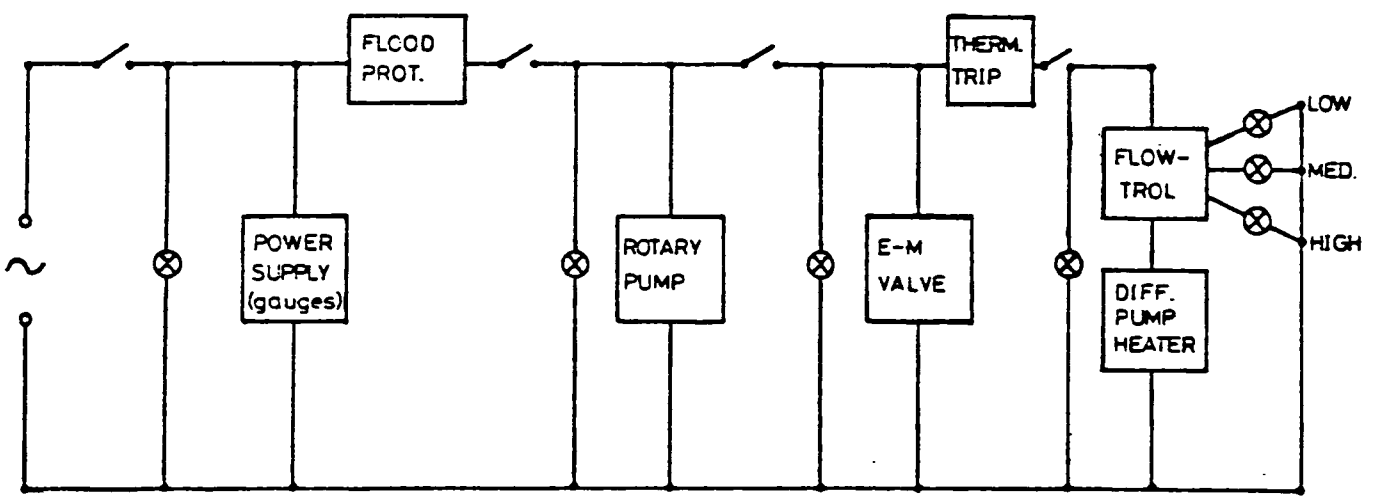


Figure 3.3
Control circuit for the vacuum system.

The multidipole device itself (main chamber) consisted of two non-magnetic stainless steel cylindrical vacuum vessels of diameter 32cm bolted together in the centre with an O-ring seal between them. The ends of the machine were called North (pump end) and South for historical reasons. Each vacuum vessel (not including the end plates) had an array of permanent magnets strapped to it for confinement (Section 3.2 and MOORE, 1979). A short range line-cusp field was used as in Figure 3.1. There were two electrical feedthroughs, one at each end and each with 9 pins. These were used for filament connections and employed copper gasket vacuum sealing because of the high temperatures near the filaments. Access for 7mm diameter probe tubes was available at two ports in the North end and three ports in the South end of the device, one of the latter ports being axial. Each port employed a double O-ring seal to allow motion of the tube. In general, polished stainless steel tubes were used to mount probes and wave transmitters. The probe arrangements used in particular experiments are indicated in Figures 4.5 and 5.1. The vacuum sealing method for the probe tubes in early experiments (Chapter 4) used Araldite which was unsatisfactory causing frequent leaks. In later experiments (Chapter 5), soldered metal-ceramic "Ferranti" seals were used on the outer ends of the tubes.

The axial probe tube was passed into the main chamber through a pumped Wilson seal (WILSON, 1941). The two O-rings in this seal were separated by a cavity which was connected to the backing vacuum line. This rough vacuum was sufficient to ensure negligable leakage when moving the probe tube. A mechanism for traversing the axial probe tube using an electric motor and a linear drive was designed and built (see Figure 3.4). The probe motion, which was sufficient to traverse the whole machine if required, was limited by variable

position end stops which disabled the electrical probe drive circuit. The probe position was measured electrically using a slide-wire potentiometer arrangement, allowing the position of the probe within the device to be recorded on an x-y plotter.

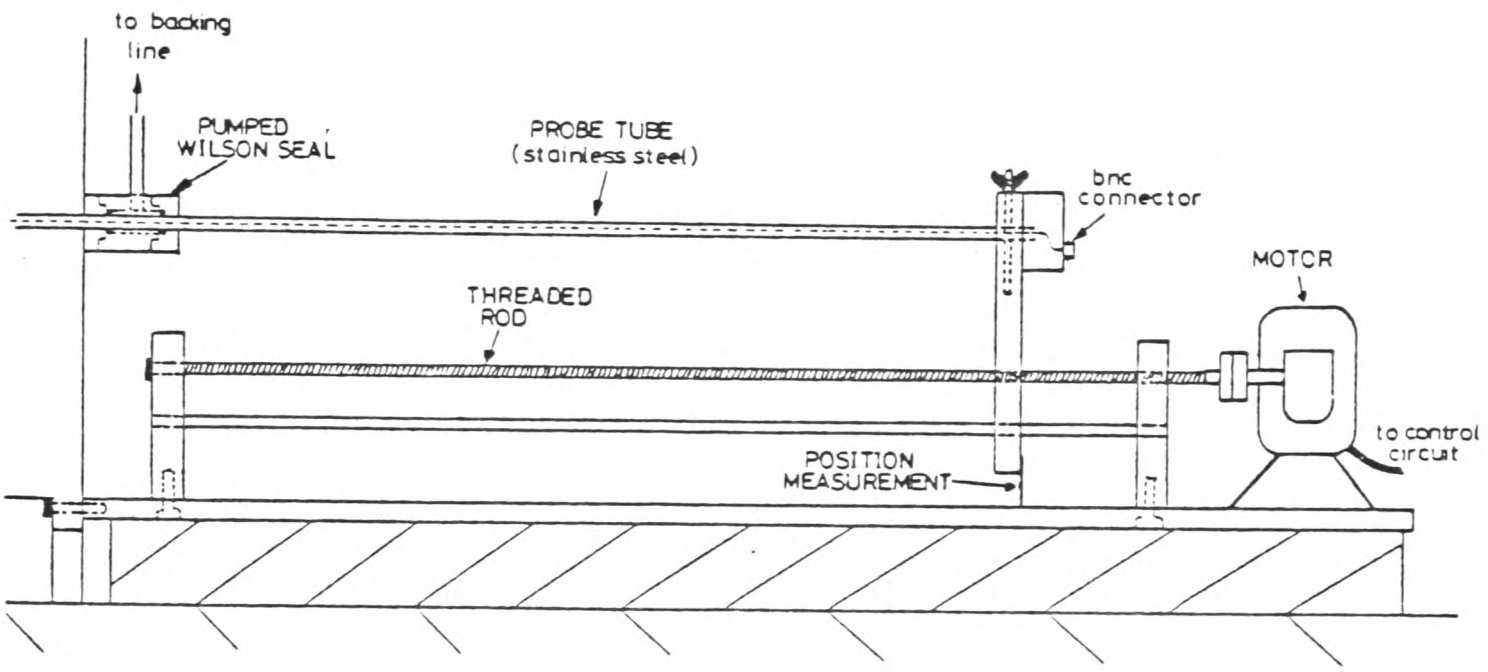


Figure 3.4
Linear drive system for the central probe tube.

3.3.2 The Electrical System

The plasma was produced using two different anode configurations; with cylindrical mesh anodes (Method A) or with the vacuum chamber as the anode and the meshes removed (Method B). Whichever of these schemes was employed two filaments were used, one at each end of the device. No significant differences in plasma properties were encountered with these different anode connections, but we shall state which is being used in each set of experiments. We shall now discuss the operation of the filaments and then examine the electrical arrangements used in both Methods A and B.

The filaments were biassed at a voltage of -50 to -70 volts with respect to the anode. They were supported in such a way that they were not within the wall magnetic fields. Each filament consisted of an 8cm long, 0.2mm diameter tantalum wire spot-welded onto a tantalum support. The filaments were heated by the passage of an electric current to a temperature of approximately 2000K (as measured using an optical pyrometer). Thus thermionic emission of electrons was achieved. The heating current necessary to obtain a particular electron emission current decreased with time of operation due to the evaporation of tantalum which caused a lower cross-sectional area. The filament lifetime was $\geq$50h.

The variation of plasma current (i.e. the current between the filaments and the anode) with electron accelerating voltage (i.e. the potential difference between these two) may be understood as follows:

(a) Negligible current was collected if the voltage was below the ionization potential of argon (15.7V).

(b) Above 15.7 volts, the current increased due to the increase in ionization efficiency with electron energy (von ENGEL, 1965). In this range the electron emission current was limited by space-charge formation.

(c) Above some critical voltage, the electron emission current (and therefore the plasma current) became temperature-limited, all thermionic electrons escaping from the vicinity of the filament. This critical voltage was approximately 40V but depended on the filament temperature.

The discharge was usually operated at a constant voltage above this critical voltage, and the plasma current was thus controlled by the filament heating current (i.e. the filament temperature). In all experiments the plasma current was kept constant by manual variations of the filament current.

Note that the voltage drop across a filament due to its resistance will lead to an initial energy spread of up to 10 volts in the emitted electrons. This will mean that the accelerated primaries will not have a monoenergetic distribution.

The Method A anode arrangement was used in the initial experiments (COATES, 1979) and for most experiments in Chapter 4. Cylindrical mesh anodes were placed within the wall magnetic fields (see Figure 3.5). The effective anode area was thus reduced even more than that of SPIELMAN et al (1976), by our use of magnetic fields. The filaments, vacuum chamber and probe tubes were all at 0V, while the grid anodes were at +50V. A plasma current of 300mA was drawn to the anodes. In this arrangement plasma potential was -12V with respect to the anodes, so that the current to the grids consisted of electrons.

The Method B anode arrangement is the one usually used in multidipole devices and was used for experiments discussed in Chapter 5. The mesh anodes were removed. The vacuum chamber and probe tubes were all at 0V, while the filaments were at -70V (see Figure 3.6). In this case plasma potential was about -15V with respect to the anodes but was dependent on whether probe tubes were earthed (see Section 4.2). The plasma current was again kept constant at 300mA. It was assumed that the anode effectively consisted of the ends of the device (where there were no magnetic

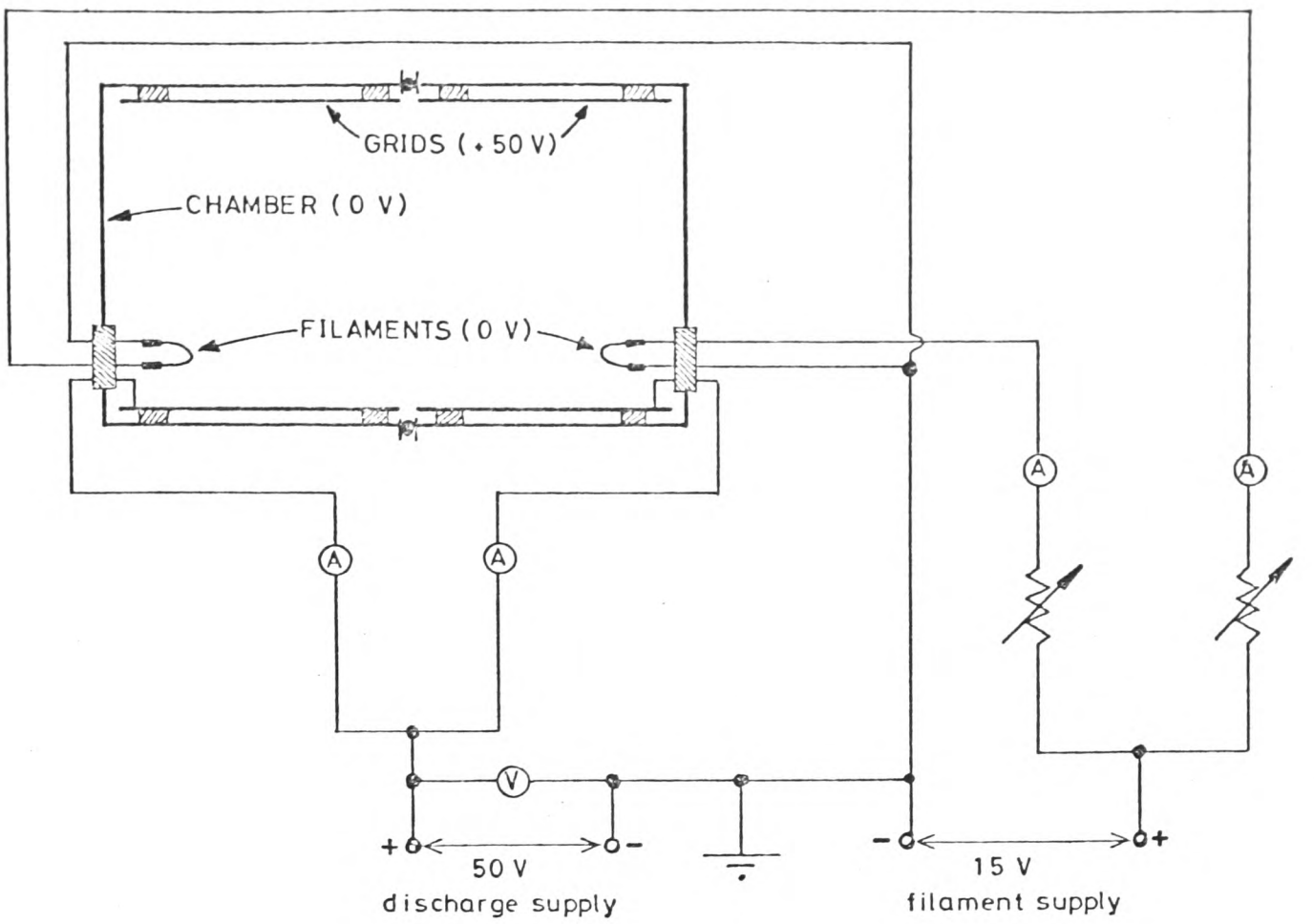


Figure 3.5
Method A electrical connections.

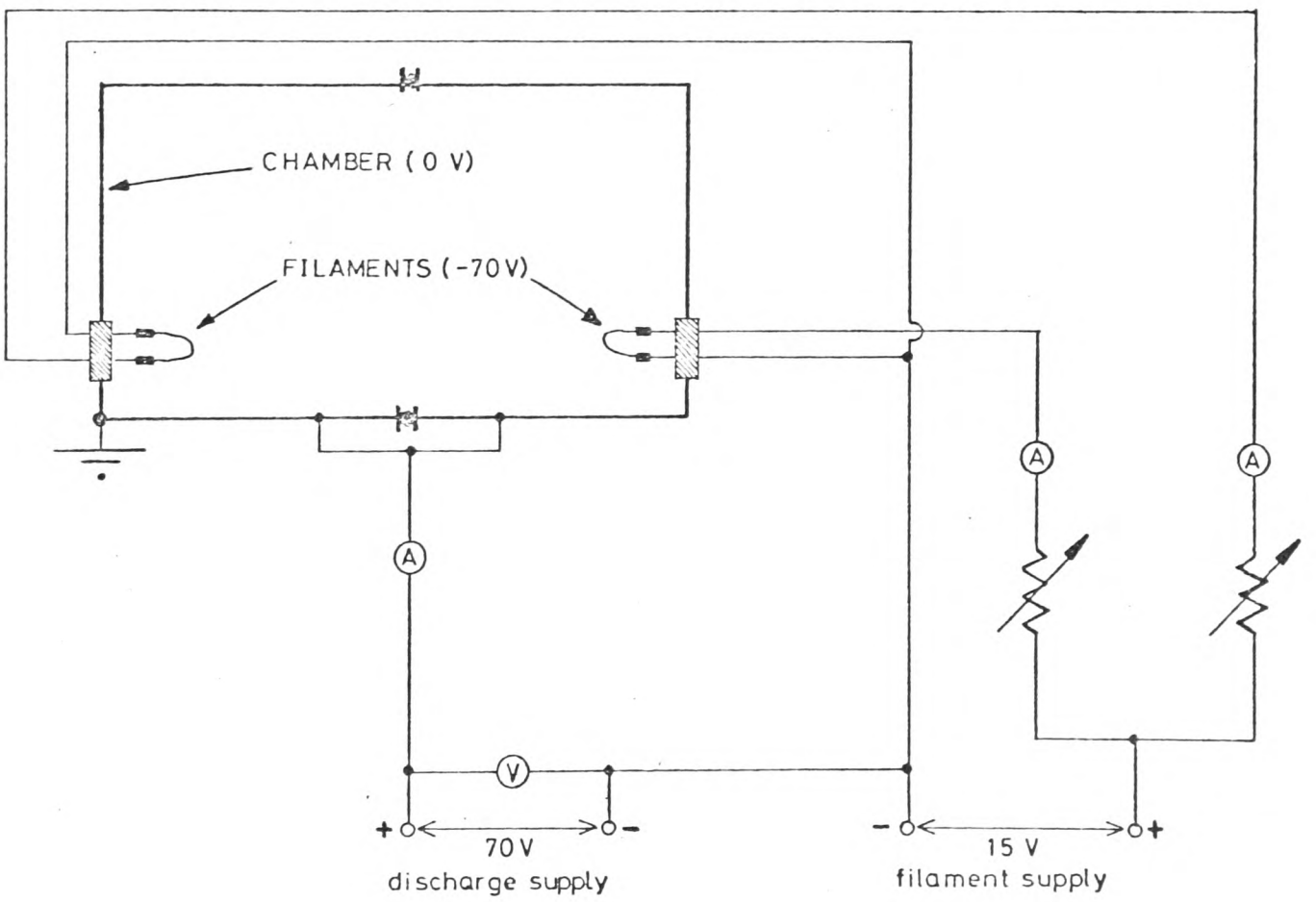


Figure 3.6
Method B electrical connections.

fields) together with the earthed metal probe tubes. Again electrons were drawn at the anode.

3.4 SUMMARY AND RUNNING CONDITIONS

A double plasma device has been modified to provide a quiescent plasma to be used in basic plasma physics experiments. The experimental details of the device have been described, including the vacuum system and the electrical arrangements.

Typical running conditions were as follows:-

Background pressure	3×10^{-6} torr
Neutral argon pressure (corrected)	3.5×10^{-4} torr
Anode-cathode voltage (Constant in particular experiments)	50 - 70 Volts
Filament current (I_{fil})	3.5 A (new filaments) to 2.5 A (old filaments)
Voltage drop across a filament	~8 Volts (new) to 11 Volts (old)
Plasma current (Variable by changing I_{fil})	300 mA

CHAPTER 4

BASIC PLASMA EXPERIMENTS

4.1 INTRODUCTION

This Chapter describes the fundamental properties of the argon plasma produced in the multidipole device. Details of the device were discussed in Chapter 3.

Standard Langmuir probe measurements determine the electron temperature, plasma density and plasma potential, and the Druyvesteyn technique is used to measure the electron velocity distribution. The ion acoustic speed, found from measurements on small amplitude ion acoustic waves and pulses, is used to provide additional information on the electron temperature. In the case of positive ion acoustic pulse excitation we shall see that care has to be taken not to draw too much electron current to the transmitter as the whole plasma is then disturbed.

The apparatus was connected using Method A (see Section 3.3.2) for all the measurements described in detail here. The differences which are observed using Method B will be discussed at the end of this Chapter; the major plasma parameters will be seen to be very similar.

4.2 LANGMUIR PROBE EXPERIMENTS

The Langmuir probe technique has been reviewed by a number of authors (CHEN, 1965a, SCHOTT, 1968, SWIFT and SCHWAR, 1970). Here we shall decribe some measurements using a cylindrical probe. The probe tip was a 6mm long, 0.3mm diameter tinned copper wire. Electrical shielding was continued almost to the probe tip using semi-rigid coaxial cable. The probe was mounted in the axial probe port in the South end of the vacuum chamber (Section 3.3.1).

4.2.1 Current-Voltage Characteristics

The simplest Langmuir probe measurement is the determination of its current-voltage characteristic. The interpretation of such measurements may not be so simple due to complicating effects such as finite ion temperature and sheath size. Nevertheless the technique gives important information concerning plasma potential, floating potential, electron temperature and plasma density.

The circuit used for these measurements is shown in Figure 4.1. Voltages were measured with respect to the anode. The characteristics were displayed either on an oscilloscope (for the linear plots) or on an x-y recorder (for either the linear or the semi-logarithmic plots). Usually data were taken with the probe in the centre of the device and with the running conditions given in Section 3.4.

A typical result is shown in Figure 4.2 where the linear and logarithmic plots are compared. From the linear plot we can see that plasma potential (V_{pl}) is approximately -12V with respect to the anode, while floating potential (V_f) is approximately -25V.

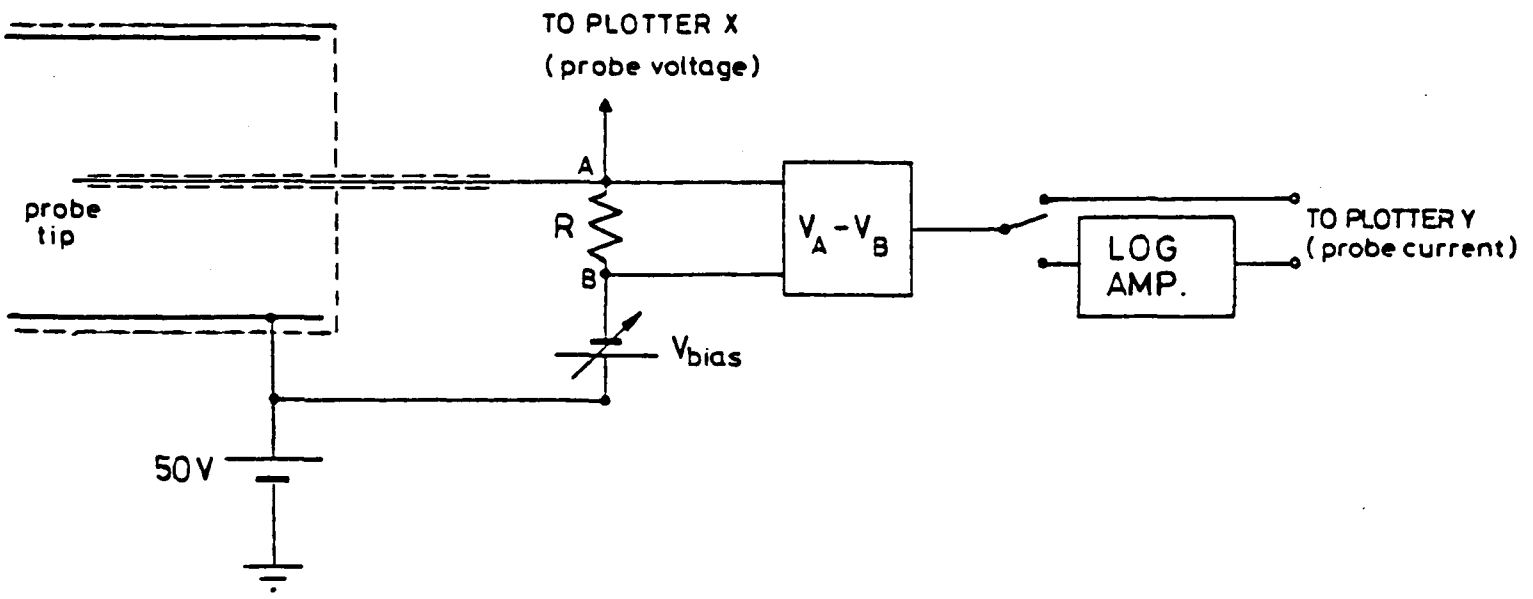


Figure 4.1
Electrical circuit for Langmuir probe current-voltage characteristics.

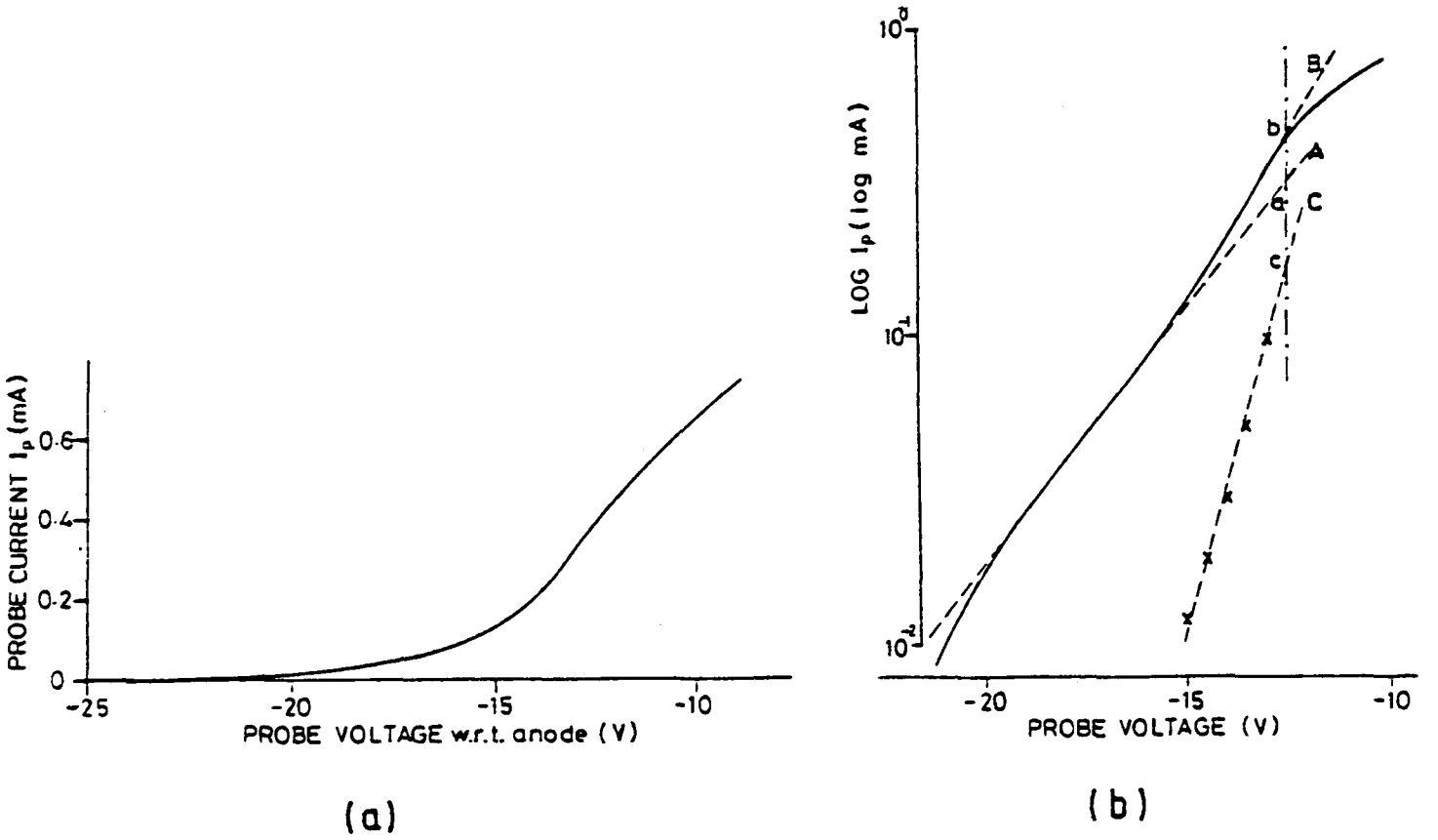


Figure 4.2
Experimental Langmuir probe characteristics (a) linear, and (b) semi-logarithmic. In (b) two straight lines A and B are evident, the line C represents a plot of (B-A).

Recalling the theoretical expression for floating potential with respect to the plasma (ALLEN, 1974), we have

$$V_{pl}-V_f = (\frac{kT}{2e})\ ln(\frac{M}{2\pi m}) \qquad (4.1)$$

assuming a Maxwellian electron velocity distribution with temperature T. The measured value of floating potential thus gives an electron temperature of approximately 2.8eV. From the semi-logarithmic plot, however, it appears that a non-Maxwellian electron velocity distribution is present. The plot, whilst indicating plasma potential (the knee b) more accurately than the linear one, appears to consist of two intersecting straight lines A and B.

Following the interpretation of similar results by OLESON and FOUND (1949) and JONES et al (1975), this behaviour may be approximated by the superposition of two Maxwellian electron velocity distributions. The line A in Figure 4.2(b) corresponds to current due to the hotter electron species. The points on line C are found from a subtraction of the current due to the extended line A from the total current B for a particular voltage. The straight line thus obtained corresponds to current due to the colder (low-energy) electron species. The relative number densities of the two components are found from the intercepts a and c of the straight lines with the vertical line which indicates plasma potential. Using this method, the results show two electron species of temperatures $T_c \simeq 1eV$ and $T_h \simeq 2.7eV$ with approximately equal densities. This description remains reasonable if the temperatures and densities are within 10% of those stated. Further evidence for this two-temperature behaviour will be presented from other measurements, and we recall that such an electron velocity distribution is not

uncommon in multidipole and double plasma devices (de HOOG and SCHOTT, 1970, SPIELMAN et al, 1976, ARMSTRONG et al, 1979). This result is reproducible and occurs even when probes have been heated to remove surface contamination by drawing electron saturation currents.

The two-temperature distribution was not previously noticed (COATES, 1979) due to the use of point-by-point as opposed to continuous logarithmic plots. Although the floating potential quoted above is sensitive to the hotter electron component, the theoretical speed of ion acoustic waves depends on the cold electron component as well, and so a detailed knowledge of the distribution is important for our moving sheath experiments.

Plasma density may be measured from the probe plots either by measuring the electron current at plasma potential or, more accurately, by measuring the ion saturation region in detail and comparing the results with the numerical curves of CHEN (1965b). Chen solved a cylindrical version of Poisson's equation as used by TONKS and LANGMUIR (1929, see Section 1.2) assuming $T_i=0$ for a variable ratio of probe radius to Debye length. Under the usual running conditions (Section 3.4), both techniques applied to our results give a value of $\lambda_D \simeq 0.3$mm and $n_o \simeq 10^{15} m^{-3}$ using the effective electron temperature of $T_{eff} \simeq 1.5$eV (see Section 4.3).

The plasma potential was also determined using a method which utilized the fact that the sheath disappears at plasma potential. A low frequency (1KHz) sinusoidal voltage was applied to a floating probe, while the DC bias voltage on a second probe was varied. The magnitude of the AC signal received on the second probe was plotted as a function of bias voltage and the maximum of this gave plasma

potential. The assumption is that the coupling from plasma to probe is most efficient when the sheath disappears. The results agree to within 1V with those obtained from the semi-logarithmic probe plot.

Noise levels in the plasma were measured by examining fluctuations in the electron saturation current, and the relative density variation $\delta n/n$ is found to be less than 0.1%. This level is uniform throughout the plasma except near the walls where the noise level increases dramatically. The noise frequency spectrum in this region is well-defined and appears to consist of a 200kHz fundamental with a few (~3) observable harmonics, though these may be spuriously generated by the non-linear characteristic of the probe sheath. These frequencies decrease slightly towards the wall. Similar observations in multidipole devices have been made by D'ANGELO et al (1978) and GLANZ and HERSHKOWITZ (1981), though the frequency spectrum was much broader. They suggested that the noise increase towards the wall was apparent, the cause being plasma waves excited by the presence of the positively biassed probe in a magnetic field.

Axial density uniformity measurements were made by plotting the ion saturation current to a probe as a function of distance. The plasma density was found to be uniform except within ~15cm of the walls of the device or near large probes and probe tubes. Density gradients with different scale lengths were found to be associated with these regions (see Figure 6.1). Plasma drift speeds associated with these gradients were measured using ion acoustic waves (Sections 4.3 and 4.4).

Some investigations were carried out using a probe while the plasma was running with different conditions to those in Section 3.4. The following general trends were noticed:-

(a) Decreasing neutral pressure causes V_{pl} and V_f to become more negative with respect to the anodes and decreases the plasma density. These effects are due to a decrease in electron collision frequency. The plasma could not be maintained below ~2×10^{-5} torr.

(b) Increasing the filament-anode voltage causes floating potential to become less negative and increases the plasma density.

(c) Increasing the filament heating current too far causes the plasma to extinguish. This effect is not understood, but may be due to local gas heating effects.

(d) Electrical connections to the metal probe tubes cause differences in plasma potential. Usually only the motor-driven probe tube on the axis of the machine was earthed while the others were allowed to float, but if these are earthed also V_{pl} and V_f become less negative with respect to the anode. This effect is particularly noticeable when the machine is connected using Method B (see Section 3.3.2) since earthed probe tubes are then at anode potential and collect electrons. Traversing a probe tube in the device changes the effective electron collecting area, and may therefore affect the properties of the plasma. Limited motion of the probe tubes was made in particular experiments so that little effect on the plasma as a whole is observed in the results.

4.2.2 Electron Velocity Distribution Measurements

The electron velocity distribution function was measured using the second derivative of the probe current-voltage characteristic (DRUYVESTEYN, 1930). This method has been widely used for the measurement of isotropic distributions (SWIFT and SCHWAR, 1970).

In the electron retarding region of the probe characteristic (i.e. when the probe voltage is more negative than plasma potential) it can be shown that

$$[f_1(E)]_{E=eV} = CV^{1/2} \frac{d^2I}{dV^2} \qquad (4.2)$$

where $f_1(E)dE$ is the number of electrons per unit volume in the energy range E to E+dE, V is the probe voltage with respect to plasma potential, I is the current to the probe and C is a constant involving the probe area and other factors. The derivation of 4.2 assumes:-

(i) An isotropic velocity distribution (ALLEN, 1978)

(ii) No ionization in the sheath

(iii) The electron contribution to $\frac{d^2I}{dV^2}$ is much larger than the ion contribution. This assumption holds for a retarding energy of up to approximately $8kT_e/e$ for argon (RICHARDS et al, 1975).

The second derivative of the probe current is measured by imposing a small alternating voltage v(t) onto the DC bias voltage of the probe V such that the total voltage applied to the probe may be written

$$V(t) = V + v(t) \qquad (4.3)$$

Then the electron current drawn to the probe I(t) may be written

$$I(t) = I_o + i(t) = F(V(t))$$

We may Taylor expand this to give

$$i(t) = F'(V).v(t) + F''(V).\frac{v^2(t)}{2!} + \ldots \qquad (4.4)$$

where the prime denotes differentiation with respect to voltage. We wish to find F''(V). To do this, it is convenient to apply an alternating voltage of the form:

$$v(t) = v(1 + \cos p_1 t)\sin p_2 t \qquad (4.5)$$

with $p_1 \ll p_2$ and $v \ll kT_e/e$. This has Fourier components at frequencies p_2 and $p_2 \pm p_1$; these will be the frequencies of the F'(V) term in equation (4.4). The F''(V) term (which is the one required) contains a DC component, and AC components at frequencies p_1, $2p_1$, $2p_2$, $(2p_2 \pm p_1)$, $(2p_2 \pm 2p_1)$. The F'''(V) term contains no components at p_1; the next one to do so is the fourth order term. It is assumed that v^4 is small enough for this term to be neglected.

The experimental technique, then, is to apply an alternating voltage of the form indicated in equations (4.3) and (4.5) and to measure the amplitude of the component of current drawn at the frequency p_1 as a function of the bias voltage V. The experimental arrangement is shown in Figure 4.3 and is similar to that used by EDGLEY (1975).

A typical result from this measurement can be seen in Figure 4.4 which shows a plot of $\frac{d^2I}{dV^2}$, which is proportional to the electron velocity distribution function (note that the electron energy distribution function can be obtained by multiplying the ordinate by

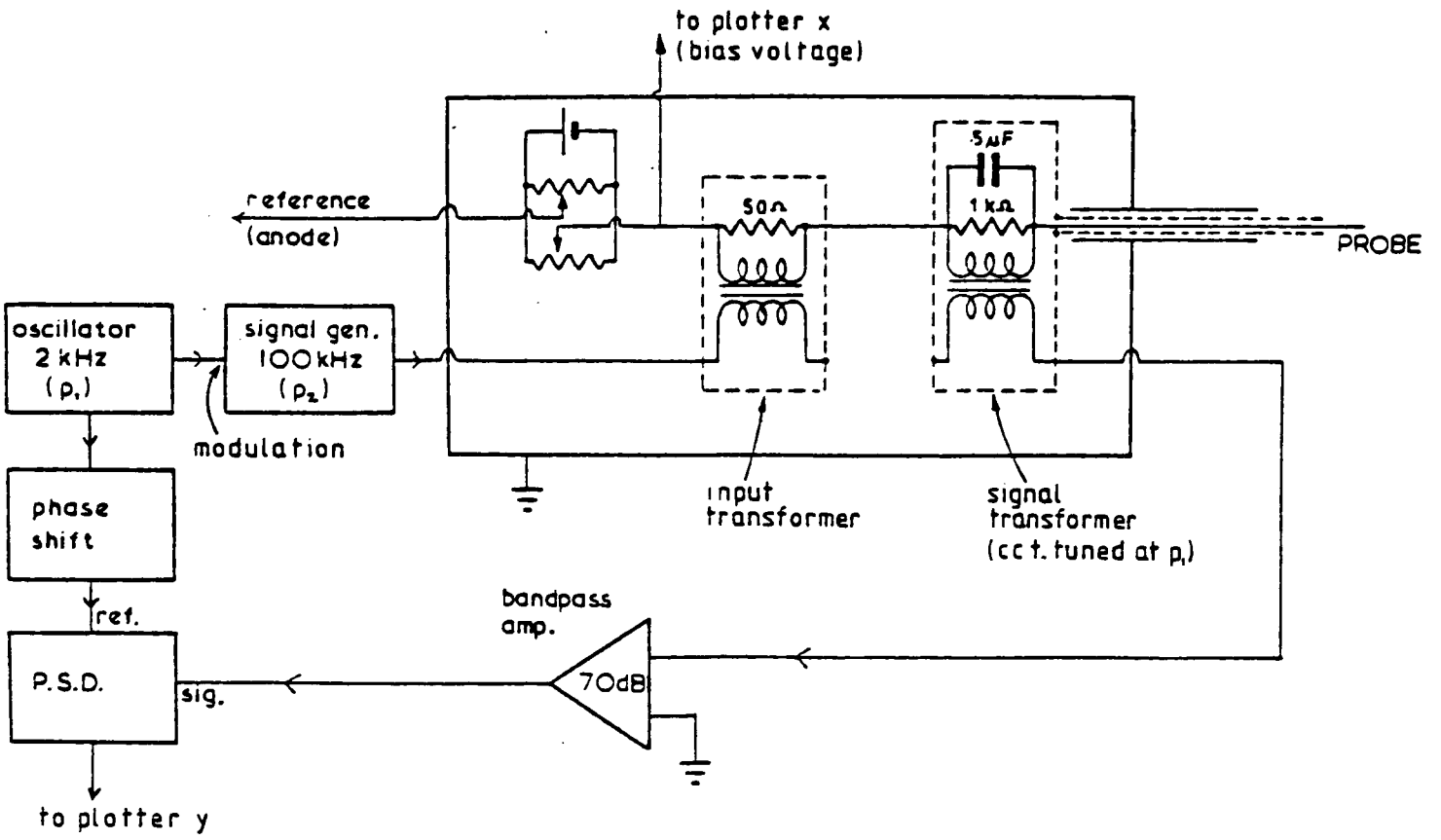


Figure 4.3

Electrical circuit to measure the second derivative of probe current with respect to voltage (I").

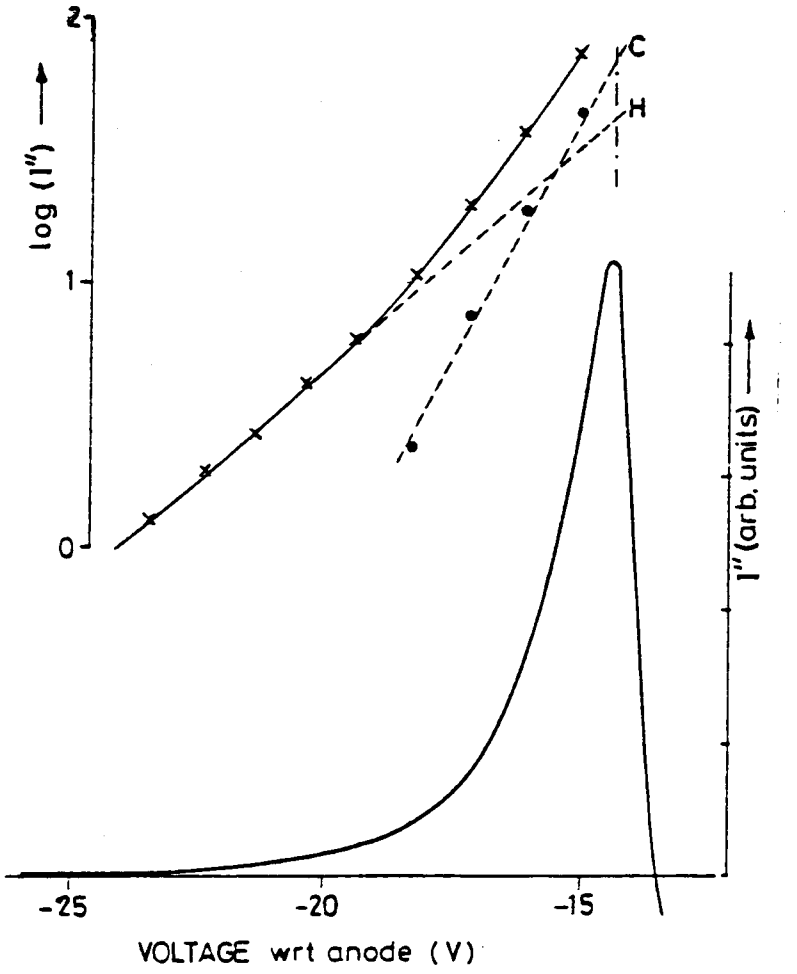


Figure 4.4

Experimental results for I" which is proportional to the electron velocity distribution. The logarithm of I" is also shown; the solid line shows experimental data and the lines H and C correspond to hot and cold electron populations (c.f. Figure 4.2).

$V^{1/2}$). Also plotted is the natural logarithm of $\frac{d^2I}{dV^2}$ which for a Maxwellian velocity distribution should give a straight line. As shown in the diagram the actual behaviour is well approximated by two intersecting straight lines, as inferred from the semi-logarithmic Langmuir probe measurements (Figure 4.2). From Figure 4.4 the "hot" and "cold" components have electron temperatures of approximately 2.4eV and 0.9eV with approximately equal densities. These results agree with those in Section 4.2.1 within experimental error (~10%).

4.3 CONTINUOUS ION ACOUSTIC WAVE PROPAGATION

The propagation of ion acoustic waves in the plasma was studied using an interferometer technique. The waves were excited by impressing an alternating voltage at frequencies well below the ion plasma frequency (amplitude about 8.5V p-p) through a capacitor onto the steady floating potential of the shielded grid structure illustrated in Figure 4.5. The shielding was used in an attempt to eliminate the capacitative coupling between transmitter and receiver. Fluctuations in electron saturation current were measured using the axial Langmuir probe as the receiver (see Figure 4.6). Electron saturation current was used because the highest signal levels are observed at this bias. The receiver probe was used to measure the phase of the signal relative to the phase of the transmitted wave as a function of distance. These were compared using a phase-sensitive detector (P.S.D.) as an interferometer, whose output as a function of distance was recorded on an x-y plotter (see Figure 4.6). The time constant on the P.S.D. was set at 1s giving a 1Hz bandwidth around the exciter frequency. The probe carriage took a time of approximately 30s for its scan of 20cm.

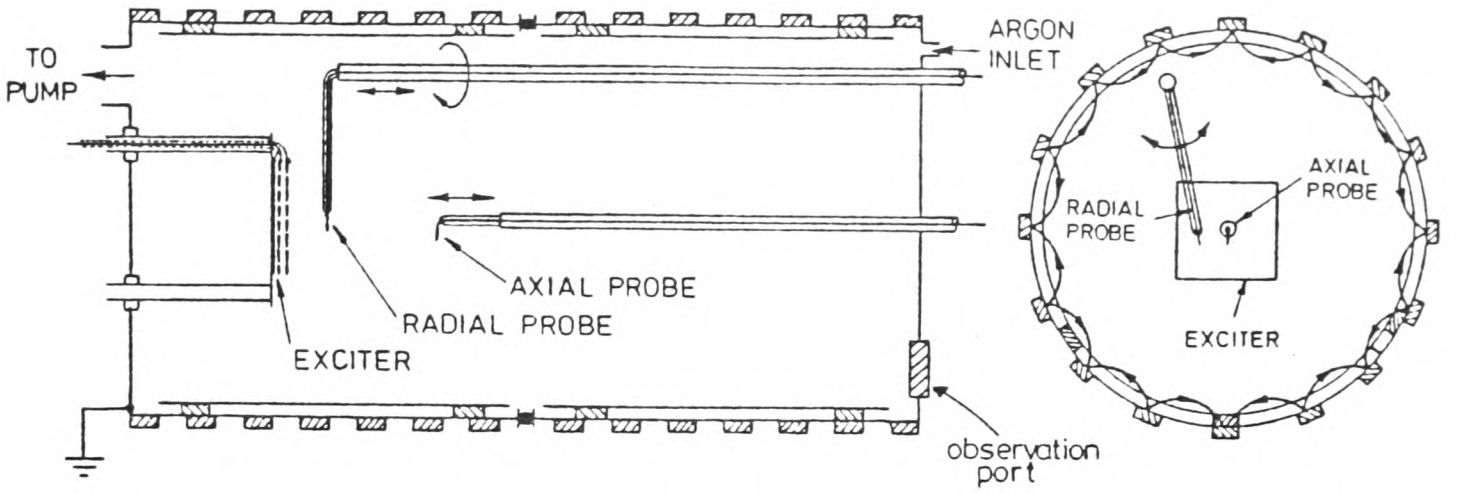


Figure 4.5
Probe configuration in the Method A anode arrangement as used in this Chapter.

Some typical interferograms at various frequencies are shown in Figure 4.7. The apparent damping rate is found to be independent of frequency although care is needed when interpreting these results since plasma fluctuations may displace part of the wave energy outside the narrow 1Hz bandwidth of the measurement.

Measurements of wave propagation in the opposite direction from probe to grid were also made and the measured wave phase velocity differs for the two cases as revealed by the frequency versus wavenumber plot of Figure 4.8. Such a result implies that a plasma drift towards the transmitter exists, in which case an average of the two speeds gives the true ion acoustic speed. The ion drift velocity can be found from the difference of the two speeds. This drift was not caused by the transmitter itself because variation of the DC bias on the grids does not affect these results. A more likely explanation is due to the slight nonuniformity of the plasma since the experiments were conducted towards the transmitter end of

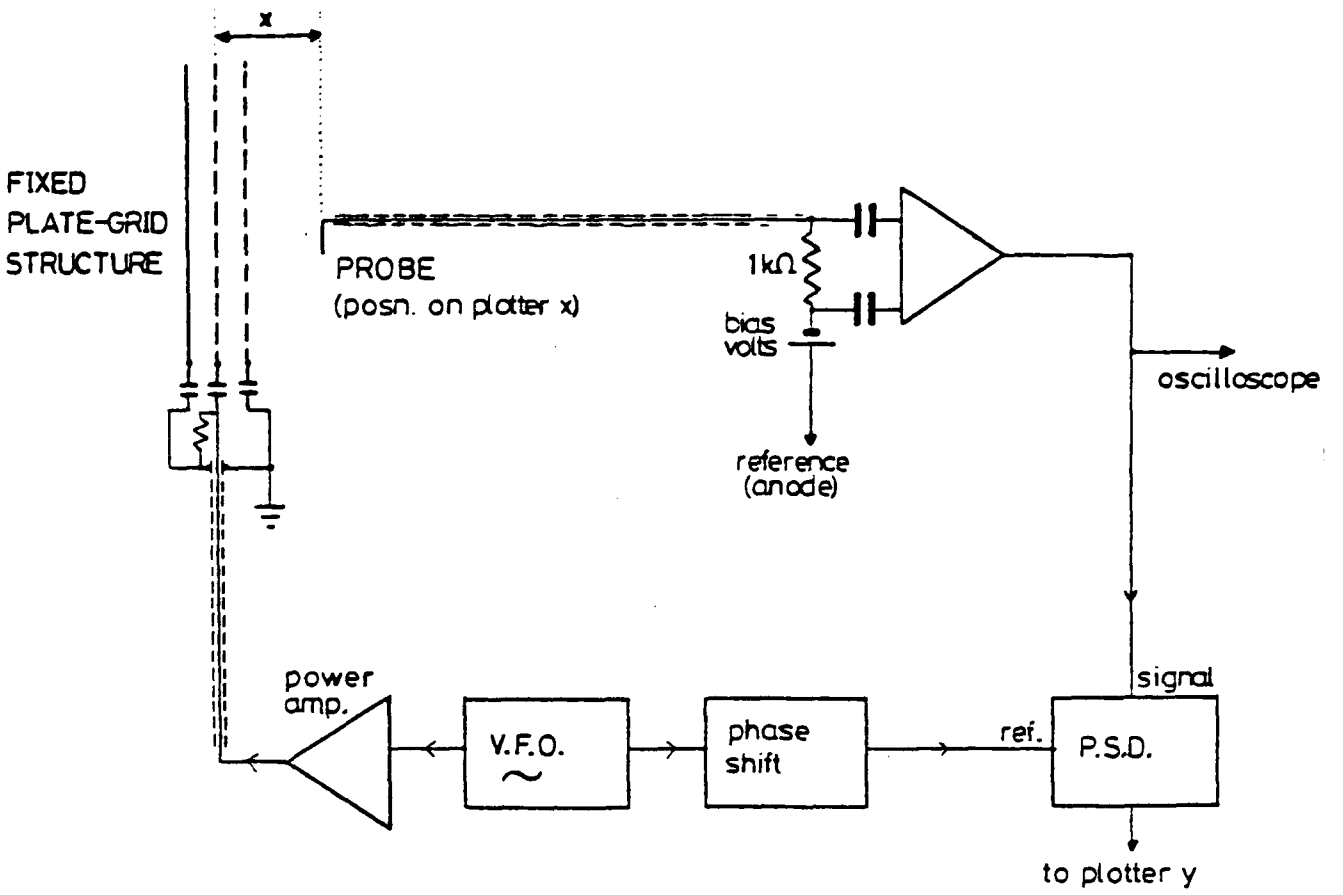


Figure 4.6

Experimental arrangement for continuous ion acoustic wave measurements. The phase-sensitive detector (P.S.D.) acts as an interferometer.

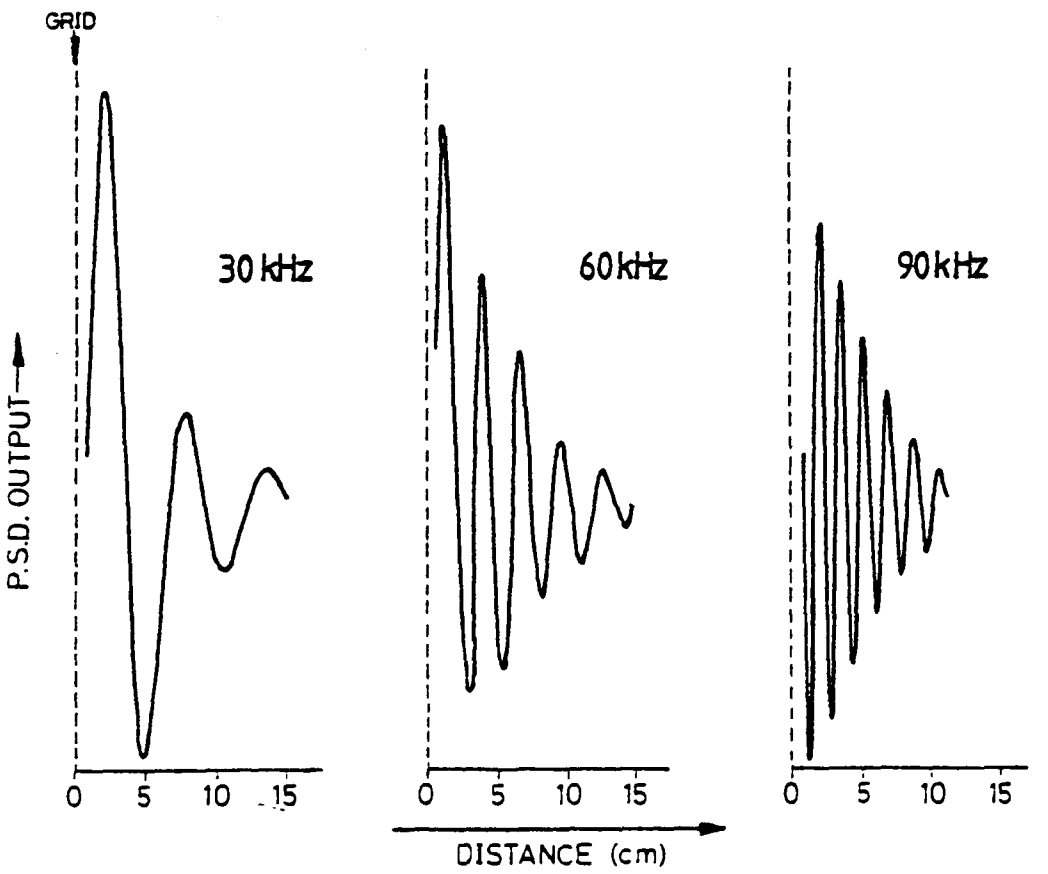


Figure 4.7

Interferograms produced for different frequencies applied to the exciter (propagation away from plate).

the device fairly near to the end wall. The measured wave speeds are thus local ion acoustic speeds in the wall presheath. Similar wave velocity changes due to plasma drifts have been observed previously (JONES and ALEXEFF, 1965, AKSORNKITII et al, 1969, MISRA and SCHOTT, 1973).

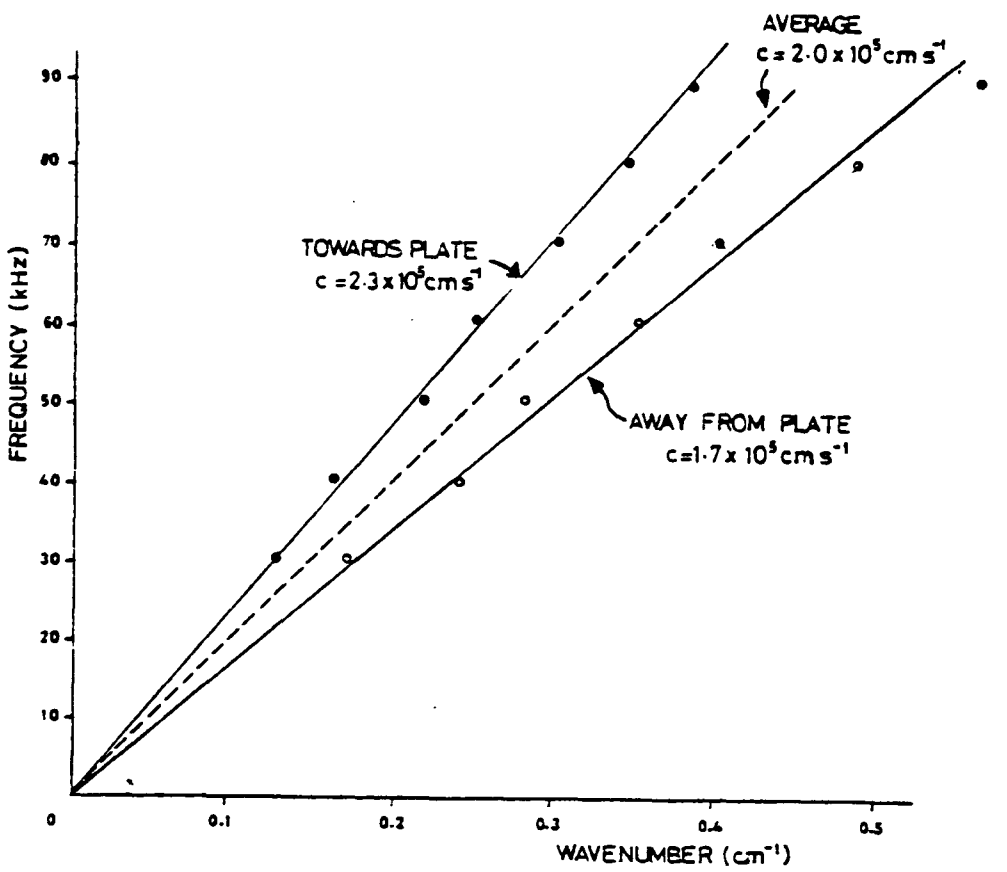


Figure 4.8
Frequency-wavenumber plot for ion acoustic wave propagation in opposite directions with respect to the plasma.

The ion acoustic wave speed c_s is found to be $2x10^3 ms^{-1}$ and the plasma drift speed is approximately $0.3x10^3 ms^{-1}$. From $c_s=(kT_e/M)^{1/2}$, the electron temperature is about 1.5eV. However, we have seen (Section 4.2) that the electron velocity distribution approximates to the superposition of two Maxwellians, so we shall now consider the theory of the propagation of ion acoustic waves in a two electron temperature plasma in order to check the experimental results. This treatment is due to JONES et al (1975).

From the fluid equations (2.1) to (2.3) with zero ionization for each of the three species (cold ions and two species of warm electrons at temperatures T_h and T_c) and using Poisson's equation the dispersion relation for ion acoustic waves is :

$$1 = \sum_{i,h,c} \frac{\omega_p^2}{(\omega^2 - \kappa^2 v_t^2)} \qquad (4.6)$$

where i, h and c refer to the three species as above, ω_p and v_t denote the plasma frequency and r.m.s. velocity for each species. The ion r.m.s. velocity is zero.

This equation may be reduced to

$$(\frac{\omega}{\kappa})^2 = c_s^2 = \frac{kT_{eff}}{M} \qquad (4.7)$$

where the effective electron temperature is given by:

$$T_{eff} = \frac{(n_c + n_h)T_c T_h}{(n_h T_c + n_c T_h)} \qquad (4.8)$$

Thus the presence of two electron groups causes a modification to the ion acoustic speed, though only one mode exists. It is interesting to note that if two warm ion species are present, two ion acoustic modes may propagate depending on the ion mass ratio (NAKAMURA et al, 1976).

Substituting our measured (Section 4.2) values of n_c, n_h, T_c and T_h into equation (4.8) gives a value for T_{eff} of 1.5eV, in excellent agreement with the temperature deduced from the measured ion acoustic wave speed. It would appear that the two-temperature description is a reasonable aproximation since the ion acoustic wave speed agrees with a detailed examination of the electron velocity distribution function.

4.4 ION ACOUSTIC PULSE PROPAGATION

To complement the results of the previous Section, and as a preliminary to the moving sheath experiments described in Chapter 5, the propagation of low-amplitude ion acoustic pulses was studied using a time-of-flight technique. Half sinusoidal pulses (negative and positive, 30V amplitude, 5-10μs width) were applied to the same transmitter as that used for the continuous wave propagation experiments, and again fluctuations in electron saturation current to the axial probe were measured. The pulse generator and receiver circuits are shown in Figure 4.9. In this experiment a boxcar detector, the operation of which is described in Section 5.2.2, was used to average the received signals over many experimental pulses. A typical output time constant was 300ms compared to a sweep time of the sampling gate across the experimental time base of 30s. Fluctuations in electron saturation current were plotted as a function of time for various transmitter-receiver separations. In this way the time of flight, and therefore the speed, of ion acoustic pulses could be measured.

Figure 4.10 shows results for negative excitation, the applied signal having a peak value of -30V from floating potential as shown in the top trace. The plasma response at various exciter-receiver separations is shown in the diagram, and a region where the plasma density is lower than its steady-state value arrives at later times for increased separations. This signal, which is shown by a dotted line, corresponds to an ion acoustic rarefaction pulse propagating into the plasma. The speed of this pulse agrees with the speed of continuous ion acoustic waves moving away from the exciter (Section 4.3).

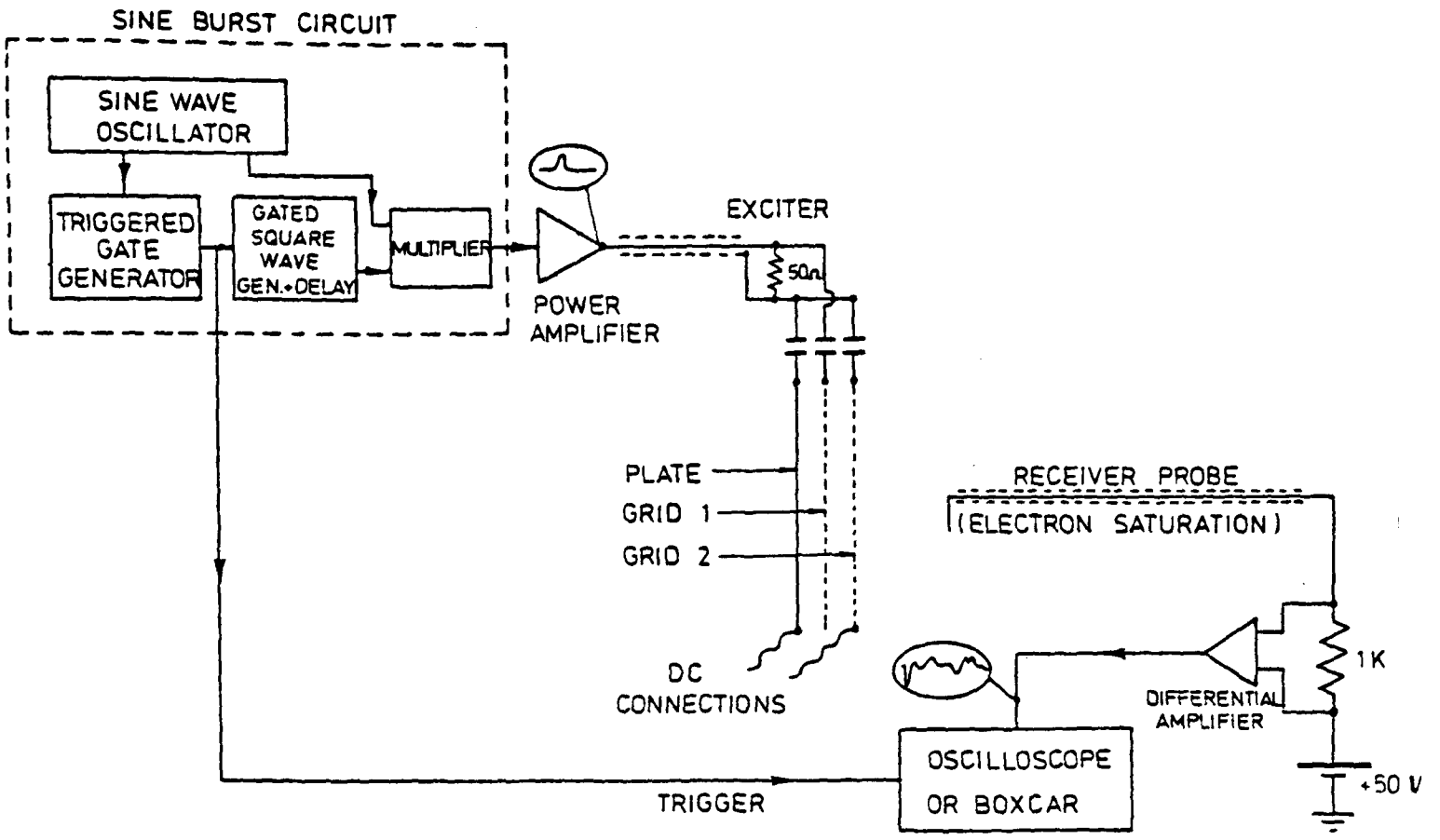


Figure 4.9

Pulse generator and receiver circuits for pulsed ion acoustic wave experiments.

Figure 4.11 shows the response of the plasma to a positive pulse as a function of time, for various transmitter-receiver separations; clearly the situation is more complex than the previous negative pulse case. Three main features are apparent. The first is a large "directly-coupled" signal observed on the receiver at the same time as the pulse is applied to the transmitter; secondly a compression pulse, shown by the dotted line, propagates into the plasma at the ion acoustic speed; thirdly a more complicated and apparently propagating structure, emphasized by the vertical broken line, is observed at later times. The apparent speed of the third structure is approximately $7c_s$. Note that in this situation the ballistic effects (or pseudowaves) usually associated with grids are not expected because part of our transmitter was a solid plate (see Figure 4.6).

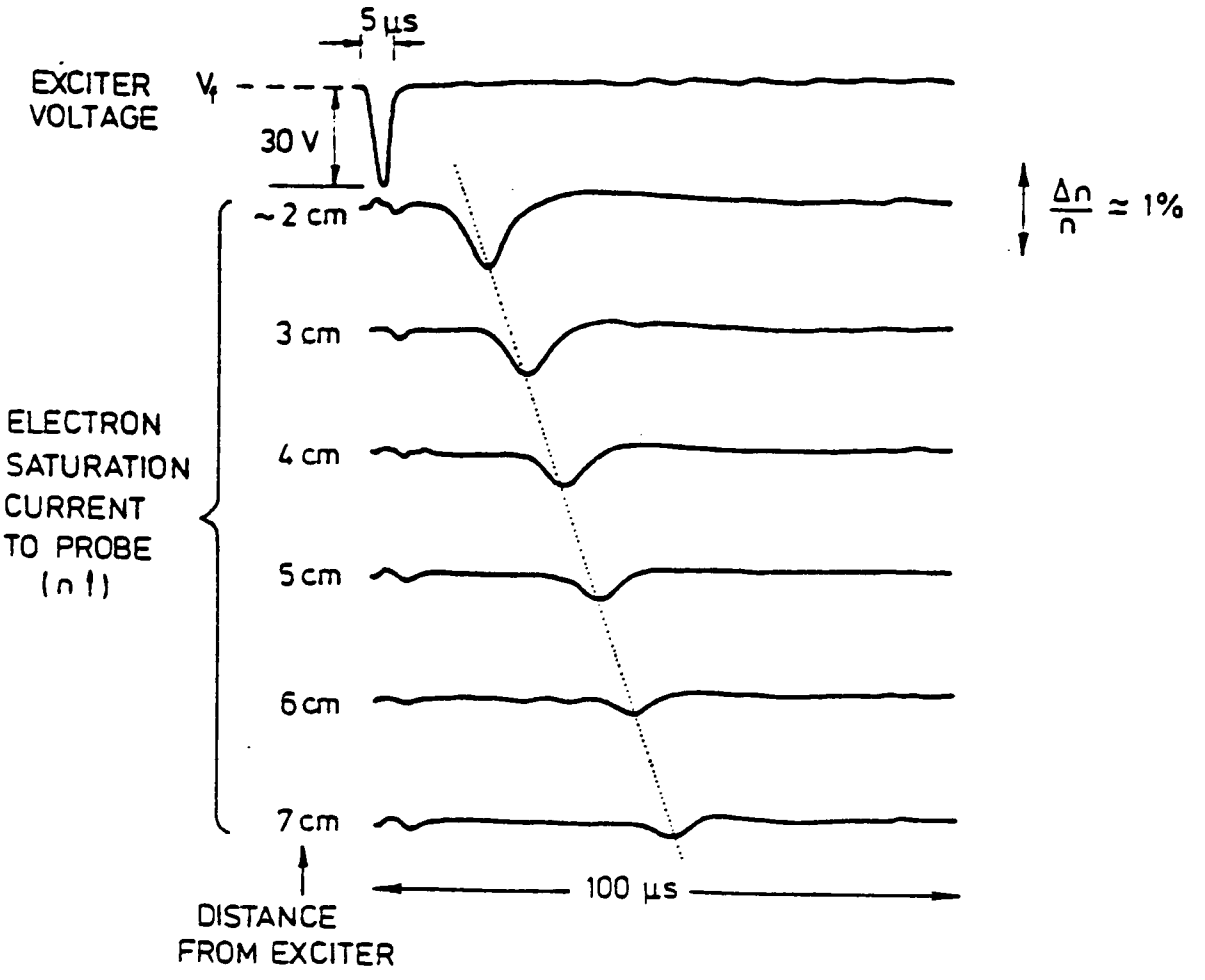


Figure 4.10

Plasma response to negative pulse (top trace) at various exciter-receiver separations. The rarefaction pulse is indicated by a dotted line.

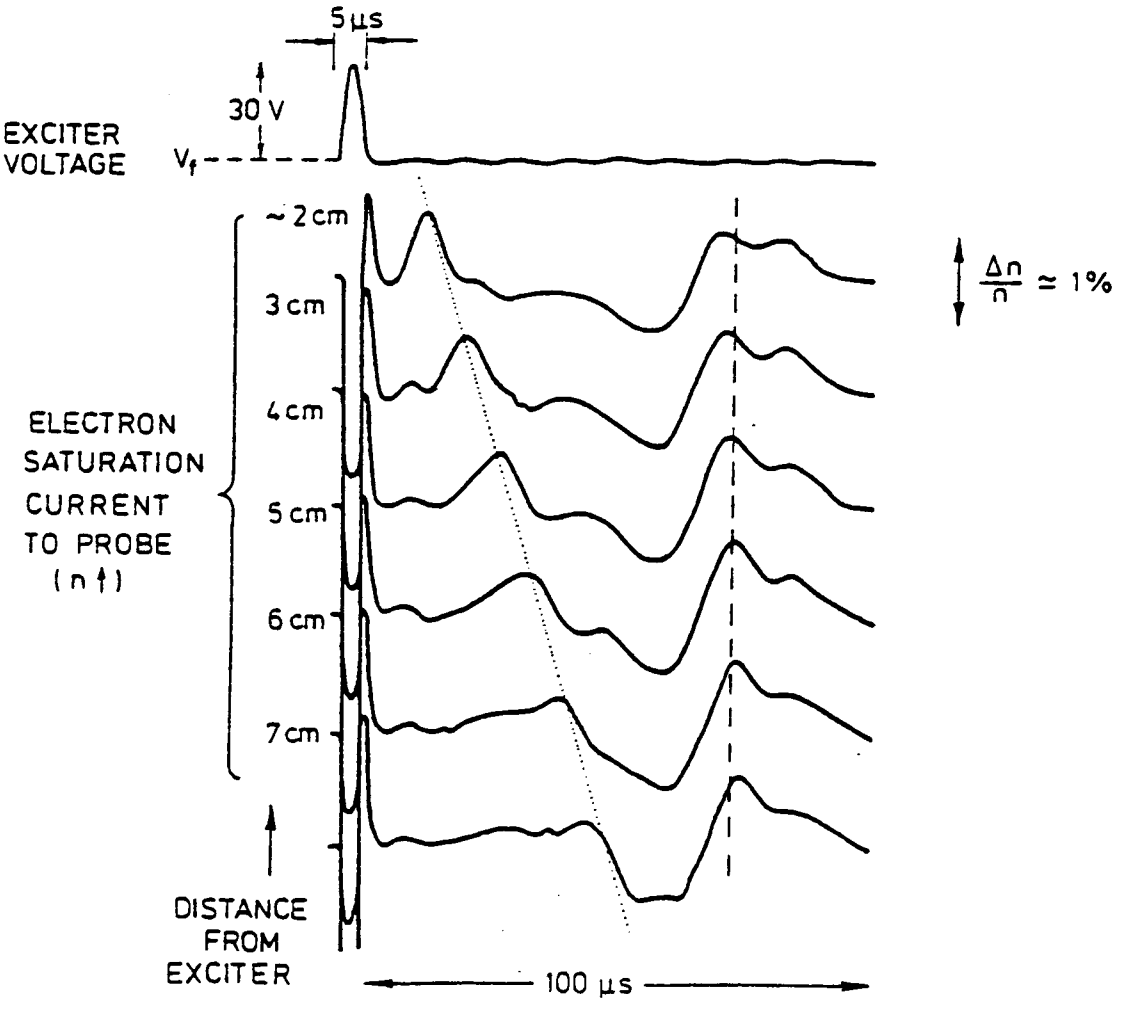


Figure 4.11

Plasma response to positive pulse (top trace) at various exciter-receiver separations. The compression pulse is indicated by a dotted line and the "fast" pulse is emphasized by a broken line.

A distance-time diagram of the rarefaction, the compression and the "fast" signal reveals that the compression arrives slightly more quickly than the rarefaction (Figure 4.12), and that a long time delay precedes the first peak of the "fast" signal. The speeds of the compression and rarefaction pulses were both in very satisfactory agreement with other measurements of the ion acoustic speed.

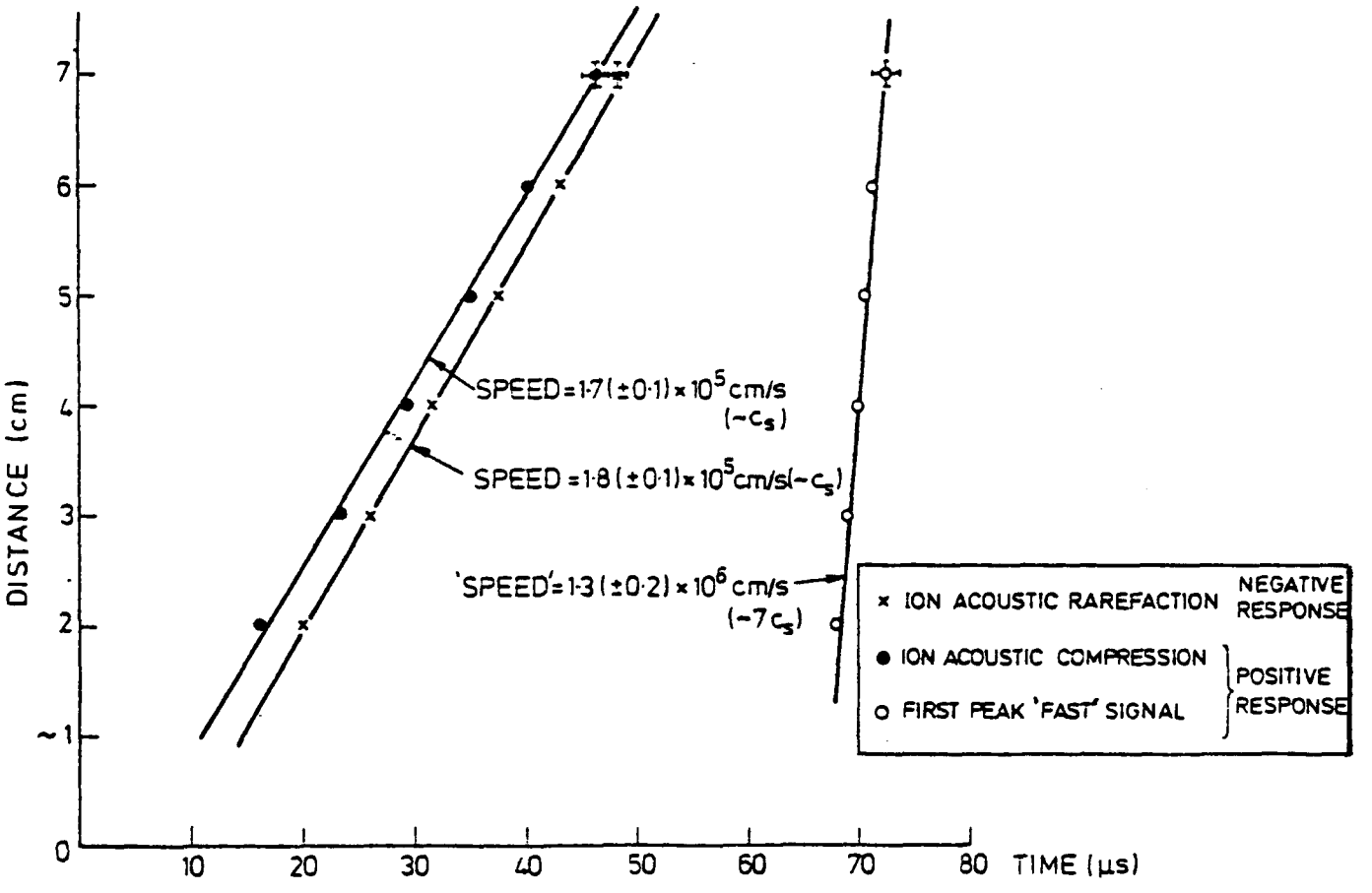


Figure 4.12
Distance-time results from ion acoustic pulse experiments.

In order to investigate the "fast" signal further, the pulse voltage was varied and the plasma response measured at a fixed position (see Figure 4.13). These results show that if the applied voltage is $\leqslant$+10V, the "fast" signal and also the direct coupled signal disappears. The ion acoustic signal (labelled I) was, in contrast, present for all voltages.

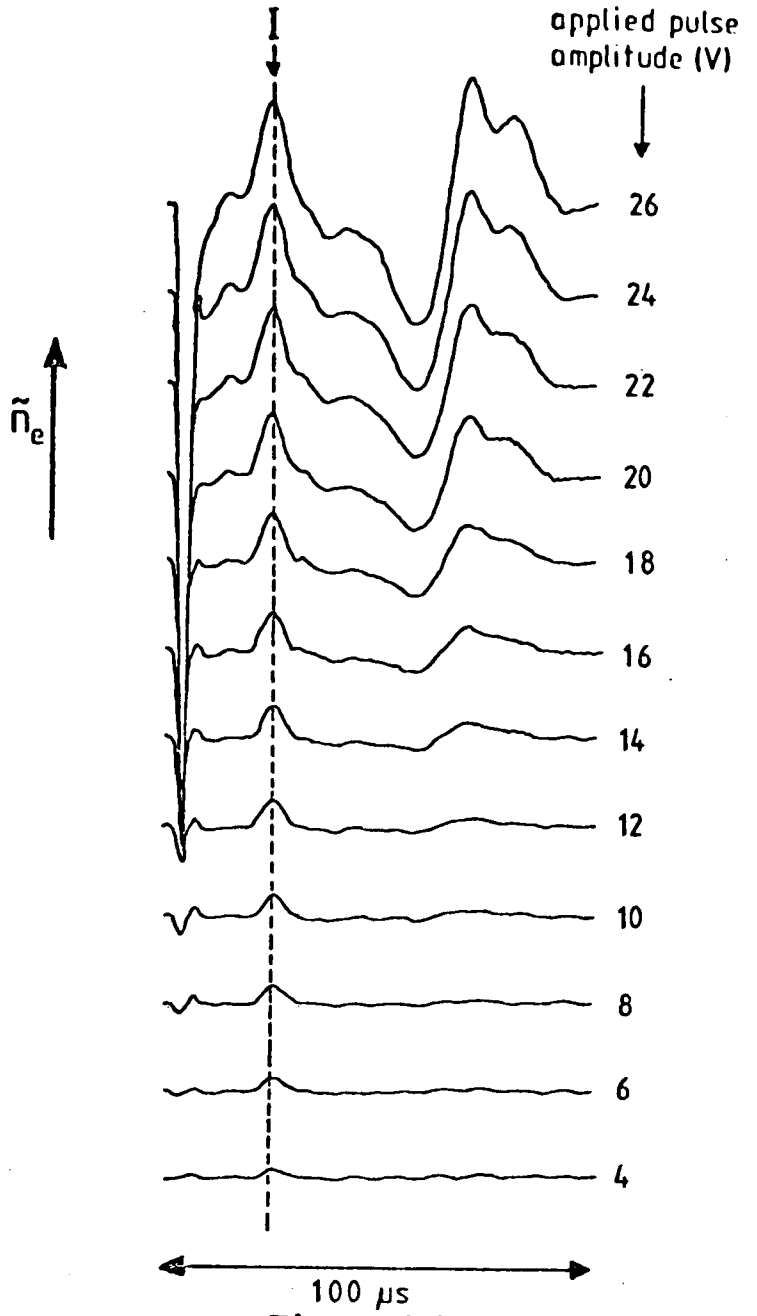


Figure 4.13

Plasma response to various amplitudes of positive excitation as in Figure 4.11 at a constant exciter-receiver separation of 3cm. The ion acoustic wave response is labelled I.

The radial variation of the response was measured by inserting a radially movable Langmuir probe and using the same detection technique as previously. The axial distance was kept constant and the response was measured at various radial positions from the axis of the device outwards. The results are shown in Figure 4.14, where it is seen that the "fast" structure splits into two separate components as the angle increases. A rarefaction is detected at earlier times and a compression at later times. This corresponds with the probe being nearer to one wall and further away from the other.

Such results lead to the conjecture that wall-excited waves are being produced. The disturbance due to the application of a pulse reaches the wall very quickly through the direct coupled signal, where its effect is to launch a cylindrically converging ion

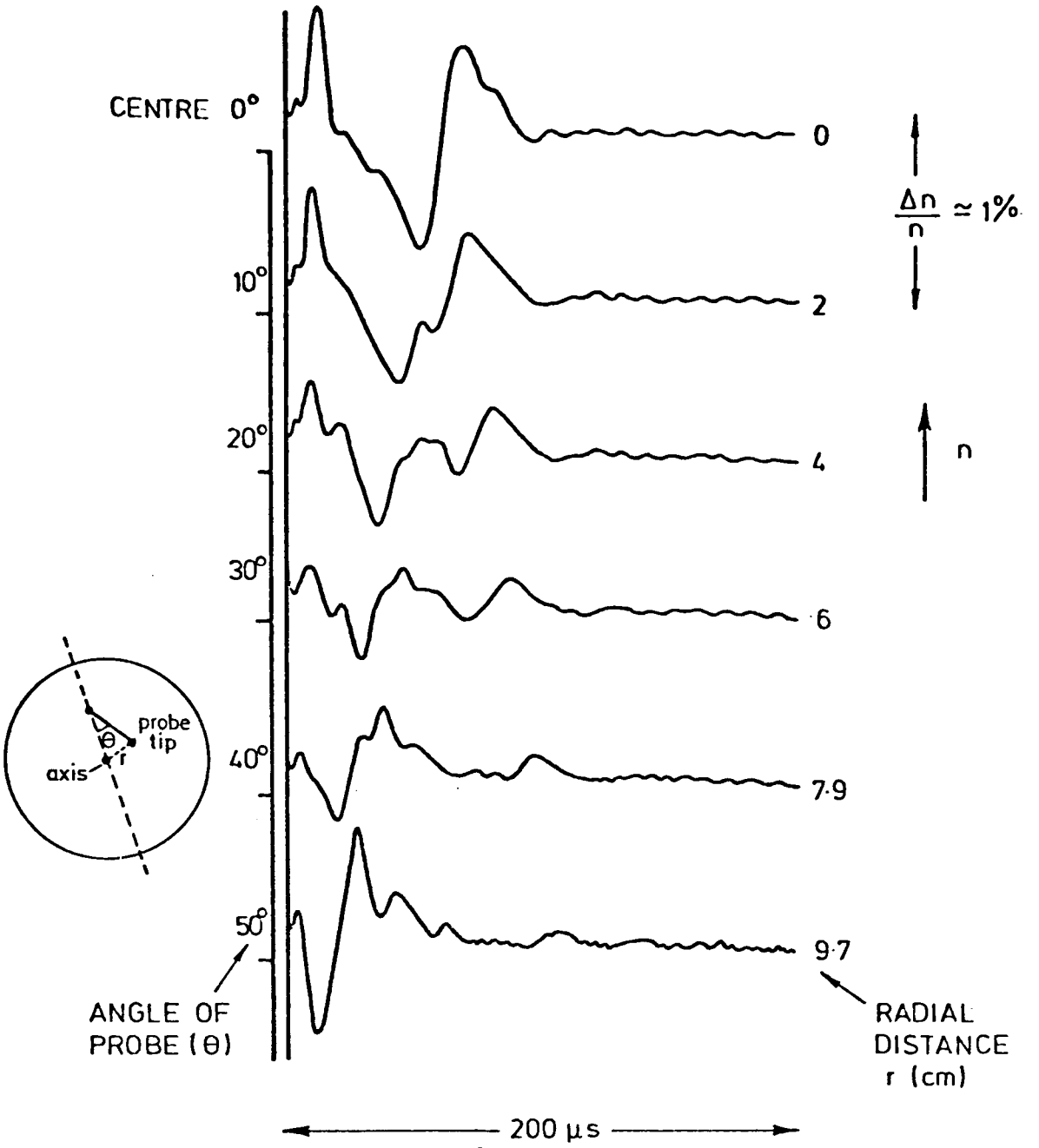


Figure 4.14

Plasma response at various radial probe positions to positive excitation (axial position constant at 2cm). The "fast" signal splits into two components with increasing θ.

acoustic pulse which is observed on the axis after a long delay time. This explanation agrees with all the observations.

Further investigation reveals some details of the mechanism. There is a transient change (increase) in floating potential on a probe during the direct coupled signal; plasma potential also increases. These effects occur with a delay time of ~0.2μs from the start of the applied pulse, corresponding to electron thermal time scales. This is now thought to be the explanation of the direct coupled signal. The increase in plasma potential is effected by a large transient electron current flowing to the transmitter causing a depletion of electrons in the plasma. This current is only drawn when the applied voltage exceeds the steady plasma potential, and the transient current taken by the transmitter is found to be $\geq$20% of the discharge current in this case. The effect on plasma

potential at the wall is then equivalent to applying a pulse to the chamber wall itself, which then acts as a transmitter but only if the applied voltage exceeds plasma potential in agreement with observations.

It is evident that care must be taken when applying positive voltage pulses to electrodes in plasmas. If a large electrode is used, large electron currents may be drawn which transiently change the plasma potential. The potential difference between the plasma and any object in it, including the containing wall, is thus changed almost instantaneously. This in turn causes the generation of an ion acoustic wave due to the motion of a sheath. Cylindrically converging ion acoustic waves may be observed.

The apparent axial propagation of the pulse, which might be expected to occur at a constant delay time for various axial probe positions, may be understood by considering the radial plasma drift speed towards the walls of the device. In further experiments this drift speed was measured by the propagation of ion acoustic waves from an axial probe to another probe near the wall of the device. By the reverse wave propagation technique it was discovered that there was an axial gradient of radial drift speed. The ion acoustic transit time from the wall probe to the axial probe agrees well with the delay time observed for the "fast" feature. In further experiments, evidence of a similar signal propagating from the end wall of the device was observed.

With a smaller probe as the transmitter (a 4mm diameter sphere), a radially propagating feature similar to that described above was again observed. For this experiment, the plate-grid system was removed from the device. The measured current, for the

same applied voltage pulse, was about 5% of the discharge current. Apparently care must be taken even with small transmitters.

4.5 DISCUSSION AND COMPARISON OF RESULTS

The experimental results discussed in this Chapter consistently indicate that the electron velocity distribution function is non-Maxwellian. An increase in the number of high energy electrons, approximating to a two-temperature distribution, is observed. It is thought that these high-energy electrons are not energy-degraded primaries, as these are thought to have a distribution which is spread-out in energy (GOEDE et al, 1980). They may be some secondary population, either due to a second ionization process (possibly involving a metastable state) or else secondary electrons from the walls caused by electron bombardment (COAKLEY and HERSHKOWITZ, 1980).

The observed axial and radial plasma drifts (speeds up to 20% of c_s) are not surprising since the multidipole device provides only a finite containment chamber. Production and loss processes balance to provide an equilibrium density profile (see Chapter 2) since volume recombination is negligible. The presence of a large plate-grid structure in the centre of the plasma with its associated sheaths may lead to further drifts. Evidence for drift towards a plate will be presented in Chapter 5. Note that the neutral gas drift speed towards the pump is negligible compared with the measured axial drift speed.

The ion acoustic wave speed measurements, which indicate the importance of taking the low-energy electrons into account, form an important basis for the moving sheath experiments to be discussed in Chapter 5. The agreement between the continuous and pulsed ion acoustic wave speeds is convincing.

In the case of positive pulse excitation the wall-excited waves are an interesting feature. When our experiments had been completed and the behaviour explained, it was found that previous experiments had observed the same phenomenon (CHRISTENSEN and HERSHKOWITZ, 1977) and a similar explanation to ours had been presented (NAKAMURA and NOMURA, 1978). Our experimental results are more complete because neither of these papers gave a radial probe scan. Since that time, the method of perturbation of plasma potential to create ion acoustic waves has been used to study nonlinear converging ion acoustic waves (SCHOTT, 1980a) and collisions of ion waves excited in opposite directions (NAKAMURA et al, 1980). Another experiment relevant to this work is the reflection of linear and nonlinear converging ion acoustic pulses on the axis of a multidipole device (TSUKABAYISHI et al, 1981). In this work it was shown that for a linear pulse a phase change of $\pi/2$ was produced on reflection. These results are supported by our own experiments (see Figure 4.14) where there is a phase change between the early time pulse and the late time pulse.

4.6 SUMMARY OF PLASMA PARAMETERS

The results of this Chapter are now summarized; all of the experiments used the multidipole device connected using Method A (Section 3.3). We conclude with a discussion of the effects on the

plasma of using Method B.

4.6.1 Summary

Langmuir probe characteristics (direct and second derivative) and ion acoustic wave measurements have been described. Normal running conditions were used as indicated in Section 3.4. The following results were found, and some derived quantities using our experimental values are included here for completeness.

ELECTRONS:	$T_h \simeq 2.7eV$, $T_c \simeq 1eV$
	$T_{eff} \simeq 1.5eV$, $n_c \simeq n_h$
ION ACOUSTIC WAVE SPEED:	$c_s \simeq 2.0x10^3\ ms^{-1}$
PLASMA DRIFT SPEED:	$v_d \simeq 0.3x10^3\ ms^{-1}$
ION TEMPERATURE:	< 0.1 eV (assumed)
PLASMA DENSITY:	$n \simeq n_e \simeq n_i \simeq 1x10^{15}\ m^{-3}$
IONIZATION FRACTION:	$n_i/n_a \simeq 10^{-4}$
DEBYE LENGTH:	$\lambda_d \simeq 0.3$ mm
ELECTRON PLASMA FREQUENCY:	$f_{pe} \simeq 300$ MHz
ION PLASMA FREQUENCY:	$f_{pi} \simeq 1$ MHz
ELECTRON THERMAL SPEED:	$v_{te} \simeq 5x10^5\ ms^{-1}$
ION THERMAL SPEED:	$v_{ti} \simeq 2.5x10^2\ ms^{-1}$

We also note some relevant mean free paths and collision frequencies (from von ENGEL, 1965 and BROWN, 1966) for argon at a pressure of $3.5x10^{-4}$ torr:

e_{2V}	$- e_{2V}$ (COULOMB)	$\lambda_c \simeq 100m$	$\nu_c \simeq 6x10^3 Hz$
e_{2V}	- A (TOTAL)	$\lambda_{es} \simeq 1.6m$	$\nu_{es} \simeq 4x10^5 Hz$
e_{50V}	- A (TOTAL)	$\lambda_{ef} \simeq 0.8m$	$\nu_{ef} \simeq 4x10^6 Hz$
e_{50v}	- A (IONIZATION)	$\lambda_i \simeq 1.9m$	$\nu_i \simeq 1x10^6 Hz$
A^+	- A (CHARGE-EXCHANGE)	$\lambda_A \simeq 0.18m$	$\nu_A \simeq 1x10^4 Hz$

DEVICE SCALE-LENGTH L≃0.7m

The plasma may be regarded as collisionless for our purposes since the electron mean free paths are greater than the distances of interest. In addition the charge-exchange mean free path is much longer than the wavelengths of interest though this process may cause collisional damping of ion acoustic waves. Had we decreased the neutral pressure still further (which is quite possible in this device) the effect would not have been so important and any collisional damping could have been detected.

The long ionization mean free path (λ_i) compared to the machine dimension L means that the primary electrons must be confined by the wall magnetic fields. In this way sufficient ionization is produced to sustain the plasma.

4.6.2 Effects Of Different Anode Connections

All the above experiments were conducted with the mesh grids as anodes (Method A, Section 3.3). We shall now consider the differences in the results when the earthed vacuum chamber was used as the anode (Method B).

From Langmuir probe experiments, a non-Maxwellian electron velocity distribution was still present with temperatures and densities approximately the same as those already described. Plasma potential was about -15V with respect to the anode; this value was found with the higher discharge voltage of 70V which was necessary in this mode. Also an earthed probe tube had a more marked effect on plasma potential in this configuration, since any earthed object in the plasma acted as an extension of the anode. It is worth

noting here that the different probe tip (tantalum) used in Method B was more prone to hysteresis than the copper probe used in method A. Tantalum was used to reduce secondary emission and, particularly, sputtering (see Chapter 5).

Ion acoustic wave and pulse experiments gave very similar results to those described above despite the use of a simple plate transmitter (as opposed to the more complicated grid structure used in this Chapter). Wall excited ion acoustic waves were also observed.

In conclusion, there were no significant differences, apart from plasma potential, between the plasmas produced by the different methods A and B.

CHAPTER 5

EXPERIMENTS ON MOVING SHEATHS

5.1 INTRODUCTION

New experiments performed to examine the effects of moving the edge of an ion-rich sheath formed on a plane probe will be described. The theory of this process was considered in Chapters 1 and 2, while previous experimental work was discussed in Chapter 1.

The basic experimental technique used here is the application of negative (with respect to plasma potential) voltage ramps, either decreasing or increasing with time, to a large plate in the multidipole device. The edge of the ion-rich sheath is moved a distance of order centimetres at a speed less than c_s either away from or towards the plate. In this way the effects of expanding and collapsing the sheath are studied separately. Electrical and optical probing techniques are used to measure the propagation of the associated plasma disturbances.

The Chapter begins with a description of the design of the experiment and of the diagnostics. The next Section concerns ion rarefaction wave generation by slow and fast negative-going ramp voltages applied to the plate. Similar experiments on ion

enhancement waves produced by positive-going ramp voltages (the voltage never exceeding floating potential) are then discussed. The results of some optical measurements are considered; these show that with the high negative voltages applied to the plate in these experiments surface ion bombardment effects cannot be ignored. An increase in the light emission from the high voltage sheath region is observed. The final Section summarizes the experimental results.

5.2 EXPERIMENTAL TECHNIQUES

The multidipole device was used with the chamber walls as anodes (Method B Section 3.3.2) for all the following experiments except where explicitly stated. The arrangement of the plate and probes is indicated in Figure 5.1.

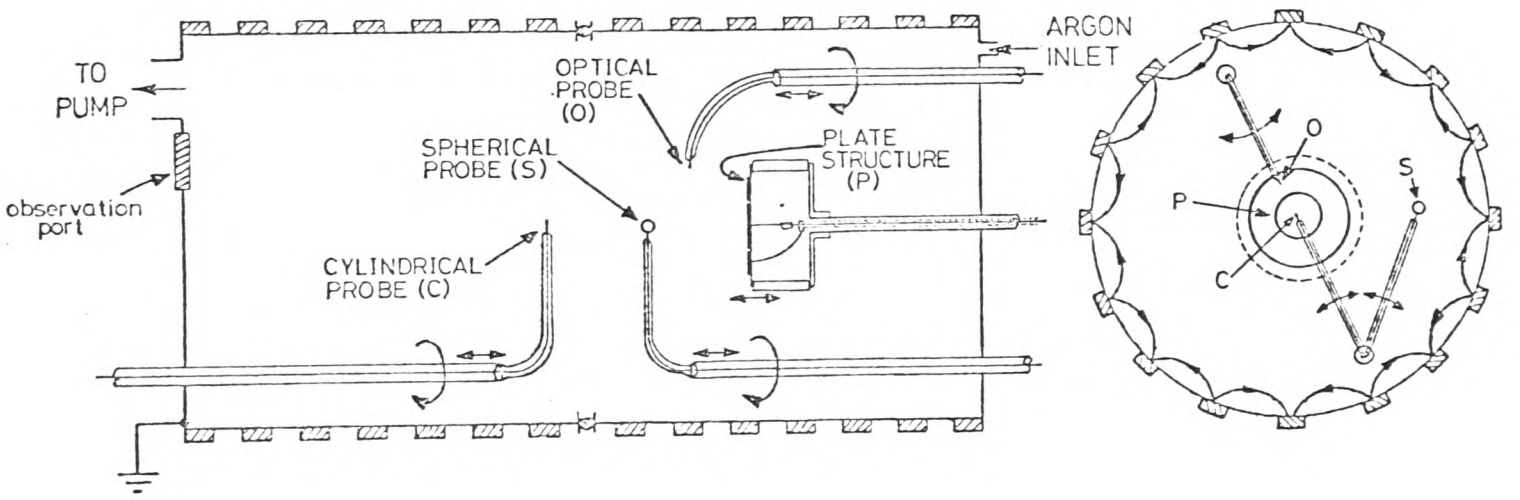


Figure 5.1
Probe configuration in the Method B anode arrangement as used in this chapter.

5.2.1 Details Of Construction

A detailed view of the plate assembly is shown in Figure 5.2. This assembly was mounted on the motor-driven axial probe tube. Electrical connections were made using semi-rigid coaxial cable

passing through a Ferranti seal soldered to the outer end of the tube. High negative voltage (up to -2kV) pulses were applied to both the inner and the outer of the coaxial cable which was insulated from the earthed probe tube using a glass tube. Two electrical connections were made to the guard-ring structure of the plate itself via tantalum wires spot-welded to the rear surfaces of the tantalum plates. The guard-ring arrangement consisted of a concentrically mounted 4cm disc and an 8cm diameter annulus spark-eroded from 0.5mm tantalum plate. These were mounted in a recessed PTFE holder of diameter 10cm. The whole structure was mounted on a 10cm diameter stainless steel disc support using insulating posts. Much of the earthed metal surface of this assembly was covered with ceramic cement to avoid drawing electron currents from the plasma.

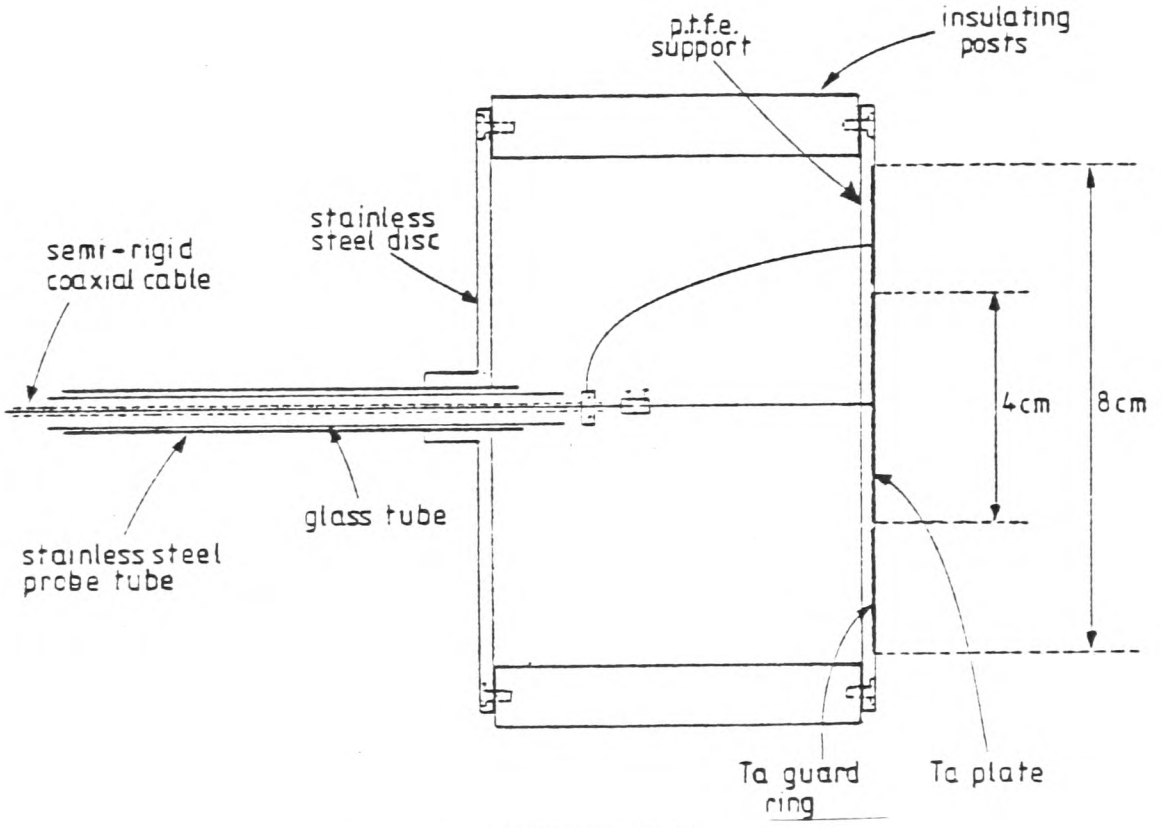


Figure 5.2
Construction of the exciter plate.

The choice of tantalum for the plate material will now be discussed. The secondary emission coefficient under 1keV A^+ bombardment is not significantly different to that of other materials (0.1-0.7 electrons per incident ion, KAMINSKY, 1965) but the sputtering rate is about 1/20 that of copper and 1/4 that of

nickel (COBINE, 1958). Further data is given by CHAPMAN (1980). Copper was used in preliminary measurements of moving sheaths (COATES, 1979) and nickel was used in similar experiments by PREWETT (1974) and WICKENS (1980). Thus there was expected to be less damage to the plate itself and also less contamination of nearby surfaces (e.g. insulators and probe supports) upon the application of large negative voltages.

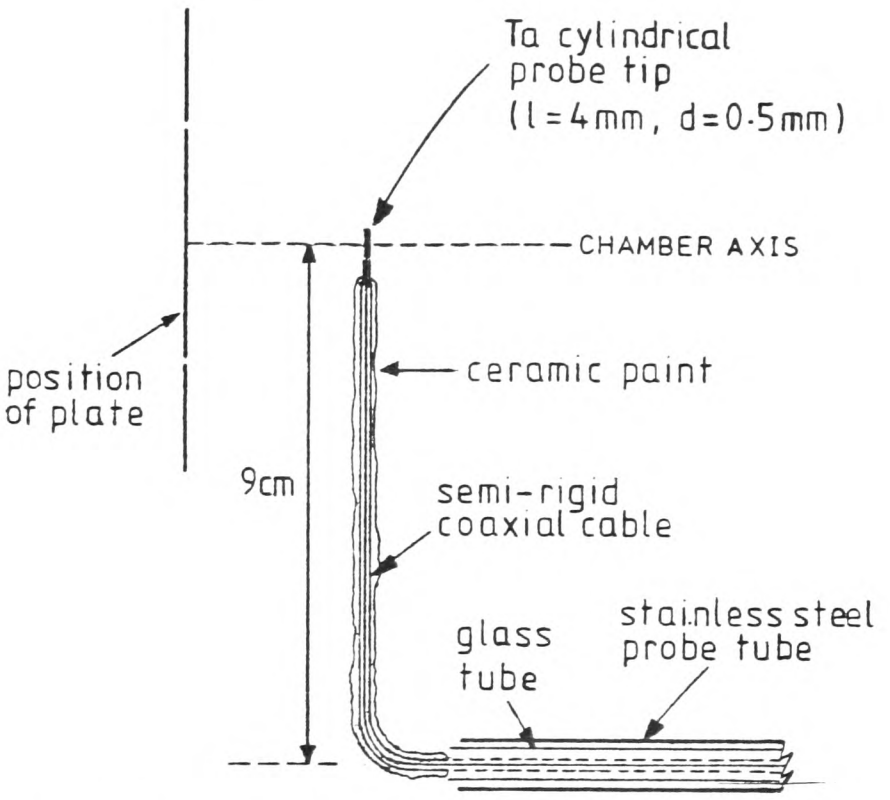


Figure 5.3
Construction of the cylindrical Langmuir probe.

The construction of the receiver probe is illustrated in Figure 5.3. The probe was mounted such that its insulating support was perpendicular to the axis of the plate (c.f. PREWETT (op. cit.), WICKENS (op. cit.) and COATES (op. cit.) all of which had the probe support parallel to the plate axis). A cylindrical probe tip was used (PREWETT and WICKENS both used plane probes). Probe current-voltage characteristic experiments showed that the tantalum probe tip used here was more prone to hysteresis than the tinned copper probe tip used in Chapter 4. This was not thought to be important when measuring fluctuations in saturation current as in most of the following experiments. The decrease in electron saturation current after cleaning the probe with a very high

electron current is shown in Figure 5.4. Approximately one minute after cleaning, the probe current was nearly constant for an appreciable time. Data were taken during this period.

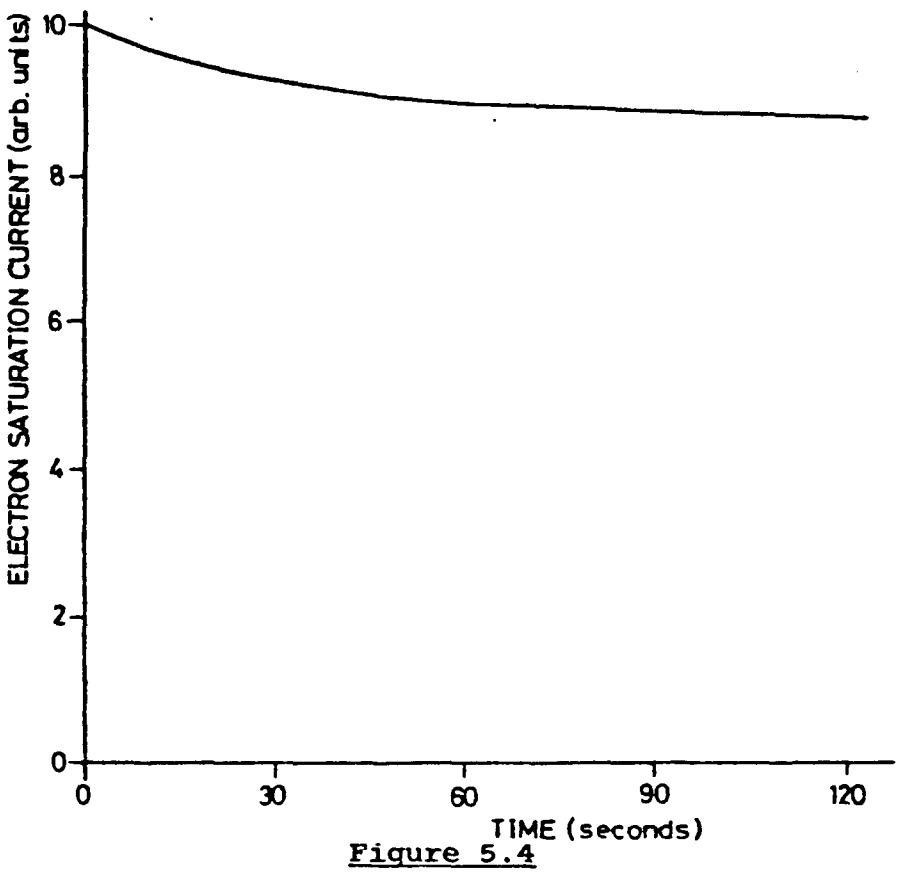


Figure 5.4

Decrease in electron saturation current with time after probe cleaning.

An emissive probe was used in some experiments. The construction of this was similar to that indicated in Figure 5.3 except that two coaxial cables were used and the heated filament consisted of a 10μm diameter Ta wire with an exposed length of 4mm.

The optical probe consisted of a quartz optical fibre with a silicone resin cladding manufactured by Quartz and Silice. The diameter of the core was 0.4mm and the total diameter was 0.85mm. This fibre was led into the vacuum chamber using a metal tube (see Figure 5.1) and was positioned 5mm from the plate and perpendicular to it. The fibre had a quoted numerical aperture of 0.17 giving a half angle for the acceptance cone of 9.8^{o} (see Figure 5.32). This limited the resolution of the optical probe which was originally inserted in an attempt to measure the propagation of the sheath edge. Despite the failure of these particular experiments, some interesting results were found using this technique (see Section

5.5).

5.2.2 Exciter And Receiver Electrical Circuits

In previous studies the negative exciter voltages for rarefaction wave experiments were large with a decaying exponential time dependence. Such single-shot waveforms were used by CHESTER (1970), PREWETT (op. cit.), WICKENS (op. cit.) and COATES (op. cit.), though WIDNER et al (1970) used a -50V "step function".

Some preliminary experimental results were obtained using anode connection Method A and a copper plate (i.e. similar to COATES (op. cit.)). A repetitive and approximately exponential negative voltage ramp was generated by discharging a capacitor with a thyratron switch. In an attempt to reproduce the results of CHESTER (op. cit.), it was found that detection of the wavefront was the most sensitive for a detector probe bias of >+10V with respect to plasma potential while the sheath edge was visible at a bias of <+5V. Previously (COATES (op. cit.)), some difficulty had been encountered in detecting the sheath edge and thus interpretation of the results was suspect. Electronic differentiation of the repetitive signal in these later experiments proved to be a sensitive detection technique, but the applied voltage waveform was not entirely reproducible, and it was decided to proceed with a different approach.

The requirements for the exciter voltage waveform were as follows:-

(i) Negative polarity, to ensure an ion-rich sheath

(ii) Linear voltage ramp, making comparison with theory possible

(iii) Variable rise times of order 100μs, to allow different sheath edge speeds

(iv) Repetitive waveform to allow signal averaging techniques rather than single-shot experiments

(v) Maximum voltage variable up to -2kV, current capability 10-20 mA, variable average voltage level

(vi) Negative or positive slopes, to allow expanding or contracting sheath experiments.

The circuit chosen to fulfil these requirements used a Servomex LF141 function generator (up to 10V truncated triangular waveform) and a Kepco OPS-2000 programmable operational amplifier power supply (2kV, 20mA) with a voltage gain of 200 (see Figure 5.5). The amplitude, rise time and repetition frequency of the output were controlled on the Servomex, while the output DC level was programmable on the Kepco. Thus it was possible to produce a linearly decreasing voltage (section A of the waveform) and a linearly increasing voltage (section B) in such a way that the effects of each could be studied separately. The quoted slew rate for the Kepco was 1V/μs, but experiments showed that the response remained fairly linear up to about 5V/μs. A convenient triggering signal for the measuring instruments was obtained from the triangular wave output on the Servomex.

The principal method used to detect plasma wave signals was that of measuring fluctuations in electron saturation current (i.e. in plasma density, see Section 5.7) in a similar manner to the ion acoustic wave experiments already described (Section 4.3) Signals were recorded either on an oscilloscope (Tektronix 551) or on an x-y plotter using a boxcar detector (Brookdeal Scan Delay

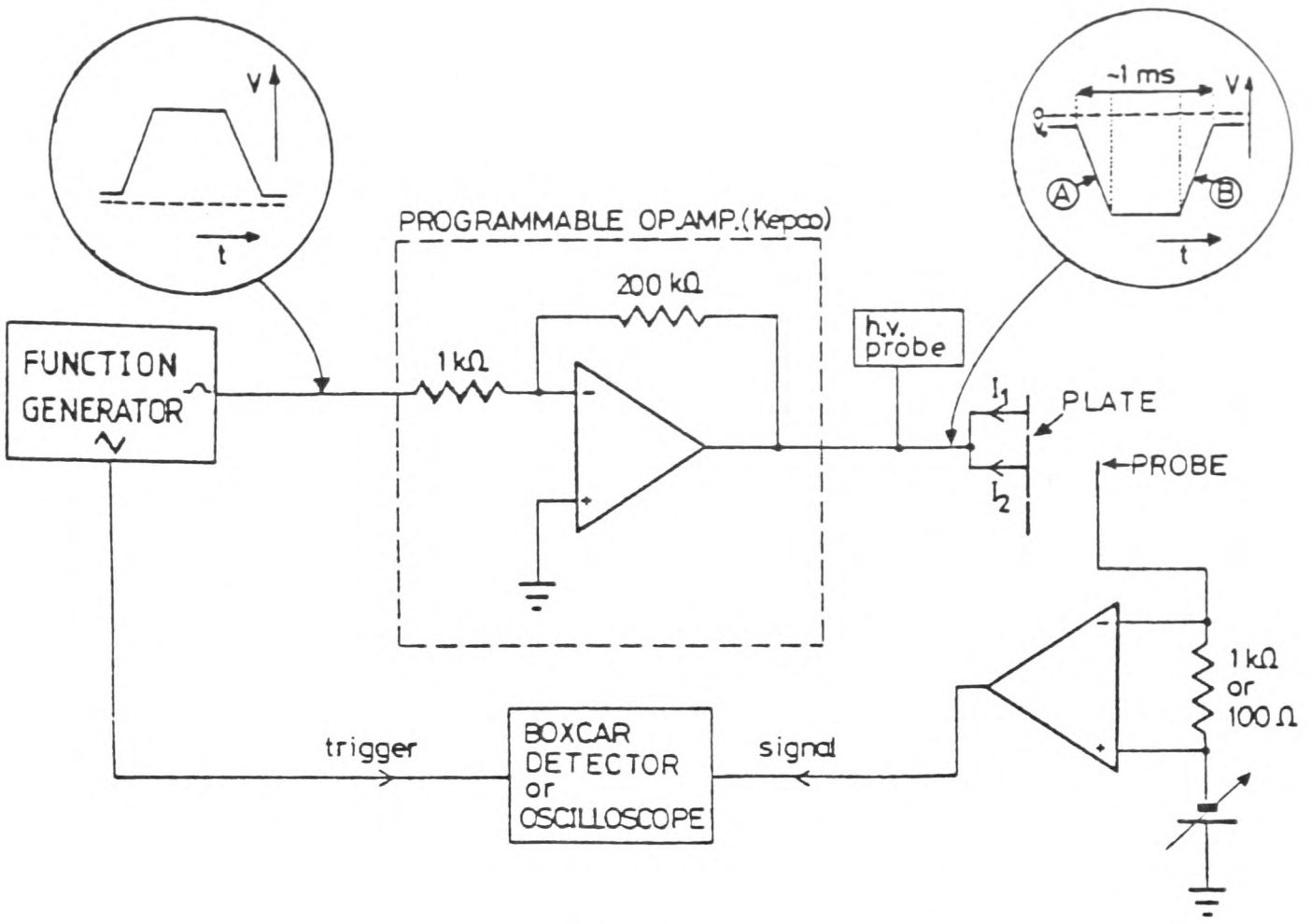


Figure 5.5
High voltage ramp generator and receiver probe circuits for slow ramp experiments.

Generator plus Linear Gate). The receiver electrical circuit is illustrated in Figure 5.5. The boxcar detector was used in two modes:-

(i) Scan mode, in which the delay time of a narrow sampling gate was automatically scanned with respect to the trigger pulse across a preset time window. An averaged waveform was thus built up on the plotter. The scan rate and output time constant were variable. The output on the x-y plotter was therefore electron saturation current as a function of time, and was effectively a sampled repetitive oscilloscope trace.

(ii) Single point mode, in which the narrow sampling gate was kept at a fixed (manually variable) delay time with respect to the trigger while the plate-probe distance was varied. The plotted output was then electron saturation current as a function of distance with time as the parameter.

Another technique was to take cold probe or emissive probe characteristics using the single point mode of the boxcar and varying the probe bias voltage. Using these methods it was possible to compare the temporal and spatial evolution of plasma density and potential in the vicinity of the moving sheath edge.

5.3 ION RAREFACTION WAVE OBSERVATIONS

It was predicted by the theory in Chapters 1 and 2 that ion rarefaction waves would be produced when an ion-rich sheath was expanded from an electrode. This Section discusses some corresponding experiments, using the portion A of the ramp waveform indicated in Figure 5.5. The results of applying a faster ramp voltage in the same sense are also discussed.

5.3.1 Slow Ramp

The range of ramp voltages applied here started from -70 V and increased to between -500 and -2200 V in a time of 100-800 μs. A wide range of 'slew rates' (i.e. $\frac{dV}{dt}$) was thus available, and qualitatively the results looked similar for the different waveforms apart from the speed of the sheath edge.

A typical oscillogram is shown in Figure 5.6, in which the top trace shows the applied negative-going voltage ramp and the second trace shows the output from the optical probe (described in Section 5.2.1) on these timescales. The light signal, which will be discussed in Section 5.5, consists of the following components on an arbitrary scale of 10:-

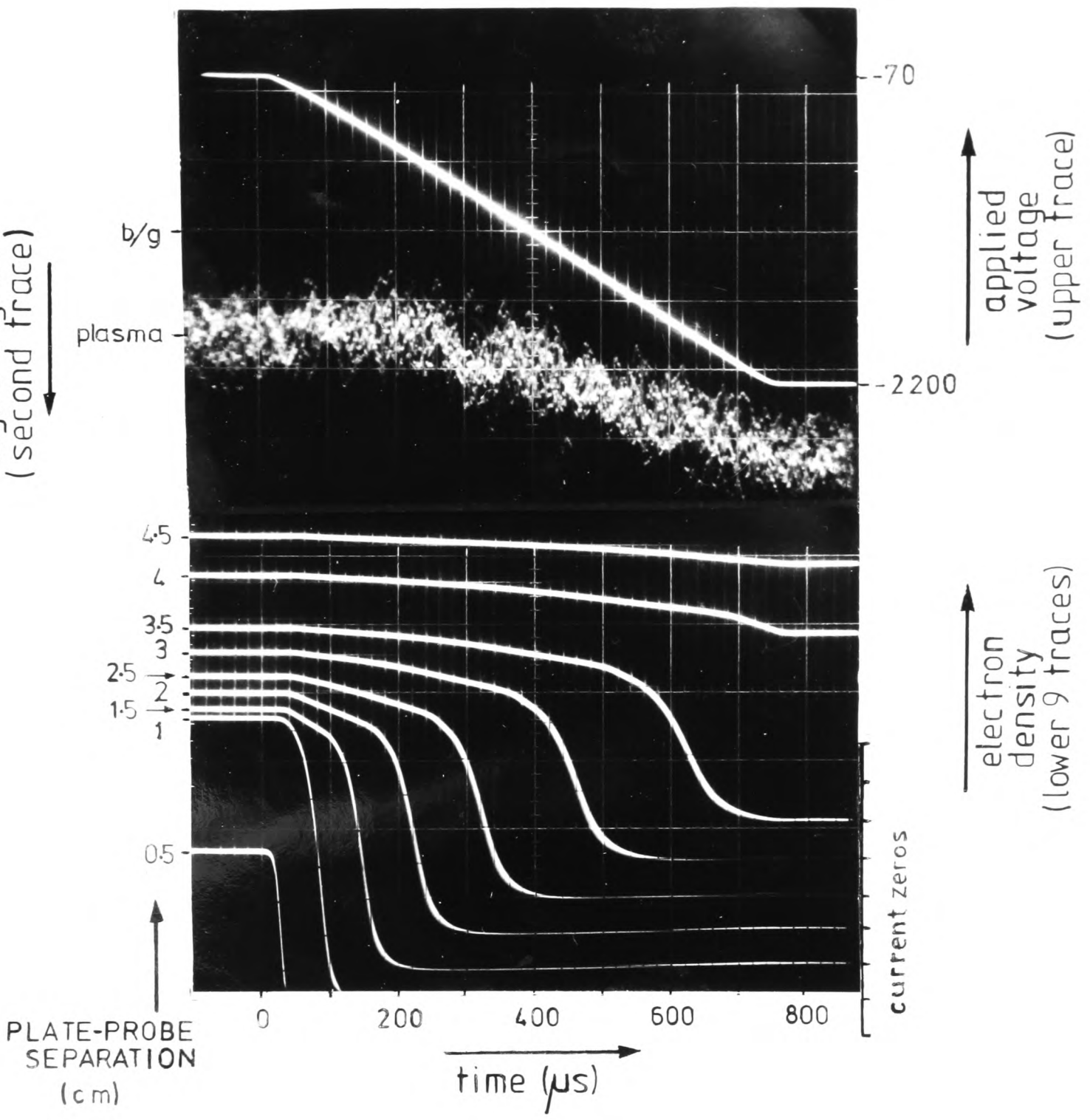


Figure 5.6

Oscillograms of applied voltage, light signal and electron saturation current during slow negative voltage ramp.

Dark noise	0.5 units
Filament light (background)	9 units
Plasma light	1 unit
Maximum signal	
(light increase for -2200 V)	1.5 units

From Figure 5.6 a measurable light increase is seen near the plate if the magnitude of the negative voltage exceeds 800V.

The nine traces at the bottom of Figure 5.6 all show electron saturation current to the Langmuir probe as a function of time in response to the ramp voltage. Upwards deflection indicates an increase in density, and the zeros of saturation current have been manually displaced for clarity. The probe is moved 0.5cm in a direction away from the plate between measurements, the trace shown at the bottom of the photograph corresponding to a plate-probe separation of 0.5cm. The results, which should be compared with those of CHESTER (see Figure 1.6) show the following features:-

(i) A plasma density decrease (the first "knee") occurs after a time which is approximately 10μs for the nearest trace but increases to about 60μs for the furthest trace.

(ii) For plate-probe separations greater than 1cm, a second density decrease (or "knee") is observed. The arrival time of this second knee also increases with distance away from the plate.

(iii) The electron saturation current collected by the probe ultimately reaches zero for plate-probe separations of less than 4cm.

The theory of Chapters 1 and 2 predicted a rarefaction front to precede the sheath edge moving into the plasma if the sheath edge speed was less than the local ion acoustic speed. In the oscillograms we identify the first knee as the rarefaction front and the second knee as the sheath edge. The electron saturation current falls to zero soon after the passage of the sheath edge. Only one knee is observed for the two traces taken near to the plate because the sheath edge speed is greater than the ion acoustic speed here and no rarefaction front is formed.

After the rarefaction front is produced, the second knee (i.e. the sheath edge) moves at approximately one tenth of the speed of the first knee (the rarefaction front). These oscillograms are essentially preliminary and the speed measurements are not accurate, but the general behaviour expected from the theory is observed.

More accurate measurements were then made using the boxcar detector in scan mode to detect the time of arrival of the rarefaction front as a function of distance. An amplified, sampled form of Figure 5.6 with better time resolution was produced. A distance-time diagram taken from this data is shown in Figure 5.7. This graph shows an increase in the rarefaction front speed with distance from the plate, finally (for distances greater than ~2cm) reaching the same speed as the low-amplitude ion acoustic waves and pulses in Figures 4.8 and 4.12. It is believed that this is the same effect as noticed by GOLDAN and LEAVENS (1970) in their careful studies of ion acoustic wave motion near a large plane transmitter. It is due to the drift of ions towards the plate at t=0 as a result of the initial presheath causing a modified (local) ion acoustic wave speed. The rarefaction front thus moves at the local ion

acoustic speed in the moving ion fluid. The reason why this speed-up was not observed in the low-amplitude ion acoustic wave experiments (Chapter 4) is that those measurements were not made sufficiently near to the plate for the effect to appear.

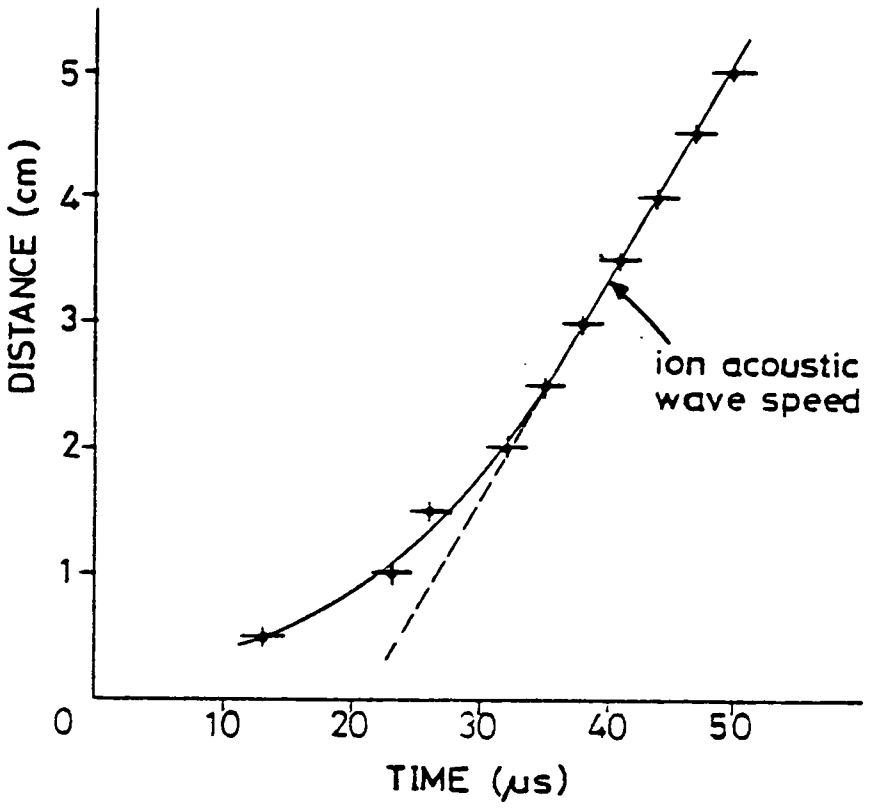


Figure 5.7
Measured distance-time diagram for the rarefaction front.

A different experiment was performed using the boxcar detector in the single-point mode. A similar but slightly faster negative ramp waveform (from -70V to -1200V in 200μs) was applied to the plate starting at t=0. The boxcar detector was used to examine the evolution of the plasma density profile. Electron saturation current (including both AC and DC components) was measured as a function of distance. The results are shown in Figure 5.8 which shows plasma density profiles at different times throughout the voltage ramp ('density snapshots'). The traces are again displaced with respect to each other for clarity. At t=0 it is clearly shown that a density gradient exists in front of the plate due to the -70V initial plate bias forming an ion-rich sheath. The sheath edge is visible as a rapid change in the density gradient. The profiles at 10 and 20 μs show the propagation of two "knees", a rarefaction front and the slower sheath edge in agreement with the previous

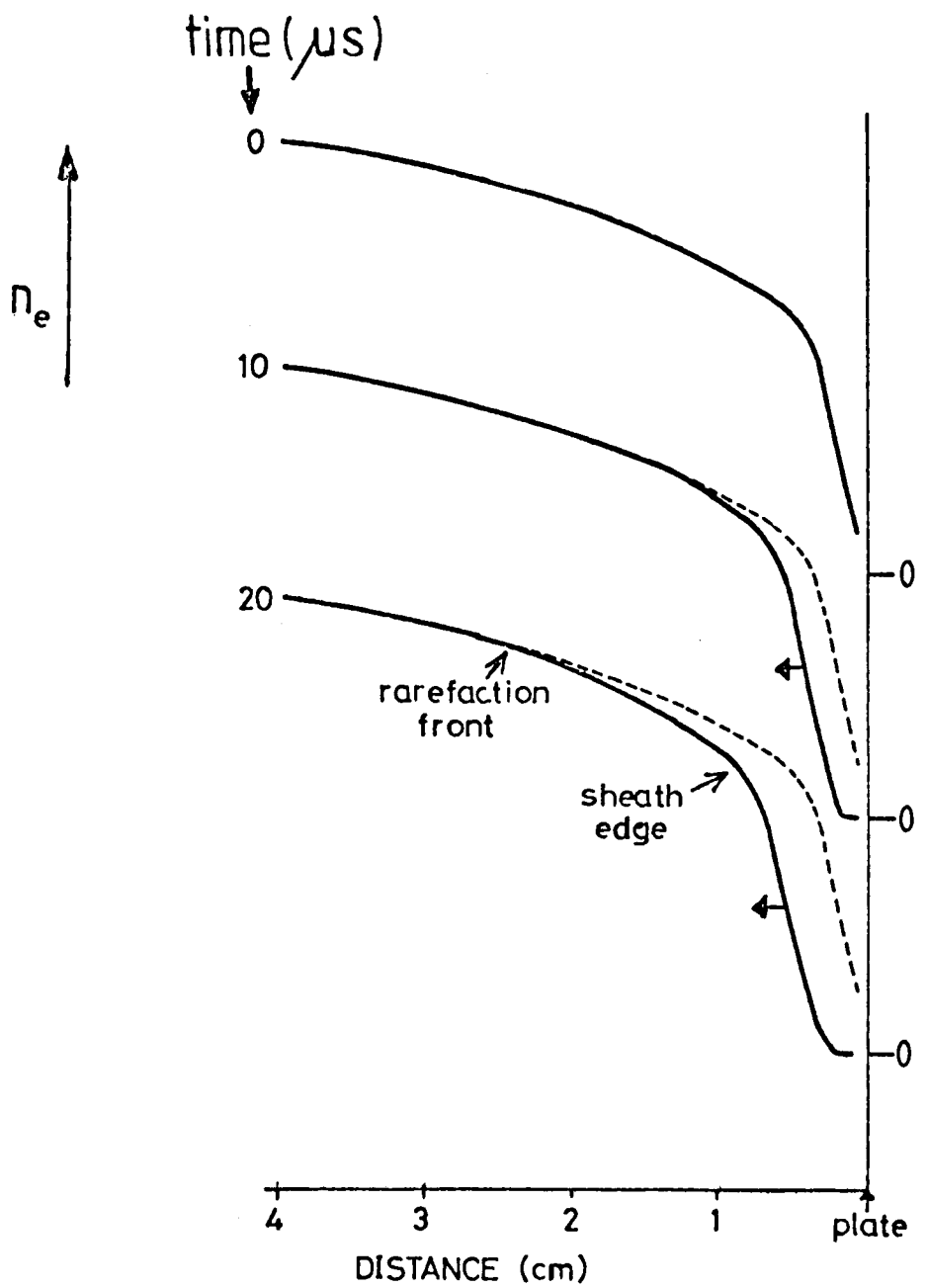


Figure 5.8

Electron number density profiles at various early times during the slow negative-going voltage ramp. The broken lines indicate the displaced t=0 density profile.

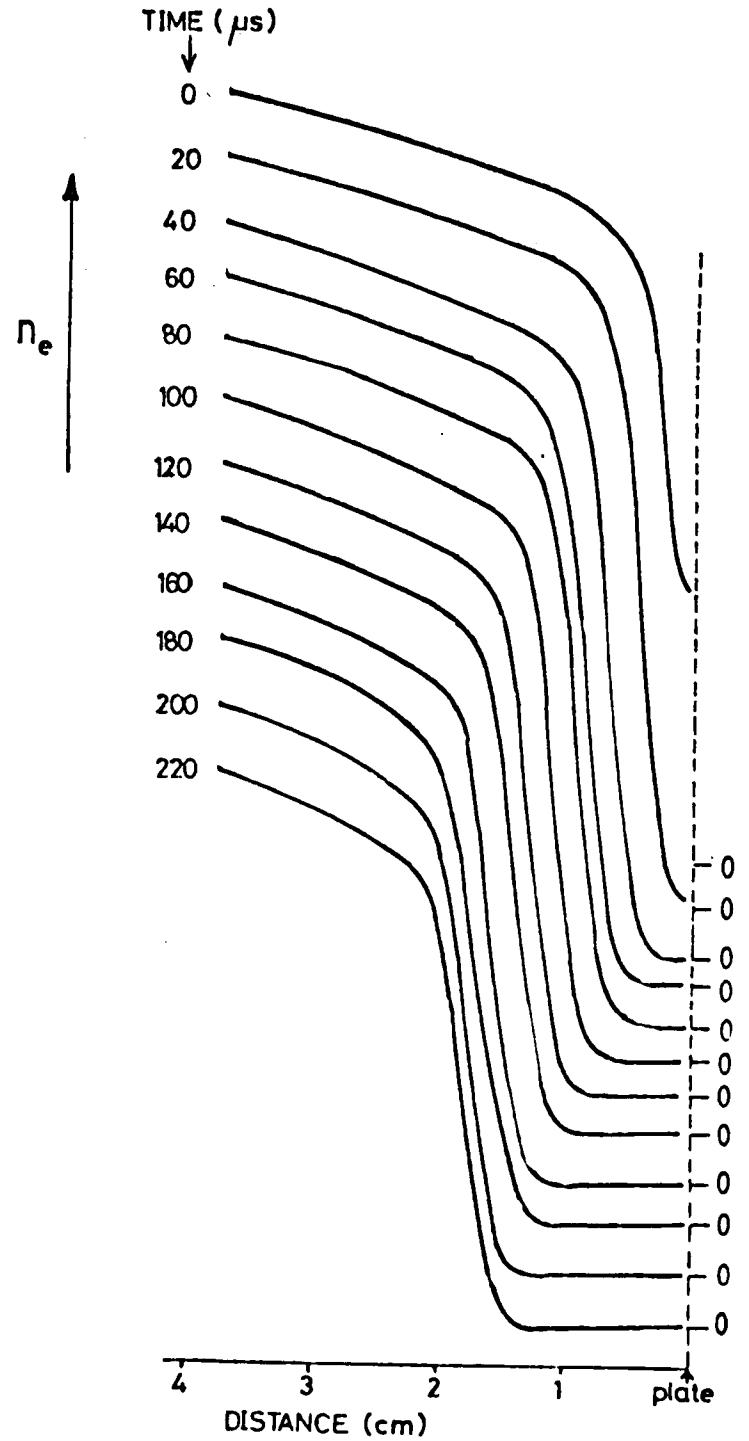


Figure 5.9

Electron number density profiles at various later times showing the propagation of the sheath edge.

results.

The density profiles in Figure 5.8 may be regarded as 'cross-plots' of the oscillograms of Figure 5.6. The propagation of the rarefaction front and sheath edge are easily determined. Similar results at later times (for a ramp of -70 to -800 V in 200 μs) illustrate the complete propagation of the sheath edge (see Figure 5.9). The rarefaction front has travelled a distance greater than 4cm at times above 20μs and so is invisible in this diagram. It is clearly seen that the sheath edge stops moving at times greater than 200 μs when the applied voltage becomes constant.

Similar results were taken for different applied voltage slew rates, and it was found that the rarefaction front speed was constant, whereas the sheath edge speed was dependent on the slew rate. A distance-time diagram for the sheath edge in response to different voltage waveforms is shown in Figure 5.10. This diagram shows that:

(i) The ultimate sheath width is larger in the case of higher applied voltages

(ii) The sheath edge speed is always less than the rarefaction front speed and is a function of the applied voltage waveform.

Further experiments were performed using the boxcar detector in fixed point mode to determine the variation of plasma potential through the rarefaction wave. Probe characteristics were sampled using a narrow sampling gate at a fixed delay time with respect to the trigger. The probe bias voltage was varied for a constant plate-probe separation to obtain a complete sampled probe characteristic. The delay of the sampling gate was then changed to

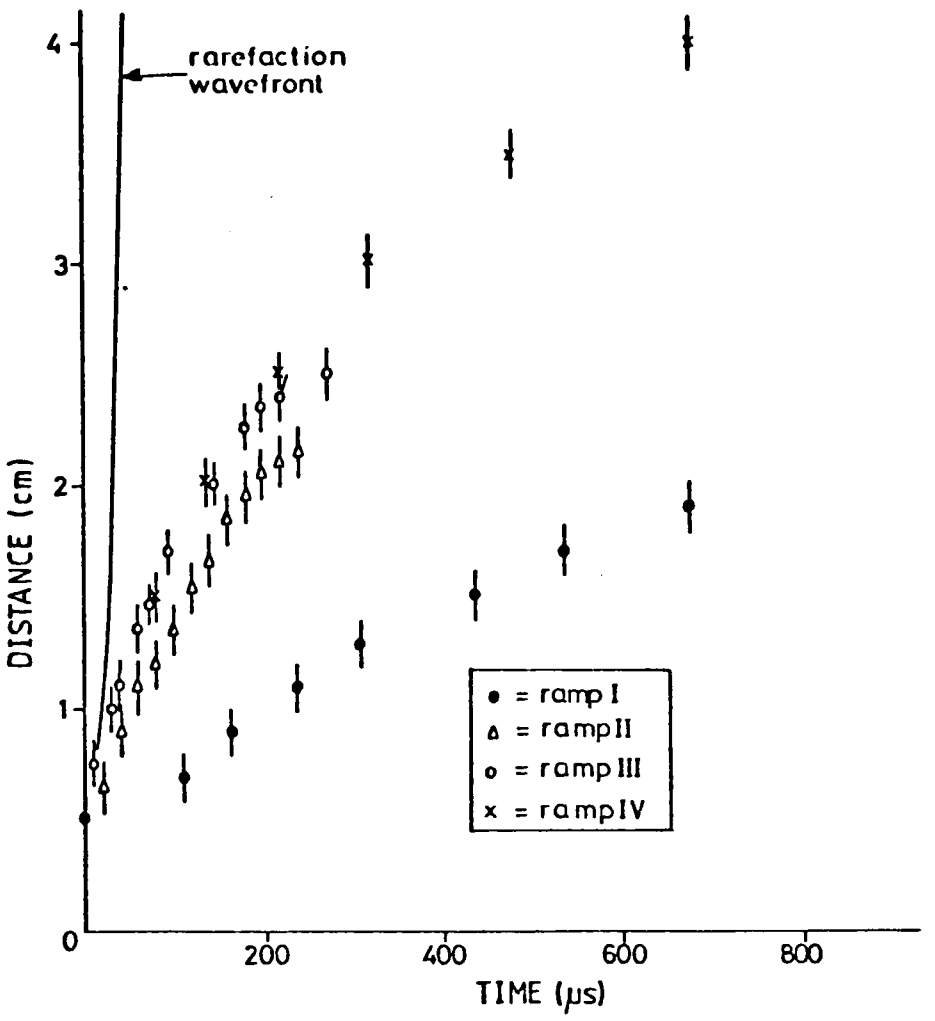
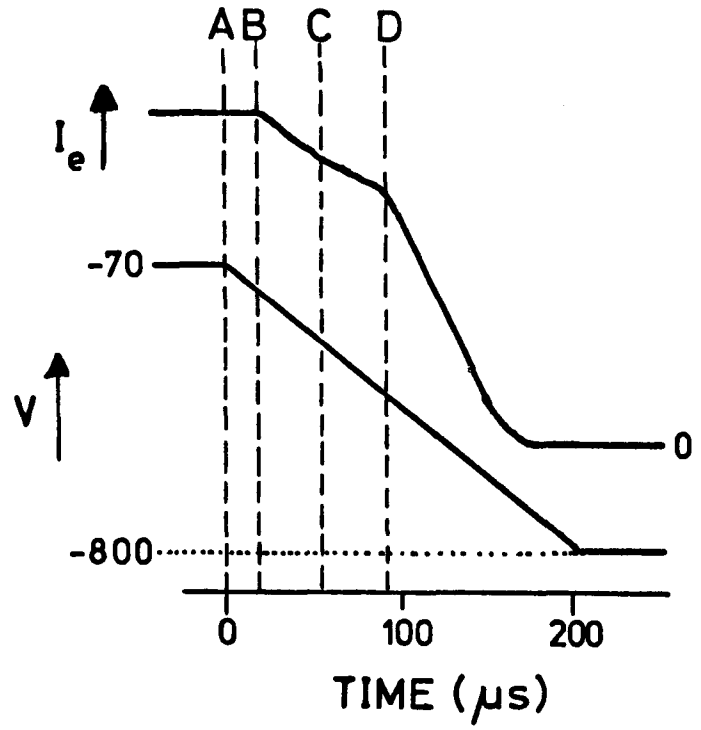


Figure 5.10

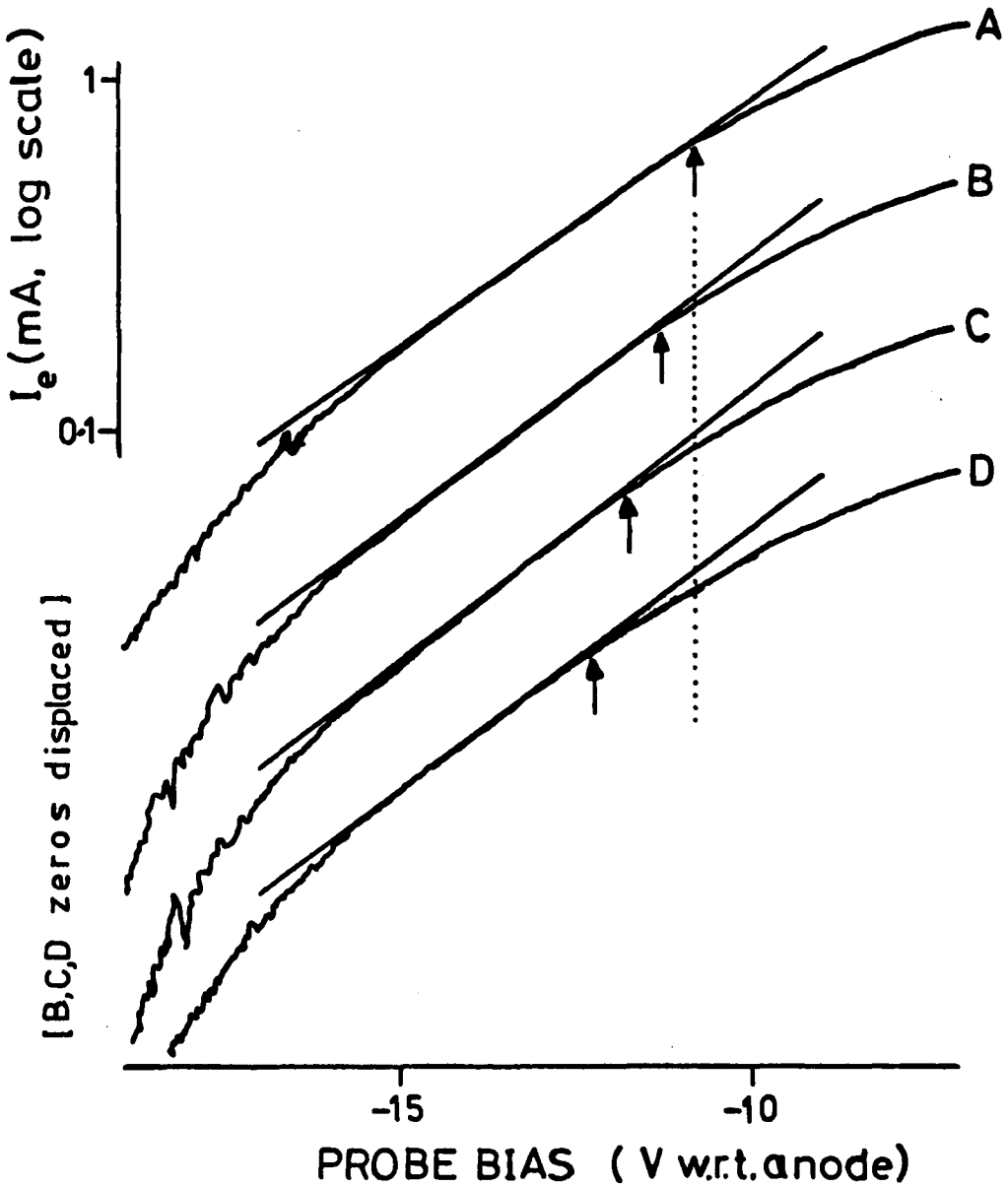
Measured sheath edge distance-time diagram for different applied voltage slew rates: (I) -70 to -800V in 700μs, (II) -70 to -800V in 210μs, (III) -70 to -1200V in 210μs and (IV) -70 to -2200V in 700μs.

a new fixed value and the experiment was repeated. By using a number of different delay times the evolution of the probe characteristic was found. It was hoped that the sampled probe characteristics thus obtained would give information about the existence of positive space charge regions. These have previously been associated with Langmuir probe characteristics which were anomalous in the ion saturation region (EMELEUS and BROWN, 1936). No such anomalous behaviour is observed in our results, even when the probe is in the sheath. Plasma potential is not clear from this measurement.

The experiment was repeated, electronically taking the logarithm of the probe current signal (as in Section 4.2.1) so that the plasma potential could be measured more accurately. These results, shown in Figure 5.11, indicate a plasma potential decrease of approximately 1V between the sampling times B and D which corresponds to approximately $kT_e/2e$ between the rarefaction front



(a)



(b)

Figure 5.11

(a) Sampling times through the rarefaction wave (c.f. Figure 5.6). Time B corresponds to the rarefaction front and D to the sheath edge.

(b) Semi-logarithmic sampled Langmuir probe characteristics at the times A - D through the rarefaction wave. Approximate plasma potential is indicated by arrows.

and the sheath edge. The measurement was not accurate (±0.3V) but a decrease in plasma potential is certainly evident.

In an attempt to improve the accuracy of the potential measurements an emissive probe was tried. Such probes have been used by various authors to give an accurate measurement of plasma potential. Relevant work includes the measurement of sheath thicknesses by WIDNER et al (1972) and the detection of ion acoustic waves by FUJITA et al (1981). The principle of the probe is as follows; a heated filament emits electrons and the filament is biassed at various voltages with respect to the plasma. If the bias voltage is above plasma potential no electrons are emitted and the current collected from the plasma is the same as for a cold probe. Below plasma potential, however, electrons are emitted causing an apparent positive ion current to the probe, which is higher than that usually collected by a cold probe. The hot and cold probe currents thus diverge giving a measure of plasma potential (CHEN, 1965a). This method still has the problem of cold probe contamination since a cold probe plot is necessary in addition to the hot probe characteristic.

Better measurements of plasma potential include that of the floating potential of an emissive probe; sampled experiments were presented by IIZUKA et al (1981). The floating potential approximates to plasma potential when the electron emission current is very high. Another measurement of plasma potential which does not require such large emission currents which may perturb the plasma is that of the inflection point of the emissive probe characteristic (SMITH et al, 1979). Time-sampling of the latter measurement as in Figure 5.11 should give the variation of potential

throughout the rarefaction wave without too much disturbance to the plasma.

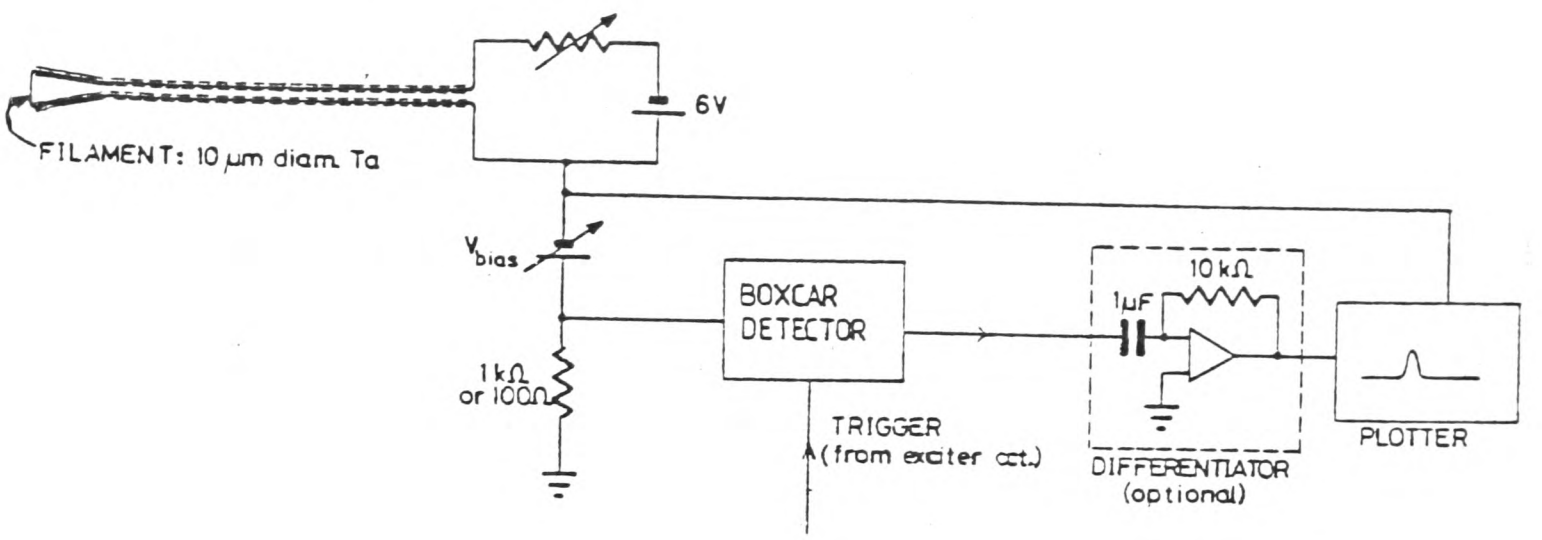


Figure 5.12
Electrical circuit for emissive probe experiments.

An emissive probe was constructed as indicated in Section 5.2.1. The electrical circuit is shown in Figure 5.12. The inflection point of the probe characteristic was detected using the differentiation circuit which gave a turning point in the differentiated signal. Typical hot and cold probe plots without differentiation are shown in Figure 5.13 where it is seen that the floating potential depends on the probe heating current. The sampled turning point measurements through the ion rarefaction wave are indicated in Figure 5.14(b) at the same sampling times as shown in Figure 5.11. Again it is shown that approximately 1V is dropped across the rarefaction front region. For comparison Figure 5.14(a) includes some similarly sampled non-differentiated emissive probe characteristics. These show a comparable decrease in the floating potential and also an associated plasma density decrease. The resolution of the method is still not good (±0.2V). Refinement of the technique may be fruitful, but was not attempted due to the likelihood of plasma perturbation with the emissive probe approach.

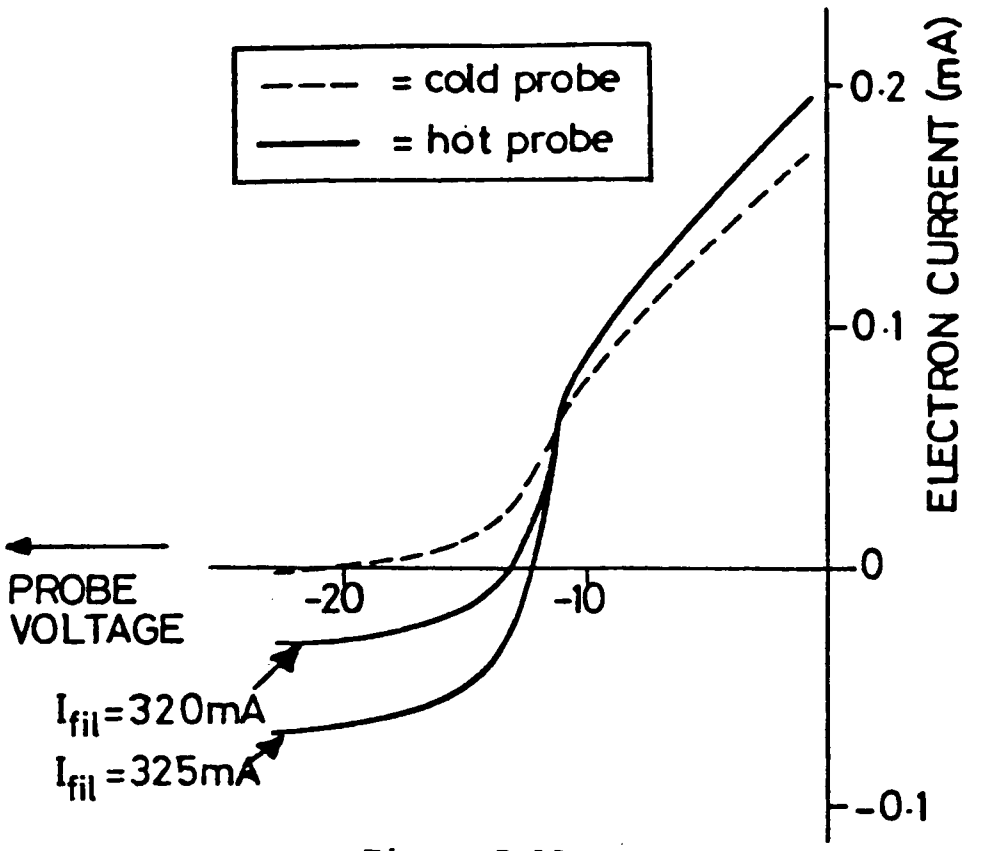


Figure 5.13

Comparison of hot and cold probe characteristics showing apparent ion current for the hot probe and contamination effects in the cold probe electron saturation region.

From these techniques some information concerning the variation of plasma potential through the rarefaction wave was built up. It was hoped that this technique would give profiles of potential with time as the parameter similar to the profiles of density shown in Figure 5.8. A limited amount of data was taken due to the poor (±0.2V) resolution and also noise problems. The results, which are shown in Figure 5.15, show trends which are qualitatvely consistent with the density profiles in Figure 5.8.

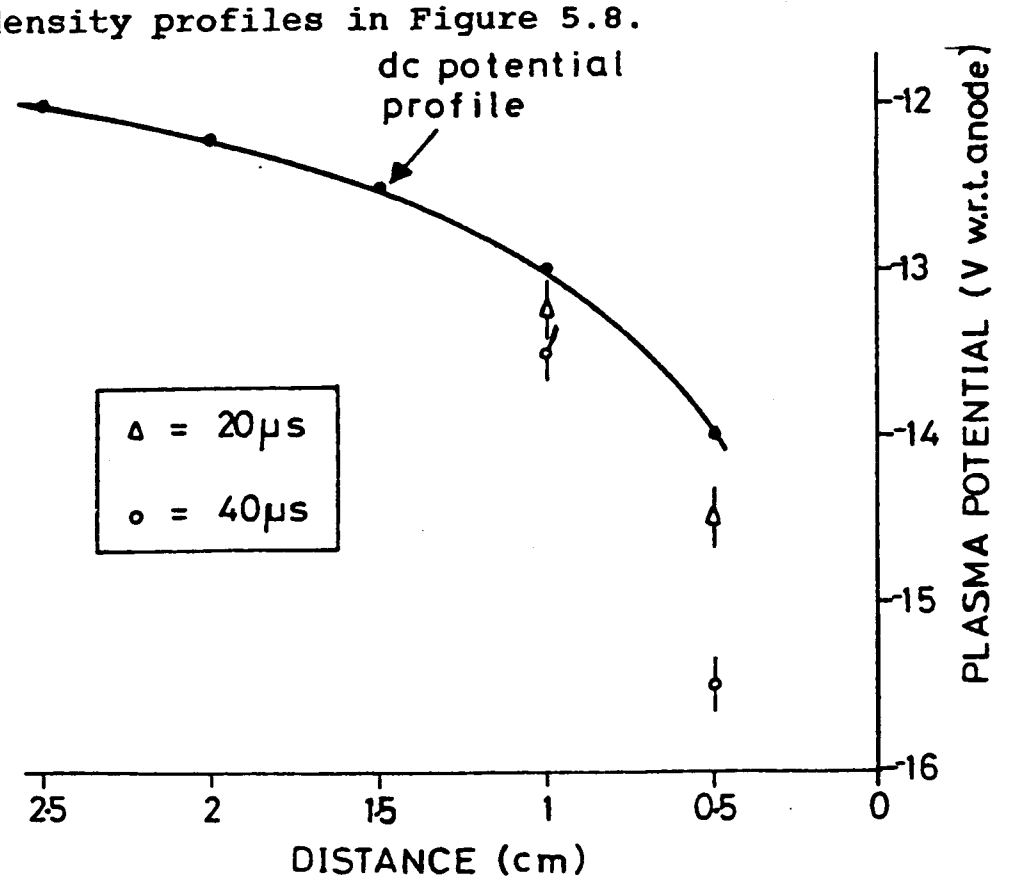
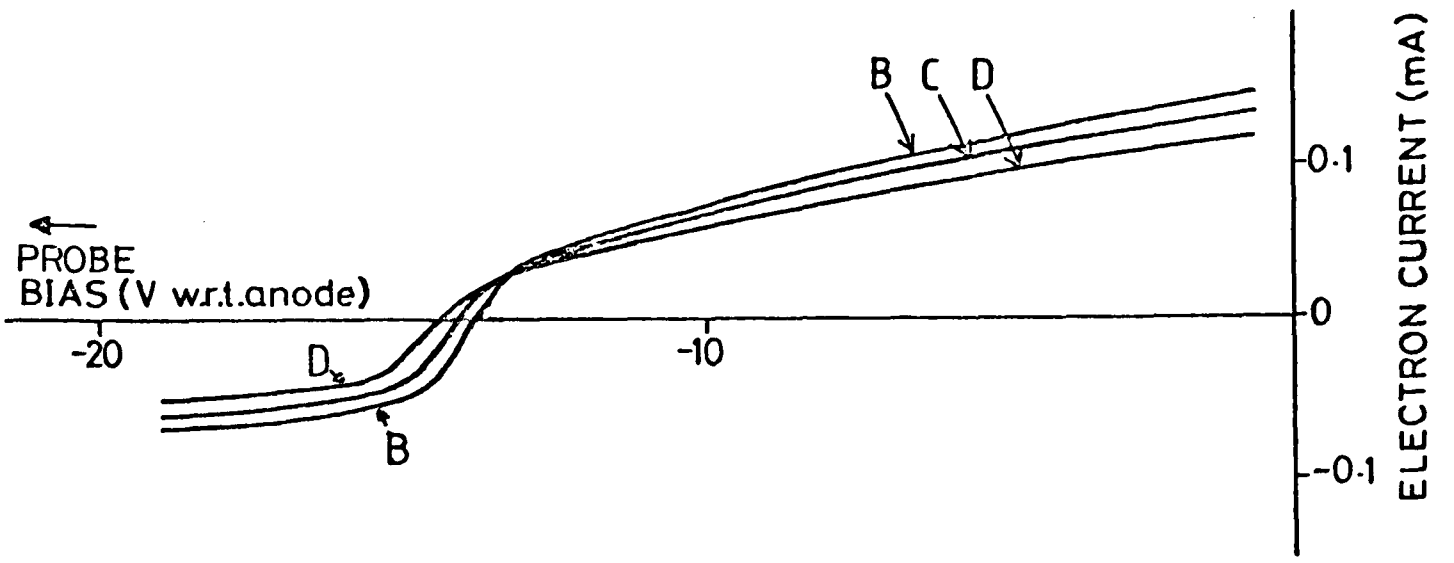
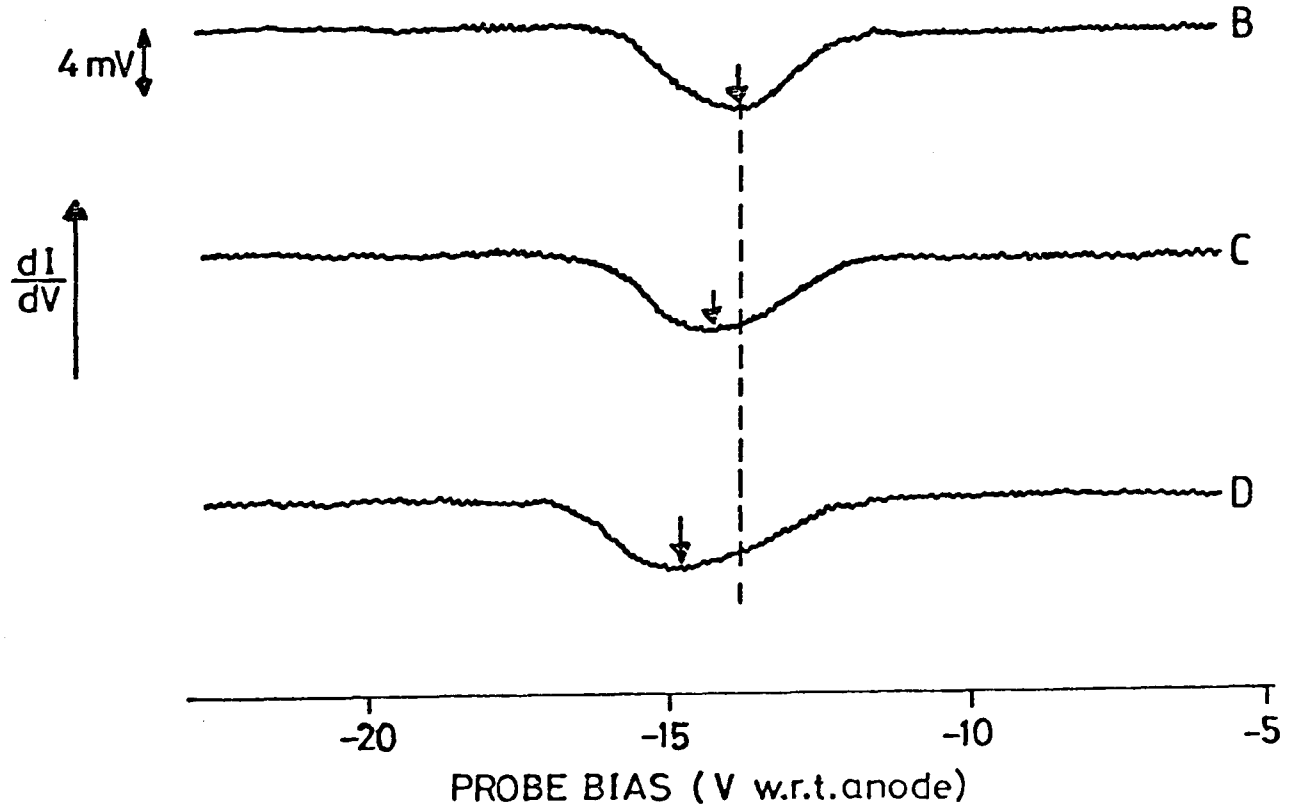


Figure 5.15

Potential profiles at various times through the rarefaction wave (c.f. Figure 5.8).



(a)



(b)

Figure 5.14

Sampled emissive probe characteristics at various times (B - D as in Figure 5.11) through the rarefaction wave:- (a) direct and (b) differentiated (arrows indicate plasma potential).

During the negative ramp pulse, the current drawn to the plate was of interest. Current was measured to the inner disc of the guard-ring construction to reduce unwanted geometrical effects. An oscillogram of the current waveform is shown in Figure 5.16 (measured using a Tektronix current probe). Note that the steady current level before pulsing is 0.85mA, while the current at the end of the ramp is higher than this. This is due to two factors:-

(i) secondary electrons emitted from the plate under energetic ion bombardment cause an apparent ion current increase

(ii) geometrical effects (thought to be small)

Measurements of the steady current to the plate at different negative bias voltages indicated that the plate current followed the dotted line shown in Figure 5.16. The waveform shows a pulsed ion current increase in qualitative agreement with theory; this will be discussed in Section 6.4.

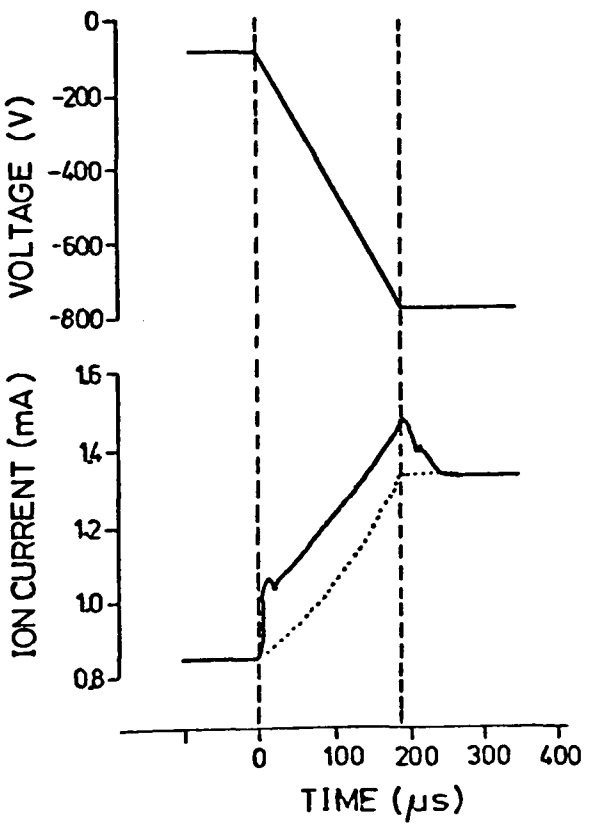


Figure 5.16

Ion current to the plate during the negative-going voltage ramp. Measurements of the current drawn by a steady negative plate voltage of the same magnitude are shown by a dotted line.

5.3.2 Fast Ramp

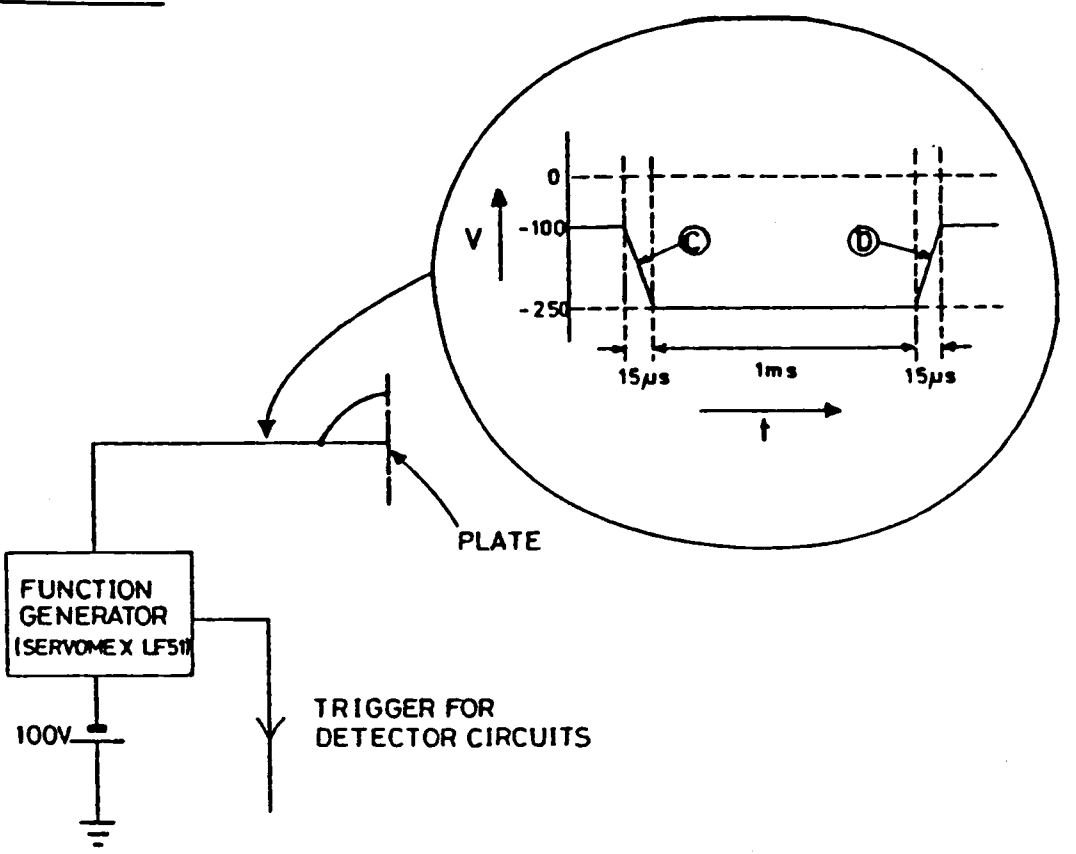


Figure 5.17
Exciter circuit for fast ramp experiments.

A different circuit was used to apply this ramp, which was faster but of lower amplitude (-100 to -250 V in 15μs). The excitation circuit is indicated in Figure 5.17. Again a repetitive signal was generated. For sheath expansion experiments, the portion C of the waveform was used. Fluctuations in electron saturation current to a nearby probe were measured using the probe circuit in Figure 5.5. The plasma response at various positions is shown in Figure 5.18. The sheath edge can only be seen at low values of plate-probe separation (<1cm) due to the relatively low applied voltages in this experiment. The following points are of interest:-

(i) The plasma disturbances are of small amplitude compared to the slow ramp experiments ($\frac{\delta n}{n} \simeq 2\%$ compared to 10-20% previously).

(ii) A rarefaction front is seen propagating away from the plate at the ion acoustic speed.

(iii) The plasma disturbance behind the front does not now consist of a monotonic density decrease as in the slower

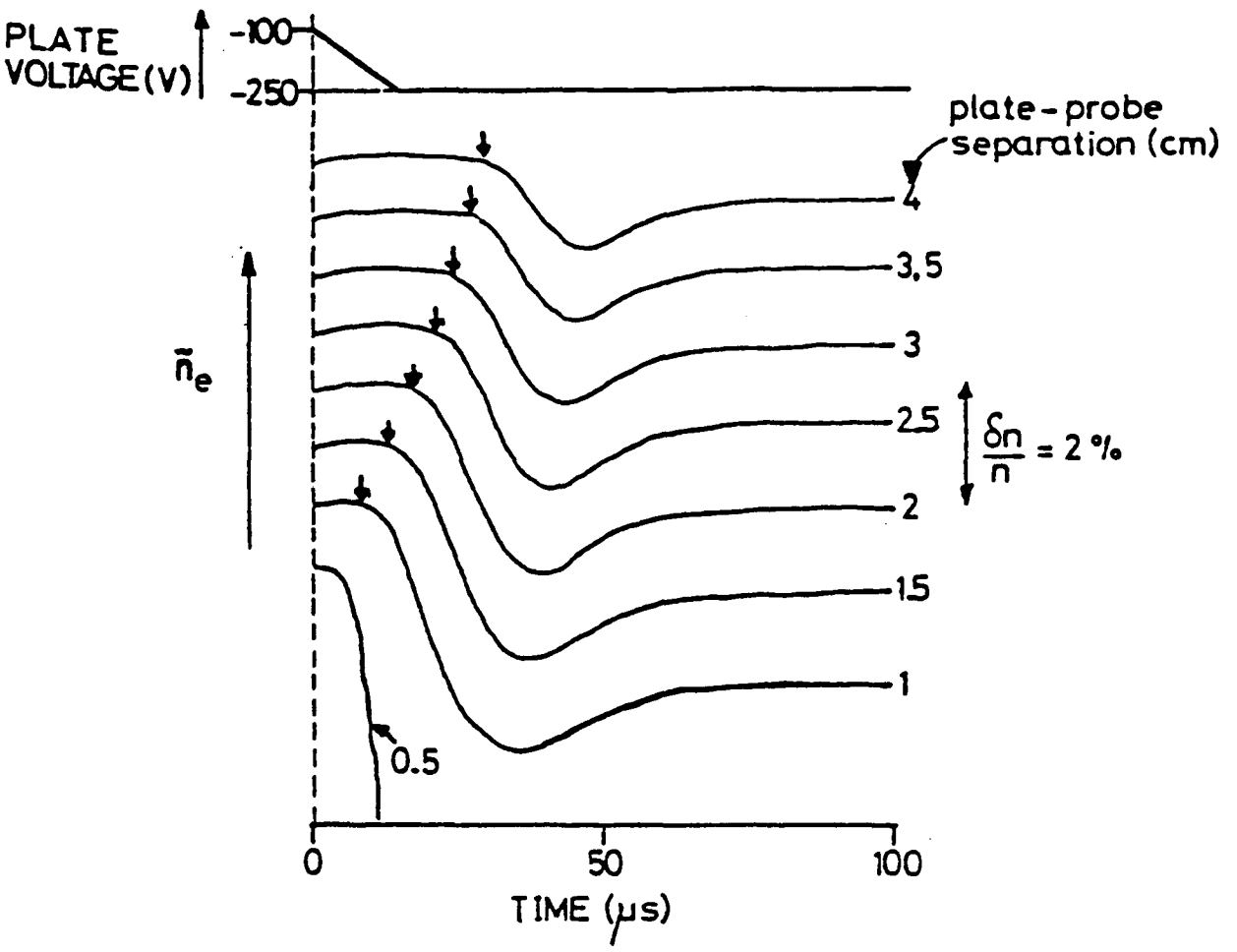


Figure 5.18

Plasma response to fast negative going voltage ramp (top trace) at various plate-probe separations. The rarefaction front is arrowed.

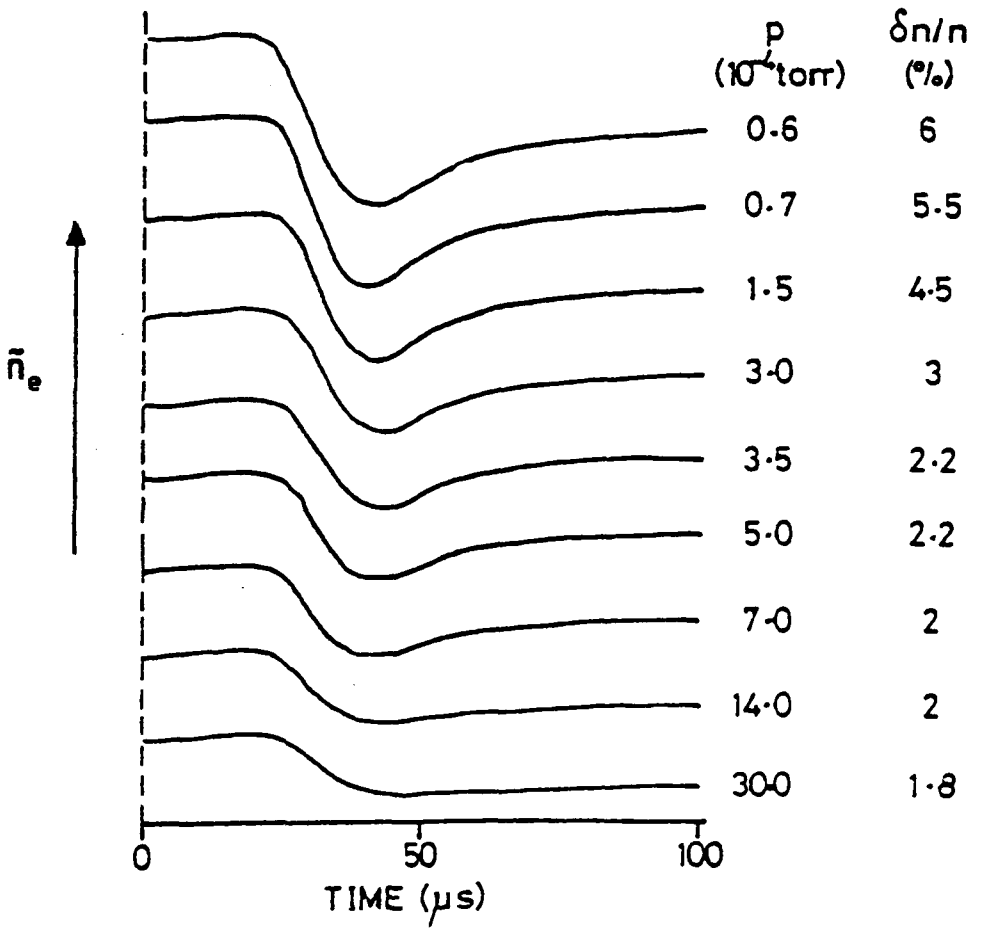


Figure 5.19

Plasma response to fast ramp at a fixed plate-probe separation (3cm) for various neutral pressures (usual conditions $p = 3.5 \times 10^{-4}$ torr). The pulsed response disappears at high pressures.

experiments, but the behaviour is better described in terms of a rarefaction front followed by a rarefaction pulse. This behaviour is not understood. In a further experiment on this phenomenon, it was noticed that the pulse disappeared and became a monotonic density decrease if the background pressure was increased. This effect is illustrated in Figure 5.19, which shows the variation of the probe response at a fixed distance of 3cm with pressures between $6x10^{-5}$ and $3x10^{-3}$ torr. The pulse response disappears at $3x10^{-3}$ torr where a monotonic decrease is observed. The excitation efficiency decreases with increasing pressure.

Further experiments using the fast ramp voltage were performed using the boxcar detector in the fixed point mode to measure the AC component of electron saturation current as a function of distance. This technique is similar to that used to obtain Figure 5.8 except that the t=0 density profile due to the initial presheath has been effectively subtracted giving a measure of the perturbed density profile only. The results are shown in Figure 5.20. In response to the fast ramp, the sheath edge moves out slightly to a distance of order 1cm from the plate and a rarefaction front moves into the plasma. The measured density decrease is not steady, in qualitative agreement with Figure 5.18. The propagation of the rarefaction front is plotted on a distance-time diagram (Figure 5.21). In agreement with the slow ramp case (Figure 5.7) a speed-up of the front is observed at low distances indicating the presence of an initial presheath.

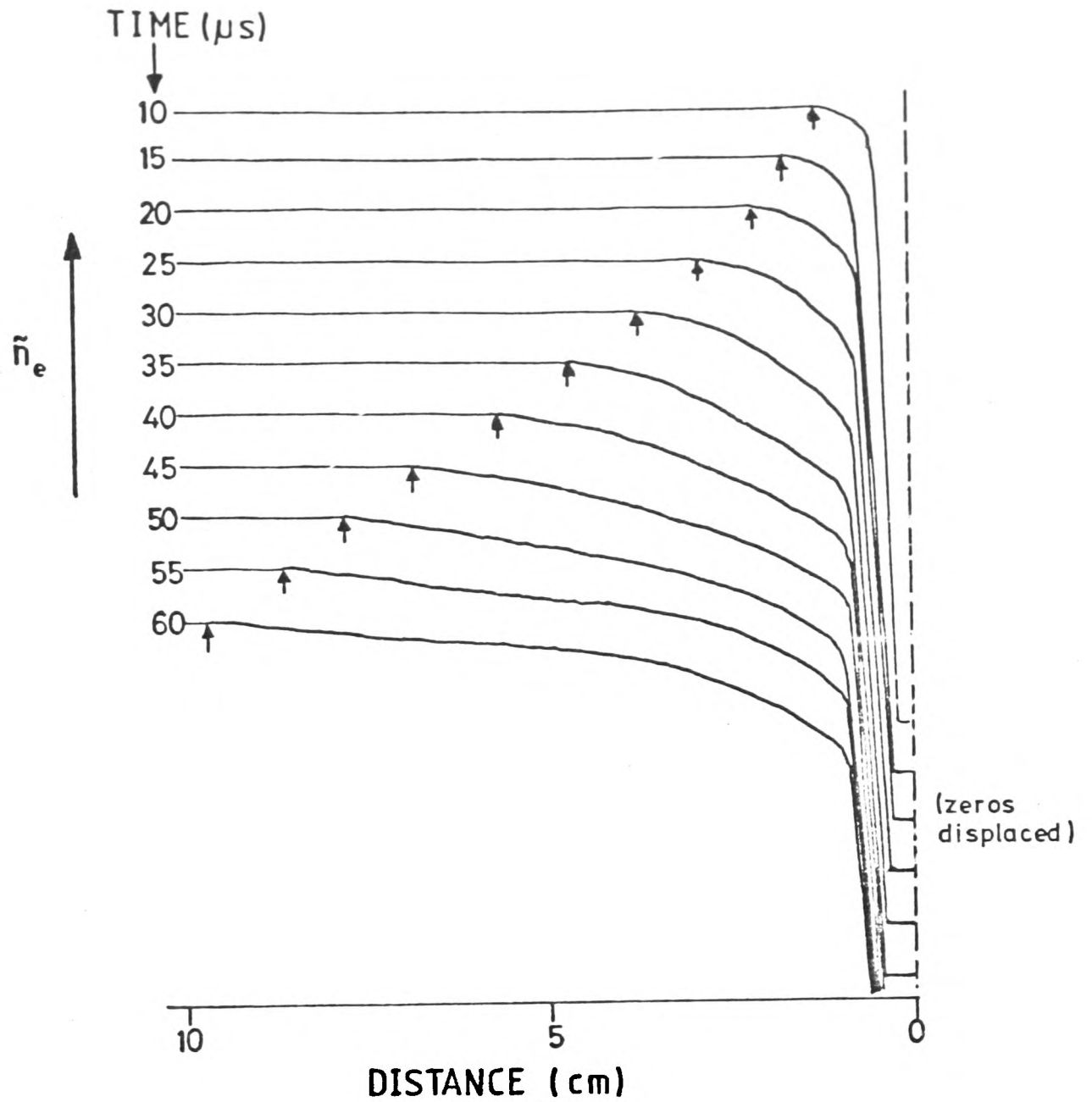


Figure 5.20

Perturbed electron number density profiles at various times during the fast negative-going voltage ramp experiment (voltage constant after 15μs). The rarefaction front is indicated by an arrow.

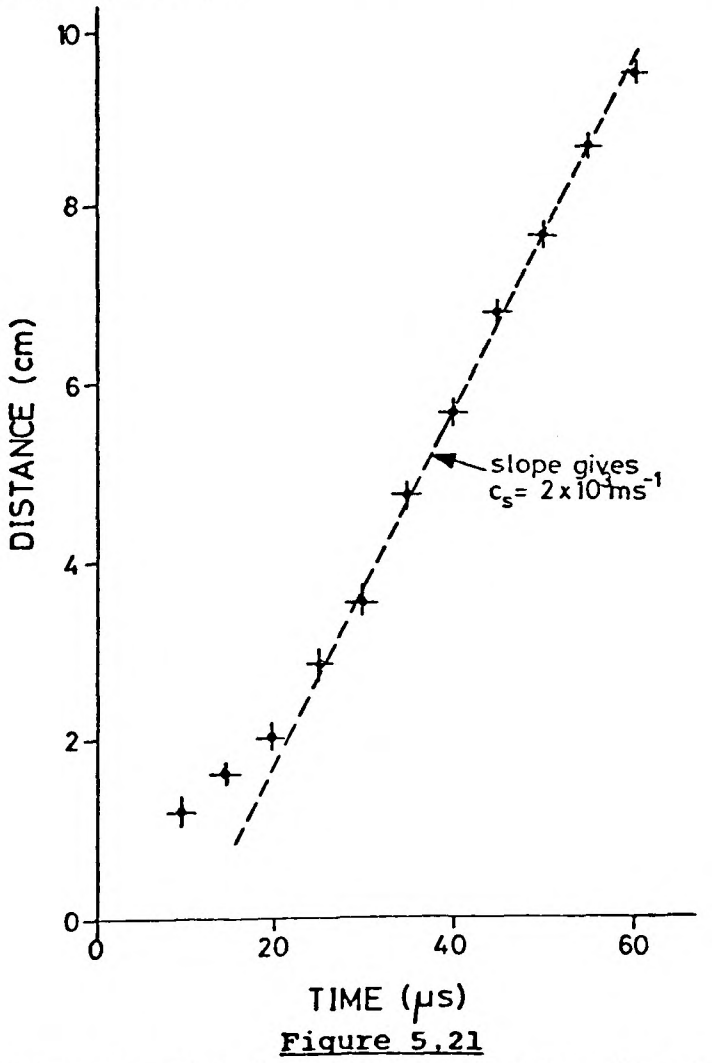


Figure 5.21

Distance-time results for the rarefaction front from Figure 5.20.

5.4 ION ENHANCEMENT WAVE OBSERVATIONS

When collapsing an ion-rich sheath towards an electrode Chapter 2 predicted that an ion enhancement wave should be produced. We shall now discuss some experimental results taken using the portion B of the slow ramp voltage waveform indicated in Figure 5.5, and then the results of some faster ramp experiments.

5.4.1 Slow Ramp

The range of slow ramp voltages used started between -500 and -2200 V and then decreased linearly to a final level of -70V in a time of 100-800μs. This was the converse of the ramp applied in the rarefaction wave experiments (Section 5.3.1). At all times an ion-rich sheath was present since the applied voltage never exceeded plasma potential. The width of the sheath decreased during the ramp.

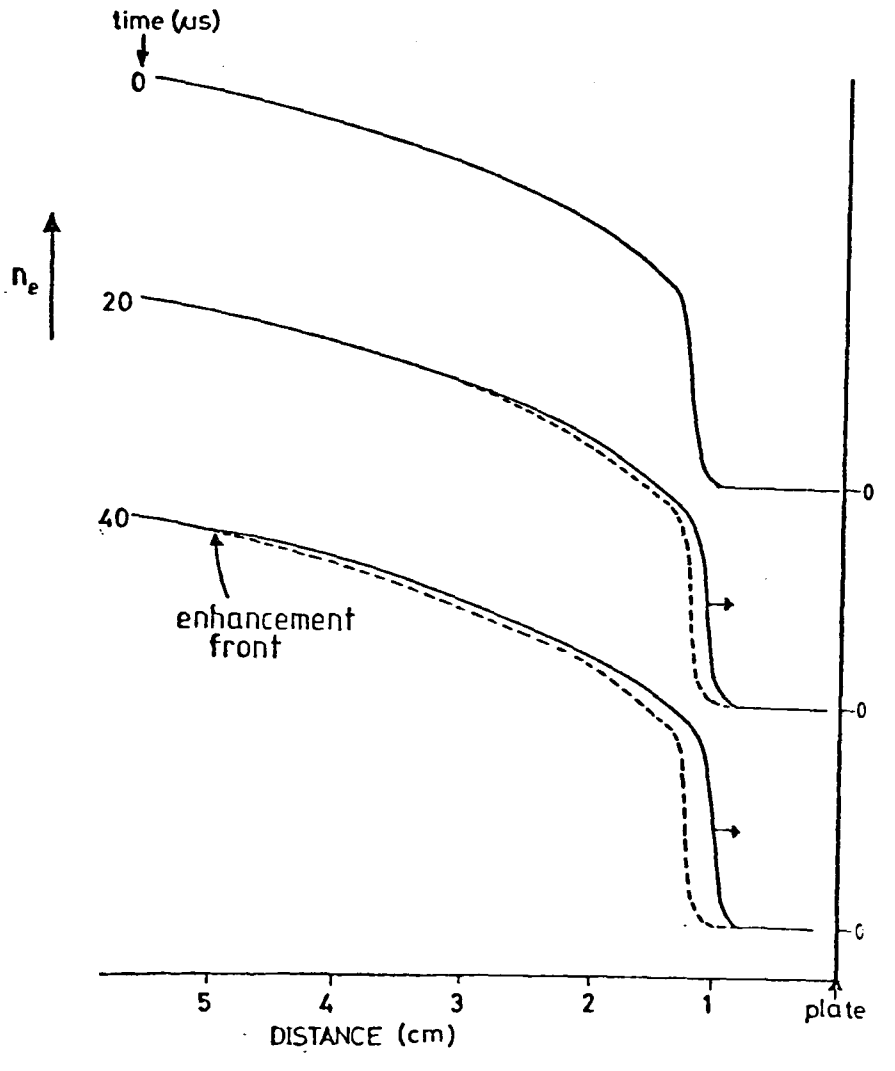


Figure 5.22
Electron number density profiles at various early times through the slow positive-going voltage ramp. The broken lines indicate the displaced t=0 density profile.

The most convenient way to present the results is in the form of a diagram similar to Figure 5.8, namely a boxcar averaged density versus distance plot with time as the parameter. Results are shown in Figure 5.22. The probe used in this experiment was the emissive probe described in Section 5.2.1. It was used as an electron-collecting probe, and the effects of probe contamination were avoided by passing a small heating current through the filament though not sufficient to cause significant electron emission. The ramp applied to produce the results in Figure 5.22 was -500V to -70V in 120μs. At t=0, a large (1.5cm) sheath is formed on the plate, with a density gradient in the plasma in front of the sheath edge. As time progresses, the sheath width decreases (indicated by arrows) and a front moves into the plasma. The dotted line on each trace represents the displaced t=0 density profile. The density at a particular position in the disturbed region increases with time. An enhancement wave is thus generated, in agreement with the theory in Chapter 2.

Figure 5.23 shows results of an experiment which continues to longer times where the traces are not displaced with respect to one another, and the collapsing sheath edge is clearly seen. The sheath edge moves towards the plate and the enhancement front moves in the opposite direction.

A distance-time diagram for the enhancement front and sheath edge is shown in Figure 5.24. An oscillogram of electron saturation current as a function of time will not show both the enhancement front and the sheath edge because distance is kept constant for each measurement and the two features move in opposite directions. For $x<x_0$ only the sheath edge is observed, while for $x>x_0$ only the

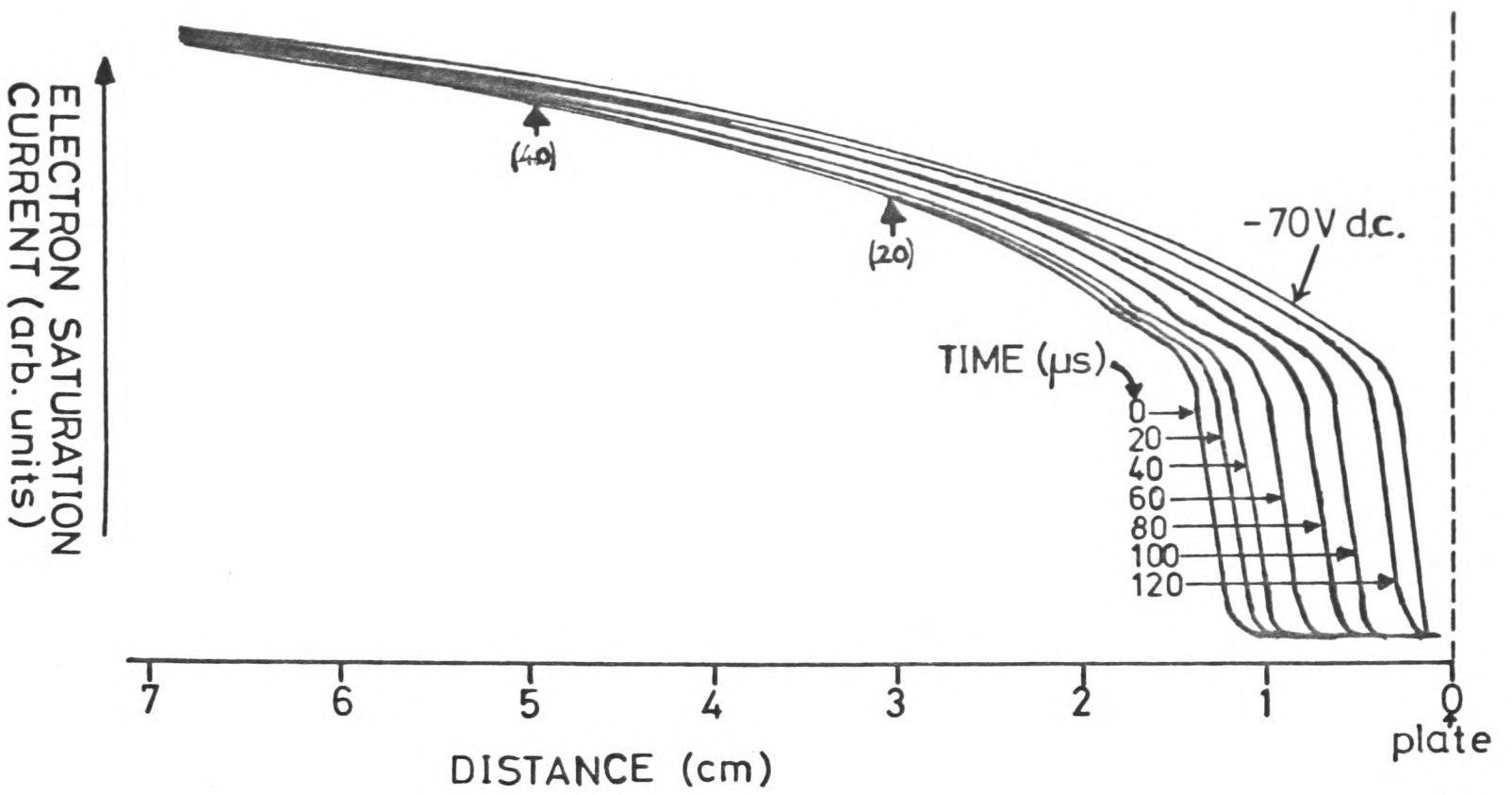


Figure 5.23

Electron number density profiles at various later times through the slow positive-going voltage ramp; the enhancement front is indicated by arrows. The density profile for a steady -70V plate voltage is also indicated.

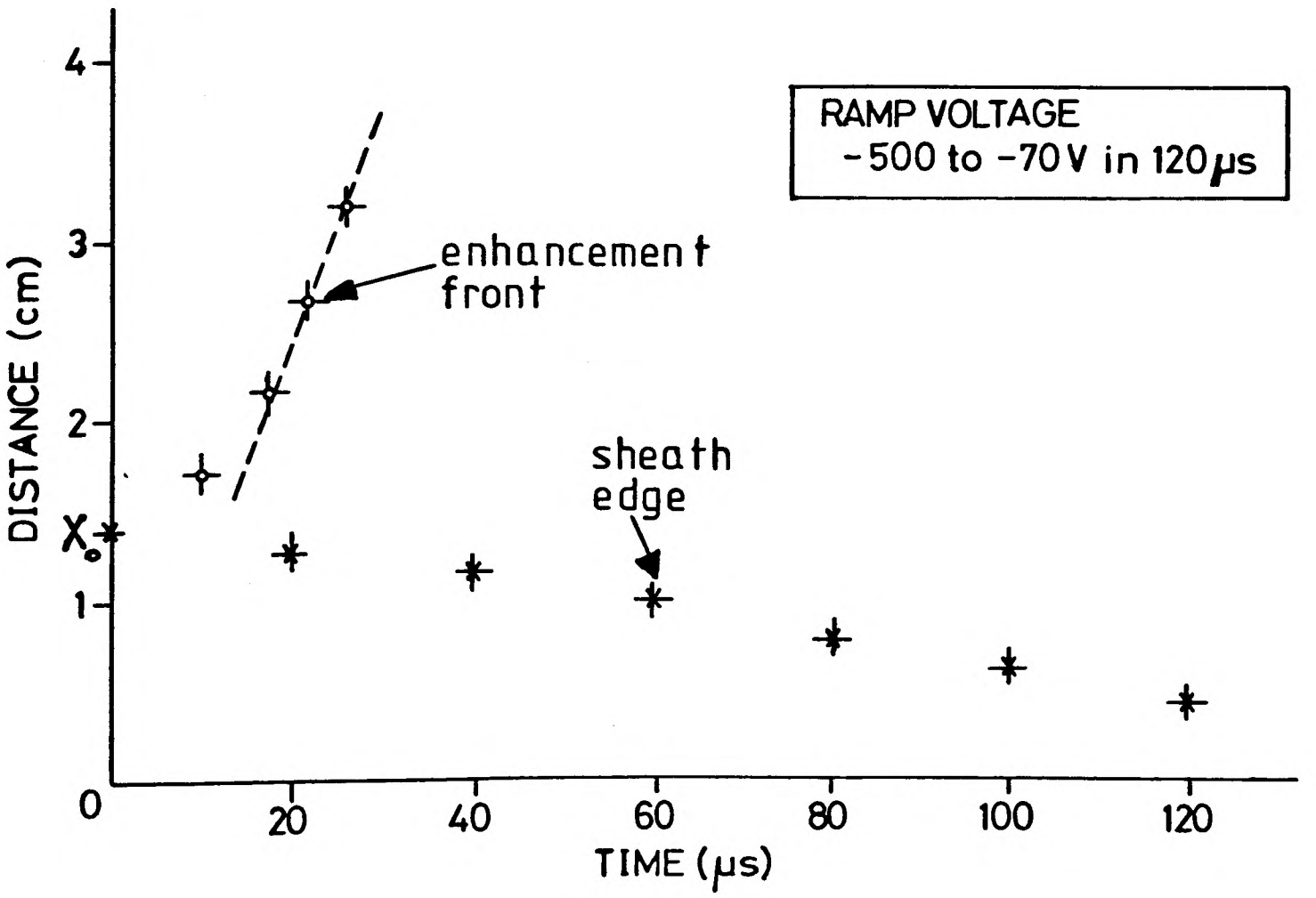


Figure 5.24

Measured distance-time diagram for the enhancement front and the sheath edge. The enhancement front speeds up with distance from the plate.

enhancement front may be detected. This behaviour was observed in experiments. Detailed measurements showed a speed-up of the enhancement front for $x>x_0$ (see Figure 5.24) in a similar manner to the rarefaction front results.

The ion current to the plate was measured as in the expanding sheath case to the inner tantalum disc. A typical waveform is shown in Figure 5.25. At t=0 a high (1.3mA) steady current is drawn, and the current returns to its usual DC level (0.85mA) at the end of the ramp when the plate is at a steady -70V. This is lower than the -800V current level because of the secondary and geometrical effects as indicated in Section 5.3.1. The waveform shows a pulsed ion current decrease in qualitative agreement with theory; this will be discussed in Section 6.4.

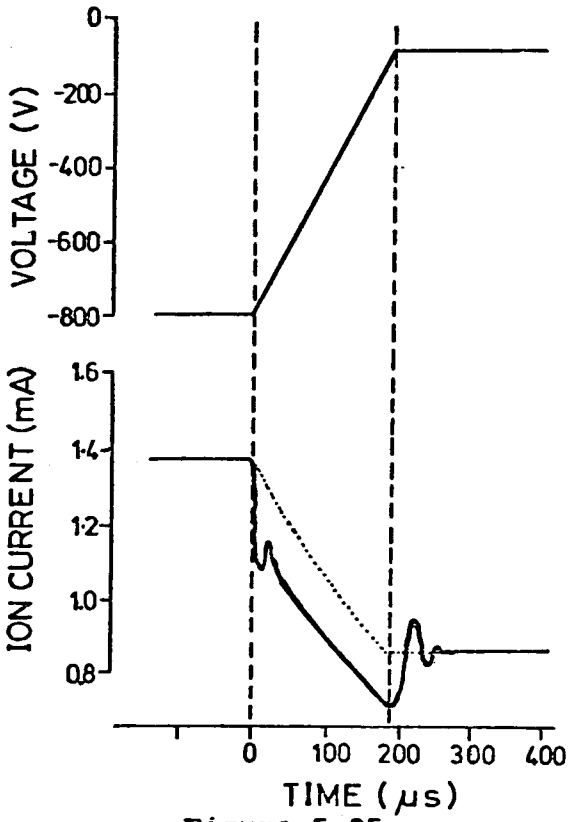


Figure 5.25

Ion current to the plate during a slow positive-going voltage ramp. Measurements of the current drawn by a steady negative plate voltage of the same magnitude as the ramp are shown by a dotted line.

5.4.2 Fast Ramp

The electrical circuit for the faster ramp experiments was shown in Figure 5.17. The portion D of the repetitive waveform was used corresponding to a voltage change of -250 to -100 V in 15μs.

The response of the plasma to this excitation was measured at various positions near the plate and is illustrated in Figure 5.26. This diagram should be compared with Figure 5.18 which was for the corresponding negative-going ramp. The following points are of interest:-

(i) $\frac{\delta n}{n} \simeq 2\%$

(ii) An enhancement front propagates away from the plate at the ion acoustic speed.

(iii) An enhancement pulse propagates behind the front. The pulse is observed to disappear, leaving simply a front, at high neutral pressures in a similar way to the rarefaction experiments in Section 5.3.2.

Some results for distances below 1cm which show the propagation of the sheath edge as well as the evolution of the enhancement front and pulse are shown in Figure 5.27. The sheath edge and the front move in opposite directions. The front, as in Figure 5.24, is never visible at the same position as the sheath edge.

Measurements of the plasma density profile were performed using the single point mode of the boxcar detector, but measuring only the AC component of electron saturation current so that the t=0 profile was subtracted (c.f. Figure 5.20). Results for the response to a collapsing sheath are shown in Figure 5.28. The apparent increase in measured density at the sheath edge (as opposed to the expected decrease as in Figure 5.20) is thought to be due to an overload of the boxcar detector, but it serves as an indication of the sheath edge position. A density enhancement front is clearly generated. The distance-time diagram for this front is shown in Figure 5.29, again showing a speed-up for small distances.

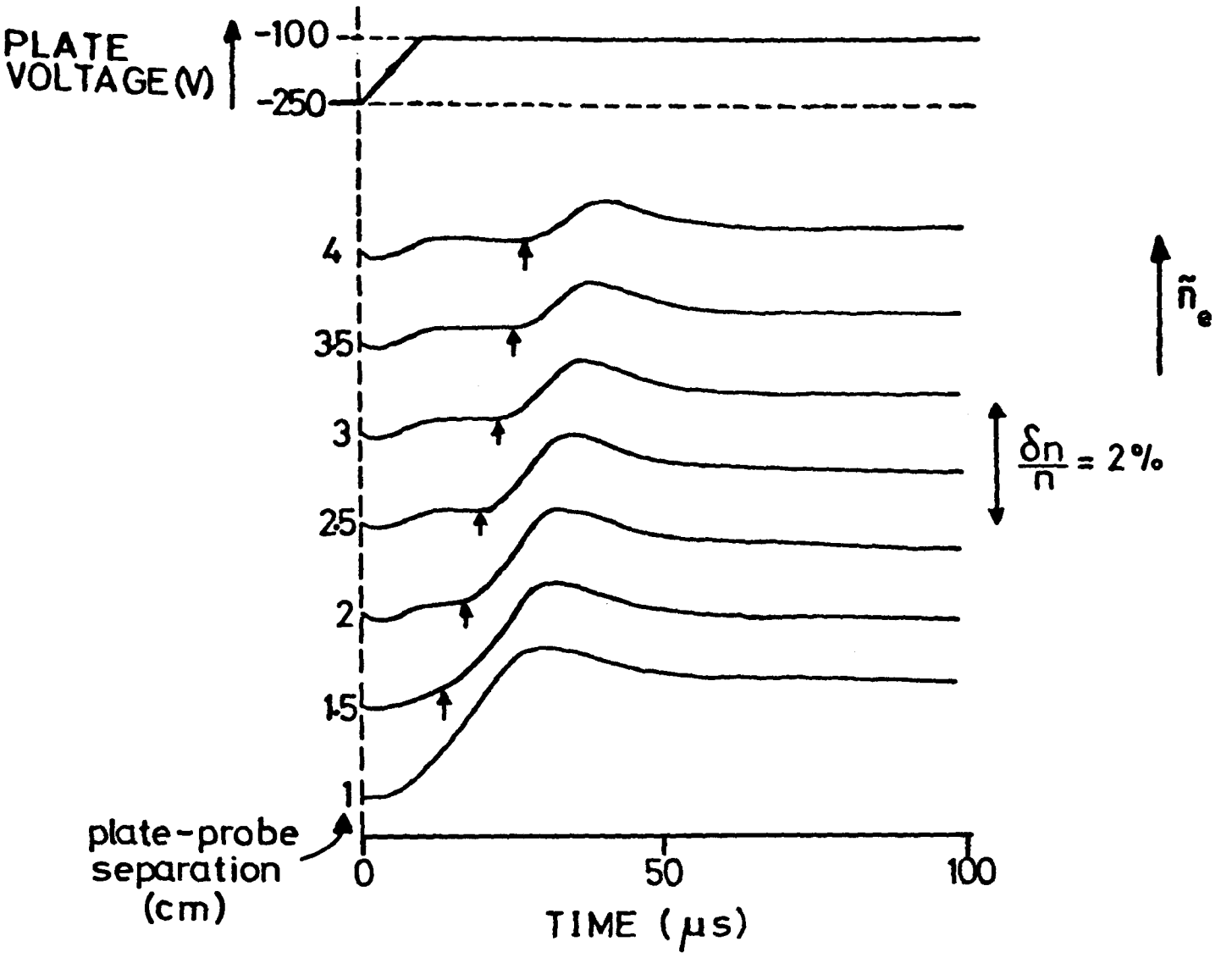


Figure 5.26
Plasma response to fast positive-going voltage ramp (top trace) at various plate-probe separations. The enhancement front is arrowed.

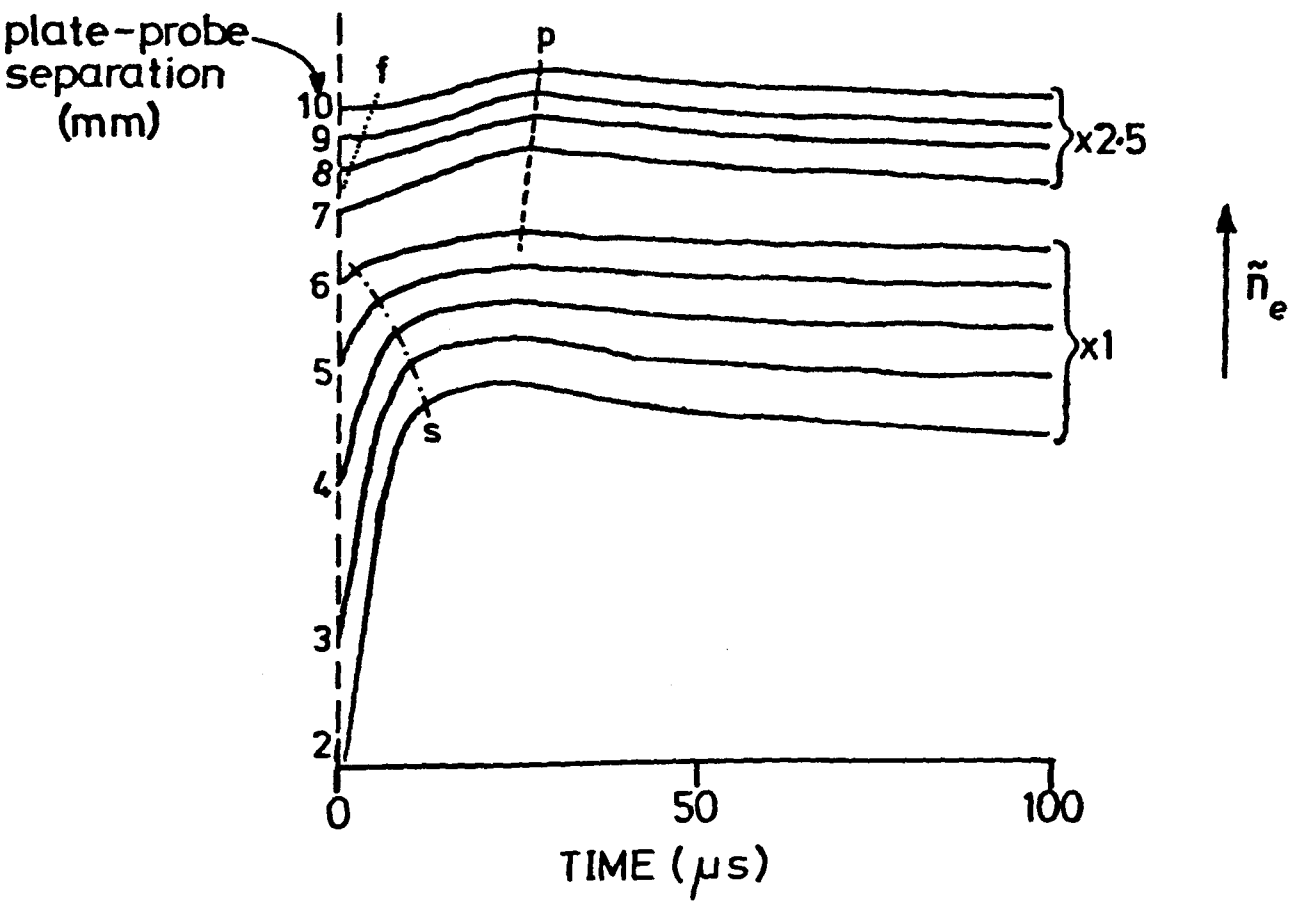


Figure 5.27
Plasma response to fast positive-going voltage ramp at positions very close to the plate; the sheath edge (s), enhancement front (f) and enhancement pulse (p) are all visible.

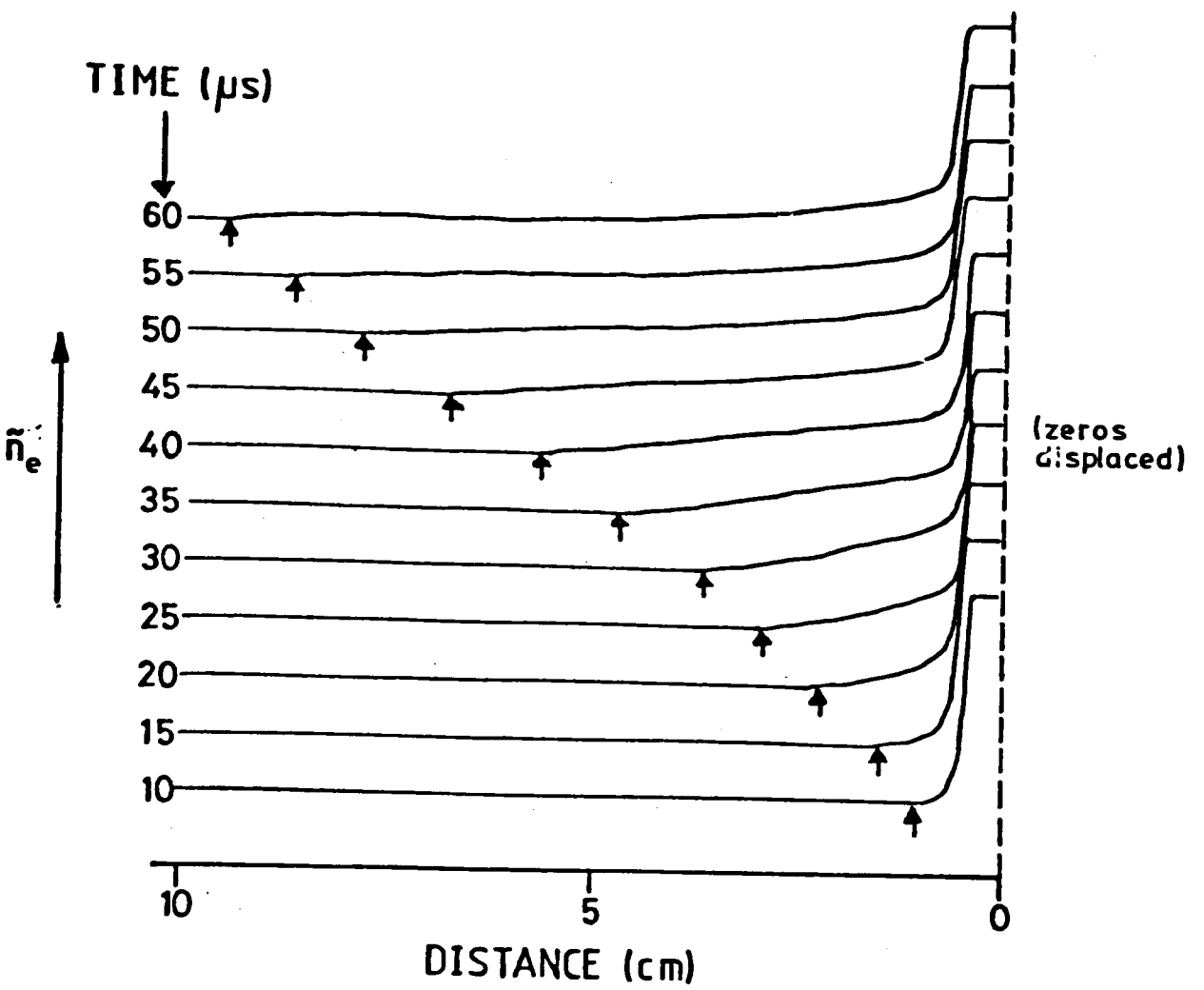


Figure 5.28

Perturbed electron number density profiles at various times during the fast positive-going voltage ramp experiment (voltage constant after 15μs). The enhancement front is indicated by an arrow.

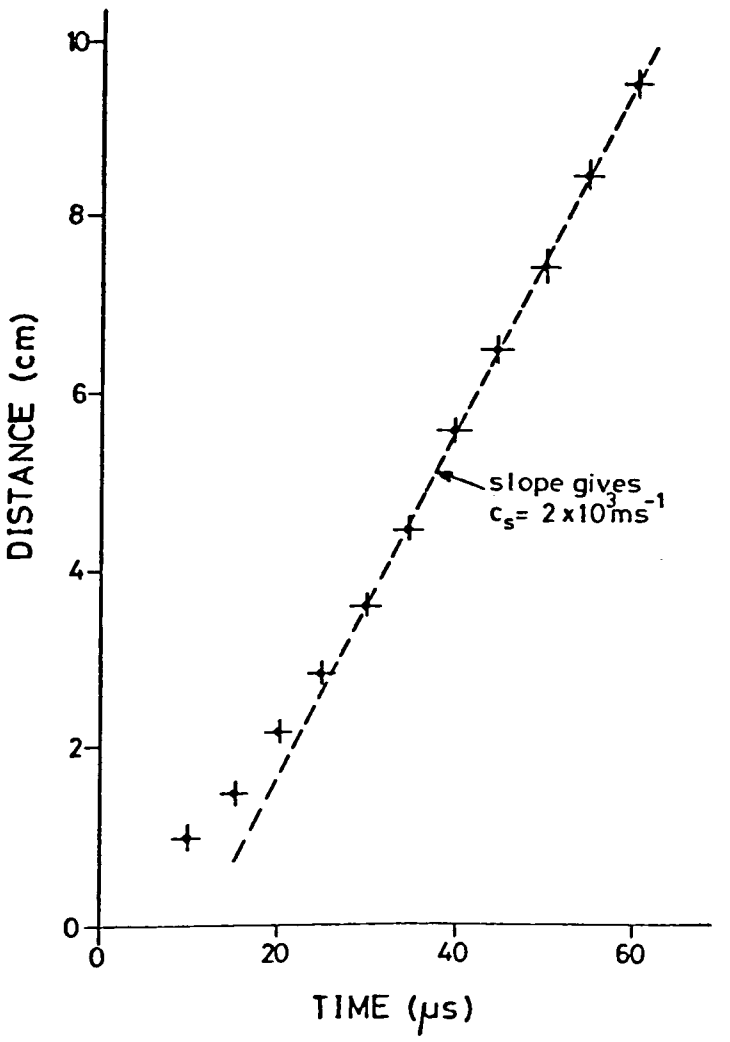
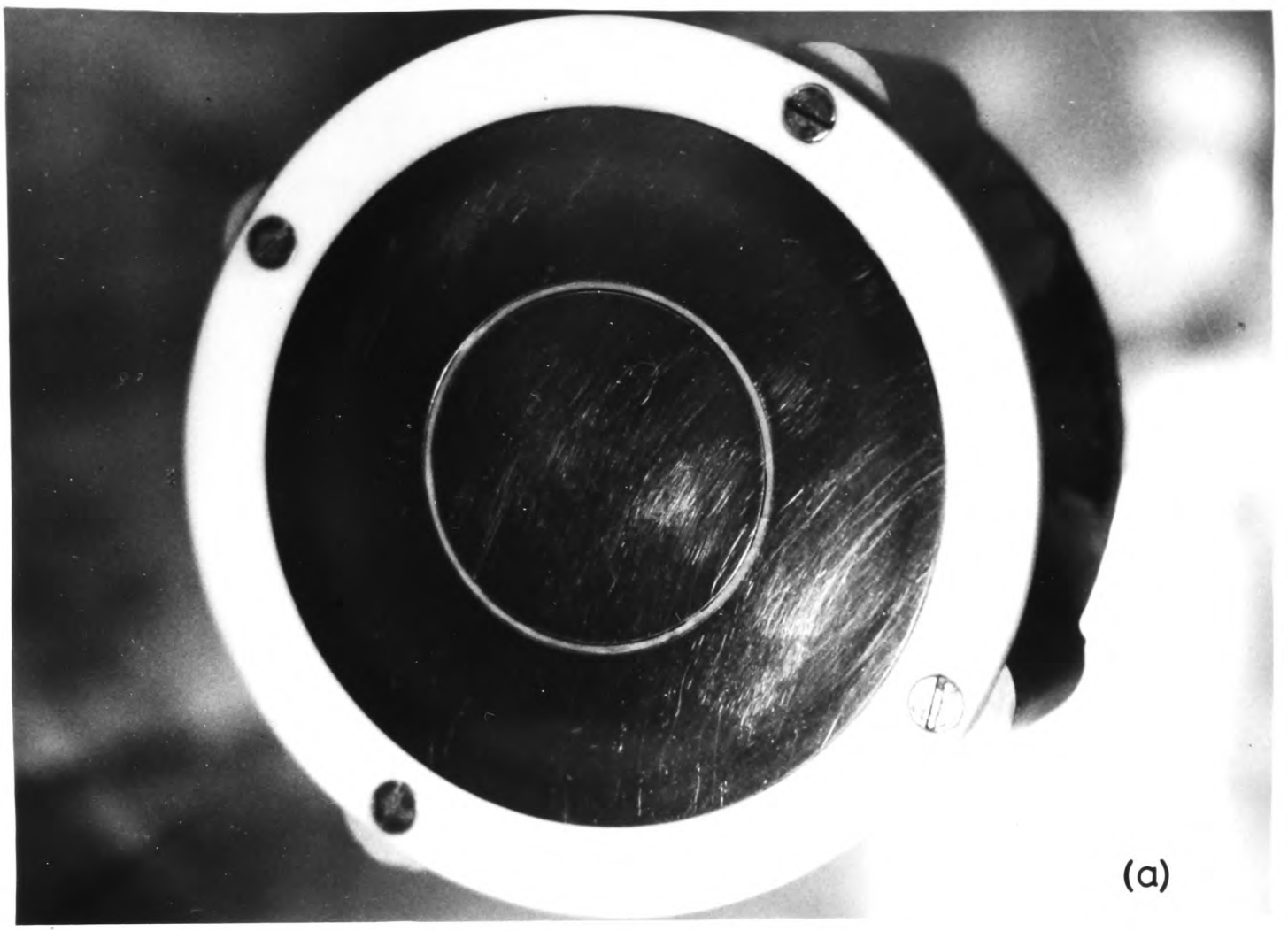


Figure 5.29

Distance-time results for the enhancement front from Figure 5.28.



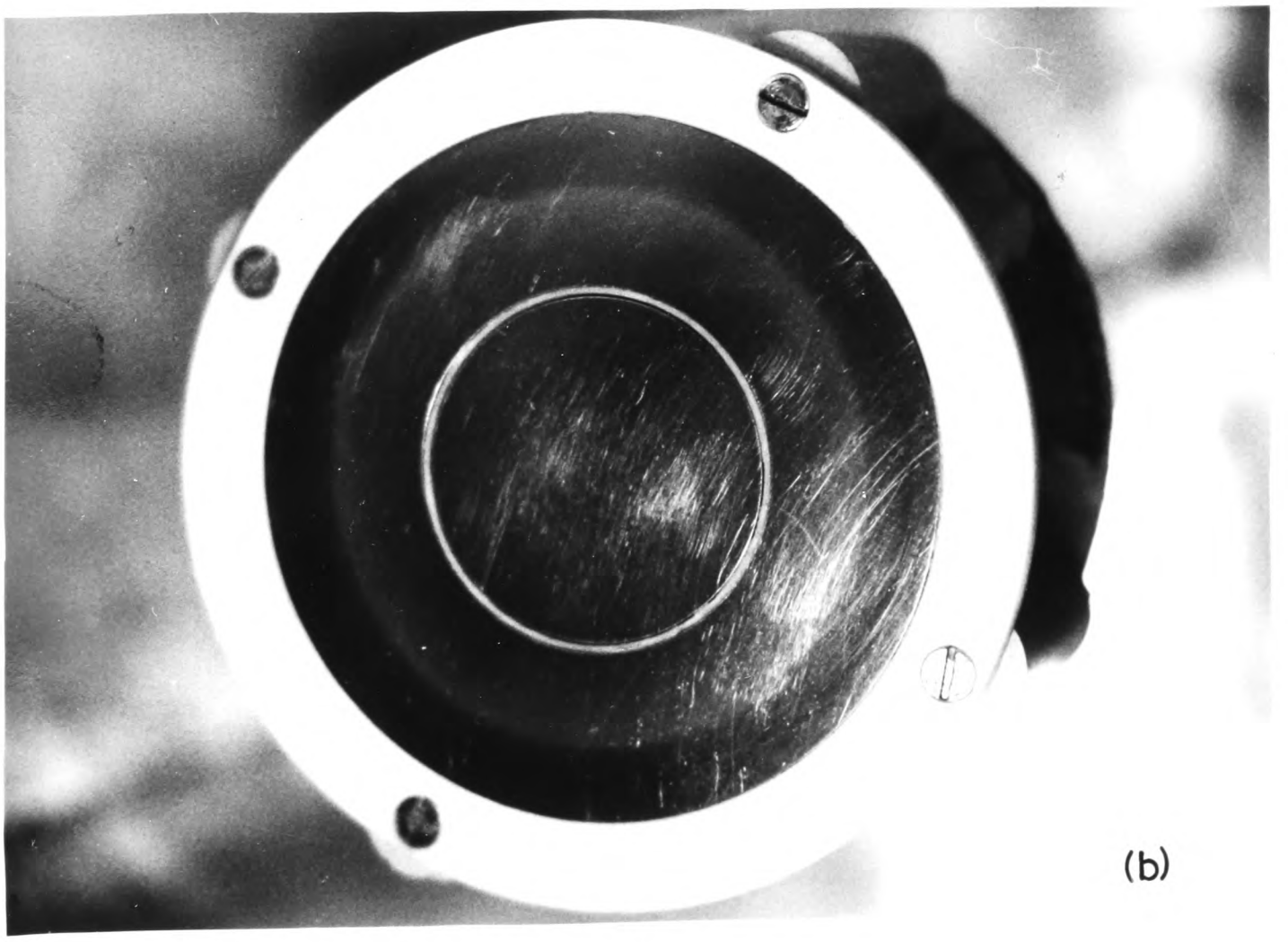


Figure 5.30
Glow on tantalum plate with large negative voltages applied (a) -1500V and (b) -2200V. Exposure time 1/60s.

5.5 OPTICAL MEASUREMENTS

In the course of some slow sheath expansion experiments it was noticed that a region near the plate appeared to illuminate when high negative voltages were applied. This effect, which was mentioned in Section 5.3.1 and is illustrated in Figures 5.6, 5.30 and 5.31, will now be discussed.

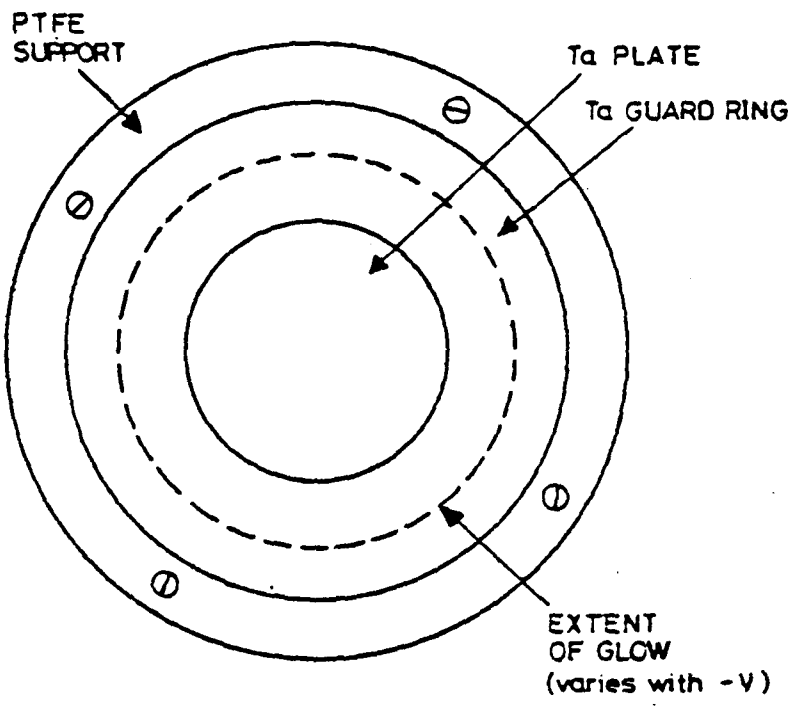


Figure 5.31
Schematic diagram of Figure 5.30. The dotted line shows the extent of the glow; the diameter of this boundary and the intensity of the glowing area within it change with applied voltage.

5.5.1 Observations

The following effects were noticed:-

(i) The appearance of the light was relevant on timescales of less than 100μs (see Figure 5.6) as well as on longer timescales of order seconds (see Figures 5.30 and 5.31). The mechanism producing the glow may thus be important for high voltage moving sheath experiments.

(ii) The light only appeared when tantalum was used. It was very much weaker (almost invisible) in the case of a copper plate.

(iii) Changing the background gas from argon to nitrogen or helium

did not change the blue colouration of the glow though the colour of the discharge was red in the case of nitrogen.

(iv) The intensity of the light was a function of the negative bias voltage applied to the plate. If the size of the plate voltage $|V_p|$ was below approximately 800V the light was invisible to the eye; if $|V_p|$ was greater than this value the light increased in intensity. The area of the glow decreased as the size of the plate voltage increased (see Figure 5.30). The edge of the glow on the plate seemed quite sharp. In addition the glow contracted radially still further if the neutral pressure (and therefore plasma density) was decreased.

(v) The glow was restricted to less than 1cm in front of the plate. This measurement was performed using the optical probe looking perpendicular to the plate axis (see Figure 5.32). The light signal transmitted through the optical fibre was measured using a photomultiplier as a function of distance away from the plate using the boxcar detector in fixed point mode. The resolution of this measurement was ~1cm because of the acceptance angle of the fibre, which meant that the actual glow probably extended less than this. This distance should be compared with the sheath width at high negative voltages which is of order cm. The glow is thus well within the sheath and near to the plate itself.

(vi) Some approximate measurements of the spectrum of the glow were made using a hand-held pocket spectrometer. Despite the large amount of background light (consisting of continuum radiation from the hot filaments with a superimposed line spectrum from the argon plasma), it was

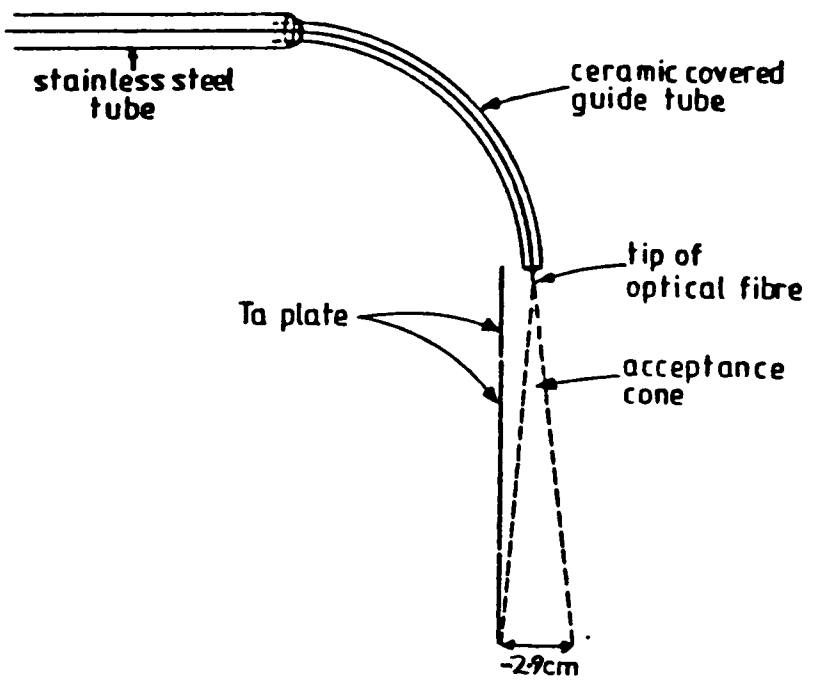


Figure 5.32
Construction of the optical probe, showing the dimensions of the acceptance cone relative to the 10cm diameter Ta plate.

possible to detect the glow which, rather than consisting of a sharp line spectrum, appeared to almost be a continuum but more intense in the blue end of the spectrum.

5.5.2 Discussion Of The Optical Results

The optical results raise a number of questions. We are interested to know if the process causing the glow affects the electrical experiments, as it would if charged particles were involved in the mechanism. We are also interested from a more fundamental point of view because similar observations have not been previously reported in plasmas. To quote from LANGMUIR and MOTT-SMITH (1924):

"In general whenever the collector was at potentials of 25 volts or more [up to 1160 V] negative with respect to the space, the positive ion sheaths seemed perfectly dark and had apparently perfectly sharp edges."

This observation was for a nickel plate in a mercury discharge, with an Hg pressure of ~1mtorr.

Our results, outlined above, seem to indicate that the glow is a property of the surface of the plate rather than of the background gas. The increase in intensity with bombarding ion energy is to be expected since the probability of most surface processes (e.g. secondary electron emission and sputtering) rises as the incident energy increases to kilovolts.

The contraction of the glow with increasing voltage is due to the charging up of the insulator (PTFE) surrounding the outer plate. This was proved as follows. A similar experiment was performed in which the full (-2200V) negative voltage was applied to the inner disc while allowing the annulus to float. A similar contraction of the glow appeared on the inner disc only. The annulus was then connected to a -200V power supply and the glow grew to cover almost the whole of the inner plate. It was thus clear that the charge on any adjacent surface controls the extent of the glow. An increase of the positive surface charge density on the insulator causes electrostatic focussing of the monoenergetic incident ions. This has the effect of forming a sharp boundary on the plate between areas where ion current was collected and not collected. The area of the glow is thus a diagnostic of the current-collecting area of the plate.

The restriction of the glow perpendicular to the plate is another proof that the glow is a surface phenomenon. The observations which indicated a continuum spectrum are unexpected. The results may be unreliable due to the poor resolution of the pocket spectrometer, but on the other hand it was possible to resolve the line spectrum of the plasma. Two possible explanations for the glow are now presented.

Firstly, incident ions are known to produce secondary electrons with an efficiency of up to 70% at these energies. Excitation of neutral particles in front of the plate (gas or tantalum) may be caused by these low energy electrons as they accelerate away from the the plate. The electrons are more likely to cause excitation than the incident ions because of their higher excitation cross-section. However, even the electrons have a mean free path of over 30m at these pressures, so that unless the neutral gas density in front of the plate is three or four orders of magnitude higher than anywhere else in the plasma chamber this process seems unlikely. Some elevation of the local neutral density may occur due to outgassing of the plate.

Secondly, incident ions produce neutral sputtered particles with an efficiency of 50-100% at these energies (CHAPMAN, 1980). It is possible that some of these may leave the surface in an excited state. Much work has been done on the topic of ion bombardment of solids, and the first spectroscopic work was reported by CHAUDHRI et al (1961). A review of the different mechanisms leading to surface light emission, together with the various typical spectra, has been given by KERKDIJK et al (1976a). Continuum radiation has been observed with certain metals (e.g. Ta, W, Mo) and a faint line spectrum was associated with others (e.g. Cu, Ni) by WHITE et al (1976). The light emission process was explained in terms of excited sputtered particles since secondary charged particles were proved not to be involved in the excitation mechanism (KERKDIJK et al, 1976b). The production of a continuum is usually explained by the sputtering of clusters rather than of individual atoms (KERKDIJK et al, 1976a). The fact that we observe the glow within 1cm of the plate indicates a short lifetime for these excited states.

More careful spectroscopy would be necessary in our experiment to vindicate this explanation completely. Some sputtering is known to occur in our case from the fact that a layer of tantalum is deposited on insulating surfaces placed adjacent to the plate. If no charged particles are involved in the mechanism the electrical experiments already described should not be affected. We should bear in mind, however, that some secondary electrons are formed as a result of the ion bombardment which will affect measurements of ion current to the plate.

5.6 SUMMARY OF EXPERIMENTAL RESULTS

The application of linearly increasing and decreasing negative voltage ramps to a large tantalum plate has given well-defined results on ion rarefaction and enhancement waves. Separating the effects of sheath expansion and collapse has been a useful technique.

Both slow and fast linearly increasing negative voltage ramps gave rise to rarefaction fronts, and sheath expansion was observed. On application of the fast ramp a rarefaction pulse was also generated. The rarefaction fronts were confirmed to move at the local ion acoustic speed into the plasma. Density and potential through the rarefaction region were measured and the results were mutually consistent.

Both slow and fast linearly decreasing negative voltage ramps gave rise to enhancement fronts and sheath collapse. The faster waveform gave rise to an enhancement pulse as well as a front. The enhancement fronts clearly moved at the local ion acoustic speed.

On the application of high negative voltages to the plate, for times $\gtrsim 100\mu s$, a glow was observed in front of the plate which was explicable in terms of excited sputtered particles.

5.7 ERRORS

The electron saturation current measurements had some associated error for the following reasons:-

(i) The cylindrical tantalum probe used in the ion rarefaction wave experiments was prone to surface contamination effects. This was avoided in the enhancement wave experiments by the use of a heated (but non-emitting) probe. More rarefaction wave results were taken with the heated probe and the previous cold probe results were confirmed.

(ii) We have so far ignored the effect of a change in plasma potential on the electron saturation current. Since neither probe shows a classical saturation, this effect may be important since we have assumed that a change in electron current for a fixed bias voltage ($>V_p$) is the result of a plasma density change.

The latter effect will now be discussed in more detail. The probe current I is a function of electron density n and probe potential with respect to the plasma ρ. If n and ρ vary, we may write

$$\delta I = \frac{\partial I}{\partial n}\delta n + \frac{\partial I}{\partial \rho}\delta \rho \qquad (5.1)$$

This expression may be considered for negative ρ (below plasma potential) and for positive ρ (above plasma potential).

Below plasma potential we have:-

$$I = I_0 \exp(-\frac{e\rho}{kT}) = ne\frac{\bar{c}}{4} A$$

Equation(5.1) now becomes

$$\delta I = I\frac{\delta n}{n} - (\frac{e}{kT})I\delta\rho$$

which vanishes for a Maxwellian electron velocity distribution. The variation of the response of an ion acoustic wave receiver has been used as a diagnostic for the measurement of plasma potential (SCHOTT, 1980b). If an emissive probe is used, δI still exists and ion acoustic waves can be detected (FUJITA et al, 1981).

For our case ρ is positive, but I still depends on ρ. For example, if the collecting probe radius is small with respect to λ_D orbital limited probe theory holds (SWIFT and SCHWAR, 1970) and I is proportional to $[1+e\rho/kT]^{1/2}$ in which case

$$\delta I = I\frac{\delta n}{n} + \frac{I}{2[1+e\rho/kT]}\frac{e.\delta\rho}{kT}$$

For large ρ, the left hand term will dominate and our measured density profiles will be fairly accurate. In our experiment $\rho \simeq 4kT/e$ and so the error is about 10%. The two effects of n and ρ perturbations add so that our experiments may give a slightly enhanced perturbed signal compared with the case where only one of these perturbations is present.

Ion saturation current is less prone to this effect, but was not used because of low signal levels and the fact that this would involve another ion-rich sheath in the measurement region which would lead to further plasma disturbance.

CHAPTER 6

DISCUSSION AND SUMMARY

6.1 INTRODUCTION

The major results presented in this thesis concern the motion of the boundary of a plasma leading to ion acoustic disturbances travelling into the plasma. In this Chapter, the theoretical (Chapter 2) and experimental (Chapter 5) results are compared. In particular, the relevance of the one-dimensional bounded plasma theory to a real three-dimensional plasma experiment is considered. The experimentally observed sheath edge velocity for the case of slow sheath expansion is then compared with a dynamic version of Child's Law. Measured current to the plate during the negative ramp voltage is also compared with theory.

The relationship of the phenomena observed in this thesis to the mechanism for ion acoustic wave generation from moving sheaths is then discussed. The Chapter ends with a summary of the results obtained in this work.

6.2 RAREFACTION AND ENHANCEMENT WAVES

In this Section we consider the theoretical and experimental results on the motion of a plasma boundary, which has been shown to lead to ion acoustic rarefactions and enhancements.

When comparing theory and experiment, three limitations on the theoretical model are :-

(i) Space charge is neglected. We are interested in disturbances of the plasma so that the assumption of quasineutrality is reasonable. The breakdown of this assumption in our theory at the moving sheath edge represents the limit of the plasma approximation. It also indicates that a more physical model was used here than in previous calculations (e.g. ALLEN and ANDREWS, 1970, ANDREWS, 1971).

(ii) The solution was found by making assumptions about the ion motion. Ions, which are born at all positions where the plasma density is finite, move at some local average speed, with no thermal spread, immediately they are produced. ANDREWS and SHRAPNEL (1972) applied a more realistic momentum equation to the case of an expanding sheath though the ions were still monoenergetic. The collapsing case would be an area for further study.

(iii) Our one-dimensional theory involves a presheath with a scale length L due to the effects of ionization. In a real experiment involving the movement of a sheath near an electrode additional presheath scale lengths may be present.

Firstly, it is known theoretically that a spherical probe in an infinite plasma has a scale length of the plasma solution which is the probe diameter (e.g. ALLEN, BOYD and REYNOLDS, 1957). For a small ion-collecting probe this will lead to a localized density perturbation which is controlled by the size and geometry of the probe. The sheath scale length will, of course, be the Debye length λ_D. Secondly, consider a small plane ion-collecting probe in a plasma. In the one-dimensional semi-infinite case, no presheath or scale length may exist. If the plasma is made finite but still one-dimensional the probe becomes one wall and the presheath scale length would be half of the inter-wall distance if an ion generation mechanism is included (c.f. Chapter 2). In a real three-dimensional plasma, if the current collected by the probe is much less than that collected by the walls, the overall plasma properties will not be significantly perturbed by the probe. A localized density change in front of the probe with a presheath scale length of order the probe diameter is to be expected. Such behaviour was observed by VAREY (1970). It is not clear whether this scale length is due to ionization or geometrical effects.

Experiment and theory may be compared for the case of expanding sheaths (c.f. Figures 5.8 and 2.9) and collapsing sheaths (c.f. Figures 5.22 and 2.6). In the former case, rarefaction waves are predicted and observed, while in the latter case enhancement waves are seen. Density and potential profiles show the same trends in both theory and experiment. In this sense there is qualitative agreement. It is not clear, however, that the theory has the correct presheath formation mechanism.

We now discuss the experimental evidence for the existence of presheaths in the multidipole device. Evidence for ion drift speeds was discussed in Chapter 4; these drifts were independent of the presence of the plate. The results may be summarized as follows:-

(i) Langmuir probe measurements showed a density profile with scale length ~15cm near the end walls of the device. This is substantiated by a variation of floating potential such that V_f is about 1V more negative near to both the end and side walls than in the centre of the plasma.

(ii) Ion acoustic wave experiments more than a few cm away from the transmitter showed the existence of both longitudinal and radial plasma drifts.

On the introduction of the metal plate at floating potential, a measurement of ion saturation current as a function of distance was made using the Method A anode connections (Section 3.3.2) and is shown in Figure 6.1. From this diagram the following effects are evident. The scale length of the wall presheath YW is approximately 20cm; the scale length of the presheath near the plate is substantially less than this. The latter region (PX) appears to be a localized perturbation occuring within one diameter of the plate. The flat region of the plot XY is not horizontal due to the effects of moving an earthed probe tube, and also uneven plasma production at the two ends of the device (because of the large insulators present in Method A). Similar trends were noticed using the Method B anode connections, but the probe tube effect was even more important in this case making experiments which involved motion of the probe by more than a few cm very difficult.

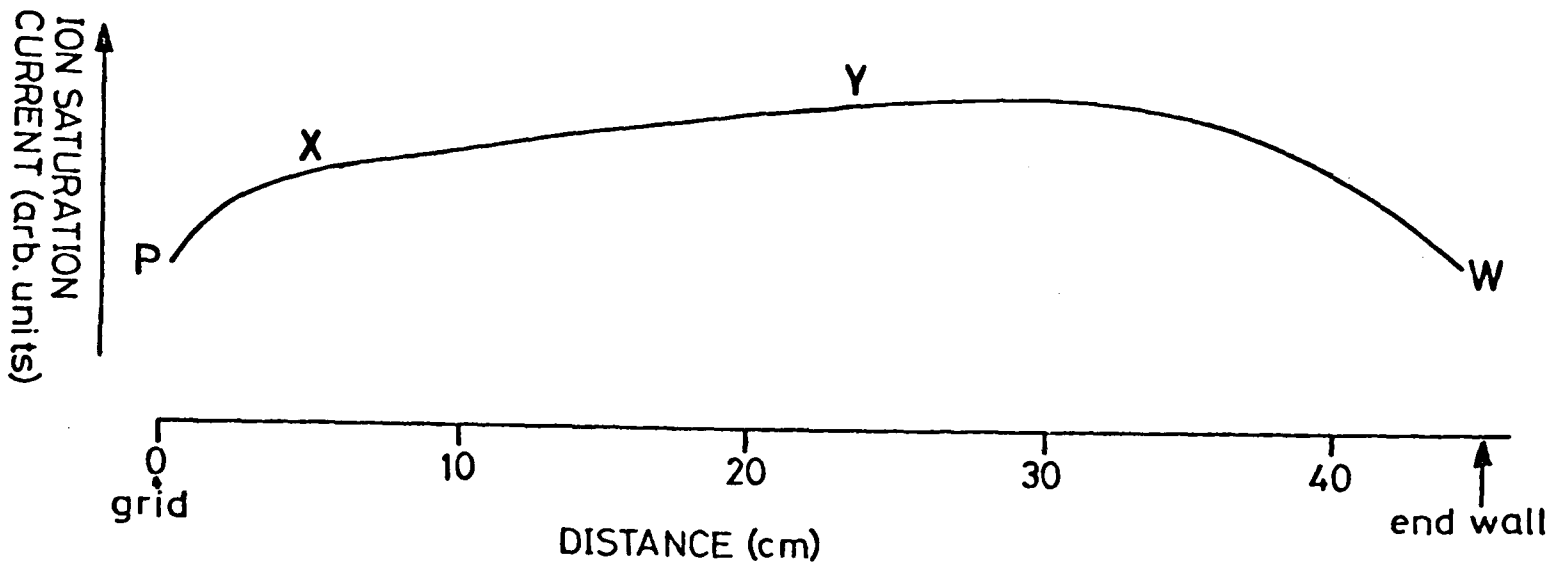


Figure 6.1
Density uniformity measurement (Method A anode arrangement).

Comparing Figure 6.1 with the theoretical steady-state density profile illustrated in Figure 2.1, the region YW approximates to the region 1<X<2 since Y is near the centre of the device. However, the region PX has a different scale length.

We now compare the theoretical and experimental distance-time diagrams for the wavefronts. The theoretical diagram is shown in Figure 2.2; measurements of the local ion acoustic distance-time relationship near the plate are shown in Figures 5.7 and 5.21 for the rarefaction case and 5.24+5.29 for the enhancement case. In the theoretical diagram, the wavefront accelerates from zero speed in the laboratory frame at X=0 and reaches a speed of c_s at X=1. It then accelerates further, due to the effects of ion drift towards the opposite wall. In the experimental diagrams a clear acceleration of the front is observed at low (≤4cm) distances after which a constant propagation speed is measured in agreement with the speed of ion acoustic waves and pulses travelling away from the plate (c.f. Figures 4.8 and 4.12). This behaviour may be approximated theoretically by viewing the local density and velocity gradients near the plate as one side of the positive column solution

(0<X<1) which matches onto another solution which has the scale length of the device. This latter scale length will appear relatively large near to the plate and so it will be ignored here. To construct the distance-time diagram the local perturbation is thus joined onto a straight line.

Figure 6.2 shows the results of comparing such a theoretical model with the experimental results in Figure 5.21 using an ion acoustic speed of 2×10^3 m/s for the denormalization of the theoretical curve. The diagram shows good agreement of experiment with the theory for an imposed scale length of 2.5cm. The distance X_0 has been included to allow for the effects of the sheath width at t=0 and a systematic probe position measurement error (2mm). Note that no transient sheath thickness has been included since the plate voltage does not change quickly enough for this to be important (i.e. the ions do have time to move in this experiment). The agreement in Figure 6.2 is not expected to be perfect because of other effects:-

(i) The scale length of the multidipole device has been ignored but it will have some effect since it is not very different from the plate scale length

(ii) At large values of X (greater than the plate radius R_p), the wavefronts are no longer plane and three-dimensional effects may be important

(iii) The model used for the curved portion of the theoretical trace is a bounded positive column solution with ionization; such a model may not apply exactly to the case of the local perturbation of density near a plane probe.

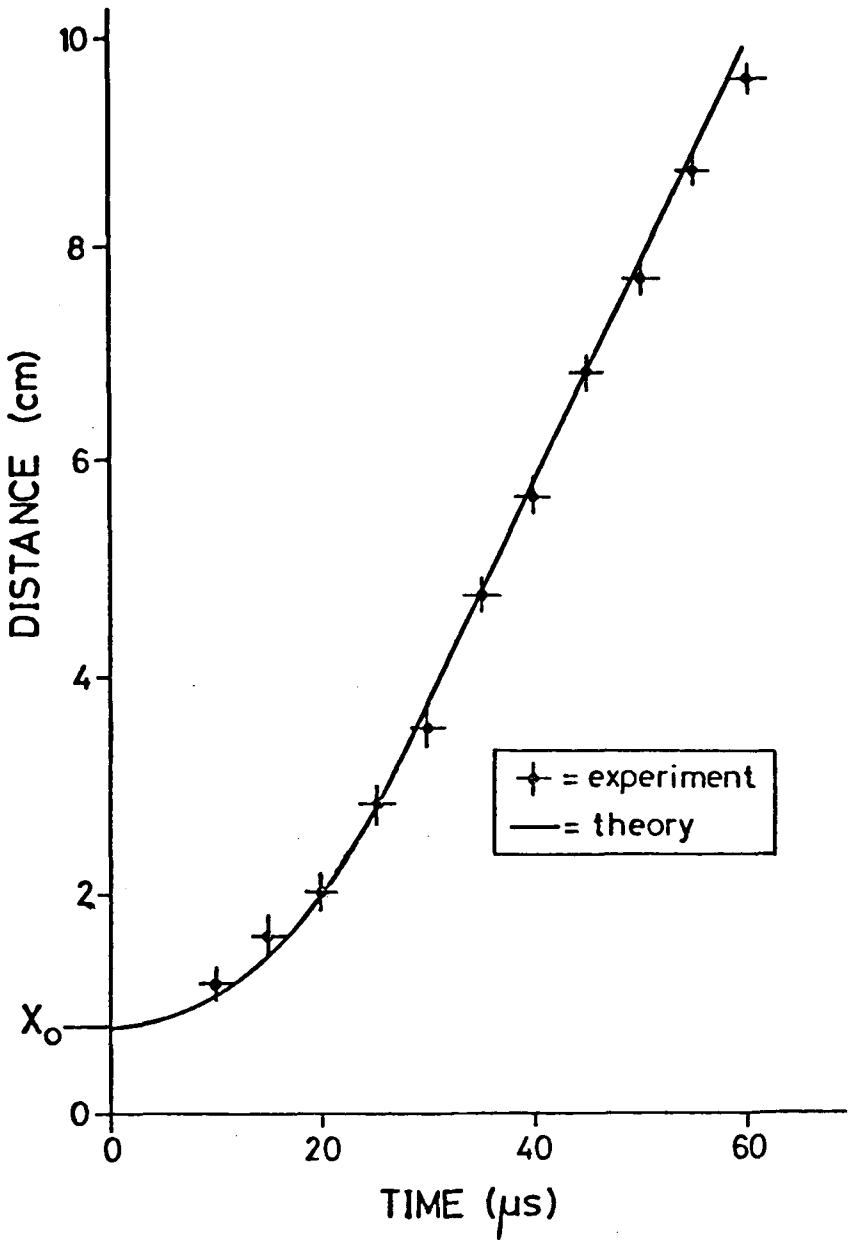


Figure 6.2

Distance-time diagram for rarefaction front (from Figure 5.21) compared with a plot of equation (2.28) using a scale length of 2.5cm matched to a constant ion acoustic speed of $2 \times 10^3 \text{ ms}^{-1}$. The enhancement front results show similar agreement.

The existence of two different scale lengths in the plasma emphasizes the difference between the one-dimensional theoretical model and the three-dimensional experiment. Note that an initial presheath will always be associated with any wave transmitter when the average applied voltage is below plasma potential.

Despite the various reservations on the application of our plane geometry theory to the experimental results, the agreement between the two is remarkably good. The only previous such comparison was made with a spherical geometry theory with no ionization by MISRA and SCHOTT (1973).

6.3 OBSERVATIONS OF THE SHEATH EDGE

The sheath edge was clearly visible in the experimental results of Chapter 5 as a sharp change in the measured density gradient. The most reliable data is from sampled-density profile measurements as in Figure 5.9. From such experiments it was possible to measure the sheath width as a function of time during the slow voltage ramps (see Figure 5.10). Previous experimental results have not been so clear (COATES, 1979) since electron current appeared to be drawn even when the probe was in the sheath. No sharp "knee" associated with the sheath edge was visible. The reason for this behaviour was not clear but may be due to the single-shot nature of the experiments or the positioning of the probe support. The results presented here show much more understandable behaviour.

For a slow voltage ramp such that ion transit times are fast with respect to times of interest it is possible to use a dynamic form of Child's Law to estimate the sheath width as a function of time (e.g. ANDREWS and VAREY, 1971). The static form of this Law was given in equation (1.2):

$$I = \alpha \frac{V^{3/2}}{s^2}$$

where α is a constant proportional to the plate area. In the case of a moving sheath edge, the voltage drop across the sheath V and the sheath width s will vary with time. Assume that I is constant as a first approximation since changes in V and s are more significant than changes in I from the experimental results. The functional form of V(t) is $(V_o + \beta t)$ so that

$$s = \left(\frac{\alpha}{I}\right)^{1/2} (V_o + \beta t)^{3/4} \qquad (6.1)$$

where V_o is the initial bias voltage and β is the slew rate $(\frac{dV}{dt})$ of the ramp waveform. This equation represents a succession of quasi-static states where the potential profile has time to reach an equilibrium with the applied plate voltage at all times during the ramp.

This expression may be compared with the experimental expanding sheath data shown in Figure 5.10. A comparison is given in Figure 6.3(a) for various different negative voltage ramps. We may also compare data from the collapsing sheath experiment with theory in a similar manner (Figure 6.3(b)). The different initial sheath distances s_0 and s_1 in the two diagrams 6.3(a) and (b) correspond to different values of the V_0 term in equation (6.1). The theoretical model is very simplified since the effects of plasma electrons are neglected (reasonable at high negative voltages) and also the ion current to the plate is assumed constant for the whole ramp. Agreement between theory and experiment is reasonable as a result of the sheath edge speeds being very slow (of order 1/10 of the ion acoustic speed). Note that the data used for Figure 6.3 are from boxcar-averaged density profiles rather than from oscillograms where the measurement errors are larger.

The sheath edge velocity functions used in Chapter 2 (see Figure 2.11) may now be compared with those measured in experiments. The different intercepts s_0 and s_1 in Figure 6.3 should be set to zero to compare with theory. Equation (6.1) shows that if the Child's law theory is correct, $\frac{ds}{dt}$ is discontinuous at t=0. This indicates that a centred wave theoretical solution would be necessary for this case. The particular expanding sheath initial conditions used in the theory are not directly comparable with those

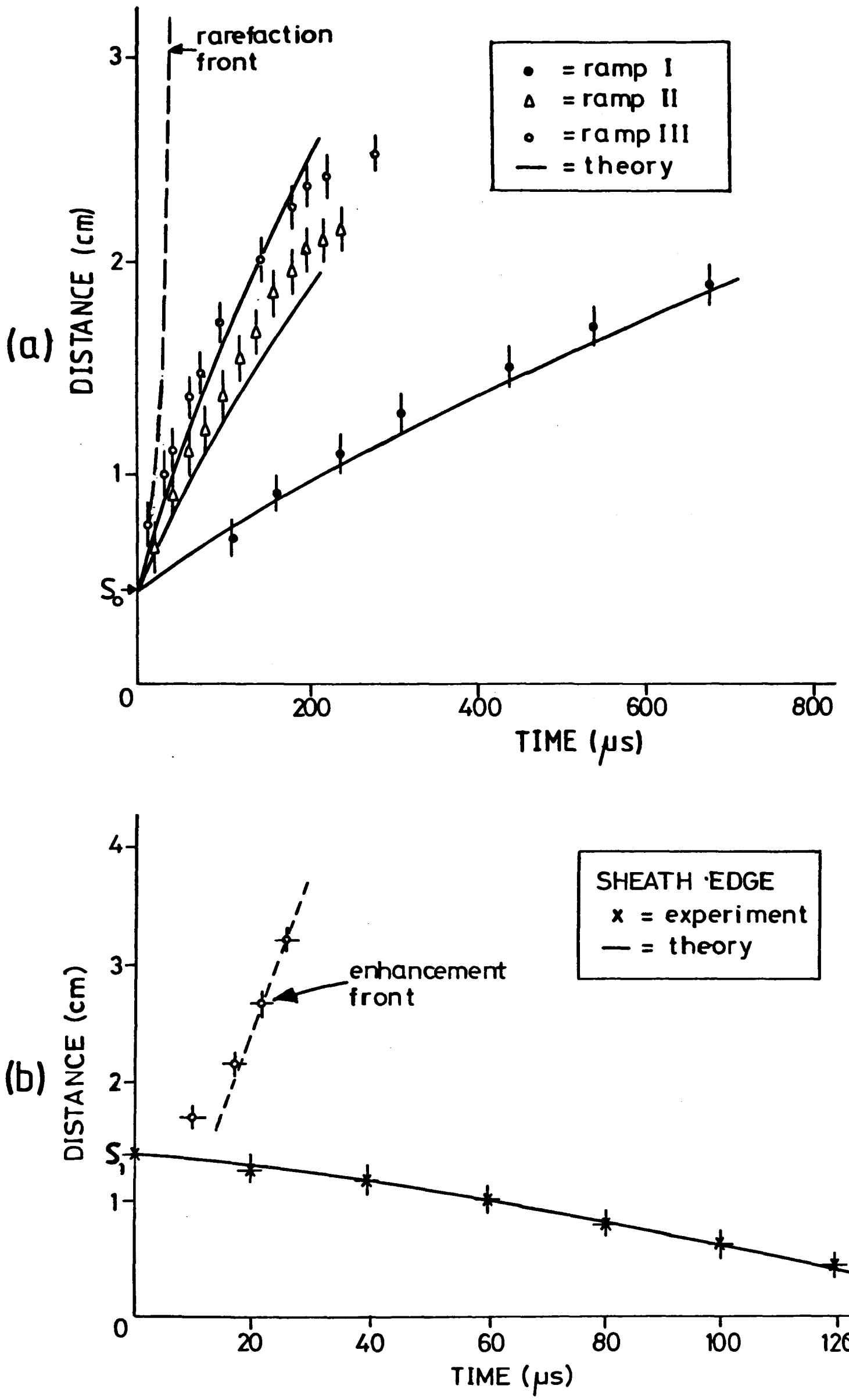


Figure 6.3

Comparison of experimental and theoretical distance-time diagrams for the sheath edge; (a) for an expanding sheath from Figure 5.10 and (b) for a collapsing sheath from Figure 5.24.

indicated in Figure 6.3(a) since the experimental curve decelerates with time. However, the speed of the sheath edge is at all times less than the local ion acoustic speed in undisturbed plasma. Further work is possible on using a more realistic sheath edge velocity function in the expanding sheath theory, but results similar to Figure 2.9 are expected. A variety of sheath edge velocity functions have been used for the collapsing sheath case, with no significant differences in the results.

6.4 CURRENT TO THE PLATE

The experimental measurements of current to the plate during the slow negative- and positive-going voltage ramps were shown in Figures 5.16 and 5.25. The results show an increase in current for an expanding sheath and a decrease for a collapsing sheath in addition to the secondary and geometrical effects already mentioned. In both cases the AC component of current is approximately 25% of the steady current at t=0. We shall now compare these results with theory.

The current density measured at the plate will equal the current density in the plasma; at the sheath edge we have

$$j = n_s e(v_i - v_e)$$

where n_s is the plasma density at the sheath edge. v_i and v_e are the ion and electron drift velocities in the laboratory frame. Now v_e is assumed to equal the speed of the plasma boundary (ALLEN and ANDREWS, 1970) so that

$$j = n_s e(v_i - v_s)$$

Using the dynamic Bohm criterion (equation 1.8) this gives

$$j = n_s e c_s \qquad (6.2)$$

This is the dynamic current to the plate (c.f. the steady case, equation (1.1)). The plasma density at the sheath edge n_s is determined by moving sheath theory.

According to the theory of ALLEN and ANDREWS (1970),

$$n_s = n_o \exp[(v_s/c_s) - 1] \qquad (6.3)$$

This expression is in qualitative agreement with our measurements since positive v_s (an expanding sheath) gives a current increase while negative v_s (sheath collapse) causes a decrease in current. Quantitatively, the results for ramp II in Figure 5.10 may be compared with Figure 5.16. The sheath edge velocity $v_s \simeq .05c_s$ so that the current increase should be approximately 5%. This is lower than the experimentally observed current, probably due to the limitations of this theory which omits a presheath.

The theory which was presented in Chapter 2 gives different variations of n_s with time depending on the applied sheath edge velocity function (see Figures 2.6, 2.14 and 2.9). This is thought to be due to the unrealistic sheath edge velocity functions used in our particular calculations. Changes in n_s are observed to be of order 10% in agreement with the measurements. Further work using this model may be fruitful.

6.5 OTHER OBSERVATIONS

An observation which was not explained and deserves further study concerns the rarefaction and compression pulses formed in addition to the respective wavefronts in the case of the fast

voltage ramp application. The effect, which disappears at high neutral pressures, is not explicable in terms of the theory presented in Chapter 2 and is not at present understood. A similar case of a pressure increase causing the disappearance of a rarefaction pulse was reported in the spherical geometry expanding sheath results of WIDNER et al (1970). The geometry of the experiments reported in this thesis is thought to be planar to a good approximation since our data were taken at plate-probe separations less than the plate diameter.

The optical emission which was observed in front of the tantalum plate on the application of either alternating or constant high negative voltages is an interesting phenomenon. The existence of light in the sheath region is thought to be a result of excited sputtered particles due to fast ion bombardment as indicated in Chapter 5. Since no other charged particles are thought to be involved in this process (for example, there is no ionization within the sheath), the observation serves as a diagnostic of the current collecting area of the plate and should not affect the results in any other way.

6.6 THE PRODUCTION OF ION ACOUSTIC WAVES

The mechanism for production of ion acoustic waves from moving sheath edges would now appear to be clear both theoretically and experimentally. Theoretically, the introduction of a local ion acoustic speed by way of a presheath scale length has removed the previous problems which meant that only ion rarefaction waves were possible. Sheath collapse has now been associated with ion "enhancement" waves, where the plasma density is larger than its

steady-state value at a particular position. The word "compression" is not used since the ionization introduces new particles into the system causing a density increase. The theory also predicts ion rarefaction waves moving at the same speed on expansion of the sheath. A combination of rarefaction and enhancement wave generation by oscillating the sheath edge position will thus lead to ion acoustic waves in the plasma. The effects of a different momentum equation (see Chapter 2) are not expected to change the results significantly in the plasma region.

The presheath, which has been seen to be so important in the generation of ion acoustic waves, is formed in our theory by the presence of ionization in a bounded plasma. An alternative method of producing a presheath would be to use spherical geometry where a finite plasma model is unnecessary. Theoretical work on spherical sheath collapse using the method of characteristics rather than a similarity approach (which allows no scale length) would be useful. Experiments are also possible.

The results of experiments on plane geometry sheath motion agree well with theory. In particular, the generation of enhancements and rarefactions has been unambiguously linked with collapsing and expanding a sheath edge. Also a speed-up of both wavefronts has been observed indicating the presence of an initial presheath. Faster alternating motion of the sheath edge has excited ion acoustic waves in agreement with many other authors.

6.7 SUMMARY AND CONCLUSIONS

In this thesis, the response of a plasma to the motion of its boundary has been studied. Chapter 1 was concerned with previous work on this topic. The theoretical problem favoured in the past was the plasma response to motion of its boundary at a speed less than the ion acoustic speed. Most of this work ignored the effects of initial ion motion; ion rarefactions were created by both the expansion and the collapse of ion-rich sheaths. Experiments were previously concerned with the effects of expanding sheaths.

A theory of the plasma response to a moving sheath which includes the effects of initial ion motion was presented in Chapter 2. A one-dimensional quasineutral plasma solution was found by using an ionization term in the fluid equations. This involved the introduction of a scale length. The method of characteristics was then used to solve time-dependent versions of these equations. Collapse of the sheath was associated with density enhancements, whilst sheath expansion caused rarefaction waves. These disturbances moved at the local ion acoustic speed, including the effects of initial ion drift velocities. The theory predicted a breakdown of quasineutrality at the moving sheath edge. This feature showed the more physical nature of these calculations compared to previous work and was shown to be expected if the dynamic Bohm criterion was applied at the sheath edge. The other boundary condition was the imposed function used for the sheath edge velocity. This was arbitrary (with the limitation that the sheath edge itself could not in general coincide with a characteristic), and here speeds less than the local ion acoustic speed were imposed. Further work could usefully consider the case of sheath collapse

both in spherical geometry and in plane geometry with a different momentum equation to that used in this work.

In Chapter 3 the experimental arrangement of the multidipole device was described. This device was used as a plasma source for the experiments described in Chapters 4 and 5.

Chapter 4 contained the results of various experiments which were carried out to measure the basic properties of the plasma. Langmuir probe and ion acoustic wave and pulse techniques were used to investigate various plasma parameters. The ion acoustic speed was found to be dependent on the electron velocity distribution function, which showed a higher number density of energetic electrons than would be expected from a single Maxwellian distribution function. Other results are summarized in Section 4.6.1. When the wave transmitter drew large electron currents (i.e. when it was near to or above plasma potential), wall-excited ion acoustic waves were observed as a result of a transient change in plasma potential.

Experiments to study the motion of a plasma boundary were discussed in Chapter 5. Large negative linearly decreasing and increasing voltage ramps were separately applied to a large tantalum plate in the plasma. The response of the plasma to slow sheath motion was measured with a Langmuir probe. Sheath expansion was clearly associated with rarefaction waves while sheath collapse produced enhancement waves. The rarefaction and enhancement fronts moved at the local ion acoustic speed into the plasma, the increase in measured speed indicating the presence of an initial presheath. Some sampled potential measurements in the rarefaction wave region showed consistent trends. Faster ramp waveforms produced a plasma

response which included both a front and a pulse. This behaviour was not understood and would be an area for further study. A glow was observed in front of the plate associated with the high negative voltages; this is thought to be due to excited sputtered particles.

In Chapter 6 a comparison of experiment with theory has been given. It is found that the two are comparable if a scale-length of order the plate radius is used in the theoretical model. The motion of the sheath edge in response to the slow ramp voltages has been shown to be in approximate agreement with a simple model involving a succession of quasi-static states. The measured current to the plate agrees qualitatively with moving sheath theory.

In conclusion it has been shown both theoretically and experimentally that the presence of an initial presheath is essential to the generation of ion enhancement waves in plasmas. Enhancements and rarefactions together constitute complete ion acoustic waves and are individually associated with the collapse and expansion of an ion-rich sheath. The theoretical and experimental separation of these processes has served to clarify the process of ion acoustic wave generation by a moving sheath.

REFERENCES

AKSORNKITII, S., HSUAN, H.C.S. and LONNGREN, K.E., (1969), J. Appl. Phys., 40, 2674.

ALEXEFF, I., JONES, W.D., LONNGREN, K. and MONTGOMERY, D., (1969a), Phys. Fluids, 12, 345.

ALEXEFF, I., HIROSE, A., JONES, W.D., LONNGREN, K. and WIDNER, M., (1969b), Proc. Int. Conf. Quiescent Plasmas, Paris, p.85.

ALLEN, J.E., (1974), "Plasma Physics" (B.E. Keen, ed.), Ch. 5, I.O.P. Conference Series no. 20.

ALLEN, J.E., (1978), J. Phys. D (Appl. Phys.), 11, L35.

ALLEN, J.E. and ANDREWS, J.G., (1970), J. Plasma Phys., 4, 187.

ALLEN, J.E., BOYD, R.L.F. and REYNOLDS, P., (1957), Proc. Phys. Soc. B70, 297.

ANDREWS, J.G., (1970), J. Plasma Phys., 4, 603.

ANDREWS, J.G., (1971), Phys. Fluids, 14, 129.

ANDREWS, J.G. and SHRAPNEL, A.J., (1972), Phys. Fluids, 15, 2271.

ANDREWS, J.G. and VAREY, R.H., (1971), Phys. Fluids, 14, 339.

ARMSTRONG, R.J., WEBER, W.J. and TRULSEN, J., (1979), Phys. Letters, 74A, 319.

BERTOTTI, B., CAVALIERE, A. and GIUPPONI, P., (1966), Phys. Fluids, 9, 265.

BEZZERIDES, B., FORSLUND, D.W. and LINDMAN, E.L., (1978), Phys. Fluids, 21, 2179.

BOHM, D., (1949), "The Characteristics of Electrical Discharges in Magnetic Fields" (A. Guthrie and R.K. Wakerling, eds.), Ch. 3, McGraw-Hill, N.Y.

BRAITHWAITE, N.St.J., (1977), M.Sc. Dissertation, Univ. of Oxford.

BROWN, S.C., (1966), "Basic Data of Plasma Physics", M.I.T.

CARUSO, A. and CAVALIERE, A., (1962), Nuov. Cim., 26, 1389.

CHAPMAN, B., (1980), "Glow Discharge Processes: Sputtering and Plasma Etching", Wiley.

CHAUDHRI, R.M., (1961), Proc. Int. Conf. Phenom. Ionized Gases, Munich, p.1175.

CHEN, F.F., (1965a), "Plasma Diagnostic Techniques", (R.H. Huddlestone and S.L. Leonard, eds.), Ch. 4, Academic Press, N.Y.

CHEN, F.F., (1965b), Plasma Phys., 7, 47.

CHEN, T. and SCHOTT, L., (1977), Phys. Fluids, 20, 844.

CHESTER, J.K., (1970), J. Sci. Tech., 37, 2.

CHILD, C.D., (1911), Phys. Rev., 32, 492.

CHRISTENSEN, T. and HERSHKOWITZ, N., (1977), Phys. Letters, 61A, 170.

CIPPOLA, J.W.,Jr., and SILEVICH, M.B., (1981), J. Plasma Phys., 25, 373.

COAKLEY, P., and HERSHKOWITZ, N., (1980), Phys. Letters, 78A, 145.

COAKLEY, P., HERSHKOWITZ, N., HUBBARD, R., and JOYCE, G., (1978), Phys. Rev. Letters, 40, 230.

COATES, A.J., (1979), M.Sc. Dissertation, Univ. of Oxford.

COBINE, J.D., (1958), "Gaseous Conductors", 2nd. Ed., Dover, N.Y.

CROW, J.E., AUER, P.L. and ALLEN, J.E., (1975), J. Plasma Phys., 14, 65.

D'ANGELO, N., HERINK, K., KOZIMA, H. and REINLEITNER,L., (1978), J. Phys. Soc. Jpn., 44, 991.

DEBYE, P., and HUCKEL, E., (1923), Phys. Z., 24, 185.

DRUYVESTEYN, M.J., (1930), Z. Phys., 64, 781.

EDGLEY, P.D., (1975), D.Phil. Thesis, Univ. of Oxford.

EDWARDS HIGH VACUUM, (1974), Catalogue.

EMELEUS, K.G. and BROWN, W.L., (1936), Phil. Mag., 22, 898.

EMMERT, G.A., WIELAND, R.M., MENSE, A.T. and DAVIDSON, J.N., (1980), Phys. Fluids, 23, 803.

ENGEL, A.H.von, (1965), "Ionized Gases", O.U.P.

FELBER, F.S., and DECOSTE, R., (1978), Phys. Fluids, 21, 520.

FRANKLIN, R.N. and OCKENDON, F.R., (1970), J. Plasma Physics, 4, 371.

FUJITA, H., YAGURA, S. and YAMADA, E., (1981), Phys. Letters, 83A, 12.

GLANZ, J. and HERSHKOWITZ, N., (1981), Plasma Phys., 23, 325.

GOEDE, A.P.H., GREEN, T.S. and SINGH, B., (1980), J. Appl. Phys., 51, 1896.

GOLDAN, P.D., (1970), Phys. Fluids, 13, 1055.

GOLDAN, P.D. and LEAVENS, W.M., (1970), Phys. Fluids, 13, 433.

GUREVICH, A.V., PARIISKAYA, L.V. and PITAEVSKII, L.V., (1966), Sov. Phys. JETP, 22, 449.

HARRISON, E.R. and THOMPSON, W.B., (1959), Proc. Phys. Soc., 74, 145.

HERSHKOWITZ, N., deKOCK, J.R., COAKLEY, P. and CARTIER, S.L., (1980), Rev. Sci. Inst., 51, 64.

HERSHKOWITZ, H., ZE, F. and KOZIMA, H., (1979), Phys. Fluids, 22, 338.

deHOOG, A.C. and SCHOTT, L., (1970), Rev. Sci. Inst., 41, 1340.

HOLMES, R. and YANABU, S., (1973), J. Phys. D (Appl. Phys.), 6, 1217.

IIZUKA, S., MICHELSEN, P., RASMUSSEN, J.J., SCHRITTWIESER, R., HATAKEYAMA, R., SAEKI, K. and SATO, N., (1981), J. Phys. E (Sci. Instrum.), 14, 1291.

IKEZI, H., KIWAMOTO, Y., LONNGREN, K.E., BURDE, C.M. and HSUAN, H.C.S., (1973), Plasma Phys., 15, 1141.

JONES, W.D. and ALEXEFF, I., (1965), Phys. Rev. Letters, 15, 286.

JONES, W.D., LEE, A., GLEMAN, S.M. and DOUCET, H.J., (1975), Phys. Rev. Letters, 35, 1349.

JOYCE, G., LONNGREN, K., ALEXEFF, I. and JONES, W.D., (1969), Phys. Fluids, 12, 2592.

KAMINSKY, M., (1965), "Atomic and Ionic Impact Phenomena on Metal Surfaces", Springer-Verlag, Berlin.

KERKDIJK, C.B., KISTEMAKER, J. and SARIS, F.W., (1976a), in "Physics of Ionized Gases", p.357, Proc. 8th. Int. Summer School, Dubrovnic, Yugoslavia.

KERKDIJK, C.B., SCHARTNER, K.H., KELLY, R. and SARIS, F.W., (1976b), Nucl. Inst. Meth., 132, 427.

LAM, S.H., (1965), Phys. Fluids, 8, 73.

LANGMUIR, I. and MOTT-SMITH, H.,Jr., (1924), Gen. Electr. Rev., 27, 449.

LANDAU, L.D. and LIFSHITZ, (1959), "Fluid Mechanics", Pergamon.

LEUNG, K.N., SAMEC, T.K. and LAMM, A., (1975), Phys. Letters, 51A, 490.

LIMPAECHER, R. and MacKENZIE, K.R., (1973), Rev. Sci. Inst., 44, 726.

MISRA, S.G. and SCHOTT, L., (1973), Plasma Phys., 15, 883.

MOORE, P.A.C., (1979), D.Phil Thesis, Univ. of Oxford.

MOORE, P.A.C., (1981), J. Phys. D (Appl. Phys.), 14, 1429.

NAKAMURA, Y., NAKAMURA, M. and ITOH, T., (1976), Phys. Rev. Letters, 37, 209.

NAKAMURA, Y. and NOMURA, Y., (1978), Phys. Letters, 65A, 415.

NAKAMURA, Y., NOMURA, Y. and ITOH, T., (1980), Proc. 4th. Int. Conf. Plasma Phys., p.119, Nagoya, Japan.

OLESON, N.L. and FOUND, C.G., (1949), J. Appl. Phys., 20, 416.

OLIVER, B.M. and CLEMENTS, R.M., (1975), J. Phys. D (Appl. Phys.), 8, 914.

PREWETT, P.D., (1974), D.Phil. Thesis, Univ. of Oxford.

PREWETT, P.D. and ALLEN, J.E., (1973), J. Plasma Phys., 10, 451.

RICHARDS, S.L.F., JONES, R.P. and LLOYD, G.J., (1975), Int. J. Electronics, 38, 551.

SCHOTT, L., (1968), "Plasma Diagnostics" (W. Lochte-Holgrevin, ed.), Ch. 11, North Holland.

SCHOTT, L., (1978), Rev. Sci. Inst., 49, 491.

SCHOTT, L., (1980a), Phys. Fluids, 23, 147.

SCHOTT, L., (1980b), Rev. Sci. Inst., 51, 383.

SELF, S.A., (1965), Phys. Fluids, 6, 1762.

SMITH, J.R., HERSHKOWITZ, N. and COAKLEY, P., (1979), Rev. Sci. Inst., 50, 210.

SPIELMAN, R.B., deGROOT, J.S. and RASMUSSEN, D.A., (1976), J. Appl. Phys., 47, 1909.

SWIFT, J.D. and SCHWAR, M.J.R., (1970), "Electrical Probes for Plasma Diagnostics", Iliffe.

TAYLOR, G.R. and LEUNG, K.N., (1976), Rev. Sci. Inst., 47, 614.

TAYLOR, R.J., BAKER, D.R. and IKEZI, H., (1970), Phys. Rev. Letters, 24, 206.

TAYLOR, R.J., IKEZI, H. and MacKENZIE, K.R., (1969), Proc. Int. Conf. Quiescent Plasmas, Paris, p.57.

TAYLOR, R.J., MacKENZIE, K.R. and IKEZI, H., (1972), Rev. Sci. Inst., 43,1675.

TONKS, L. and LANGMUIR, I., (1929), Phys. Rev., 33, 1070, 34, 876.

TSUKABAYISHI, Y., NAKAMURA, Y. and OGINO, T., (1981), Phys. Letters, 81A, 507.

VAREY, R.H., (1970), J. Phys. D (Appl. Phys.), 3, 1107.

VAREY, R.H. and SANDER, K.F., (1969), Brit. J. Appl. Phys. (J. Phys. D), 2, 541.

WATANABE, S., (1975), J. Plasma Physics, 14, 353.

WHITE, C.W., TOLK, N.H., KRAUS, J. and van der WEG, W.F., (1976), Nucl. Inst. Meth., 132, 419.

WICKENS, L.M. (1980), D. Phil Thesis, Univ. of Oxford.

WICKENS, L.M. and ALLEN, J.E., (1979), J. Plasma Phys., 22, 167.

WICKENS, L.M. and ALLEN, J.E., (1981), Phys. Fluids, 24, 1894.

WICKENS, L.M., ALLEN, J.E. and RUMSBY, P.T., (1978), Phys. Rev. Letters, 41, 243.

WICKENS, L.M., BRAITHWAITE, N.St.J. and COATES, A.J., (1982), Phys. Letters, 88A, 147.

WIDNER, M., ALEXEFF, I. and JONES, W.D., (1971), Phys. Fluids, 14, 795.

WIDNER, M., ALEXEFF, I. and JONES, W.D., (1972), J. Appl. Phys., 43, 1532.

WIDNER, M., ALEXEFF, I., JONES, W.D. and LONNGREN, K.E., (1970), Phys. Fluids, 13, 2532.

WILSON, R.R., (1941), Rev. Sci. Inst., 12, 91.

WONG, A.Y., MOTLEY, R.W. and D'ANGELO, N., (1964), Phys. Rev., 133A, 436.

A WAVE OF ION DENSITY ENHANCEMENT FOLLOWING SHEATH CONTRACTION

L.M. WICKENS [1], N.St.J. BRAITHWAITE and A.J. COATES
Department of Engineering Science, University of Oxford, Oxford, OX1 3PJ, UK

Received 14 October 1981

The method of characteristics is used to study disturbances generated by the contraction of ion-rich sheaths. It is shown that an enhancement of ion density propagates into the plasma at the local ion acoustic speed. This complements the density rarefactions associated with expanding sheaths.

It is well established that sheath edge motion can be accompanied by rarefactive disturbances travelling at the ion acoustic speed [1,2]. The generation of compressive features by sheath edge motion is less well understood, although both rarefactive and compressive components are necessary if an oscillating sheath is to launch ion acoustic waves. In order to study the effects of sheath edge motion on a plasma, it is necessary to specify the steady state into which the disturbance is to propagate. For example, fluid models without [1,2] and with [3] ionization terms may be employed. Not only are models without ionization restricted to a semi-infinite description, but also, in planar geometry, when the plasma boundary is moved either into or away from the plasma, such models can only give rise to rarefactive disturbances. The absence of a compression-like feature is an artefact of an ionization-free steady state, which necessarily excludes gradients of ion density and velocity in the undisturbed plasma. The inclusion of an ionization term introduces an additional degree of freedom that allows a self-consistent steady-state model (e.g. a positive column), with the ionization balancing the wall losses. It is shown here that with this latter model compressive features can be generated by a contracting sheath. The boundary conditions applied here lead naturally to the breakdown of quasi-neutrality at the moving sheath edge; this was not the case for the boundary conditions used in [3].

[1] Now at the Theoretical Physics Division, AERE Harwell, Didcot, Oxon. UK.

A voltage waveform applied to an electrode immersed in a plasma causes the ion space-charge sheath between it and the plasma to expand, or contract, by moving the sheath–plasma boundary [4]. This boundary communicates information regarding its motion into the bulk of the plasma via characteristic propagation paths (or characteristics). The characteristic delimiting the undisturbed plasma from the disturbed plasma travels with the local ion acoustic speed (i.e. the speed of ion acoustic waves in the moving ion fluid) and corresponds with the wavefront. The conditions in the disturbed region between the wavefront and the sheath edge are studied here, paying particular attention to the boundary conditions to be employed at the wavefront and the sheath edge.

In the steady state, when the ion velocity reaches the ion acoustic speed, the quasi-neutral solution breaks down since there is a singularity in the electric field (cf. the Bohm criterion [5]). It is assumed that a positive ion sheath forms at this point. For the present problem, the static sheath boundary condition needs to be extended to the case of a moving sheath edge; that is, the velocity at which the ions leave the plasma must be defined.

The same problem of a collapsing sheath with ionization in the plasma has been studied using the boundary condition that ions cross the collapsing sheath edge with the acoustic speed in the laboratory frame [3]. This condition was supposed to represent the breakdown of the plasma solution at the sheath edge but the numerical results did not support this supposition.

0 031-9163/82/0000–0000/$ 02.75 © 1982 North-Holland

Moreover, the analytic derivation of this boundary condition was incorrect because it appealed to infinities obtained through divisions by quantities which were identically zero. It has been shown [2,6] that a more appropriate boundary condition would be for the ions to leave the plasma at the acoustic speed in the rest frame of the sheath edge; this might be referred to as a "kinetic sheath (or Bohm) criterion". The calculations described here have employed this latter boundary condition in investigating a collapsing sheath. The results are now consistent with the breakdown of the plasma solution at the moving sheath edge.

The initial conditions at time $t = 0$ and for positions $0 < x < 2L$ are those of a self-sustaining positive column (symmetrical about $x = L$) consisting of isothermal electrons, temperature T, density n_e, with cold ions, density n, such that:

$$n = n_e = n_0 \exp(e\phi/kT), \tag{1}$$

where ϕ is potential, e is the electronic charge and k is the Boltzmann constant. For $x < 0$ and for $x > 2L$, at $t = 0$, there are space-charge sheaths and for $t > 0$ the region $x < 0$ becomes progressively occupied by the expanding plasma.

The one dimensional continuity and momentum equations for the ions are:

$$\partial n/\partial t + \partial(nv)/\partial x = \lambda n, \tag{2}$$

$$\partial v/\partial t + v\,\partial v/\partial x = -(e/M)\,\mathrm{d}\phi/\mathrm{d}x, \tag{3}$$

where v is the ion velocity, M is the ion mass and λ is the ioniaztion rate.

The steady-state solution of eqs. (1)–(3) with the boundary conditions specified earlier is [3]:

$$u = 2\cos\{[\cos^{-1}(1 - X) + 4\pi]/3\}, \tag{4}$$

$$\eta = -0.5u^2, \tag{5}$$

where $X = x/L$, $\eta = e\phi/kT$ and $u = v/c$, where c is the ion acoustic speed ($\sqrt{kT/M}$). This solution breaks down at the sheath edge where $u = -1$ and, from eqs. (1) and (5), $n/n_0 = \exp(-1/2)$. $X = L$ is a plane of symmetry, at which both u and η are zero (see figs. 3 and 4).

To solve the time-dependent problem, eqs. (1)–(3) are put into characteristic form [7]. To do this linear combinations are sought such that only one directional derivative enters each new equation. The required linear combinations are:

$$[\partial/\partial\tau + (u + 1)\partial/\partial X](u + \eta) = 2/3, \tag{6}$$

$$[\partial/\partial\tau + (u - 1)\partial/\partial X](u - \eta) = -2/3, \tag{7}$$

where $\tau = ct/L$. There are thus two sets of characteristic propagation paths passing through every point in the (X, τ) plane, with the defining equations

$$(\mathrm{d}X/\mathrm{d}\tau)_f = u + 1, \tag{8}$$

$$(\mathrm{d}X/\mathrm{d}\tau)_g = u - 1, \tag{9}$$

corresponding with upstream (f) and downstream (g) characteristic directions. The characteristics propagate with the ion acoustic speed relative to the plasma ions. Integrating eqs. (6) and (7) along the appropriate characteristic paths in the (X, τ) plane [given by eqs. (8) and (9)] shows that along f and g characteristics:

$$u + \eta = 2\tau/3 + C_f, \tag{10}$$

$$u - \eta = -2\tau/3 + C_g, \tag{11}$$

where C_f and C_g are constant along a chosen f or g characteristic.

Solving for the characteristic propagation paths has now given enough information to determine the response of the plasma for $t > 0$, given the boundary conditions along the wavefront and sheath edge. By substituting the initial sheath edge conditions of $u_w = -1$ and $\eta_w = -1/2$ at $\tau = 0$ into eq. (10), the Riemann invariant (C_{fw}) along the wavefront is obtained and hence the position of, and the ion velocity at the wavefront are [3]:

$$X_w = 4[0.5\tau_w + (1 - \tau_w/3)^{1.5} - 1],$$

$$u_w = 1 - 2(1 - \tau_w/3)^{0.5}.$$

The speed of the wavefront ($\mathrm{d}X_w/\mathrm{d}\tau$) is found to be the local ion acoustic speed, which increases with distance across the column.

The plasma response to the collapse of one of the sheaths bounding a one dimensional positive column is investigated by constructing a mesh of f and g characteristics using eqs. (8)–(11). The f and g characteristics communicate the sheath edge and wavefront boundary conditions, respectively, to the disturbed plasma. The characteristic paths for a sheath edge collapsing with a constant speed of $v_{sh} = -0.5c$ are shown in fig. 1.

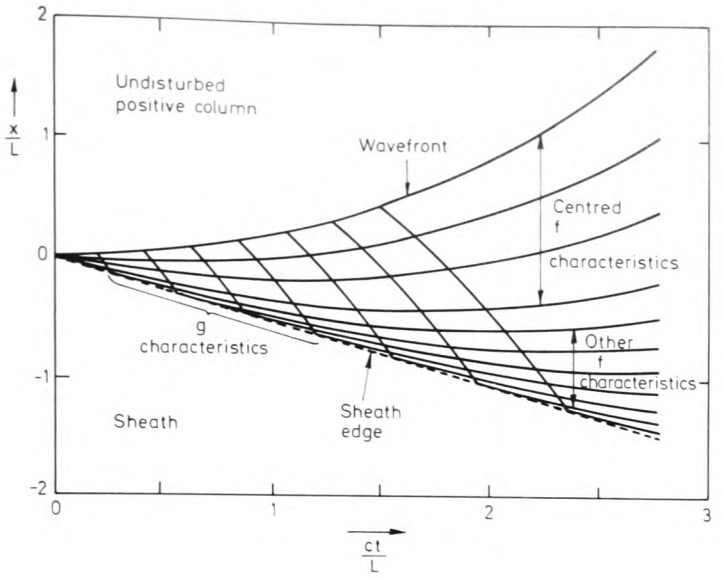


Fig. 1. Some characteristic paths calculated for constant velocity sheath collapse ($v_{sh} = -0.5c$). Information propagates along the characteristics with increasing time.

Note that the "kinetic Bohm criterion", that is the sheath edge boundary condition on the ion velocity ($u_{sh} = v_{sh} - 1$), gives the slope of the f characteristics at the sheath edge as v_{sh} from eq. (8). Thus the f characteristics leave the sheath tangentially. The centered f characteristic fan that leaves the origin represents the dispersal into the disturbed region of the step change in the sheath edge velocity at time $\tau = 0$. This centered component of the solution is bounded above by the wavefront and below by that f characteristic which is tangential to the sheath edge at the origin.

The ion number density profiles are deduced from the computed mesh of characteristics in the (X, τ) plane together with eqs. (1), (10) and (11). Fig. 2

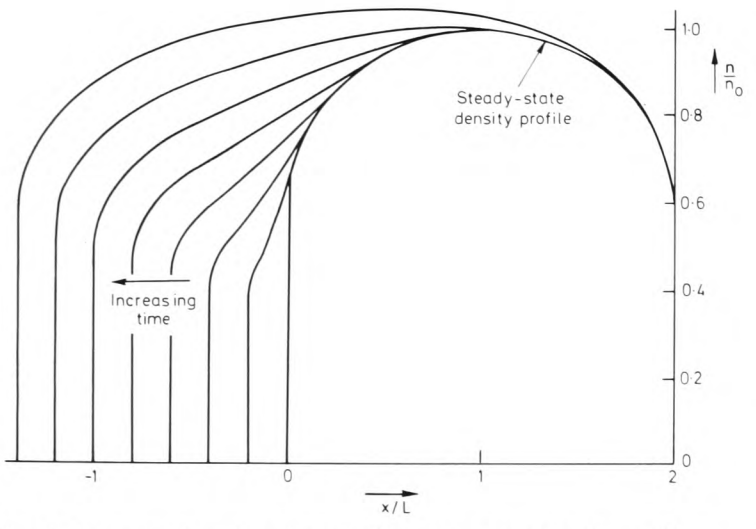


Fig. 2. Ion number density profiles at successive times ($\Delta\tau = 0.4$) for constant velocity sheath collapse (v_{sh} as for fig. 1).

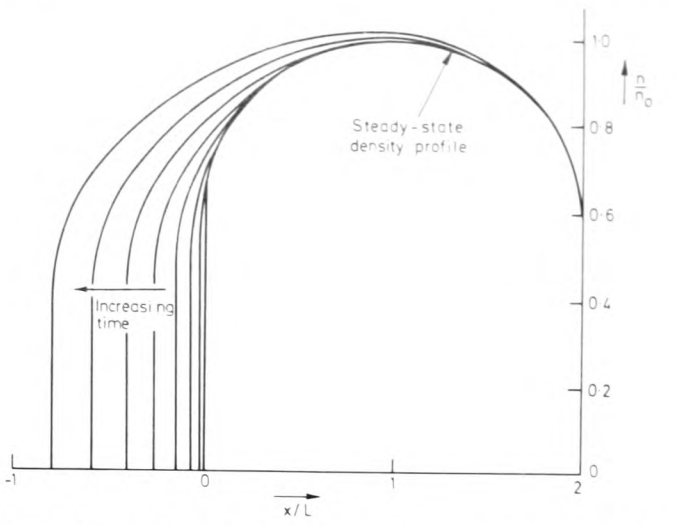


Fig. 3. Ion number density profiles at successive times ($\Delta\tau = 0.4$) for an accelerating sheath edge ($v_{sh} = -0.2c\tau$).

shows such profiles plotted at successive times for a constant velocity sheath collapse. A point of particular interest is that a compression-like feature, an ion density enhancement wave, propagates into the undisturbed plasma at the local ion acoustic speed. Moreover, the gradients of density and potential tend to infinity at the sheath edge, consistent with the breakdown of quasi-neutrality at this point (cf. ref. [3] where this is not the case).

Fig. 3 shows similar computations of ion number density for the case of sheath collapse with sheath edge velocity accelerating from zero. In this case a centered characteristic fan is not generated. Fig. 4 shows the ion velocity profiles corresponding with fig. 3. Note that the ions are accelerated to supersonic speeds in the laboratory frame before they leave the quasi-neutral plasma.

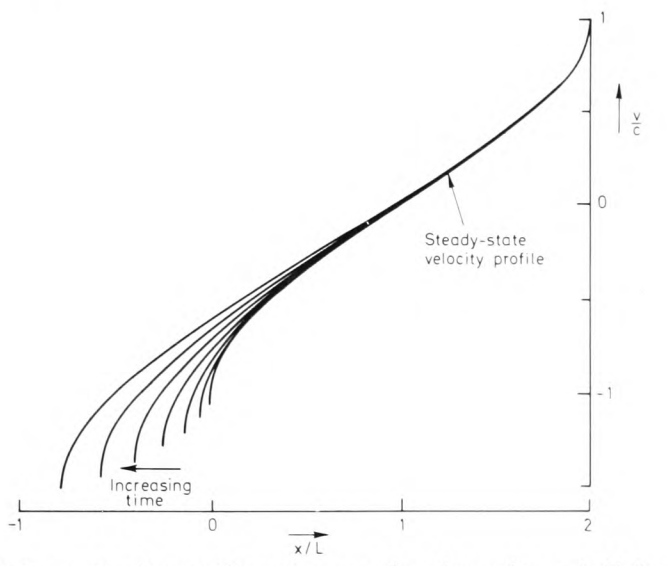


Fig. 4. Ion velocity profiles at successive times ($\Delta\tau = 0.4$) for an accelerating sheath edge (v_{sh} as for fig. 3).

In conclusion it has been demonstrated that, with a kinetic sheath edge boundary condition, the collapse of an ion-rich sheath bounding a self-sustained plasma gives rise to an ion enhancement wave. (The same sheath edge boundary condition applied to an expanding sheath results in an ion rarefaction wave; details of these results are beyond the scope of this letter.) The enhancement wave may be important in explaining how ion acoustic waves are launched by oscillating sheath edges.

Discussions with Dr. J.E. Allen and Mr. S.F. Hehir are gratefully acknowledged and one of us (A.J.C.) acknowledges financial support from the Science and Engineering Research Council, UK.

References

[1] J.E. Allen and J.G. Andrews, J. Plasma Phys. 4 (1970) 187.
[2] P.D. Prewett and J.E. Allen, J. Plasma Phys. 10 (1973) 451.
[3] J.G. Andrews, Phys. Fluids 14 (1971) 129.
[4] J.K. Chester, J. Sci. Tech. 37 (1970) 2.
[5] D. Bohm, in: The characteristics of electrical discharges in magnetic fields, eds. A. Guthrie and R.K. Wakerling, Ch. 3 (McGraw-Hill, New York, 1949).
[6] J.W. Cipolla Jr. and M.B. Silevitch, J. Plasma Phys. 25 (1981) 373.
[7] L.M. Wickens, D. Phil. thesis, Plasmas with moving boundaries (1980), Oxford University.